CZECH TECHNICAL UNIVERSITY IN PRAGUE

Faculty of Civil Engineering

Department of Steel and Timber Structures

NUMERICAL CALCULATION OF MEMBERS AND JOINTS AT ELEVATED TEMPERATURE

NUMERICKÝ VÝPOČET PRUTŮ A SPOJŮ PŘI ZVÝŠENÉ TEPLOTĚ

DOCTORAL THESIS

Mgr. Batuhan Der

Doctoral study programme: Civil Engineering

Branch of study: Building and Structural Engineering

Doctoral thesis tutor: prof. Ing. František Wald, CSc.

Prague, 2024

CZECH TECHNICAL UNIVERSITY IN PRAGUE
Faculty of Civil Engineering
Thákurova 7, 166 29 Praha 6

DECLARATION

Ph.D. student's name: Mgr. Batuhan Der

Title of the doctoral thesis: Numerical calculation of members and joints at elevated temperature

I hereby declare that this doctoral thesis is my own work and effort written under the guidance of the tutor prof. Ing. František Wald, CSc.
All sources and other materials used have been quoted in the list of references.

The doctoral thesis was written in connection with research on the project: TAČR Merlion III FW01010392, Pokročilý návrh konstrukčních detailů/prvků pomocí strojového učení, Advanced design of structural details/elements using machine learning.

In Prague on 02.02.2024

.....
signature

Abstract

The failure of steel joints may result in the collapse of the entire building at elevated temperatures due to their influences on internal forces distribution and overall deformation. Hence, the resistance of steel joints at elevated temperatures should be accurately predicted to understand the structural fire performance. In the fire, stiffness and strength of steel members have significant reductions at elevated temperatures, leading to a decrease in the ultimate load capacity. EN 1993-1-2 suggests that simplified analytical methods may be used to design of isolated steel members subjected to fire assuming a uniform temperature in the cross-section considering the mechanical properties of steel at elevated temperatures can be analysed using. The experimental investigation is the most accurate way to calculate the fire resistance of steel members and joints. Due to the high cost of full-scale fire tests and the size limitations of existing furnaces, these valuable fire tests are not easy to conduct frequently. The prEN 1993-1-14 describes two design methods for finite element models: numerical simulation (NS) and numerical design calculation. prEN-1993-14 [2] defines numerical simulation as an extension of physical experiments to determine the direct resistance of a structure. NS method generally uses an advanced numerical model including the solid elements, the measured material properties, geometrical imperfections, and residual stresses in order to simulate the response of structural components. Advanced solid finite element models have significant advantages in accurately predicting the fire behaviour of steel joints; however, they also come with certain disadvantages. Advanced solid finite element models utilize higher-order elements, and it leads to high computational costs. Another challenge is generating a high-quality mesh for solid models, particularly for irregular or complex geometries. A solid model and a shell model are developed using Abaqus to study the behavior of bolted lap joints and steel beam at elevated temperatures, respectively. The proposed models are validated against experimental results to verify the CBFEM models. The main drawback of analytical models for steel joint design is that it does not accurately reflect the nonlinear behavior of steel joints. They may not be sufficient to accurately evaluate the stress and strain values of steel joints. Therefore, NDC can be used for the static design check of steel joints which may be used to calculate the resistance as stated in prEN1993-1-14. At the design level, analytical models can be replaced by numerical design calculations for predicting the fire resistance of steel joints. This study proposes a numerical design calculation using the CBFEM model to predict the mechanical response of steel joints and members at elevated temperatures. To assess the accuracy and reliability of the proposed model, verification and validation studies are carried out. The model is verified against the results from analytical models or other finite element models. The experimental results are used to validate the steel joint models in terms of load-deformation curves, fire resistance, and failure modes at high temperatures. To predict the resistance of the steel joints and members at ambient and elevated temperatures, the 5% plastic limit strain recommended in EN 1993-1-5 for steel plate elements and the analytical model for the bolts and welds proposed in EN 1993-1-8 were used in the CBFEM model. The influence of temperature on the resistance is considered using the reduction factors for carbon steel and bolts presented in EN 1993-1-2. It can be concluded that CBFEM is a good alternative to analytical models for the design of joints and members at elevated temperatures because it uses advantages of FEM which are not considered by analytical models.

Key words: CBFEM, steel joints, steel members, shell element, numerical design calculation, elevated temperature

Abstrakt

Porucha ocelových spojů může mít za následek zřícení celé budovy při zvýšených teplotách v důsledku jejich vlivu na rozložení vnitřních sil a celkovou deformaci. Odolnost ocelových spojů při zvýšených teplotách by proto měla být přesně předpovídána, aby bylo možné porozumět chování při požáru konstrukce. Při požáru dochází k výraznému snížení tuhosti a pevnosti ocelových prvků při zvýšených teplotách, což vede ke snížení únosnosti. EN 1993-1-2 navrhuje, že návrh izolovaných ocelových prvků vystavených ohni za předpokladu jednotné teploty v průřezu s ohledem na mechanické vlastnosti oceli při zvýšených teplotách lze analyzovat pomocí zjednodušených analytických metod. Experimentální zkoumání je nejpřesnější způsob výpočtu požární odolnosti ocelových prvků a spojů. Kvůli vysokým nákladům na zkoušky ohněm v plném měřítku a omezením velikosti stávajících pecí není snadné provádět tyto cenné testy ohně často. PrEN 1993-1-14 popisuje dvě metody návrhu pro modely konečných prvků: numerickou simulaci (NS) a numerický návrhový výpočet. prEN-1993-14 definuje numerickou simulaci jako rozšíření fyzikálních experimentů ke stanovení přímé odolnosti konstrukce. Metoda NS obecně používá pokročilý numerický model zahrnující pevné prvky, měřené materiálové vlastnosti, geometrické nedokonalosti a zbytková napětí za účelem simulace odezvy konstrukčních součástí. Pokročilé pevné modely konečných prvků mají významné výhody v přesném předpovídání požárního chování ocelových spojů; mají však i určité nevýhody. Pokročilé pevné modely konečných prvků využívají prvky vyššího řádu, což vede k vysokým nákladům na výpočetní techniku. Další výzvou je generování vysoce kvalitní sítě pro objemové modely, zejména pro nepravidelné nebo složité geometrie. Pevný model a model skořepiny jsou vyvinuty pomocí Abaqus ke studiu chování šroubovaných přeplátovaných spojů a ocelového nosníku při zvýšených teplotách. Navržené modely jsou validovány proti experimentálním výsledkům pro ověření modelů CBFEM. Hlavní nevýhodou analytických modelů pro návrh ocelových spojů je to, že přesně neodrážejí nelineární chování ocelových spojů. Nemusí být dostatečné pro přesné vyhodnocení hodnot napětí a deformace ocelových spojů. Proto lze NDC použít pro statickou návrhovou kontrolu ocelových spojů, které lze použít k výpočtu odporu podle prEN1993-1-14. Na úrovni návrhu lze analytické modely nahradit numerickým návrhovým výpočtem pro predikci požární odolnosti ocelových spojů. Tato studie navrhuje numerický návrhový výpočet s použitím modelu CBFEM k předpovědi mechanické odezvy ocelových spojů a prvků při zvýšených teplotách. Pro posouzení přesnosti a spolehlivosti navrženého modelu se provádějí verifikační a validační studie. Model je ověřován na základě výsledků z analytických modelů nebo jiných modelů konečných prvků. Experimentální výsledky jsou použity k ověření modelů ocelových spojů z hlediska křivek zatížení-deformace, požární odolnosti a poruchových režimů při vysokých teplotách. Pro předpovídání odolnosti ocelových spojů a prvků při okolních a zvýšených teplotách se doporučuje 5% mezní plastické přetvoření doporučené v EN 1993-1-5 pro ocelové plechové prvky a analytický model pro šrouby a svary navržený v EN 1993-1- 8 byly použity v modelu CBFEM. Vliv teploty na odpor je uvažován pomocí redukčních faktorů pro uhlíkovou ocel a šroub uvedených v EN 1993-1-2. Lze konstatovat, že CBFEM je dobrou alternativou k analytickým modelům pro navrhování styčníků a prvků při zvýšené teplotě, protože využívá výhod MKP, které analytické modely nezohledňují.

Klíčová slova: CBFEM, ocelové spoje, ocelové prvky, skořepinový prvek, numerický návrhový výpočet, zvýšená teplota

Acknowledgement

I dedicate this thesis to my wife, Tereza, and my sons, Artuk and Salur. I hope the sacrifices you have endured for me to pursue this dream will be repaid to you with many opportunities for having great times together in our future.

I would like to extend my sincere thanks to Prof. Wald for his willing attitude to the dissertation leading, technical and methodological support.

My deepest thanks belong to my parents and brother, who supported me during my studies.

https://doi.org/10.14311/dis.fsv.2024.005

Table of Contents

1. Introduction

1.1. Background

Structural steel has become a dominant construction material, from residential buildings to carparks to schools and skyscrapers. The essential advantages of using structural steel are strength and durability, convenience for large spans, light in weight, easy installation and speed in construction, flexibility, ductility, and easy fabrication in different sizes, whereas there are some disadvantages such as buckling, availability only at steel plants and low corrosion resistance. The most common applications of structural steel in buildings are sections, reinforcing bars, sheet products, and internal fittings. The main members of steel structures are beams, columns, and joints. In practice, steel joints may be either welded or bolted.

Steel joints play a critical role in structural engineering since they transfer forces and moments between individual structural members. Effective load transfer ensures that the applied loads may be properly distributed over the entire structure. The behaviour of steel joints has a significant influence on the integrity of steel structures. The failure of steel joints may result in the progressive collapse of the whole structure. Elevated temperatures can significantly influence the performance of steel joints in structures. The increase in steel temperatures depends on the severity of the fire, the area of steel exposed to the fire and the amount of applied fire protection [1]. High temperature leads to changes in material properties, loss of strength and stiffness, and potential failure modes of steel joints. As the temperature increases, the yield strength and ultimate tensile strength of steel, bolt, and weld decrease. Therefore, the load-carrying of the steel connection may be remarkably influenced by the reduction in strength.

Accurate modelling of steel joints and members at elevated temperatures is important to ensure the safety and structural integrity of the steel structures in a fire. Finite element models may predict temperature distribution within the steel joint during a fire considering radiation, convection, and conduction. FEM allows for the detailed modelling of joint components, such as bolts, welds, and plates to investigate the behaviour of mentioned components at elevated temperatures. Designers can predict the fire behaviour of the steel joint, including deformations, stresses, and strains, under the influence of elevated temperatures. Accurate modelling of steel joints and members may significantly decrease the use of fire protection materials and it can minimize the ecological footprint of steel buildings.

1.2. Numerical Design Calculation

The prEN 1993-1-14 [2]describes two design methods for finite element models: numerical simulation (NS) and numerical design calculation (NDC). prEN-1993-14 defines numerical simulation as an extension of physical experiments to determine the direct resistance of a structure. NS method generally uses an advanced numerical model including the solid elements, the measured material properties, geometrical imperfections, and residual stresses in order to simulate the response of structural components. Advanced solid finite element models have significant advantages in accurately predicting the fire behaviour of steel joints; however, they also come with certain disadvantages. Advanced solid finite element models utilize higher-order elements, and it leads to high computational costs. Another challenge is generating a high-quality mesh for solid models, particularly for irregular or complex geometries. The main drawback of analytical models for steel joint design is not accurate reflecting the nonlinear behaviour of steel joints. They may not be sufficient to accurately evaluate the stress and strain values of steel joints. Therefore, NDC can be used for the static design check of steel joints which may be used to calculate the resistance as stated in prEN1993-1-14. At the design level, analytical models and solid models can be replaced by numerical design calculations for predicting the fire resistance of steel joints and members. Der et al.

[3-5] validated and verified the component-based finite element model to model bolted steel joints at elevated temperatures.

1.3. Component Based Finite Element Method

Component-based Finite Element Method (CBFEM) is a method to analyse and design joints of steel structures. The CBFEM is the combination of the analytical component method and the numerical finite element method (FEM). The finite element method is used to solve the distribution of internal forces. Figure 1.1 depicts the configuration of the CBFEM modelling for beam-to-column joints. Analytical models implemented into FEM as components model the behaviour of connectors. Šabatka et al. [6] define the following components for joint models:

- Generating steel plates using 2D shell element;
- Force interpolation of welds;
- nonlinear springs for bolts in shear and tension;
- contact phenomena;

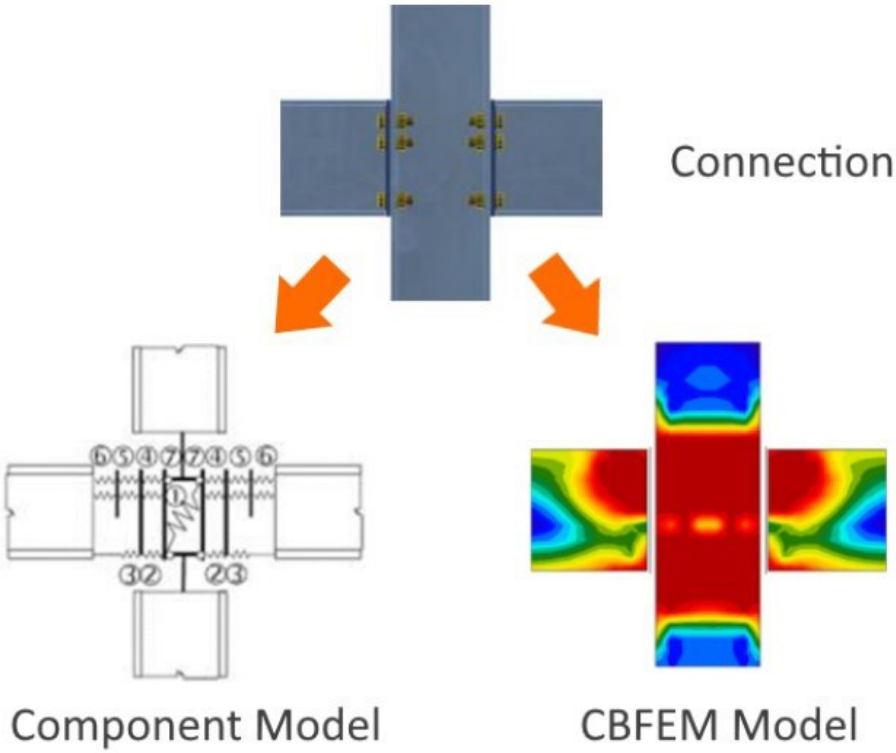

Figure 1.1. Modelling of joints using CBFEM [7]

The CBFEM is widely used to design steel joints at ambient temperatures. The benchmark studies of CBFEM are presented in the study of Wald et al [7]. CBFEM is an example of NDC. The design of joints by finite element method is not a replication of the physical experiment. The designer is interested in the limited yielding of steel plates and the failure of fasteners. CBFEM is taking advantage of accurate modelling of component behavior based on experiments and accuracy of discrete analysis of steel plate by FEM. The distribution of internal forces in connection is analyzed by finite element method. The connectors' behavior is modelled by analytical models as nonlinear springs. The use of the CBFEM models needs to be verified and validated to model the steel joints and steel members at elevated temperatures.

2. Research objectives

Predicting the behaviour of steel joints has been the object of intensive research over the past 30 years. Cardington structural fire test programme [8] and the progressive collapse of the 47-storey steel-framed World Trade Center 7 [9] building on 11 September 2001 have demonstrated the complexity of joint behaviour in fire. Several experimental tests were performed in different typologies of joints and under different boundary and loading conditions, and analytical and numerical models were developed in order to predict the steel joint behaviour. The current Eurocode on structural steel design for fire safety [10] has the only the variation of strength and elastic modulus of steel and fasteners at elevated temperatures and some guidance on thermal gradient in the connection region.

FEA has become a common research method since fire tests on an entire structure or even part of a structure are costly and time-consuming. Detailed finite element modelling using software such as ABAQUS [11] can provide sufficient accuracy, but the creation of structural models using 3D solid elements is time-consuming, and the analysis can be computationally demanding. Therefore, using shell elements in finite element method is an alternative to decrease the computational time. In addition to the finite element models, the component-based method [7] is also common models to evaluate joint behaviour at elevated temperatures. In the component-based method, a joint is considered as an assembly of nonlinear springs, each of which has its individual characteristics. This simplified model is able to represent the key behaviour of certain joint elements to an acceptable accuracy.

In this thesis, the behaviour of steel joints and members at elevated temperatures is investigated using the component-based finite element method (CBFEM). Different steel joint types are selected to analyse the component behaviours at elevated temperatures. The selected joint types are bolted lap joints, T-stubs, welded lap joints, flush endplate joints, and fin plate joints. Bolted lap joints and fin plate joints, which are simple joints, are chosen to study the bolts in shear, bearing plate, and net section failure, The reason for the selection of T-stubs and flush endplate joints is the investigation of the possible failure modes of equivalent T-stubs proposed in EN 1993-1-8 [12]. This study proposes a numerical design calculation for these joints at elevated temperatures using the component-based finite element models at elevated temperatures, since there is a lack of research on the CBFEM at elevated temperatures. The solid model is generated to predict the mechanical behaviour of bolted lap joints at elevated temperatures. However, the use of solid elements may cause an increase in computational costs. The CBFEM models use shell elements to model the steel plates to decrease the computation time. This thesis aims to show the applicability of shell elements to simulate the accurate response of steel joints and members. However, the failure criteria play a critical role in determining the resistance of steel joints and members. EN 1993-1-5 [13] recommends a 5% plastic limit strain for the failure of steel at ambient temperature, but there is no recommendation for elevated temperatures. Therefore, this thesis aims to investigate the effect of a 5% limit strain on the fire resistance of steel joints. The bolt failures are captured by the CBFEM models using the design equations for bolts in tension, in shear, and in the interaction of shear and tension presented in EN 1993-1-8. The CBFEM considers the influence of high temperatures on the material properties of bolts, welds and plates decreasing by the reduction factors proposed in EN 1993-1-2 [10]. Validation and verification are important steps to ensure the accuracy and reliability of a finite element model. The verification of the CBFEM models is performed by comparing the failure modes and resistances of steel joints obtained from the CBFEM and the analytical models. The experimental studies are used to validate the CBFEM models. In this research, experimental studies are performed for bolted and welded lap joints at elevated temperatures. Test results from the literatures are utilized for the validation of the CBFEM models to investigate the fire response of T-stubs, fin plate joints, and flush endplate joints. The main goal of the thesis is to present the numerical design calculation for steel members and joints at

elevated temperatures. Furthermore, the CBFEM may be a new design tool for the fire design of steel joints and members as an alternative to the analytical models.

2.1. Outline of research

The thesis is divided into 5 main chapters.

In Chapter 3, a comprehensive literature review on the effect of elevated temperature on steel structures, material properties of steel, bolts, and welds, and the experimental and numerical studies on the steel joints and members at high temperatures. The numerical modelling techniques are presented for bolts and welds in addition to solid models. The reduction factors proposed in different studies are summarized in Section 3.2. There are several experimental studies on the isolated parts and full-scale tests at elevated temperatures. Previous numerical models for modelling of steel joints and steel members at elevated temperatures are described in Section 3.4.

Chapter 4 gives details about the experimental study on the bolted lap joints at elevated temperatures. The testing procedure is explained, and the heating record of the joints is graphically presented. Furthermore, the load-deformation curves and failure modes of tested specimens are given at ambient temperature, 400°C, and 600°C.

In Chapter 5, the numerical models are described for modelling steel joints and members at elevated temperatures. The generated solid model for modelling of bolted lap joints, the developed shell element, and the CBFEM models for steel joints and members at elevated temperatures are described. Since the verification and validation procedure is essential to understand the reliability of the proposed numerical models. Chapter 4 indicates the verification and validation studies of the numerical models.

Chapter 6 presents the summary of the thesis. Conclusions drawn from the whole thesis and recommendations for future work are provided.

3. Literature Review

3.1. Steel Structures in Fire

Fires are severe events that involve high levels of uncertainty. The main factors influencing the response of steel structures in the fire are the elevated temperatures in the steel members, the fire limit state loads on the structure, the mechanical properties of the steel, and the geometry and design of the structure.

In fire engineering design, the mechanical properties and thermal properties of steel must be considered since the changes in material properties can cause complex structural behaviour. Steel buildings are generally vulnerable to fire, due to the high thermal conductivity and low specific heat of steel. Nevertheless, one of the major weaknesses of steel is reduction in strength and stiffness at elevated temperatures [1]. Therefore, structural steel members are normally protected by protective materials against fire. However, the cost of fire-protecting steel is an important disadvantage. Fire safety precautions are required to minimise the loss of life and financial loss incurred as a result of damage. To prevent these failures due to high temperatures in fire design, passive fire protection is required. When steel is galvanized, the fireproofing system may be provided, thanks to the presence of the zinc coating. Hot-dip galvanized steel has many advantages compared to uncoated steel as follows: lower emission factor, slower heating rate, and delay in the critical temperature [14]. A significant amount of experimental, numerical, and analytical research has been performed to investigate the mechanical response of steel structures at elevated temperatures. The Cardington program [3] was one of the most comprehensive experimental studies to understand the fire response of steel structures. The floor system and the structural integrity were able to deal with severe fire exposure without collapse, although fire protection was not presented.

3.2. Material Properties at elevated temperatures

Thermal and mechanical properties of materials with increasing temperature must accurately be determined to predict the correct temperature-time curve of structural members and the response of structures under fire loads. The required material thermal properties for structural fire engineering are emissivity, thermal conductivity, specific heat capacity, and thermal expansion. Emissivity represents the relative ability of its surface to radiate its absorbed heat. A value of 0.7 is proposed for structural steels in EN-1993-1-2 [10]. Emissivity has a significant effect on the temperature increase in steel surfaces. Therefore, galvanized steel is proposed to protect the steel structures from the severity of a fire since the emissivity of galvanized surfaces is calculated as 0.35 [14]. The thermal conductivity of a material is a measure of its ability to conduct heat. Specific heat measures the quantity of heat per unit mass to raise to temperature by 1°C. Thermal conductivity and specific heat are the temperature-dependent properties, which means that the values vary with temperature.

There are two different methods for material testing: steady-state test and transient heating test. In a steady-state test, the coupon is heated to the target temperature level then it is loaded to fracture under constant temperature. The transient heating test keeps the stress in the coupon constant and increases temperature until a fracture occurs.

3.2.1. Structural Steel

The thermal properties of structural steel such as density, thermal expansion, thermal conductivity and specific heat need to be taken into account for predicting the temperature distribution in steel joints. The density of steel given in EN-1993-1-2 [10] is 7850 kg/m³, and this value is assumed to be independent of temperature increase. Generally, simple fire engineering calculations neglect the thermal expansion of materials. However, the steel member with concrete slabs is exposed to “thermal bowing” towards the fire in the lower range of temperatures due to the differential thermal expansion. The thermal expansion strain (ε_{th}) of steel is given by Eq. 1. (EN 1993-1-2).

$$\varepsilon_{th} = \begin{cases} -2.416 \times 10^{-4} + 1.2 \times 10^{-5}T + 0.4 \times 10^{-8}T^2 \; for\; T \leq 750°C \\ 0.011 \qquad\qquad\qquad\qquad\qquad\qquad for\; 750°C < T \leq 860°C \\ -0.0062 + 2 \times 10^{-5}T \qquad\qquad\qquad\qquad for\; T > 860°C \end{cases} \quad (1)$$

Thermal conductivity is in W/(m·°C) or W(m·K) the ability of material to conduct heat. Heat flux is calculated by Fourier's law and its unit is joules per second per square meter in the case of °C. The thermal conductivity of steel, λ_s (W/mK), can be determined by the following equations:

$$\lambda_s = \begin{cases} 54 - 0.0333T \;\; for\; 20°C \leq T < 800°C \\ 27.3 \qquad\qquad for\; 800°C \leq T \leq 120°C \end{cases} \quad (2)$$

The specific heat in J/(kg·°C) or J/(kg·K) measures the quantity of heat per unit mass to raise to temperature by 1°C. The specific heat of steel increases rapidly at around 750ºC, resulting from the presence of the phase change in steel, in which the atom structure transits from a face centred cubic to a body centred cubic structure.

$$c_s = \begin{cases} 425 + 0.773T - 1.69 \times 10^{-3}T^2 + 2.22 \times 10^{-6}T^3 \quad for\; 20°C \leq T < 600°C \\ 666 + \frac{13002}{738-T} \qquad\qquad\qquad\qquad\qquad for\; 600°C \leq T < 735°C \\ 545 + \frac{17820}{T-731} \qquad\qquad\qquad\qquad\qquad for\; 735°C \leq T < 900°C \\ 650 \qquad\qquad\qquad\qquad\qquad\qquad\qquad for\; 900°C \leq T \leq 1200°C \end{cases} \quad (3)$$

The strength and the stiffness of the structural steel reduce with increasing temperature. The yield strength of structural steel around 550°C is only about half of that at ambient temperature. To determine the strength reduction factors for hot rolled steel is dependent not only on the material but also on the test method, the heating rate, and the strain limit used to determine steel strength. It is clear that there is a marked loss in strength and stiffness of structural steel between 400°C and 700°C.

Table 3.1. Reduction factors for structural steel in EN 1993-1-2

Steel Temperature (°C)	Yield Strength Reduction Factor	Modulus of Elasticity Reduction Factor
20	1	1
100	1	1
200	1	0.9
300	1	0.8
400	1	0.7
500	0.78	0.6
600	0.47	0.31
700	0.23	0.13
800	0.11	0.09
900	0.06	0.068
1000	0.04	0.045
1100	0.02	0.023
1200	0	0

The stress-strain relationship of steel at elevated temperatures, which is proposed by EN 1993-1-2 [10], is formed by two straight lines connected with an elliptical curve. The elastic material behaviour

is characterized by the first linear part until the proportional limit ($f_{p,\theta}$) is reached. The general stress-strain relationship is presented in Figure 3.1. The equations that are used to develop the stress-strain relationship for carbon steel are listed in Table 3.2.

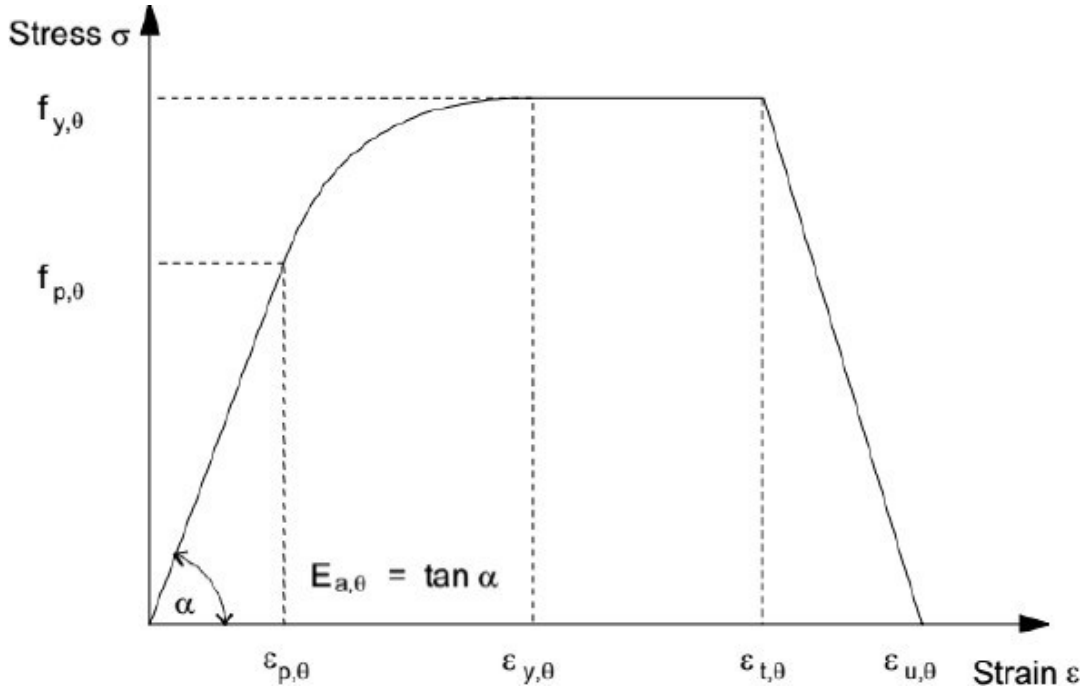

Figure 3.1. Stress-strain relationship for carbon steel at elevated temperature ([10])

Table 3.2. Stress-strain curve equations (EN 1993-1-2, 2005)

Strain range	Stress σ
$\varepsilon \leq \varepsilon_{p,\theta}$	$\varepsilon E_{a,\theta}$
$\varepsilon_{p,\theta} < \varepsilon < \varepsilon_{y,\theta}$	$f_{p,\theta} - c + (b/a)\,[a^2 - (\varepsilon_{y,\theta} - \varepsilon)^2]^{0.5}$
$\varepsilon_{y,\theta} < \varepsilon < \varepsilon_{t,\theta}$	$f_{y,\theta}$
$\varepsilon_{t,\theta} < \varepsilon < \varepsilon_{u,\theta}$	$f_{y,\theta}[1 - (\varepsilon - \varepsilon_{t,\theta})/(\varepsilon_{u,\theta} - \varepsilon_{t,\theta})]$
$\varepsilon = \varepsilon_{u,\theta}$	0

where a, b and c in the above table are parameter functions which are defined as:

$$a^2 = (\varepsilon_{y,\theta} - \varepsilon_{p,\theta})(\varepsilon_{y,\theta} - \varepsilon_{p,\theta} + c/E_{a,\theta}) \quad (4)$$

$$b^2 = c(\varepsilon_{y,\theta} - \varepsilon_{p,\theta})E_{a,\theta} + c^2 \quad (5)$$

$$c^2 = \frac{(f_{y,\theta} - f_{p,\theta})^2}{(\varepsilon_{y,\theta} - \varepsilon_{p,\theta})E_{a,\theta} - 2(f_{y,\theta} - f_{p,\theta})} \quad (6)$$

Traditionally, there are two methods to determine the stress-strain relationships at elevated temperature. The stress-strain relationship of steel at a specific temperature can be obtained directly in the steady state test.

3.2.2. Bolts

There is no extensive information on the mechanical properties of bolts at elevated temperatures. Sakumoto et al. [15] reported some experimental studies on the mechanical properties of high-strength fire-resistant bolts (F10T torque-control bolts) at high temperatures and proposed reduction factors for the elastic modulus of tested bolts. Experimental studies showed that there is an important reduction in bolt strength between 300°C and 700°C. Kirby [16] performed a series of tests on Grade 8.8 bolts, which are widely used in steel construction, in order to determine the reduction of the bolt strength in fire. A significant decrease in strength and Young's modulus was observed in this study between 300°C and 700°C. The following strength reduction factors (SRF) were recommended:

$$SRF = \begin{cases} 1.0 \; for \; T \leq 300°C \\ 1.0 - (T - 300) \times 0.2128 \times 10^{-2} \; for \; 300°C < T \leq 680°C \\ 0.17 - (T - 680) \times 0.5312 \times 10^{-3} \; for \; 680°C < T \leq 1000°C \end{cases} \quad (7)$$

Li et al. [17] established mathematical expressions for yield strength, limit strength, Young's modulus, and elongation testing 30 coupons of material experiencing the same heat treatment as in the real bolt manufacturing process. The tested bolt type was chosen as high-strength steel 20MnTib. In EN-1993-1-2, there is no consideration for the elastic modulus of bolts and welds, therefore only the strength reductions factor can be found for tension and shear. However, studies on the deterioration of bolts in fire are still lacking. Yu [18] studied the mechanical response of ASTM A325 and A490 bolts under double shear loading at temperatures up to 800°C. These tests revealed that A325 bolts are equivalent to Grade 8.8 bolts in terms of strength at ambient temperature. On the other hand, A325 bolts do not behave similarly compared to Grade 8.8 bolts. At elevated temperatures, A490 bolts have a similar decreasing trend as Grade 8.8 bolts have. Hu et al. [19] performed a series of tests for Grade 8.8 high-strength bolts complying with recent British and European standards (BS 4190:2000 and EN ISO 4014, 4017 respectively). The following strength reduction factors (SRF) were proposed based on these tests:

$$SRF = \begin{cases} 1.0 - (0.2275 \times T - 4.55) \times 10^{-3} \; for \; T \leq 300°C \\ 0.9363 - 0.24 \times (T - 300) \times 10^{-2} \; for \; 300°C < T \leq 600°C \\ 0.5407 - (1 - T/1000) \; for \; 600°C < T \leq 1000°C \end{cases} \quad (8)$$

Kodur et al. [20] conducted steady-state single shear and tension at a temperature range of 20– 800°C in order to evaluate high-temperature thermal and mechanical properties of Grade A325 and A490 high-strength steel bolts. The findings of this study indicated that the reduction in the strength properties of A325 and A490 high-strength steel bolts is greater than those of conventional steel and also that A325 steel has slightly lower strength and stiffness properties than A490 at 20-800°C. Peixoto et al. [21] carried out tests on high-strength structural A325 and A490 bolts exposed to double shear loading at elevated temperatures. Pang et al. [22] performed an experimental program to investigate the elevated-temperature material properties for three types of high-strength bolts with property classes 8.8, 10.9, and 12.9. Rezaeian et al. [23] investigated the influence of temperature on the mechanical properties of Grade 10.9 steel bolts. The results indicated that Grade 10.9 bolts experience rapid decreases in strength at temperatures exceeding 400°C and respectively reach 40% and 5% of their original strength when heated to 600°C and 800°C. Ban et al. [24] presented standard tensile coupon tests on high-performance (HP) bolts at temperatures ranging from 20 to 900°C. Furthermore, constitutive models and prediction equations were proposed to describe the material properties of the HP bolts at different temperatures. Table 3.3 gives the strength reduction factors for bolts, which are proposed by different authors, at elevated temperatures and Figure 3.2 is a graphical representation of these data.

Table 3.3. Reduction factor for tensile resistance of bolts

Temperature [°C]	**Sakumoto et al.** [16]	**Kirby** [16]	**Li et al.** [17]	**EN 1993-1-2**	**Hu et al.** [19]
20	1	1	1	1	1
100	1	1		0.968	0.982
150	1	1		0.952	0.97
200	1	1	1.004	0.935	0.959
250		1			0.948
300	0.959	1	0.938	0.903	0.936
350		0.894			0.816
400	0.874	0.787	0.742	0.775	0.696
450		0.681			0.576
500	0.747	0.574	0.438	0.55	0.456
550	0.624	0.468			0.336
600	0.43	0.362	0.213	0.22	0.216
650	0.273	0.255			0.189
700	0.166	0.159	0.091	0.1	0.162
750		0.133			0.135
800	0.074	0.106		0.067	0.108
850		0.08			0.081
900		0.053		0.033	0.054
950		0.027			0.027
1000		0		0	0

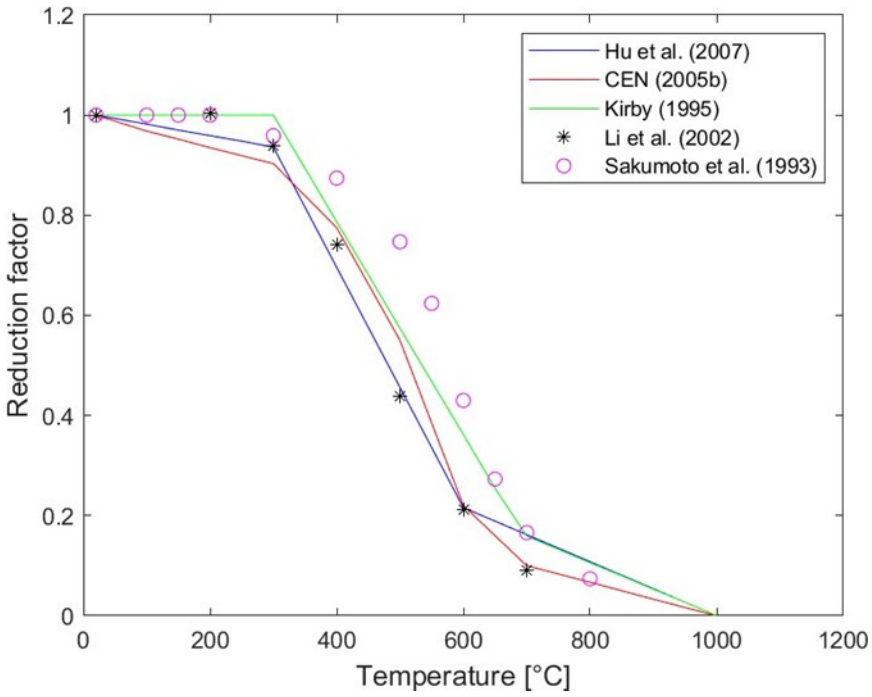

Figure 3.2. Reduction factors for bolts

3.2.3. Welds

The behaviour of welds at elevated temperatures has a significant influence on predicting the response of a welded joint. Welds are used to carry a combination of axial and shear forces at elevated temperatures. Therefore, a longitudinal weld, that is oriented parallel to its applied load, may have a component of loading that is oriented perpendicular to its length, possibly making it behave like a transverse weld. The reduced strength per unit length of a fillet weld at elevated temperature can be evaluated through reduction factors indicated in Table 3.4.

Table 3.4. Reduction factors for welds in Eurocode

Temperature (°C)	Weld Strength Reduction Factor
20	1
100	1
150	1
200	1
300	1
400	0.876
500	0.627
600	0.378
700	0.13
800	0.074
900	0.018
1000	0

Yu [25] presented reports on a set of experiments on the ultimate strength and fractural performance of structural steel welds at elevated temperatures. The proposed reduction factors are depicted in Figure 3.3. The ultimate failure resistance fluctuated up to 400°C. Rezaeian et al. [26] presented results from an experimental investigation on the high-temperature mechanical characteristic of steel welds made using the shield metal arc welding (SMAW) process, and E6013 and E7018 electrodes. The ultimate strength of welds increased up to 400°C. Test data also showed that the yield stress of steel welds decreases faster than that of structural steel at 450-800°C.

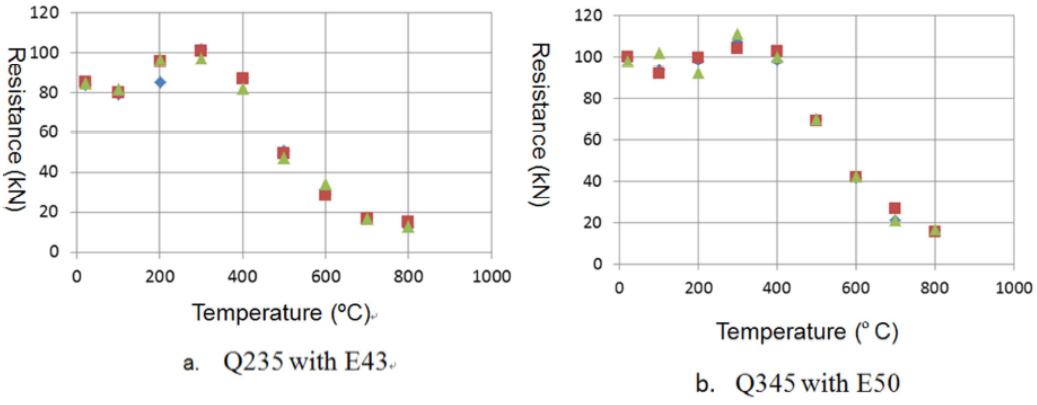

Figure 3.3. Reduction of the weld resistances with temperature [25]

3.3. Behaviour of steel members and joints at elevated temperatures

In recent years, research on the behaviors of steel structures in case of fire has become very popular. The structural response of steel structures under fire action depends on the material degradation, loss of stiffness and strength, thermal gradient, and restraints for expansion. The influences of thermally induced forces and deformations on the fire response of steel structures are poorly understood and are not properly standardized. Most research studies focused on the response of semi-rigid joints to determine their resistance and stiffness characteristics. Simões da Silva and Girão Coelho [27] stated that the following phenomena make much more complicated the prediction of fire response of a steel connection than ambient design: changes in material properties of steel with increasing temperature, accurate prediction of time-temperature variation within the various joint components, elongation difference between the various joint components because of increasing temperature and proper definition of fire development models within the building. The first three phenomena are needed to predict the moment-rotation behaviour of steel joints.

Traditionally, the joints are considered as either pinned or rigid in design. However, the actual behaviour of the joints in real life is neither absolutely rigid nor pinned, but semi-rigid. The mechanical behaviour of steel joints is a complex phenomenon in terms of strength, stiffness, and rotation capacity. The current design codes predict the resistance of structures at elevated temperatures based on isolated member tests subjected to standard fire conditions. In real structures, the interaction between members results in global or local failure of the structure, stresses, and deformations due to the restraint to thermal expansion. These phenomena can't be observed or predicted from the isolated member tests. Standard fire curves are not able to represent the natural fire curves which are characterized by three phases: a growth phase, a fully developed phase, and a decay phase [28].

Due to the high cost of the fire tests and the limited furnace size, the experimental results on the response of steel joints under fire conditions are relatively limited. The importance of joint response on the overall performance of the structure was seen through full-scale tests and fire accidents. It is traditionally assumed that beam-to-column joints have sufficient fire resistance due to their cooler temperatures and a slower rate of heating than the connected members, induced by the large concentration of thermal mass in the connection. However, the failure of the World Trade Centre [9] on 11th September 2001, the full-scale fire tests in Cardington [8] and the subsequent research demonstrated that it is not a correct assumption that beam-to-column joints have sufficient fire resistance caused by the large concentration of thermal mass in the joint since there is a change in internal forces from moment and shear at ambient temperature to moment, shear and compression due to restrained thermal expansion of the beams in the early and intermediate stages of a fire, and finally to shear and tension in the later stage when catenary action starts. These realistic loading conditions can't be obtained by experiments on isolated joints and sub-structures. The real response of joints at elevated temperatures has been gathered from large-scale furnace tests [29-31].

3.3.1. Experimental studies on steel joints at ambient and elevated temperatures

CTICM [32] and British Steel [33] carried out the first reported experimental fire tests on joints, on six joint types ranging from flexible to rigid under the ISO 834 fire curve. The tests focused on investigating the performance of high-strength bolts at elevated temperatures. The results indicated that the bolts and their connected elements could suffer considerable deformations at elevated temperatures.

Lawson [29] conducted the early fire tests of steel and composite joints, with different major-axis joints under constant load, exposed to the standard fire, as seen in Figure 3.4. Three types of bolted joints have been studied including flush endplate, extended endplate, and web cleat joints. The purpose of the tests was to develop a design approach for steel beams considering the joint rotational

restraint. The failure of bolts and welds were not observed in tests despite relatively large deformations of the joints. It was observed that up to two-thirds of the ambient temperature design moment capacity could be protected in standard fire conditions. The test results provided insufficient data to generate the moment-rotation curves. The experimental observations showed that the temperatures in the joint were much lower than that of the lower flange of the steel beam, which is usually the element that defines the limiting temperature of the beam. In addition, it was suggested that composite action at elevated temperatures contributed to the enhanced moment capacity of the joints.

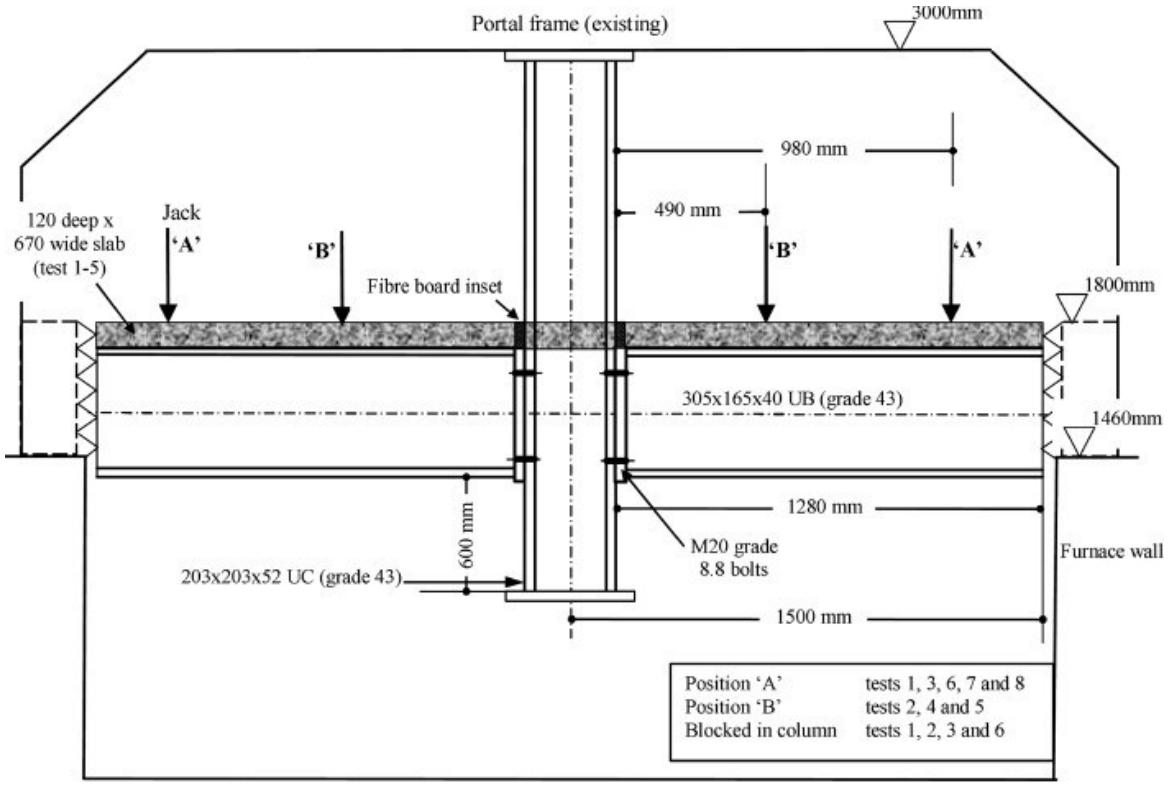

Figure 3.4. Arrangement of the fire tests on beam-to-column joints [29]

A collaborative research programme involving the Building Research Establishment, the University of Sheffield and the Steel Construction Institute in the UK have firstly attempted to characterise the moment-rotation behaviour of commonly used joints at elevated temperatures. The programme included two phases. In the first phase, Leston-Jones et al. [34] conducted a total of eleven tests on cruciform joints with flush endplates, including two tests at ambient temperature, for both bare-steel and composite joints. The test setup is shown in Figure 3.5. The significant deformation of the column web in the compression zone and of the column flange in the tension zone was observed in the tests at ambient temperature. The failure modes observed at high temperatures and at room temperature were similar. The test results at high temperatures have also shown a remarkable reduction in both the moment capacity and stiffness of the joint. The critical temperature range of the connection was between 500-600ºC. In the second phase, the scope of this test programme was extended by Al-Jabri [31] to the effect of parameters such as member size, joint type, and different failure mechanisms.

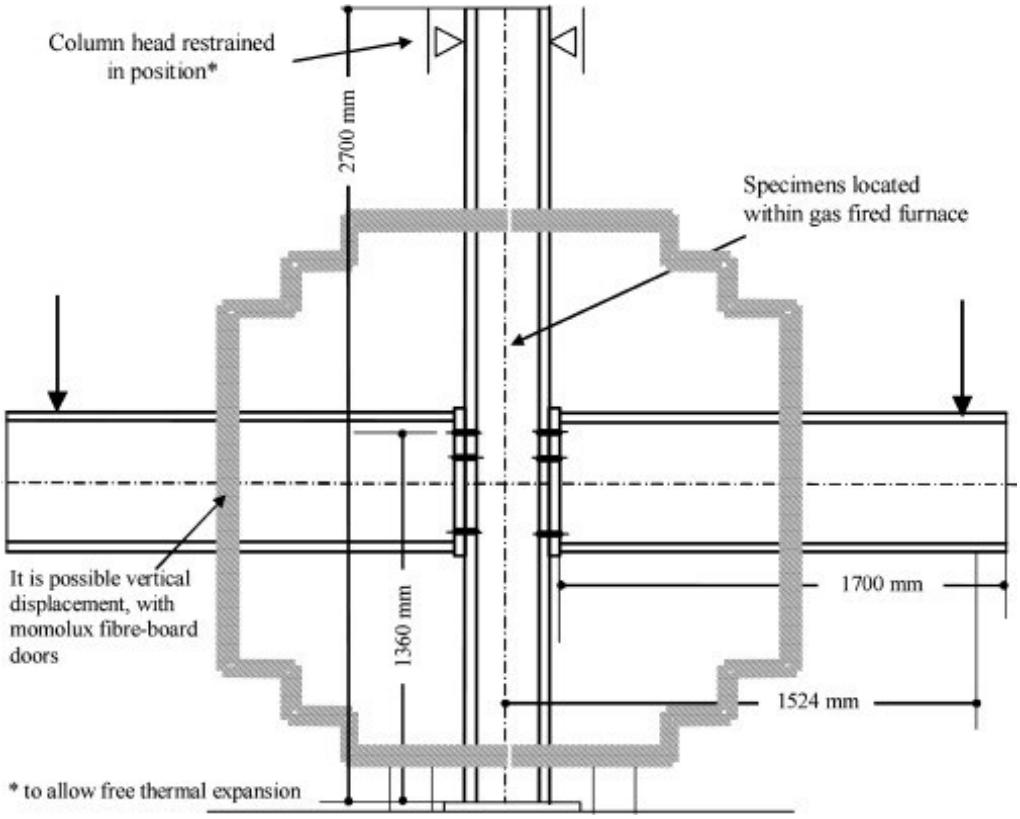

Figure 3.5. High temperature test: schematic arrangement [30]

The universities of Sheffield and Manchester studied the capacity and ductility of common types of steel joints under fire loads [35-40]. In the test programme the joints were exposed to combinations of shear force and tying force and loaded to large deformation and fracture. Yu et al. [35] studied the tying capacities and rotational capacities of web cleat joints under tying force at elevated temperatures.

A series of tests on flush end plate joints subjected to combinations of tying force and shear force at elevated temperatures were performed by Yu et al. [38]. The tested joint consists of a UC254x89 column and a UB305x165x40 beam. In all the tests the steel column and the steel beams were made of S355 and S275, respectively. A typical endplate joint was designed with three rows of bolts in accordance with UK design recommendations [41]. The 325 mm deep x 200 mm width flush endplates made of grade S275 were connected to the beams with M20 Grade 8.8 bolts. The specimens were tested under steady-state conditions. The characteristics of test specimens are presented in Table 3.5. The plate thickness used in tests varied from 8, 10, and 15 mm. The load is applied to the test specimens through a special connector with an angle described in Table 3.5. The test specimens were loaded with three different angles 35, 45, and 55° at room temperature, 450°C, 550°C and 650°C. The test specimens used to validate the CBFEM model include three rows of bolts as shown in Figure 3.6. At 20 and 450°C, the test specimens with three-bolt rows and 10 mm plate thickness failed due to the endplate fracture. At 550°C and 650°C, the bolt failure was observed with very ductile behaviour.

Table 3.5. Lists of the test specimens

Test Specimen	Plate thickness [mm]	Number of rows	Temperature [°C]	Nominal Load Angle [°]
Test 2	10	3	450	35
Test 3	10	3	550	35
Test 4	10	3	650	35
Test 6	10	3	450	45
Test 7	10	3	550	45
Test 8	10	3	650	45
Test 9	10	3	20	55
Test 10	10	3	450	55
Test 11	10	3	550	55
Test 12	10	3	650	55
Test 13	8	3	20	35
Test 14	8	3	550	35
Test 15	15	3	550	35

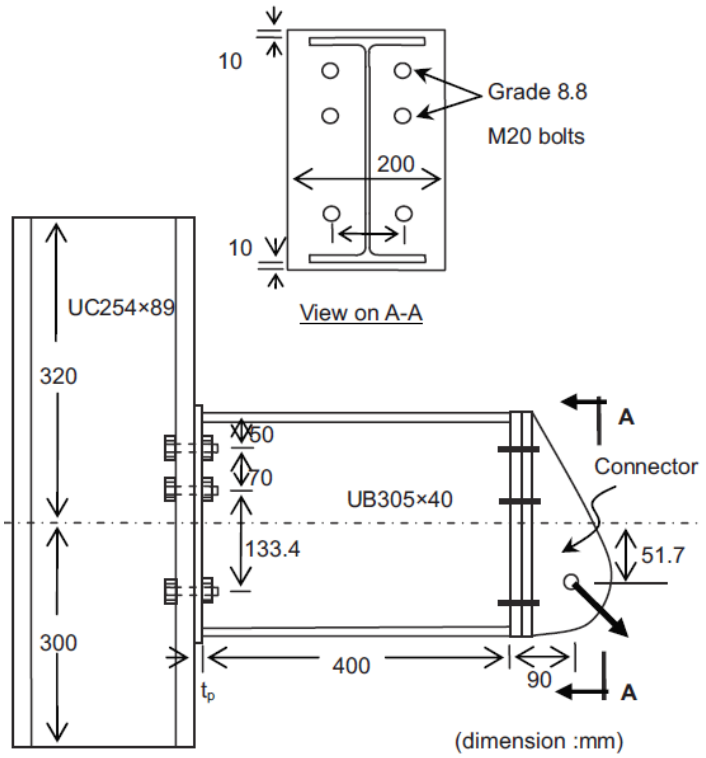

Figure 3.6. The geometry of the test specimen [38]

The nominal characteristics values of steel material properties are used to model the joints since the CBFEM is a design-oriented finite element model. This thesis aims to provide accurate and safe results to structural fire engineers at the design level; therefore, this experimental study will be used for validation of the CBFEM model in Section 5.3.5. The values for bolts are taken from the study [38]. Table 3.6 presents the material properties used in the CBFEM models to simulate Sheffield's test. The test results stated that flush end plate joints have relatively stiff responses compared to other simple connection types.

Table 3.6. Material properties used in Sheffield's test.

Parts	Elastic Modulus	Yield Strength	Ultimate Strength
	[MPa]	[MPa]	[MPa]
Beam	210000	275	430
Column	210000	355	490
Plate	210000	275	430
Bolts	206009	692	865

Yu et al. [39] reported 14 test results on typical fin plate joints subjected to combinations of shear and tying forces. All fin plates with M20 Grade 8.8 bolts failed by bolt shear fracture. The elevated temperature did not change the failure mode, whereas the resistance of the fin plate joints was significantly reduced. The experimental study [39] was performed at the University of Sheffield to investigate the behavior of fin plate joints when subjected to significant catenary forces. The tests were designed considering the following factors: the size of joints should fit the practical design; the joints should be subjected to the load combination of shear force and tensile force and the joints should be loaded till a fracture occurs. A flange of a UC 254×89 section column was connected to a UB 305×165×40 section sup-port-beam using a fin plate joint. The fin plate was 200 mm deep x 8 mm thick. Twelve fin-plate connection specimens with a single column of bolts were tested at different temperature levels as shown in Figure 3.7. All the bolts used were fully threaded. Ten specimens were performed using bolt grade 8.8. The bolt diameter was also varied with M20 and M24. Additionally, two specimens were tested with bolt grade 10.9 M20 at 20° and 550°C. At ambient temperature standard coupon tests were performed on the test specimens to determine their properties; however, the properties at elevated temperatures were not tested directly. The average tensile resistance of tested bolts was measured as 224 kN at ambient temperature. A standard tensile test specimen was conducted from the upper flange of the beam cross-section. The measured elastic modulus, yield strength, and ultimate strength were calculated as 176.35 kN/mm^2, 356 N/mm^2, and 502 N/mm^2. The CBFEM model which is generated by the author for modelling of fin plate joints will be validated by test results obtained from this study in Section 5.3.4.

First, the furnace was heated, and the temperature of the furnace was kept constant at the targeted temperature. Then, the specimens were loaded with a measured angle until failure. The study [39] determined two different angles: 35° and 55°. However, the measured initial angles were different than the nominal values. During the loading process, these angles changed. Table 3.7 indicates the initial and final angles, maximum forces, and failure mode for each test specimen. The failure modes of all the tests using Grade 8.8 M20 bolts were bolts in shear. At ambient temperature, visible plate bearing out of plate bending in beam web and fin plate were observed in addition to bolt in shear. The failure modes of test specimens with increased bolt diameter (M24) and higher bolt grade (10.9) were

similar. Significant bearing deformation occurred in the three bolt holes at room temperature. At elevated temperatures, the failure resulted from a bolt in shear with remarkable bearing deformations around the bolt holes.

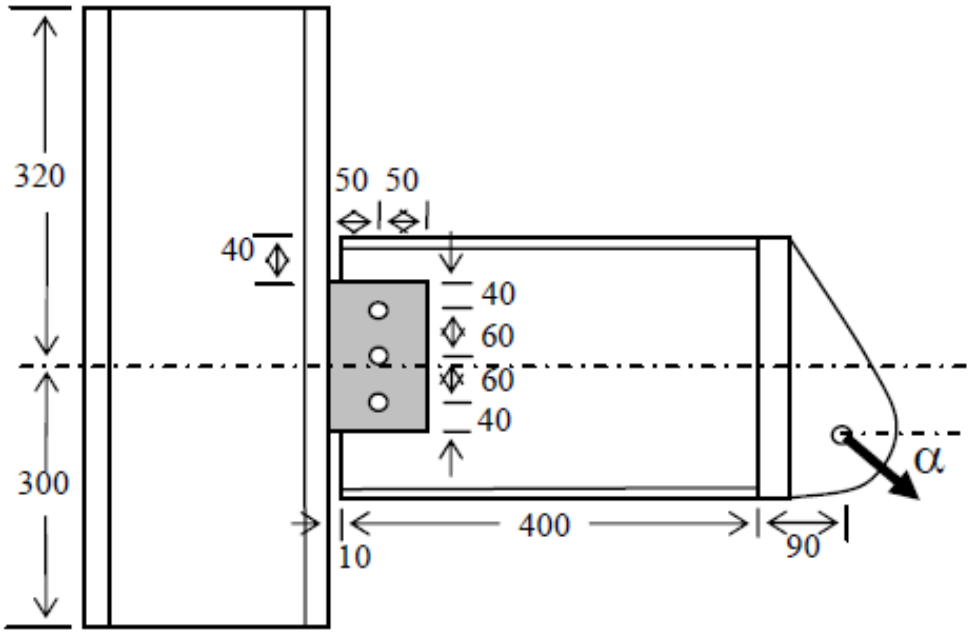

Figure 3.7. Test configuration for fin plate joint test [39]

Table 3.7. Test results for fin plate joint

Test Specimens	Initial angle (°)	Final angle (°)	Max. Force (kN)	Failure Modes
20-35	33.80	34.06	185.10	One bolt fracture and visible bearing
450-35	39.04	33.52	84.47	Bolt in shear
550-35	40.94	31.51	37.46	Bolt in shear
650-35	40.50	30.60	19.30	Bolt in shear
20-55	53.85	32.41	145.95	2 bolts in shear
450-55	51.47	41.37	70.48	Bolt in shear
550-55	53.44	42.68	34.81	Bolt in shear
650-55	53.09	44.02	17.99	Bolt in shear
20-M24	37.38	29.67	203.1	Bearing
550-M24	42.10	29.06	74.02	Bolt in shear
20-10.9	36.53	29.80	213.00	Bearing
550-10.9	40.85	23.90	56.82	Bolt in shear

Liu et al. [42] conducted experimental tests at the University of Manchester in order to investigate the effects of restraint on thermal expansion of unprotected beams, from protected columns and adjacent cooler beams. The test setup for the high-temperature test is displayed in Figure 3.8. The main focus of this experimental work was investigating the influence of different connection types on the failure temperature of the connected members at different load levels. The results from the Cardington full-scale frame fire tests were used to complement the experimental work. These tests included flush endplate and web cleat joints, coupled with three levels of loading (20%, 50%, and 70% of the moment capacity of the beam) and three degrees of horizontal restraint (8 kN/m; 35 kN/m and 62 kN/m).

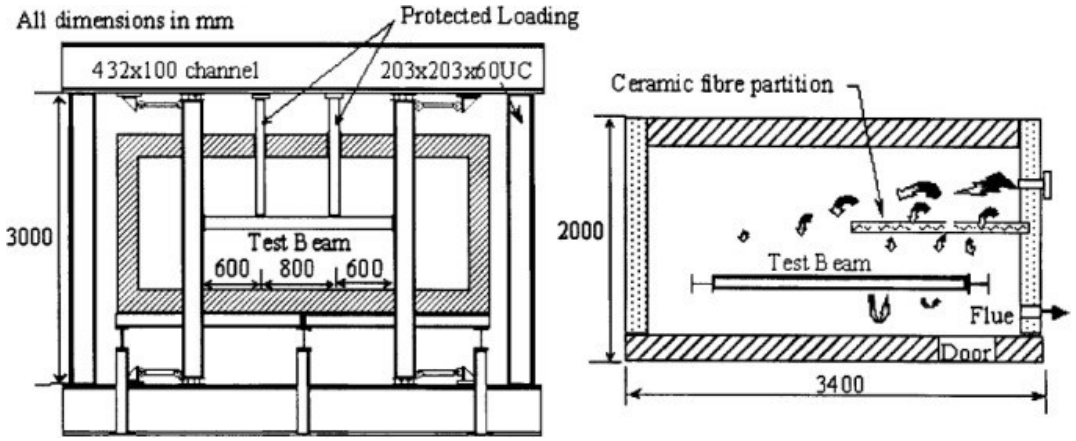

Figure 3.8. (a) High temperature test, (b) Section through furnace [42]

It was observed that web-cleat joints had very little influence on the behaviour of the beam until the beam came into contact with the column and was able to transfer a much less bending moment to the column than the flush end-plate joints. Qian et al. [43] tested the mechanical response of six internal extended end-plate joints at temperatures between 400°C and 700°C. These tests aimed at obtaining the moment- rotation-temperature characteristics under these isothermal conditions and providing beam web in shear as the main failure mode. It was noticed that axial restraint force has a significant effect on steel joint moment capacity. Santiago [44] performed experimental and numerical studies of six steel subframes exposed to natural fire conditions. The aim of this study was the investigation of investigate joint behaviour under combined bending moment and the axial force developed during a natural fire. The study focused on three types of connection: header plate, flush endplate, and extended endplate. Wang et al. [45] performed ten fire tests on medium-scale restrained steel subframes to investigate the relative behaviour and robustness of different types of steel joints in steel frames, as indicated in Figure 3.9. The studied joint types are fin plate, web cleat, flush endplate, flexible endplate, and extended endplate joints. structures in fire. The top flange of the beam was protected to consider the effect of the concrete slabs. The column ends were restrained to study the influences of axial restraint on the beam and the joints. Very large deflections were observed in the medium-scale steel beams without failure. The best performance was obtained from the web cleat joint. Khonsari et al. [46] carried out a three-dimensional frame in order to investigate the behaviour of bare steel flush end-plate joints with relatively low thicknesses at elevated temperatures. The main observed failure modes included weld fracture, bolt rupture, thread stripping, lateral-torsional buckling of the beams, local buckling of the beam flanges, and finally large inelastic deformation of the endplates.

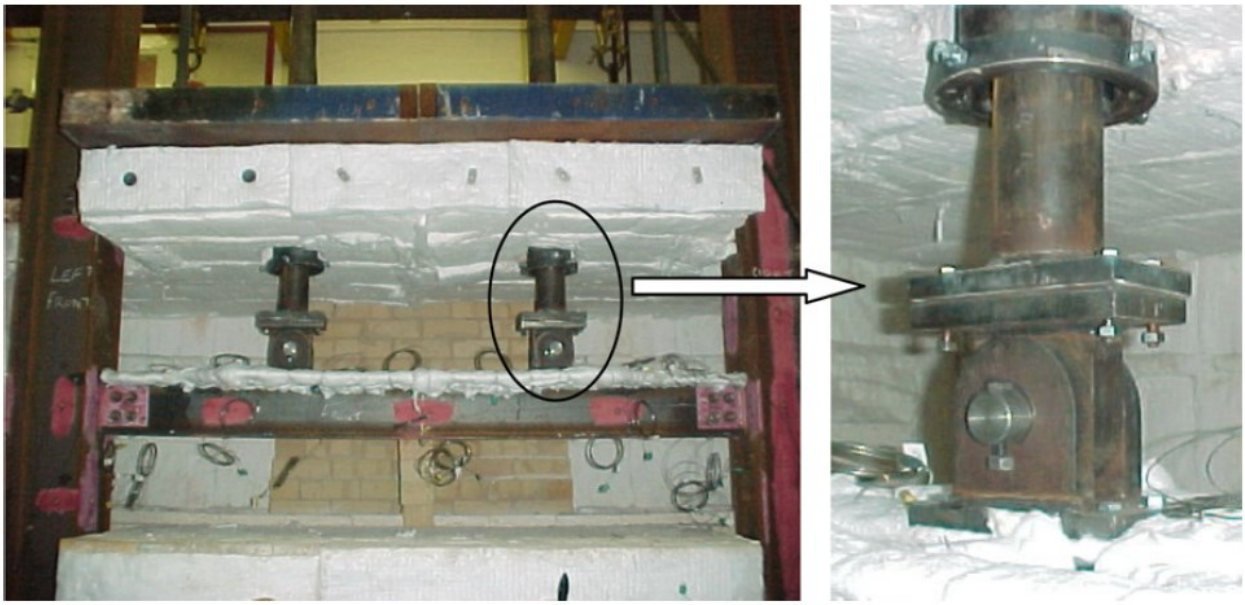

Figure 3.9. Test setup [45]

A series of experimental tests on the welded T-stub component at ambient and elevated temperatures were carried out by Barata et al [47]. The deformation capacity of the bolts indicated a significant increase with the temperature, T-stubs with bolt failure also presented a large deformation capacity. Barata et. al [47] study experimentally the behaviour of the welded T-stub specimen exposed to static loading, at ambient and elevated temperatures The study includes T-stub specimens with three different thicknesses of flange (t_f= 10 mm, 15 mm, and 20 mm) at 20°C, 500°C, and 600°C. M20 bolts, grade 8.8 was used to fasten T-stub specimens with the flanges (t_f= 10 mm and 15 mm), while the 20 mm flange was connected using M24, grade 10.9 bolts.

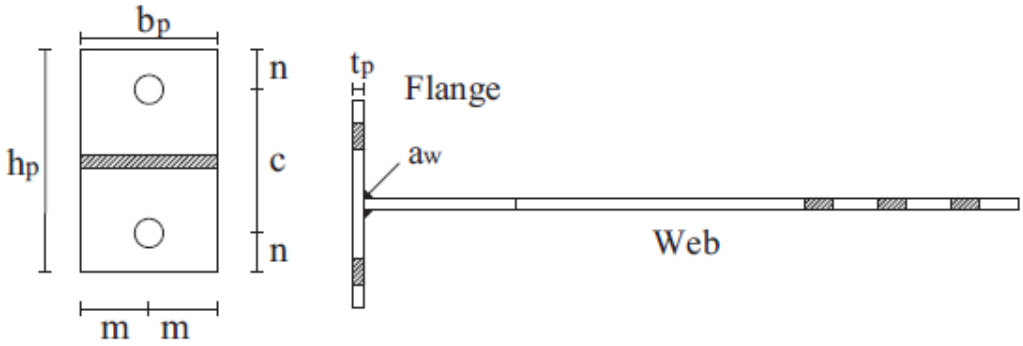

Figure 3.10. Details of the T-stub specimens [47]

The measured elastic modulus, yield strength, and ultimate strength values for the flanges are 205,500 MPa, 385 MPa, and 588 MPa, respectively. The measured modulus of elasticity for the M20 bolts, grade 8.8, and for the M24 bolts, 10.9 are 202,500 MPa and 195,050 MPa, respectively. The yield strength and the ultimate strength of grade 8.8 were measured as f_y is 684 MPa; f_u is 1002 MPa. For bolt grade 10.9, 942 MPa and 1293 MPa are values for the yield strength and the ultimate strength. The 20 mm flange is fastened using M24 bolts with a grade of 10.9, while the flanges with 10 mm and 15 mm thickness are bolted with M20 bolts of grade 8.8. The author of this thesis numerically extended the number of tested studies to perform parametric studies in Section 5.3.3. Therefore, specimens entitled by PS were added to Table 3.8. In the parametric studies, the bolt diameter is decreased to M16 for the specimen PS-1 using the flange with 15 mm thickness. The PS-2 investigated the effect of the value of m on the behaviour of T-stubs with 20 mm thick flange. The

width of the flange is increased to 200 mm in the specimen PS-3. Parametric studies were performed at 500°C and 600°C. Table 3.8 summarizes the geometrical dimensions of the T-stub specimens used in the verification study. All dimensions presented in Table 3.8 are in mm.

Table 3.8. Nominal dimension values for geometrical characteristics of T-stub specimens.

Specimen	t_p	b_p	h_p	c	n	m
FL-10	10	105	170	110	30	52.5
FL-15	15	105	170	110	30	52.5
FL-20	20	105	185	120	32.5	52.5
PS-1	15	105	170	110	30	52.5
PS-2	20	125	185	120	32.5	62.5
PS-3	10	105	200	120	40	52.5

You et al. [48] performed an experimental study to investigate the tensile behaviour of T-stubs connected by Thread-fixed One-side Bolts (TOB) at ambient and elevated temperatures. The study indicated that the ductility of the connection increases, initial stiffness, and the tension strength of TOB bolted T-stubs decrease with the elevation of temperature. Hole thread failure was not observed during the test.

Jiang et al [49] performed experimental and numerical studies to predict the resistance of S700 high-strength steel double-shear bolted joints subjected to tension at ambient temperature. In this thesis, the test specimens each containing two bolts arranged parallel to the load transfer direction were used to validate the numerical models. The inner and outer plates were both made of S700MC high-strength steel and grade 12.9 high-strength M22 was used to connect the inner and outer plates. Table 3.9 presents the measured geometric dimensions of the inner plates of each S700 high-strength steel double-shear bolted connection specimen. This study will be used to validate the proposed solid model at ambient temperature in Section 5.1.5.

Table 3.9. The measured geometrical characteristics

Specimen	b [mm]	d_0 [mm]	e_1 [mm]	e_2 [mm]	p_1 [mm]	t [mm]	Failure mode
pa-03	57.6	23.8	59.1	28.8	52,7	6	Net section
pa-04	119.9	23.9	28	59.8	71.9	6	Bearing
pa-05	119.4	23.6	34.9	59.7	71.9	6	Bearing
pa-06	121	23.8	46.9	60.5	71.9	5.9	Bearing
pa-07	119.1	23.8	35.3	59.6	60.2	6	Bearing
pa-08	120.5	23.8	35.3	60.3	52.9	6	Bearing

3.3.2. Experimental studies on steel members at elevated temperatures

In the fire, stiffness and strength of steel members have significant reductions at elevated temperatures, leading to a decrease in the ultimate load capacity. EN 1993-1-2 [10] suggests that the design of isolated steel members exposed to fire assuming a uniform temperature in the cross-section considering the mechanical properties of steel at elevated temperatures can be analysed using simplified analytical methods. Experimental investigation is the most accurate way to calculate the fire resistance of steel members. Mesquita et al. conducted a set of fifteen experimental full-scale tests using IPE 100 beams. Fork supports were used to simulate a simple supported beam. The critical temperature was measured for several laterally unrestrained beams and results depicted that Eurocode formulae may lead to conservative results. Dong and Li [50] investigated the behaviours of 14 H-section steel beams in the fire. The influence of connection, boundary condition, and axial restraint on the behaviours of steel beams was also studied. The test results showed that local buckling and lateral torsional buckling of H-section steel beams occur in a fire. Dharma and Tan [51] performed an extensive experimental programme to investigate the rotational capacity of steel I-beams under fire conditions. The results showed a considerable reduction in the rotational capacity at elevated temperatures. Ramesh et al. [52] presented an experimental response of unprotected W16 × 26 steel beams subjected to localized fire. Beam specimens were either simply supported or connected to steel columns via all bolted double-angle joints. The measured outputs were thermal and structural responses of the steel beams, the heat release rate, and applied loads. All specimens failed by lateral-torsional buckling regardless of fire loading and end support conditions. Wozniczka [53] presented the results of experimental research on lateral-torsional buckling of steel plate girders with slender webs exposed to fire conditions.

A simply supported beam as shown in Figure 3.11, was tested by Torić et al. [54]. The studies were created on the basis of several fire experiments previously carried out by the University of Split. Details regarding the experiments conducted can be found in the literature [55] and this study will be utilized to validate the shell model generated in Abaqus in Section 5.2. The experimental program, as indicated in Figure 3.11, included heating steel beams with a span of 2,5 m by applying transient heating and subsequently loading them in different ways (flexure and flexure combined with axial compression). Mechanical properties of the steel S355 were determined experimentally with the following values: $f_{y,20°C} = 362.4$ MPa and $E_{y,20°C} = 209\ GPa$ where $f_{y,20°C}$ is the yield strength at 20°C and $E_{y,20°C}$ is the modulus of elasticity at 20°C. Table 3.10 presents testing parameters and results for tested steel beams. Figure 3.12 illustrates the temperature distribution in each part of the heated steel beams.

Table 3.10. Testing parameters for steel beams

Testing method		Transient	
Load type		Flexure	Flexure + axial force
Member (Steel S355)		Test 1	Test 3
Test time (min)		115	190
Force (kN)	Axial	-	400
	Vertical	200	200

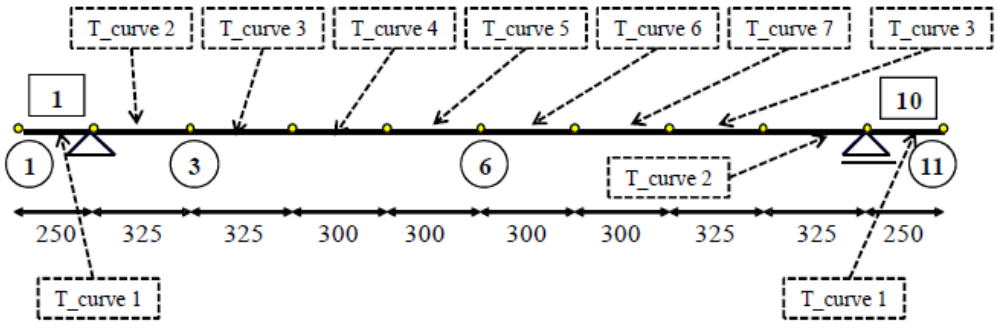

Figure 3.11. Discretization scheme for partially heated steel beam [54]

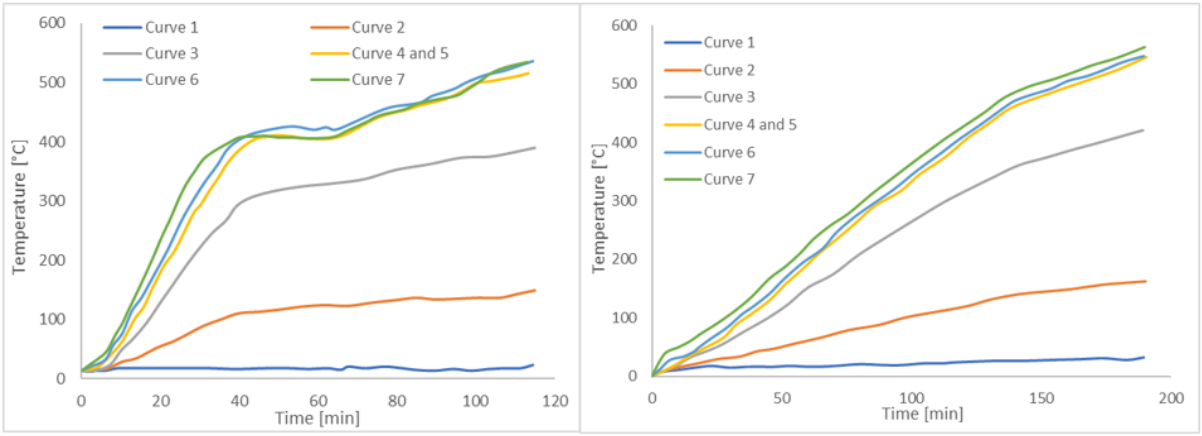

Figure 3.12. Heating history in parts of the beam

Large deformations may lead to local and global buckling of a steel column due to a mechanical load applied to the element. The reduction in strength and stiffness and the nonlinear stress-strain relationship of carbon steel at elevated temperatures results in a much lower resistance of the steel section than at ambient temperature. Therefore, the risk of buckling is much higher at elevated than at ambient temperatures. Choe [56] performed experimental tests to investigate the structural-thermal response of A992 wide flange steel columns subjected to axial loads and elevated temperatures. Yang and Hsu [57] conducted a series of experimental studies to examine the behaviour of SN490 steel columns subjected to axial load in the fire condition. The study factors were the width-to-thickness ratio of flanges, the slenderness ratio of steel columns, and residual stresses. It was observed the failure mode of steel columns changes from inelastic global buckling at room temperature to inelastic local buckling at elevated temperature. Pauli et al. [58] reported results of comprehensive fire tests, with regard to material behaviour and cross-sectional capacity as well as fire tests on slender columns and beam-columns, covering important aspects of the structural resistance of steel members in the fire. Wang et al. [59] investigated the behaviour of restrained high-strength steel columns at elevated temperatures obtained from full-scale fire tests. The obtained failure modes of steel columns from fire tests are shown in Figure 3.13. Wang et al. [60] tested six high-strength Q460 steel columns with welded H shape to determine the creep buckling strength at elevated temperatures. The effects of the slenderness ratio, load ratio, and elevated temperature on failure time corresponding to creep buckling were investigated.

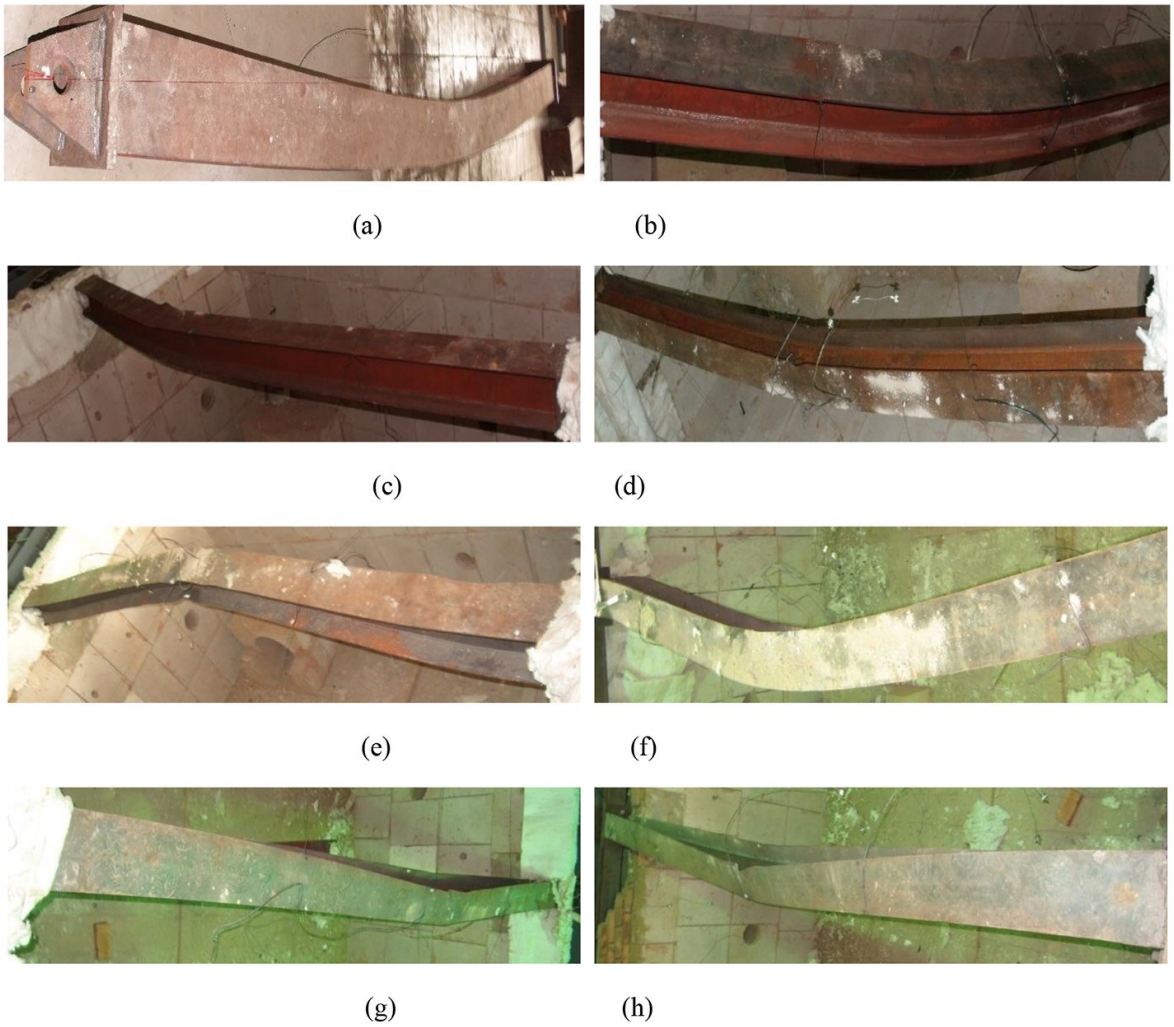

Figure 3.13. Failure modes in test specimens [59]

3.3.3. Experimental studies on complete building structures and observation of real fire even

A complete structure also includes floor slabs, walls and other non-structural members in addition to the structural members. Although extremely expensive, fire tests on complete buildings are essential in order to understand the response of a complete building in fire. The Broadgate fire accident [61] and the Cardington full-scale fire tests [62] are the most comprehensive tests to predict the structural behaviour of a complete building at elevated temperatures. Six full-scale fire tests were conducted inside the building at various locations, as shown in Figure 3.14, during 1995 and 1996. These tests have been well documented in these studies [63][64]. The fire event at the World Trade Center, NY [65] was a catastrophe to see the connection failure under elevated temperatures in real life. Orabi et al. [66] revisited the collapse of WTC7 and its investigation and then explored the hypothesis that a potential hydrocarbon fire may have compromised the large transfer structure within the mechanical space of the building. The fire tests in the Cardington laboratory [67] showed that during the heating phase of a fire, the temperature of the joints is lower compared to the beam. In the cooling phase of the fire, the temperature of the joints is higher. That is, joints cooled more slowly than the beams. The shear tabs had higher temperatures compared to the bolts, and the temperature of lower bolts was higher than upper ones. The elongations of the holes in the beam webs and shear tabs due to the associated large connection rotations were observed in the tests. Wang [68] presented the results of an analysis of the global structural behaviour of the 8-storey steel framed building at Cardington during the two BRE large-scale fire tests. These tests were performed to study the behaviour of whole

building structures under realistic fire conditions and to provide accurate test results to validate numerical models. Dong et al [69] conducted some full-scale fire experiments of steel composite frames under furnace loading. The tests showed that the fire-resistance design of structures may not be based on the performance of single separated elements in tests only. Interactions between members in a whole structure need to be considered.

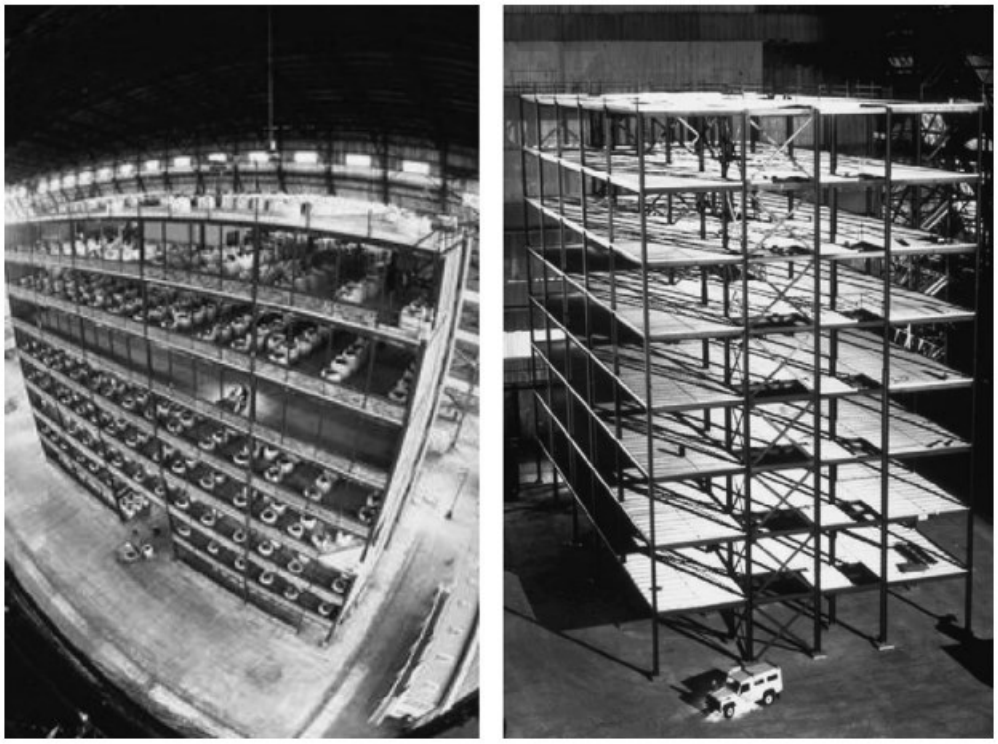

Figure 3.14. The eight-storey building at the Cardington Laboratory [68]**.**

3.4. Modelling of steel joints at elevated temperatures

Joints may be generally exposed to different forces, including moments, shear forces and axial forces, due to the interactions between them and adjacent structure members. Therefore, the mechanical behaviour of joint can be characterized by rotational stiffness (the initial stiffness of its moment-rotation curve), strength, and rotation capacity. Experimental fire tests are quite expensive to represent the behaviour of different types of joints.

In general, the moment-rotation curve can be characterized by six different simulation methods:

- simplified analytical method,
- mathematical expressions – curve-fit method,
- mechanical model – the component method,
- finite element method
- component-based finite element method
- artificial neural network (ANN) method

Finite element methods, component methods, and component-based finite element methods are mentioned in this study.

3.4.1. Component Methods

The logic behind the component method is decomposing a joint into compression, tension, and shear zones. Several basic components are used to describe the behaviour of each zone. The overall joint behaviour can be calculated by assembling the contributions of individual joint components which are

represented by rigid links and translational springs with the nonlinear force-displacement response, either in parallel or series where appropriate. The component-based method is also known as the spring-stiffness method. For end-plate connection, the component method is an assembly of spring elements in the tension, compression, and shear zones as shown in Figure 3.15.

The application of the component-based method requires the following three steps [70]:

(1) Identification of the active components within the joints;

(2) Evaluation of the stiffness and resistance characteristics for each basic component;

(3) Assembly of all the basic components to evaluate the overall stiffness and resistance characteristics of the whole connection.

The component-based method has been standardized to analyse semi-rigid joints at ambient temperatures in EN 1993-1-8 [12]. Eurocode 3 Part 1.8 lists different joint components with stiffness and strength based on the literature review. For a bolted extended end-plate joint under a simple bending moment, the active joint components according the EN 1993-1- 8 are column web in shear (cws); column web in compression (cwc); column web in tension (cwt); column flange in bending (cfb); end-plate in bending (epb); bolts in tension (bt); weld (w); beam web and flange in compression (bwc, bfc) and beam web in tension (bwt). Eurocode considers the effect of temperature on the components reducing the material properties by the reduction factors in EN 1993-1-2 [10].

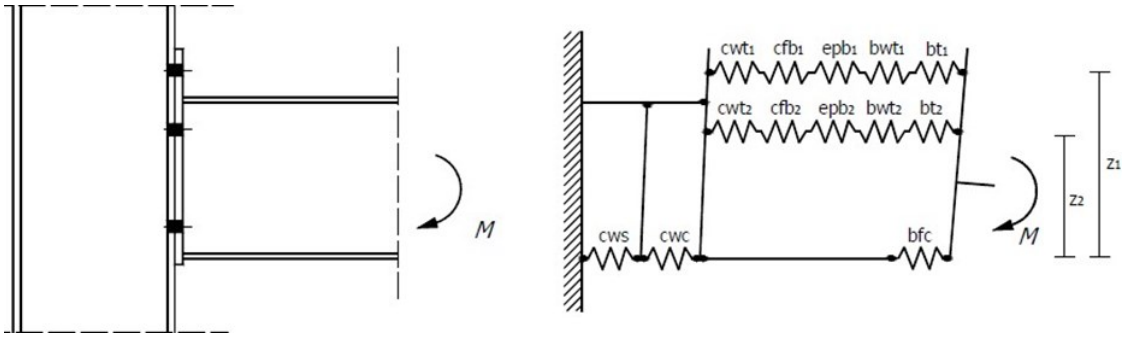

Figure 3.15. Component model of an extended end-plate joint adopted by EN 1993-1-8 [12]

$$M_{j,Rd} = F_{Rd} z \tag{9}$$

Leston-Jones [34] developed an elevated temperature component model to predict the response of bare-steel and composite flush end-plates joints with two bolt rows. In this model, the basic components are the column flange in bending, the bolts in tension, the end- plate in bending and the column web in compression, as seen in Figure 3.16. The validation results show good agreements with experimental data [34]. The validation results showed good agreements with experimental data.

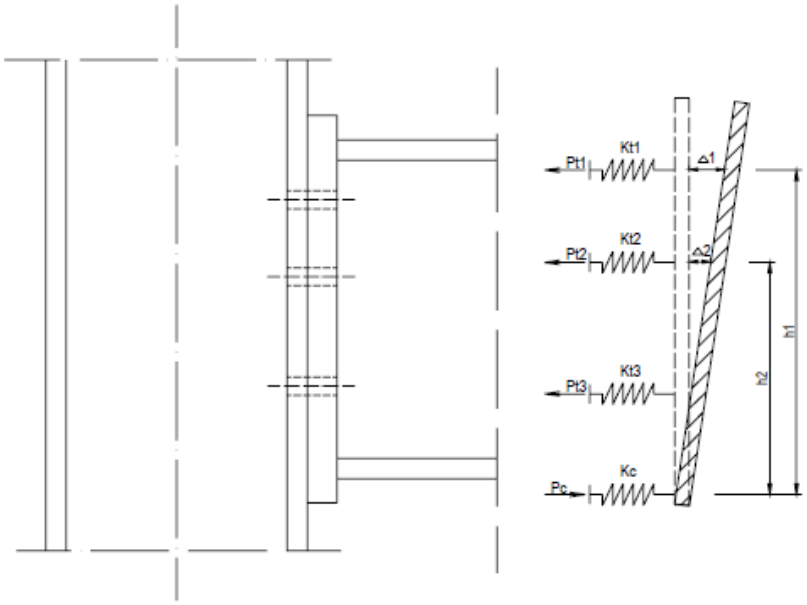

Figure 3.16. Idealized Spring Stiffness Model for Bare-Steel Flush End-plate Joint [34]

Al-Jabri [31] extended the work of Leston-Jones [34] to model the fire response of bare-steel and composite flexible end-plate joints. The active components in this model were chosen as bolts, column flange endplate in tension zone, and column web panel in compression zone.

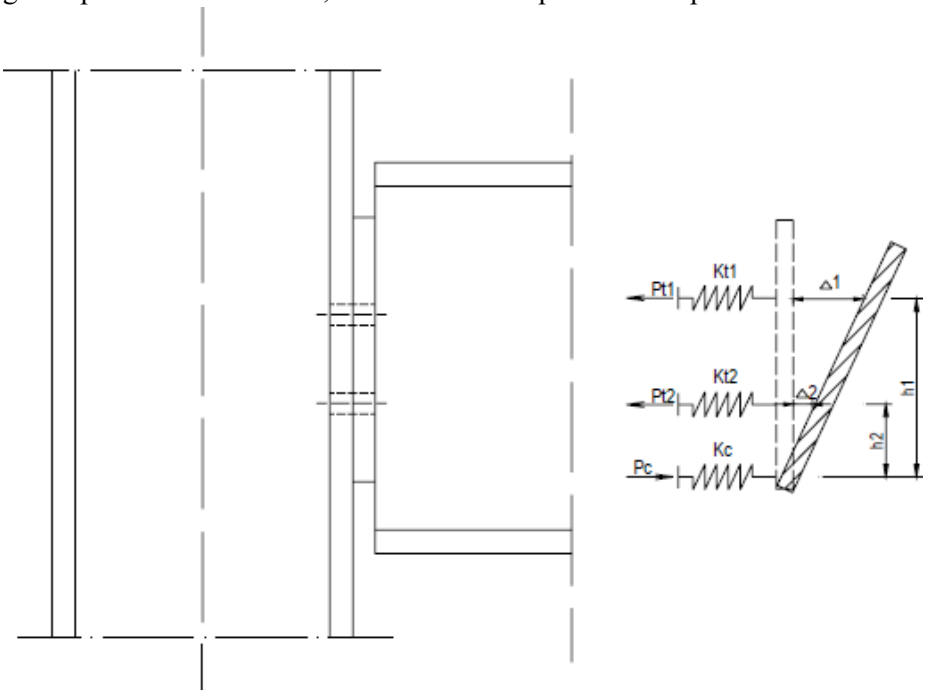

Figure 3.17. General Spring Model for Flexible Endplate Joint [31]

Simoes da Silva et al. [71] aimed at extending the component method to evaluate the fire response of steel joints. Therefore, they suggested an analytical procedure to predict the moment-rotation behaviour including the variation of yield stress and elastic modulus of the various components with increasing temperature. temperatures. The model was validated based on the fire tests conducted on flush end-plate joints by Al-Jabri [31]. A component-based method was developed by Spyrou [72] in order to investigate the behaviour of components within the tension and compression zones of flush end-plate joint at ambient and elevated temperatures. The active components required to represent a real end plate joint were the endplate in bending, column

flange in bending, bolts intension, and column web in compression. Block et al. [73] developed a component-based element for end-plate joints in fire topredict the moment-rotation curves of connection experiments at ambient and elevated temperatures, as seen in Figure 3.18. Their study expresses the derivation of the stiffness matrix of this new elementand the integration of the element into the non-linear finite element program Vulcan. The missing components in the presented connection element are group effects in the bolt rows, shear deformation in the column-web, shear deformation in the beam-end zone, local buckling of the bottom flange of the beam and bolt behaviour during cooling. The new element is able to combine the component method with detailed connection behaviour overall.

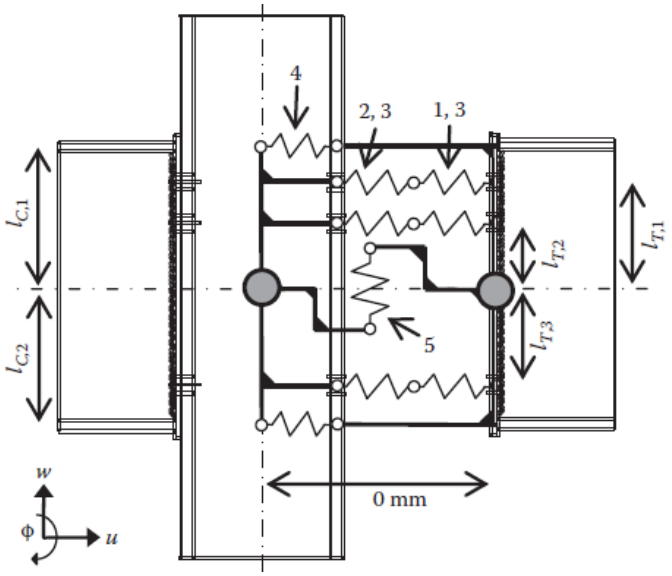

Figure 3.18. Block component method [73]

Sarraj et al. [74] utilized the component-based method to depict the behaviour and robustness of steel fin plate joints subjected to elevated temperatures and proposed a simplified mechanical model consisting of three components: plate bearing, bolt shearing, and web-to- plate friction. Wang et al. [75] developed a component-based model to predict the behaviour of extended end-plate joints under fire conditions. They investigated the effect of rib stiffener and thickness of theendplate on the fire resistance of the connection. Santiago [76] developed a general model divided into four partial models for flush endplate and extended end-plate joints. Each partial model is valid for a combination of axial force (tension or compression) and bending moment (hogging or bending). Taib [77] developed a component-based model to focus on the behaviour of fin-plate joints under fire conditions. Quan et al. [78] generated a component-based model of the buckling zone. The proposed model considered both beam-web shear buckling and bottom-flange buckling. The proposed model provided a reasonably accurate and conservative prediction of the force–deflection relationship for Class 1 and 2 beams.

The main components in the bolted end-plate connection can be represented using equivalent T-stubs [12] which have been traditionally applied to represent the components in the tension zone. Therefore, the end-plate connection can be regarded as an assembly of the column flange T-stub and the end-plate T-stub. Previous research indicates three different failure modes [72] for a T-stub assembly, depending on the ratio between the resistance of the flange and the resistance of the bolts. T-stub assemblies can fail according to the three possible failure modes;

1. Yielding in the T-stub flange, followed by yielding and fracture of the bolts,
2. A complete yield mechanism in the T-stub flange
3. The T-stub flange remains elastic until the fracture of the bolts

The T-stub model is a good, simplified model to simulate the response of the tension zone of

bolted joints, which has a significant contribution to the deformability of the whole joint. The equivalent T-stubs represent two T-shaped connected through the flanges by means of one or more bolt rows. Figure 3.19 shows the possible failure modes of a T-stub specimen.

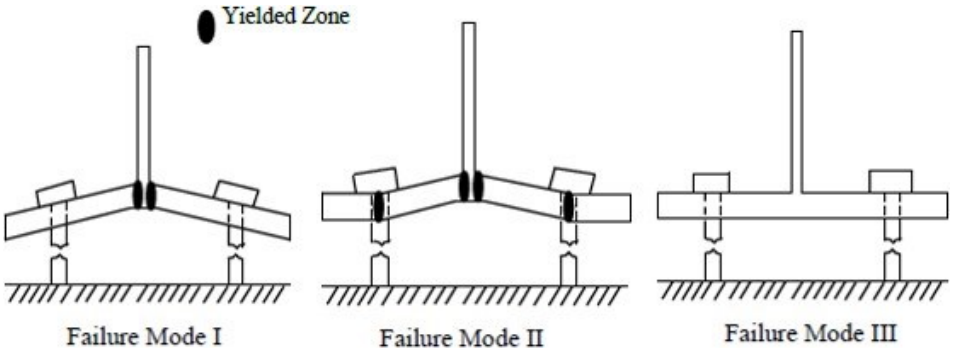

Figure 3.19. Three failure mechanisms of a T-stub

The generated CBFEM models in this thesis will be verified using the analytical formulas proposed in EN 1993-1-8 [12] in Section 5.3. EN 1993-1-8 provides design equations for calculating the shear resistance of a bolt per shear plane as follows:

$$F_{v,Rd} = \frac{\alpha_v f_{ub} A}{\gamma_{M2}} \tag{14}$$

where f_{ub} is the ultimate bolt material strengths, A is the nominal unthreaded or threaded body areas of the bolt and α_v is a coefficient dependent on bolt class — for classes 4.6, 5.6 and 8.8 it is equal to 0.6 and for classes 4.8, 5.8, 6.8 and 10.9 it is equal to .5. EN 1993-1-8 defines the bearing resistance per bolt as follows:

$$F_{b,Rd} = \frac{k_1 \alpha_b f_u d t}{\gamma_{M2}} \tag{15}$$

where d is the nominal bolt diameter, f_u is nominal ultimate tensile strength of the plate, t is the thickness of connected material and γ_{M2} is the partial factor with the recommended value of 1.25. Parameters α_b and k_1 are determined considering mainly geometrical parameters as given below: perpendicular to the direction of load transfer for edge and inner bolts, respectively

$$k_1 = min\left(2.8\frac{e_2}{d_0} - 1.7; 1.4\frac{p_2}{d_0} - 1.7; 2.5\right) \tag{16}$$
$$k_1 = min\left(1.4\frac{p_2}{d_0} - 1.7; 2.5\right)$$

- in the direction of load transfer

$$\alpha_b = min\left(\alpha_d; \frac{f_{ub}}{f_u}; 1\right) \tag{17}$$
$$\alpha_d = \frac{e_1}{3d_0}\ for\ end\ bolts$$
$$\alpha_d = \frac{p_1}{3d_0} - 0.25\ for\ inner\ bolts$$

where d_0 is the diameter of the bolt hole, f_{ub} is the ultimate strength of the bolt, f_{up} is the ultimate strength of the plate, e_1 is end distance, e_2 is edge distance. The material safety factor of 1.25 is removed to compare the ultimate resistances. Parameters α_b and k_1 are determined considering mainly geometrical parameters which are explained in EN 1993-1-8 [12]. For the design resistance of bolts at elevated temperatures, the term f_{ub}/γ_M should be replaced by $k_{b,\theta}f_u/\gamma_{fi}$. In all cases, γ_{fi} is a national determined parameter with a recommended value γ_{fi}=1.0 in EN 1993-1-2 [10]. Eurocode 3-1-2 recommends the same strength reduction factors for for tension and shear loading of bolts at elevated temperatures up to 1000°C. The fire design resistance of bolts loaded in shear should be determined from:

$$F_{v,t,Rd} = F_{v,Rd} k_{b,\theta} \frac{\gamma_{M2}}{\gamma_{M,fi}} \quad (18)$$

$k_{b,\theta}$ is the reduction factor determined for the appropriate bolt temperature from Table D.1;
$\gamma_{M,fi}$ is the partial factor for fire conditions.
The design bearing resistance of bolts in fire should be determined from:

$$F_{b,t,Rd} = F_{b,Rd} k_{b,\theta} \frac{\gamma_{M2}}{\gamma_{M,fi}} \quad (19)$$

$k_{b,\theta}$ is the reduction factor determined for the appropriate bolt temperature from Table D.1.
The tension strength of bolted T-stubs failed by flange yielding at elevated temperatures could be calculated as follows:

$$F_{T,1,Rd,\theta} = \frac{4M_{pl,1,Rd,\theta}}{m} \quad (22)$$

$$M_{pl,1,Rd,\theta} = 0.25 \sum l_{eff,1}\, t_f^2 f_{y,\theta} / \gamma_{M0}$$

where $\gamma_{M0} = 1.0$ is the partial factor provided by Eurocode, $f_{y,\theta}$ is the yield strength of T-stub flange at high temperature θ. $M_{pl,1,Rd,\theta}$ is the bending strength of T-stub flange at high temperature θ. $l_{eff,1}$ is the total length of the yielding line of the T-stub. EN 1993-1-8 provides equations to calculate the tension strength of the bolted T-stub fails by flange yielding accompanied with bolt failure at ambient temperatures.

$$F_{T,2,Rd,\theta} = \frac{2M_{pl,2,Rd,\theta} + n \sum F_{T,Rd,\theta}}{m+n} \quad (23)$$

$$M_{pl,2,Rd,\theta} = 0.25 \sum l_{eff,2}\, t_f^2 f_{y,\theta} / \gamma_{M0}$$

$$F_{T,Rd,\theta} = \frac{k_2 f_{ub,,\theta} A_s}{\gamma_{M2}}$$

where e is the distance between axis of bolt hole and edge of T-stub flange, l_{eff} is the total length of the yielding line of T-stubs, $f_{ub,,\theta}$ is the ultimate tensile strength of bolt at high temperature θ, $M_{pl,2,Rd,\theta}$ is the bending strength of T-stub flange at high temperature θ. A_s is the effective cross section area of a bolt, the coefficients $\gamma_{M2} = 1.25$ and $k_2 = 0.9$ are provide by Eurocode.

$$l_{eff,1,2} = \min (l_{eff,cp}, l_{eff,np}, l_{eff,bp}) \quad (24)$$

$l_{eff,cp} = 2\pi m$ circular pattern

$l_{eff,np} = 4m + 1.25n$ non-circular pattern

$l_{eff,bp} = b$ beam pattern

The tension strength of bolt failure at elevated temperatures could be calculated by

$$F_{T,3,Rd,\theta} = \sum F_{T,Rd,\theta} \quad (25)$$

where $F_{T,Rd,\theta}$ is the tension resistance of bolts at temperature θ.
The design resistance per unit length of a fillet weld in fire should be determined from:

$$F_{w,t,Rd} = F_{w,Rd} k_{w,\theta} \frac{\gamma_{M2}}{\gamma_{M,fi}} \quad (26)$$

where $k_{w,\theta}$ is obtained from Table D.1 for the appropriate weld temperature; $F_{w,Rd}$ is determined from clause 4.5.3.3 in EN 1993-1-8 [12]. The design tension resistance of an individual bolt in fire should be determined from the following equation:

$$F_{ten,t,Rd} = F_{t,Rd} k_{b,\theta} \frac{\gamma_{M2}}{\gamma_{M,fi}} \quad (27)$$

where $F_{t,Rd}$ is the design bearing resistance at room temperature, determined from Table 3.4 of EN 1993-1-8. EN 1993-1-5 [13] recommends a 5% limit strain for the failure of plates at ambient temperature.

3.4.2. Finite Element Method

For several decades great effort has been devoted to the study of the modelling of steel joints using finite element models. The finite element method is a powerful tool, which is able to accurately predict the mechanical behaviour of joints. The finite element method is capable of dealing with nonlinear material properties, large deformations, and interactions between bolts and plates. The important parameters affecting the accuracy of finite element modelling are the optimum mesh size, simulation of bolts, choice of elements, material behaviour, and most importantly modelling of the contact and gap elements [79].

Numerical modelling of joints at elevated temperature is an alternative to experimental testing in order to investigate joint behaviour. There are several ways to model bolted and welded joints using finite element methods. The plates can be modelled using solid and shell elements. Bolts are a more complex part of modelling of bolted connection. In previous studies, many methods were proposed by several authors. Spyrou [72], [80] adopted a finite element model to predict the joint behaviour under high temperatures by modelling the elements as 3D T-stubs. Al-Jabri et al. [80] modelled steel flush endplate joints in fire to generate their moment-rotation characteristics. Sarraj et al. [74] simulated the behaviour of fin-plate joints at elevated temperatures. Selamet and Garlock [81] investigated the behaviour of three types of shear joints (single-plate, single-angle, and double-angle joints) under fire conditions. Gernay and Franssen [82] performed a numerical study using SAFIR to indicate the influence of semi-rigid joints on the global structural response at elevated temperatures. The important point in modelling connection using a finite element model is how to simulate the behaviour of connectors (bolts and welds). There are several ways to model bolts and welds using finite element models.

Modelling of Bolts in FEM

There are different methods to model bolted joints in FE, e.g. the plates can be modelled with solid elements or shell elements. Solid models are very time-consuming and expensive and therefore the shell models are good alternative. Bolts can be modelled by using a point-to- point connection, which means the fastener element is a link between two nodes. The following ways are used to present bolts in Abaqus:

- Beam elements
- Connector elements
- Rigid elements
- Solid elements
- Spring elements

In this study, solid and spring elements will be studied. Bursi and Jaspart [83] discussed the modelling of bolts in bolted joints at ambient temperature using the general commercial program ABAQUS. A “spin” model uses beam elements to simulate bolts. The proposed model is illustrated in Figure 3.20. This was verified against 3D solid models for simple problems such as T -stubs, and then used in more complicated endplate joints.

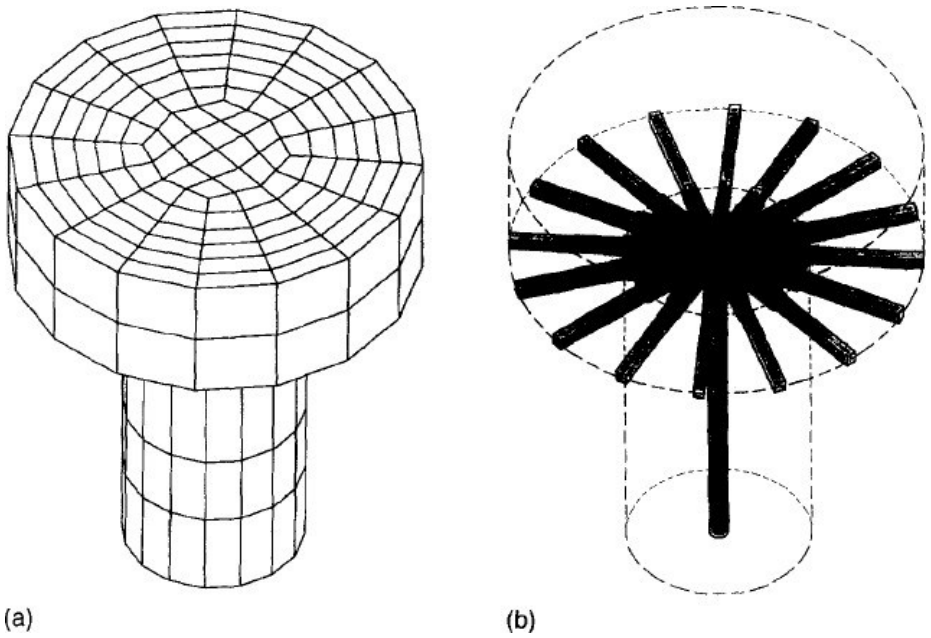

Figure 3.20. Modelling of bolt performed by [83]**: (a) solid model; (b) spin model.**

Using structural shell elements in finite element analyses saves computational time compared to the solid models. Kim et al. [84] introduced four kinds of finite element models, which are a solid bolt model, a coupled bolt model, a spider bolt model, and a no-bolt model, to investigate a modelling technique of the structure with bolted joints, as shown in Figure 3.21. All the proposed models take into account pretension effect and contact behaviour between flanges to be joined. Among these models, the solid bolt model, which is modelled by using 3D solid elements and surface-to- surface contact elements between head/nut and the flange interfaces, provides the best accurate responses compared with the experimental results.

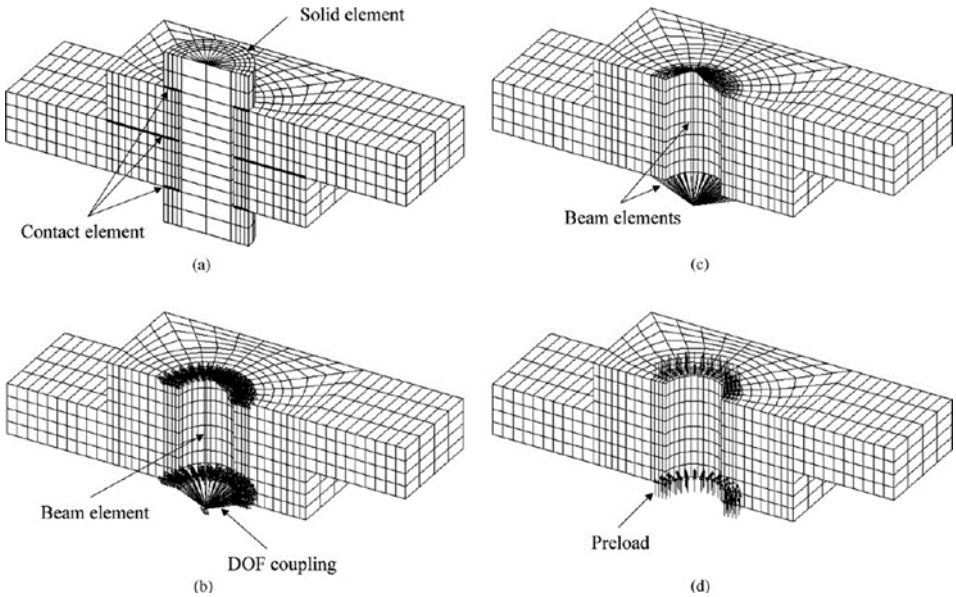

Figure 3.21. Finite element models for bolted joints proposed by [84]**. (a) Solid bolt model, (b) coupled bolt model, (c) spider bolt model and (d) no-bolt model.**

Rutman et al. [85] developed simplified bolt models using beam, spring, and gap elements with any combination of shell or solid elements. The studies highlighted that numerical calculations can be

used to replace analytical models by engineers at the design level of structural fire engineering. Gödrich et al [86] developed the numerical model using solid element based the model by Wu et al. [87] and beam element. The solid and simplified numerical model using beam elements are shown in Figure 3.22.

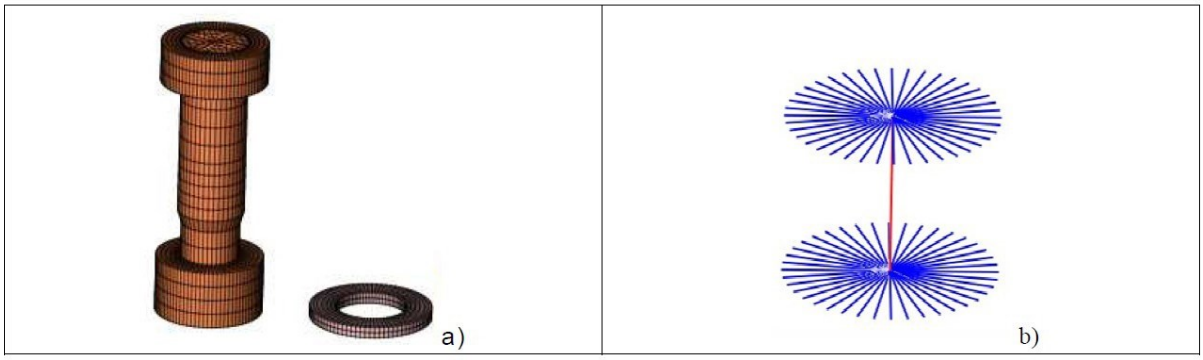

Figure 3.22. a) Solid model of the bolt b) Beam model of the bolt (Gödrich et al. [86]**)**

Modelling of Welds in FEM

In this chapter, the most frequently used weld modelling techniques are presented. The geometry and stiffness of the welds can be easily modelled using solid elements. In shell element models the stress value at welded regions can be dependent on the weld modelling technique. Aygül [88] summarized the modelling techniques to simulate weld using solid and shell elements. In shell element models, the welds in a welded joint can be represented using oblique shell elements as recommended by Niemi [89]. The length of inclined shell elements can be chosen as shown in this figure. The thickness of oblique shell elements can be defined same as the throat thickness of welds. The proposed model for weld is illustrated in Figure 3.23.

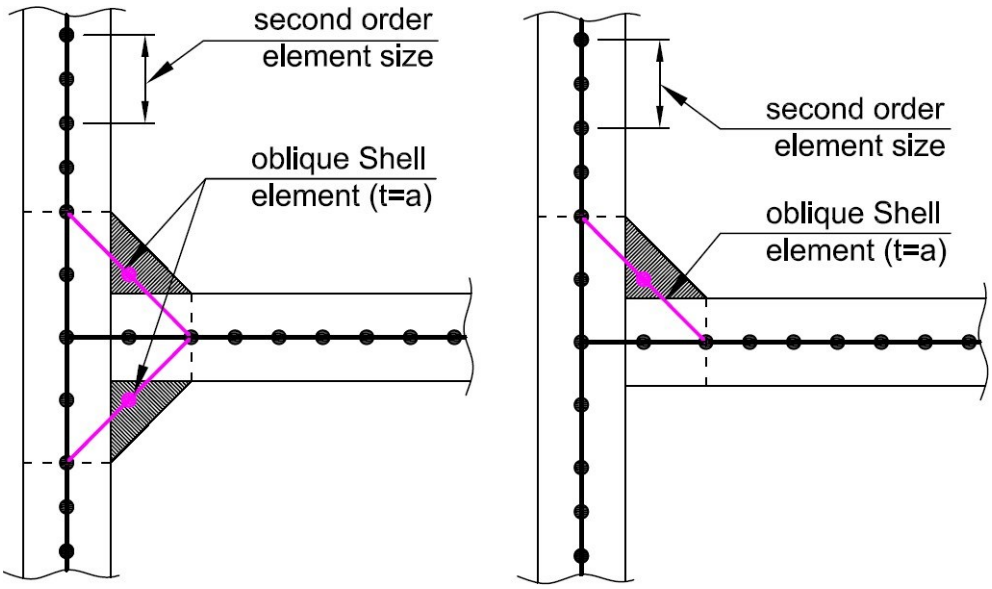

Figure 3.23. Weld modelling using oblique shell elements [89]

Weld modelling technique using rigid links was suggested by Fayard et al. [90], as shown in Figure 3.24. This technique aimed at computing hot spot stress at the weld toes and required the use of 4-node shell elements is recommended for this technique.

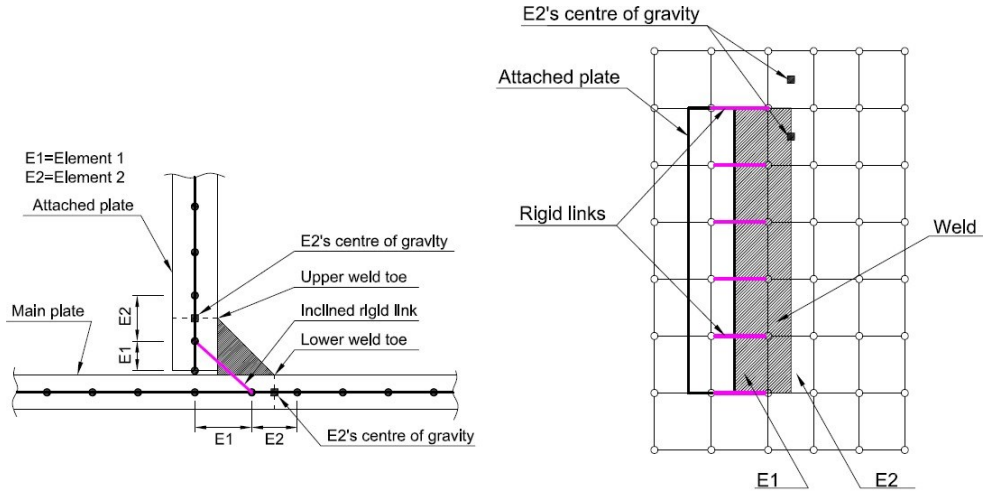

Figure 3.24. Single-side weld modelling with rigid links proposed by [90]

Niemi [89] suggested using shell elements with increased thickness in the intersection region of welded joints in order to predict the stiffness of the welds in welded joints. This method is based on two important geometry configurations: increased thickness and size/length of finite elements. Eriksson et al. [91] suggested two rows of shell elements with increased thickness, e.g. increased thickness elements both in the attached plate and the parent plate when considering a double-sided filled weld. Figure 3.25 indicates the model welds using shell elements with increased thickness for T-joints.

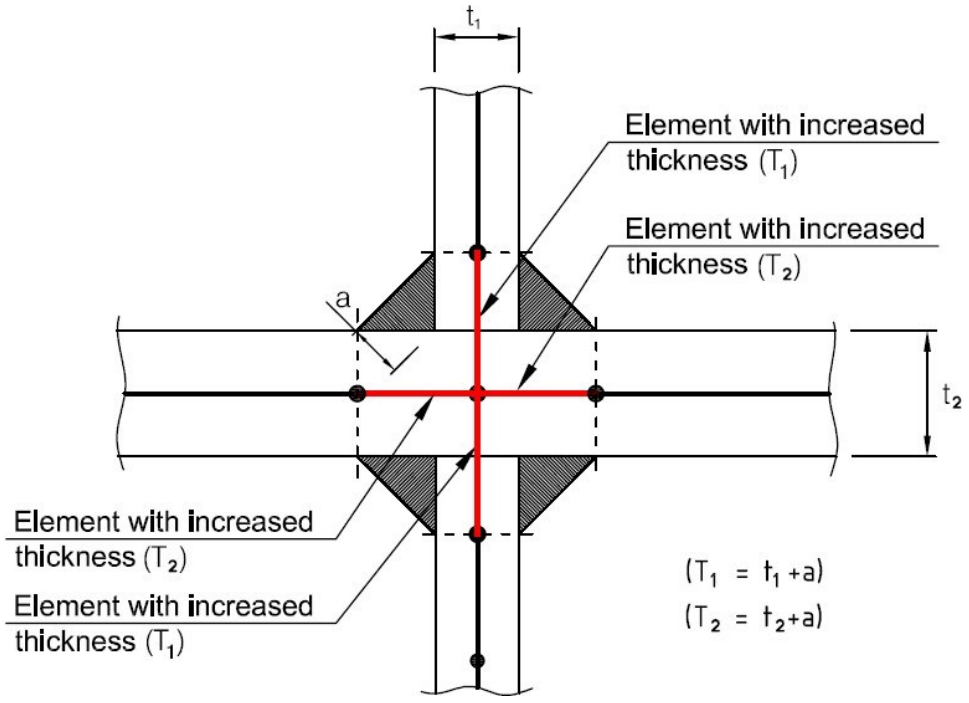

Figure 3.25. Modelling welds using shell elements with increased thickness [91]

For cover plate joints when modelling the welds, it is suggested that rigid elements can be used to join the attached plate to the parent plate while shell elements with increased thickness can be used in the parent plate using the recommended length as shown in Figure 3.26.

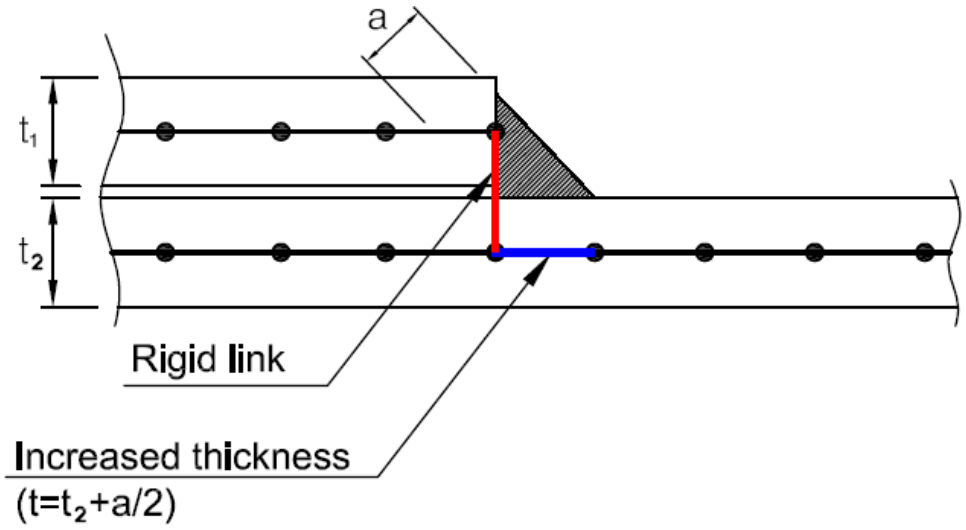

Figure 3.26. Modelling cover plate weld using shell elements with increased thickness and rigid links [92]

3.4.3. Component-Based Finite Element Methods

The CBFEM is a method to analyse and design joints and members of steel structures. It is a combination of the component method and the finite element method. The stresses, strains, and internal forces are calculated using the advantages of the finite element method to check the individual components according to design specifications (EN 1993-1-2; EN 1993-1-8). The CBFEM splits the entire joint into separated components including steel plates, welds, bolts, anchors, and concrete blocks. The CBFEM model of steel joints may consist of plates, bolts, anchors, and welds. Two numerical methods presented in the prEN 1993-1-14 are numerical simulation and numerical design calculation. The CBFEM is an NDC model since it uses simplified material models to design steel joints.

In numerical simulations, the material properties from coupon tests are generally used to simulate the behaviour of steel joints. However, the NDC models use simplified material curves based on design specifications. The CBFEM models the plates with elastic-plastic material with a nominal yielding plateau slope $\tan^{-1}$ (E/1000) according to EN1993-1-5. The von Mises yield criterion governs the material's response under stress. It is considered to exhibit elastic behaviour until it reaches the design yield strength (f_{yd}). EN 1993-1-5 recommends the value of a 5% plastic limit strain for simulating the behaviour of plates. Figure 3.27 indicates the theoretical true and engineering stress-strain curves and the material model utilized in the CBFEM. The yield strength and the elastic modulus of steel are reduced by reduction factors listed in Table 3.1.

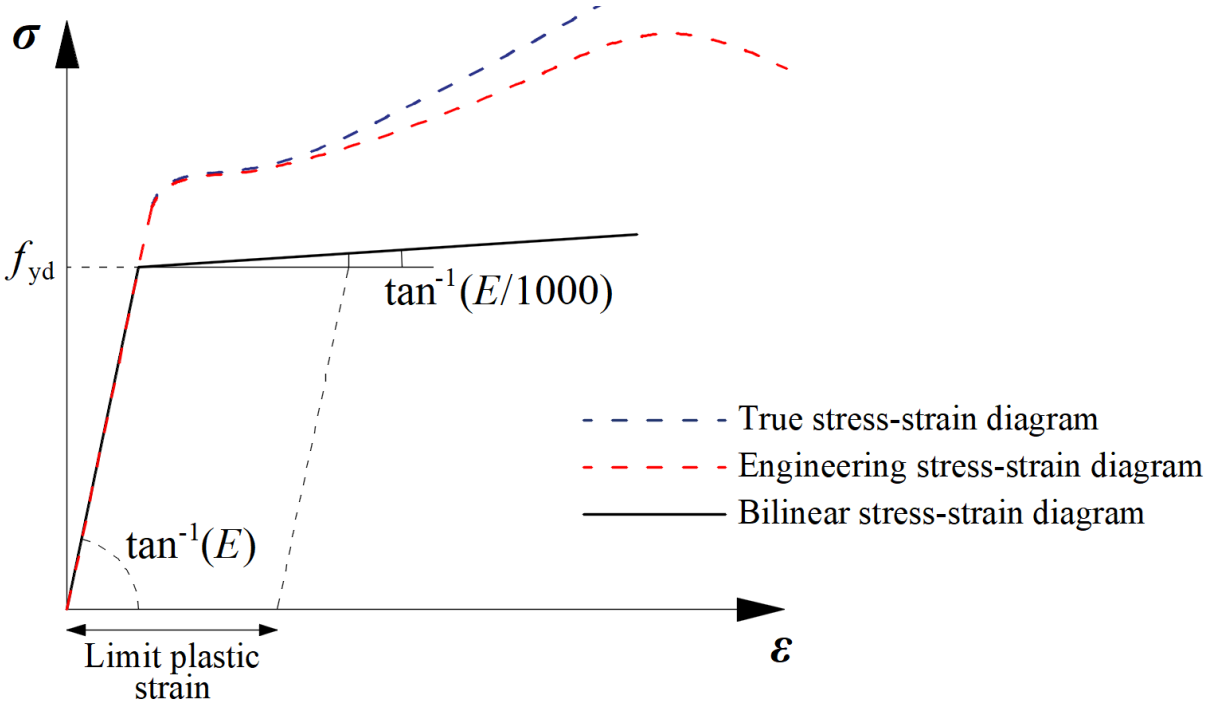

Figure 3.27. Material models used in FEM models [92]

The plates are modelled using 4-node quadrangle shell elements with nodes at their corners. Each node considers six degrees of freedom: 3 translations (u_x, u_y, u_z) and 3 rotations (φ_x, φ_y, φ_z). The plates in IDEA StatiCa are modeled with elastic-plastic material with a nominal yielding plateau slope according to EN1993-1-5 [13], as illustrated in Figure 3.27. The material behavior is based on the von Mises yield criterion [93]. It is assumed to be elastic before reaching the design yield strength (f_{yd}).

The bolt in tension is described by spring with its axial initial stiffness, design resistance, initialization of yielding, and deformation capacity, as shown in Figure 3.28. The initial axial stiffness is derived analytically in the guideline VDI [94] and Agerskov [95] as follows:

$$D_{Lb} = \frac{L_s + 0.4 d_b}{E_\theta A_{ss}} \tag{28}$$

$$A_{pp} = \frac{0.75 D_H (L_w - D_H)}{D_{W1}^2 - D_{W2}^2}$$

$$A_{P1} = \frac{\pi}{4}(D_H^2 - D_{W1}^2)$$

$$A_{P2} = \frac{1}{2}(D_{W2}^2 - D_H^2)\tan^{-1} A_{pp}$$

$$A_P = A_{P1} + A_{P2}$$

$$D_{LW} = \frac{L_W}{E_\theta A_P}$$

$$k = \frac{1}{D_{LB} + D_{LW}}$$

where d_b is bolt diameter, D_H is bolt head diameter, D_{w1} and D_{w2} are washer inner and outer diameter, L_W is washer thickness, L_s is bolt grip length, A_{ss} is bolt gross area and E is the

temperature-dependent modulus of elasticity. The force-deformation diagram for bolts in tension is constructed using the following equations:

$$k_t = c_1 k \tag{29}$$

$$F_{t,el} = \frac{F_{t,Rd}}{c_1 c_2 - c_1 + 1}$$

$$u_{el} = \frac{F_{t,el}}{k}$$

$$u_{t,Rd} = c_2 u_{el}$$

$$c_1 = \frac{f_{ub,\theta} - f_{yb,\theta}}{0.25 A E_\theta - f_{yb,\theta}}$$

$$c_2 = \frac{A E_\theta}{4 f_{yb,\theta}}$$

where $F_{t,Rd}$ is the bolt design resistance in tension, $f_{yb,\theta}$ is the yield strength of bolt, $f_{ub,\theta}$ is the ultimate strength of bolt and A is elongation after fracture. Figure 3.28 presents the characteristics of bolt behaviour in shear. The initial stiffness and the design resistance of a bolt in shear is defined by following formulas:

$$k_{el} = \frac{1}{\frac{1}{k_{11}} + \frac{1}{k_{12}}} \tag{30}$$

$$k_{11} = \frac{8 d_b^2 f_{ub,\theta}}{d_{M16}}$$

$$k_{12} = 12 k_t d_b f_{up,\theta}$$

$$k_t = \left(2.5, \frac{1.5 t_{min}}{d_{M16}}\right)$$

$$k_s = \frac{k_{el}}{1000}$$

where d_b is the bolt diameter, $f_{ub,\theta}$ is the temperature-dependent bolt ultimate strength, d_{M16} is the diameter of the reference bolt M16, $f_{up,\theta}$ is the temperature-dependent ultimate strength of the connected plate and t_{min} is the minimum thickness of the connected plate. The spring for bolt in shear has a bi-linear force deformation behaviour response. The characteristics of load-deformation in shear can be calculated as follows:

$$F_{v,el} = 0.999 F_{v,Rd} \tag{31}$$

$$\delta_{pl} = \delta_{el}$$

where δ_{pl} and δ_{el} are bolt in shear plastic and elastic deformation, $F_{v,el}$ is bolt shear elastic resistance and $F_{v,Rd}$ is bolt shear resistance. The effect of temperature on the elastic modulus, yield strength and ultimate strength of bolts and structural steel is represented by the reduction factors proposed in EN 1993-1-2. Therefore, the temperature-dependent parameters introduced in previous equations are multiplied by the reduction factors at the targeted temperature.

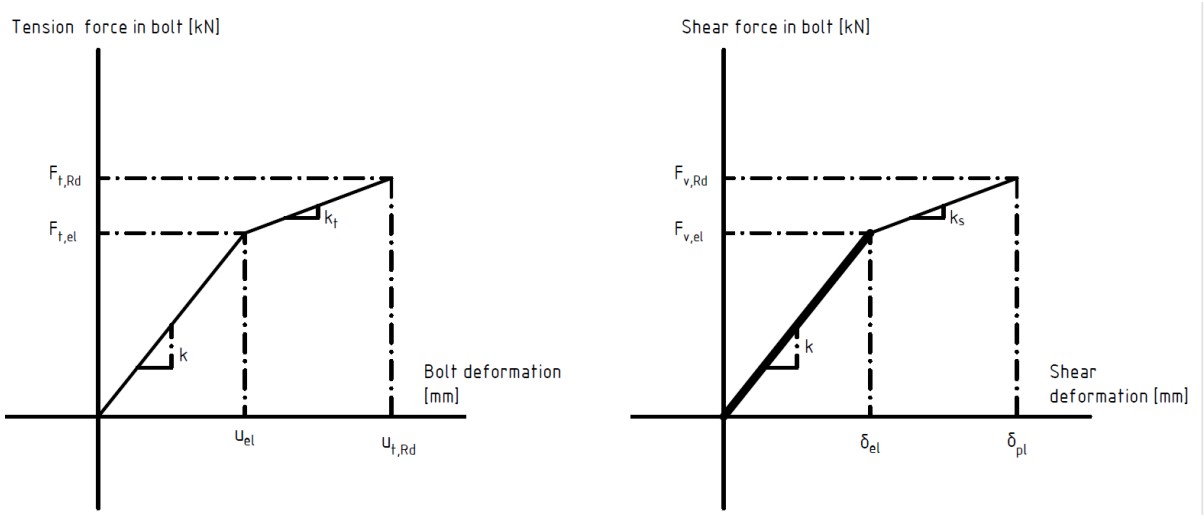

Figure 3.28. The load-deformation behaviour of bolts in tension (left) and in shear (right)

There are several parameters are mentioned in Eqs 10-13. The required parameters for building the force-deformation behaviour of the bolts in tension and shear are listed in Table 3.11. These design values are taken from the ISO 898 [96]. These parameters depend on the bolt grade.

Table 3.11. Bolt parameters in tension

Bolt Grade	A [%]	c_1 [-]	c_2 [-]
4.8	14	0.011	21.6
5.6	20	0.02	35
6.8	8	0.032	8.8
8.8	12	0.03	9.5
10.9	9	0.026	5

A direct merge of meshes is used to model the butt weld, as shown in Figure 3.29. The load is transmitted between plates by a force-deformation constraints based on the Lagrangian formulation. Plate edges are connected by multi-point constraints (MPC).

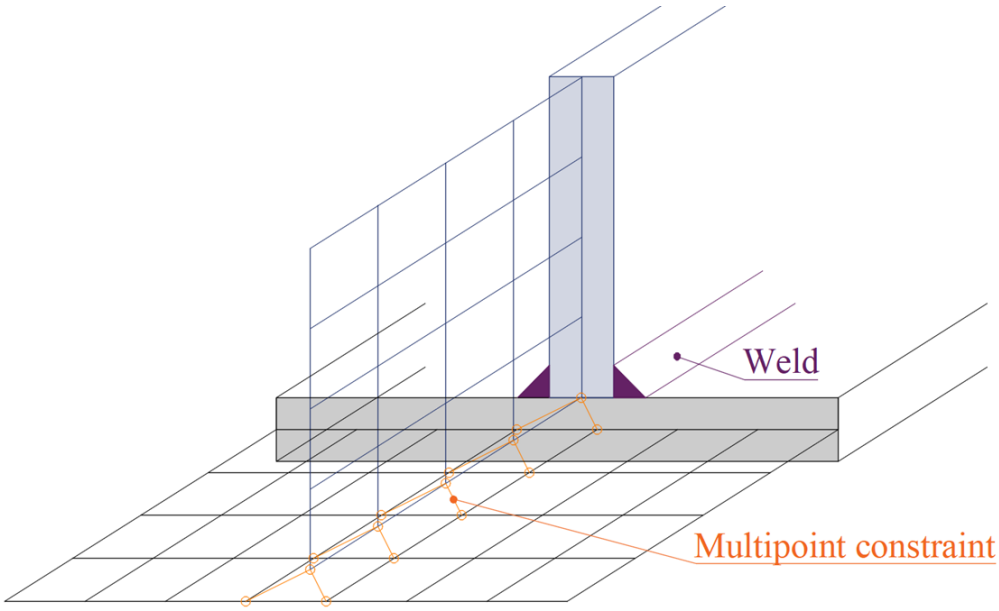

Figure 3.29. Constraint between mesh nodes (butt weld) [97]

The multi-point constraints derive the load distribution in the weld; therefore, the stresses are evaluated in the weld throat. The stiffness of the weld is neglected in this model. Conservative stress distribution is obtained. The resistance of the weld is calculated from stress at the end of plate edges. A special elastoplastic model is utilized to simulate the weld behaviour. The element is affected by the weld throat thickness, position and orientation. Equivalent weld shell element is located between plates with the corresponding weld dimensions as shown in Figure 3.30. The stress peaks are redistributed along the weld length applying the nonlinear material analysis.

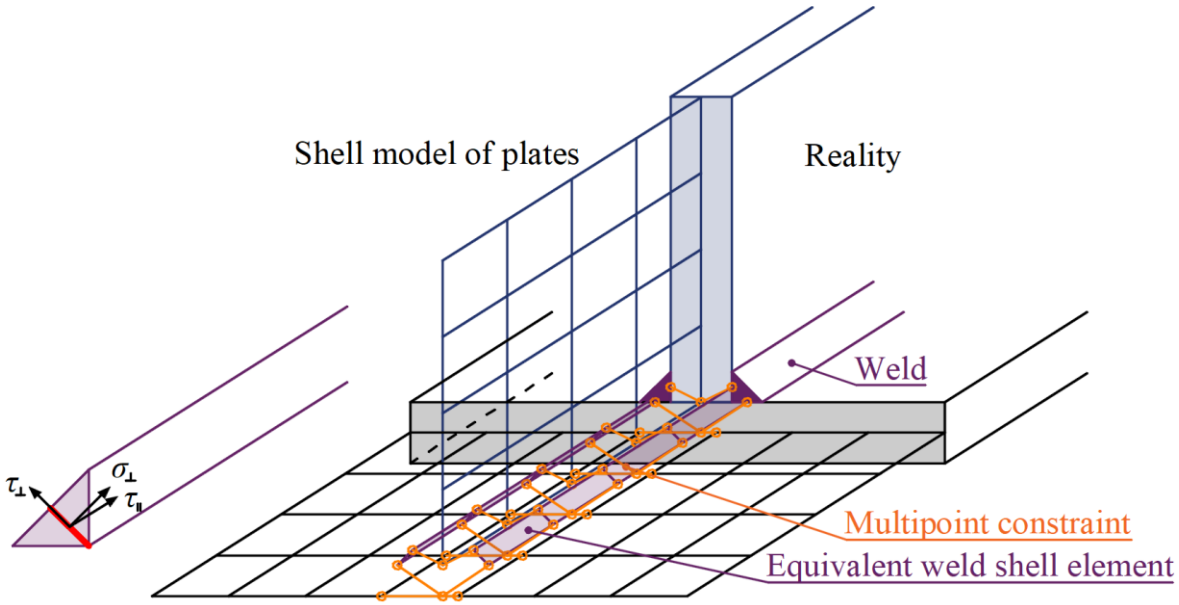

Figure 3.30. Constraint between weld element and mesh nodes (fillet weld) [7]

The weld model used in the CBFEM does not consider residual stresses or weld shrinkage. The design weld models are verified for their resistance according to relevant codes at ambient temperature. The plastic strain is 5% of the weld throat thickness and it confirms with the maximum plastic strain of plates. In this thesis, the verification of fillet welded lap joints will be presented in section 5.3.2 at

elevated temperature. The modulus of elasticity and strength of welds are decreased by Eurocode reduction factors.

CBFEM employs the standard penalty method to simulate contact between plates. Penalty stiffness is introduced in case of penetration between a node and the opposing plate. A heuristic algorithm governs the adjustment of penalty stiffness throughout the nonlinear iteration, enhancing convergence. The solver autonomously identifies penetration points and addresses the distribution of contact forces between the penetrated node and nodes on the opposing plate.

3.4.4. Numerical Studies on the steel members at elevated temperatures

Numerical studies allow us to assess the safety of steel structures in fire conditions without conducting physical experiments. Numerical studies enable researchers to conduct parametric studies, exploring a wide range of variables that affect the behaviour of steel members in the fire. Tan and Huang [98] studied the mechanical responses of generally restrained steel beams under fire conditions by the finite-element method. A linear elastic spring and semirigid rotational spring were utilized to represent the axial restraint and the rotational restraint, respectively. Numerical simulations showed that the critical temperature is reduced by axial restraint but increased by semirigid rotational restraint. Yin and Wang [99] performed a numerical study to investigate the large deflection behaviour of steel beams at elevated temperatures with different elastic axial and rotational restraints at the ends. They used shell elements of type S4R in the ABAQUS software to generate the model of steel beams. The numerical studies showed that a steel beam may survive very high temperatures without a collapse if axial restraints can induce catenary action. Heidarpour and Bradford [100] proposed a novel numerical method to describe the nonlinear behaviour of a restrained steel beam at elevated temperatures. The model incorporated moderately large displacement effects, material nonlinearity, and the development of catenary action effects with an increase in the temperature. Kucukler [101] numerically investigated the lateral torsional buckling behaviour and design of steel beams in the fire. The finite element models were generated using a four-noded reduced integration S4R shell element. Couto et al. performed a numerical study considering several cross-sections submitted to compression or bending about the major axis using SAFIR. The resistance of several cross-sections where local buckling can occur under axial compression and bending was investigated at elevated temperatures. Fang and Chan [102] presented an investigation on the structural performance of welded S460 steel columns exposed axial compression at high temperatures using finite element analysis. A finite element model, generated by the four-node shell element S4R with reduced integration, was developed and validated against the available test data for welded S460 steel columns under axial compression at room and elevated temperatures. Murtaza and Kucukler [103] proposed a structural fire design approach using second-order inelastic analysis with strain limits. The finite element analysis software Abaqus was used to create shell finite element models capable of replicating the structural response of steel columns in fire. Shell finite element models were developed and validated against experimental results performed on steel columns at elevated temperatures.

4. Experimental Study

4.1. Test Description

In order to evaluate the behaviour of bolted double lap joints at elevated temperatures, a total of 9 bolted double lap joints were studied at 20°C, 400°C, and 600°C in this experimental program performed at the Laboratory of the Czech Technical University in Prague. Three test specimens were tested for each temperature level. The test specimens were composed of three elements, which were cover plates, inner plates, and bolts, as shown in Figure 4.1. The cover and inner plates were both made of S355 steel (nominal material strengths f_y=355 MPa, f_u=490 MPa), with the respective nominal thicknesses equal to 8 mm and 16 mm. The inner plate was inserted between two cover plates with two or four M16 8.8 bolts to form a double lap joint with bolts in double shear. The first specimen was tested with 4 bolts at ambient temperature. Then, the number of bolts was decreased to 2 bolts due to the capacity of the testing machine. To study the fire-structural response of bolts, all specimens were designed to undergo bolt-in-shear failure at ambient and elevated temperatures. The characteristics of test specimens are displayed in Figure 4.1.

The experimental work was performed on 9 double-lap joints with two or four bolts positioned perpendicular to the loading direction. The test program was performed to measure the resistance of double lap joints at elevated temperatures. The tests on the bolted lap joints have been carried out by the Shimadzu Autograph AG-X plus machine under monotonic loading conditions. The maximum load capacity of the machine is 300 kN. The loads have been applied under displacement control with a speed equal to 0.65 mm/min. Table 4.1 shows the summary of the dimensions of 9 tests utilized in this study. The values of pitch p_1 and end distances e_1 were selected according to EN 1993-1-8 [12] from the minimum allowed distances to the most common ones. The edge distance e_2 was constant for all specimens and was equal to $4.5d_0$ to avoid net cross-section failure. The width of both plates is 80 mm. The test specimens were designed for bolt shear failure.

Table 4.1. Summary of test specimens

Specimen	θ [°C]	n_{bolt} [-]	e_1 [mm]	p_1 [mm]	e_2 [mm]	d [mm]
Test 1	20	4	35	50	40	16
Test 2-3	20	2	35	50	40	16
Test 4-6	400	2	35	50	40	16
Test 7-9	600	2	35	50	40	16

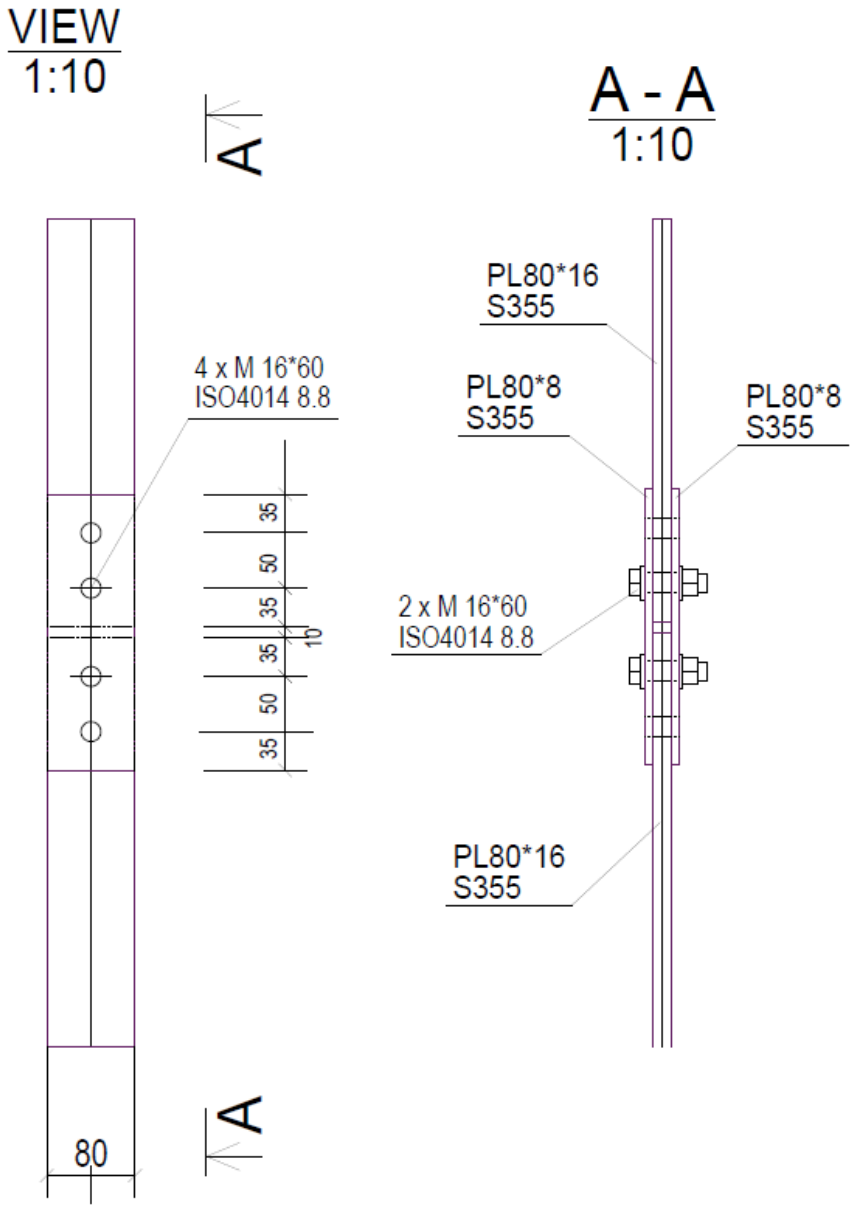

Figure 4.1. Dimensions of test specimens.

4.2. Test Setup

The commonly used methods are the steady state test method and the transient state test method in the tests of structures under fire conditions. Generally, for the transient state test method, the specimen is loaded to a certain level and then heated until it fails, whereas, for the steady-state test method, the specimen is heated to a predetermined temperature level. In this study, the mechanical response of double-bolted lap joints at elevated temperatures was investigated experimentally using the steady-state test method. After reaching the pre-selected temperature level, the constant temperature was maintained for 15 min and then loaded until it failed. The heating process is indicated in Figure 4.2. This process allows to ensure that the specimen temperature reaches the target value and is uniformly distributed. Before the heating stage started, the lower end of the specimens was gripped. The upper end was free during the heating to prevent axial force caused by thermal expansion.

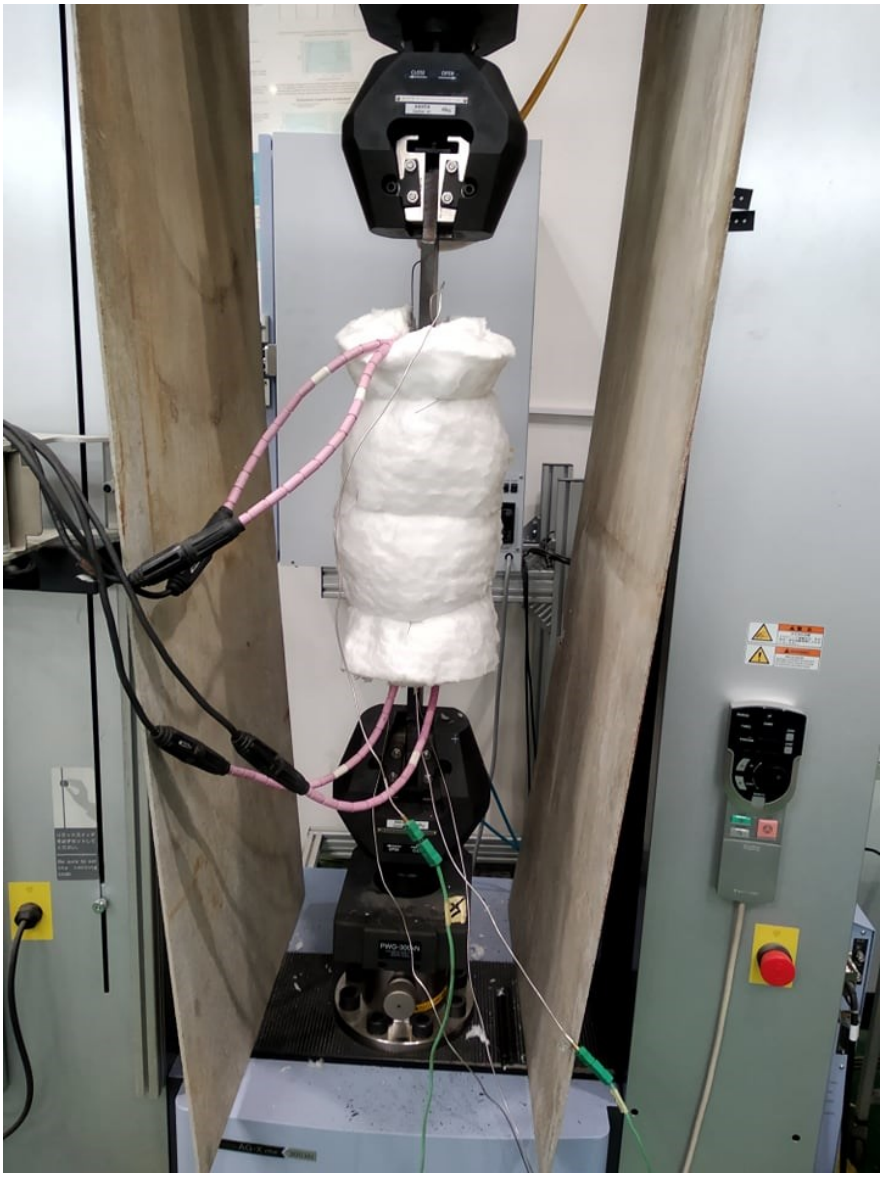

Figure 4.2. Test setup at elevated temperature

The specimens were tested at 3 different nominal temperature (T) levels, namely, at 25 °C (ambient temperature), 400 °C and 600 °C. Each of these tests used a high-temperature ceramic fiber blanket to heat the specimen. The test setup for the specimens at elevated temperatures is shown in Figure 4.2. Both testing series used the same test setup and instrumentation. Three K-thermocouples were attached to the face of the specimens to record the change of the temperature. When the temperature near the shear plane of the bolt reached the targeted degree, loading was applied to the specimen while holding the target temperature constant. Figure 4.3 and Figure 4.4 present the recorded temperature-increasing history of bolted lap joints at 400°C and 600°C.

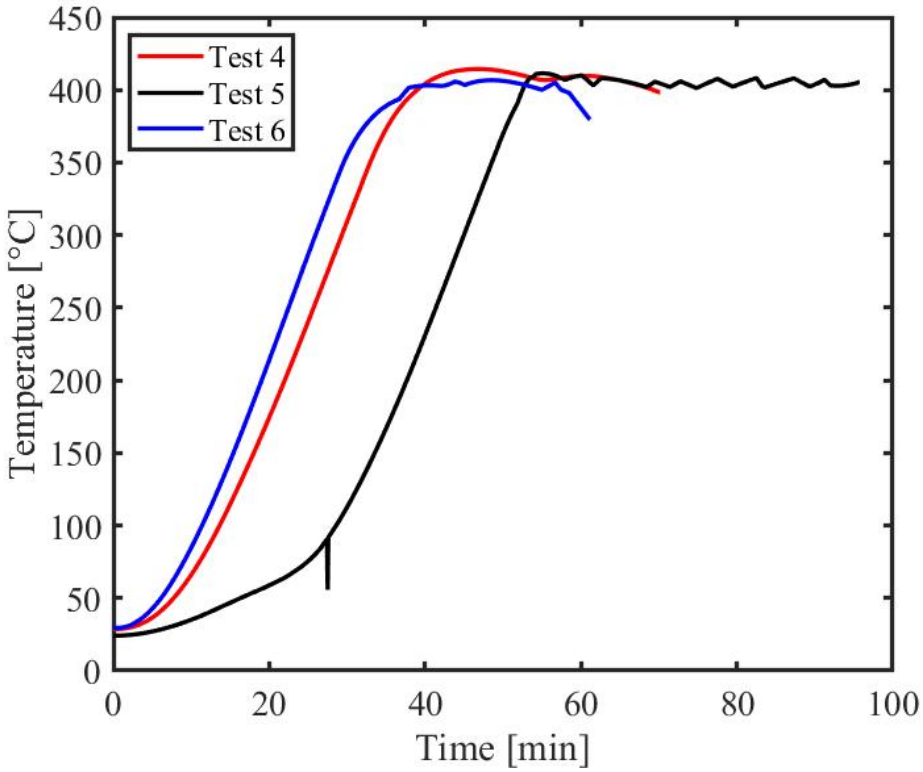

Figure 4.3. The heating process during tests at 400°C

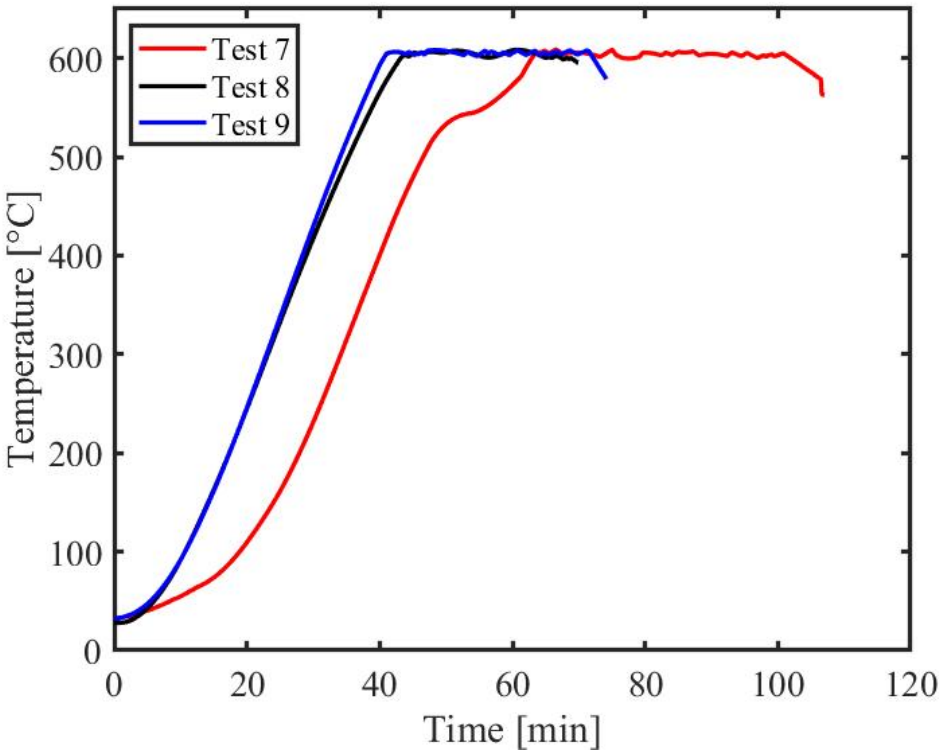

Figure 4.4. The heating process during tests at 600°C

4.3. Failure Modes

The bolted lap joints were tested at different temperature levels: ambient temperature, 400°C and 600°C. The tested specimens were heated to the targeted temperature then the specimens were loaded up to failure. Each specimen experienced the same failure mode at each temperature. The bolts were exposed to double shearing as seen in Figure 4.7. Figure 4.6 shows that the cover plates curled up after exposing heating and loading procedure. The obtained failure modes are utilized to validate the solid and CBFEM models.

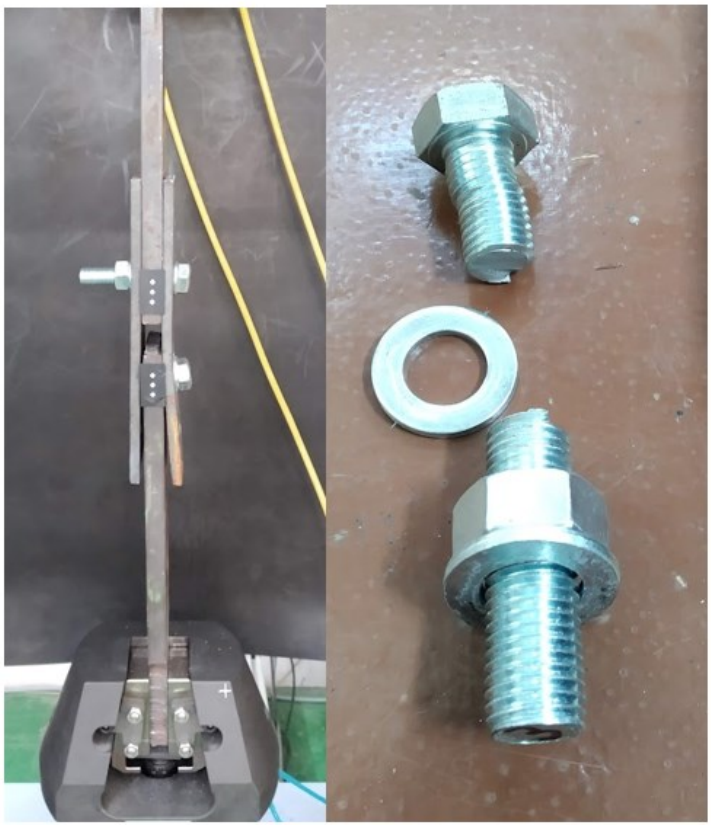

Figure 4.5. Failure modes of tested specimens at 20°C

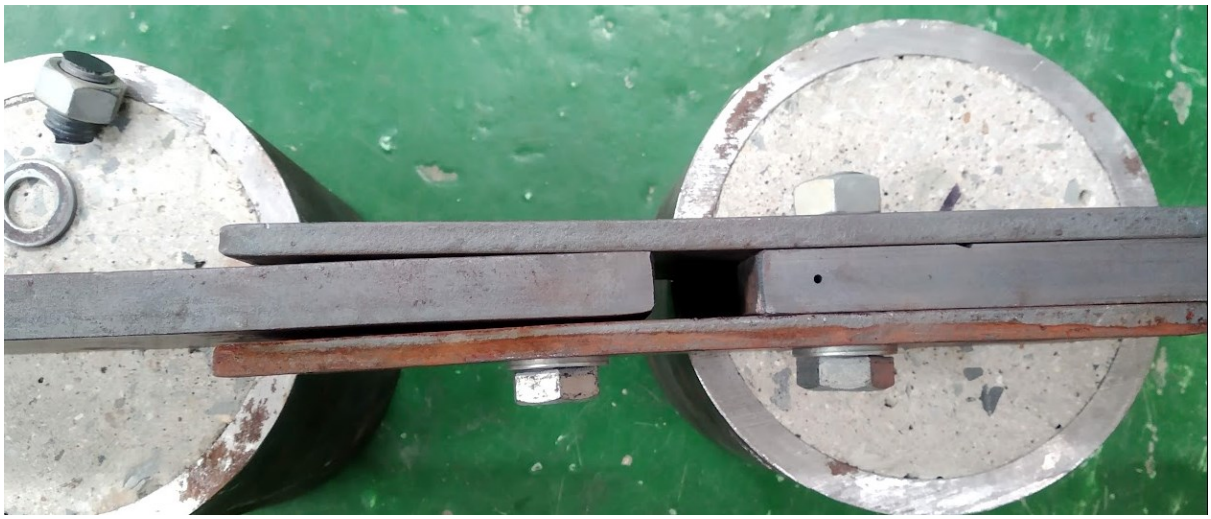

Figure 4.6. Failure modes of tested specimens at 400°C

Figure 4.7. Failure modes of tested specimens at 600°C

4.4. Load-Deformation Curves

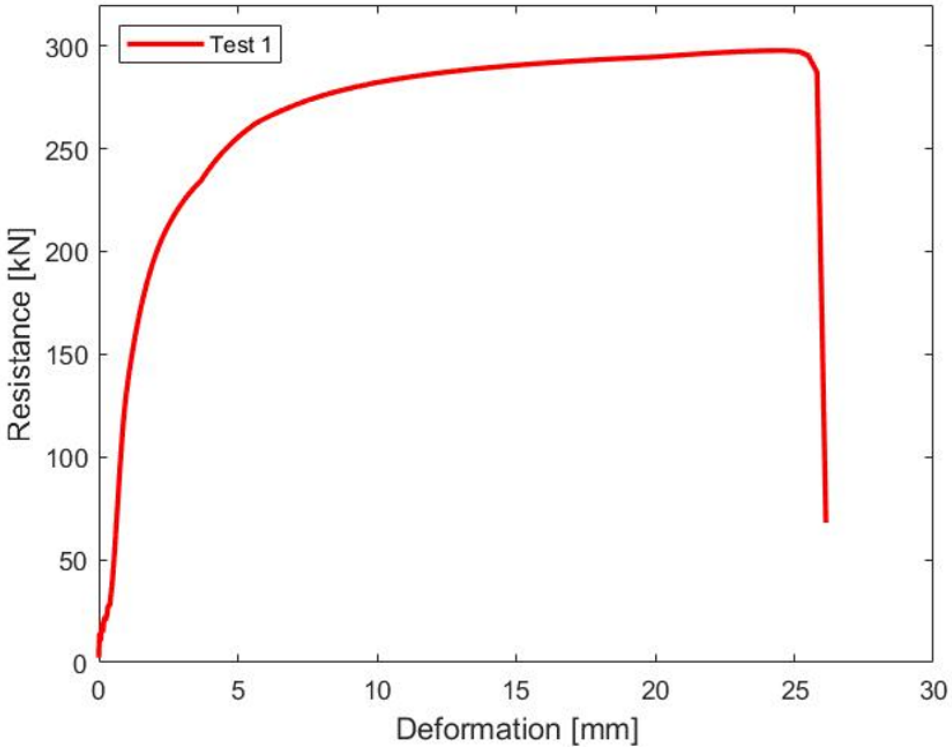

Figure 4.8. Load-deformation curve for test specimen with 4 bolts at ambient temperature

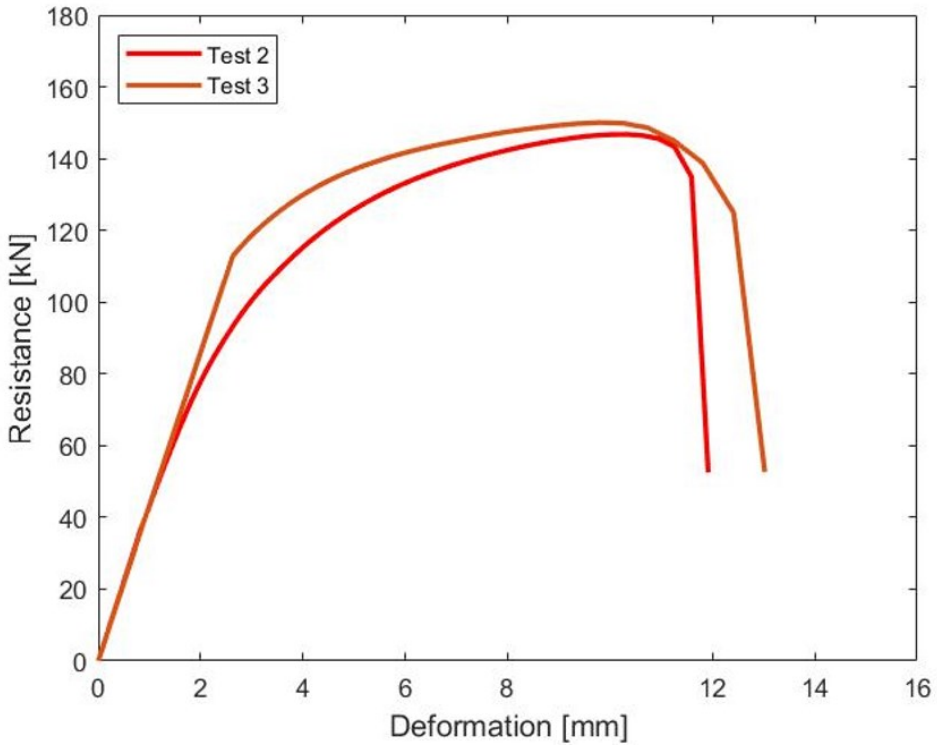

Figure 4.9. Load-deformation curves for test specimens with 2 bolts at ambient temperature

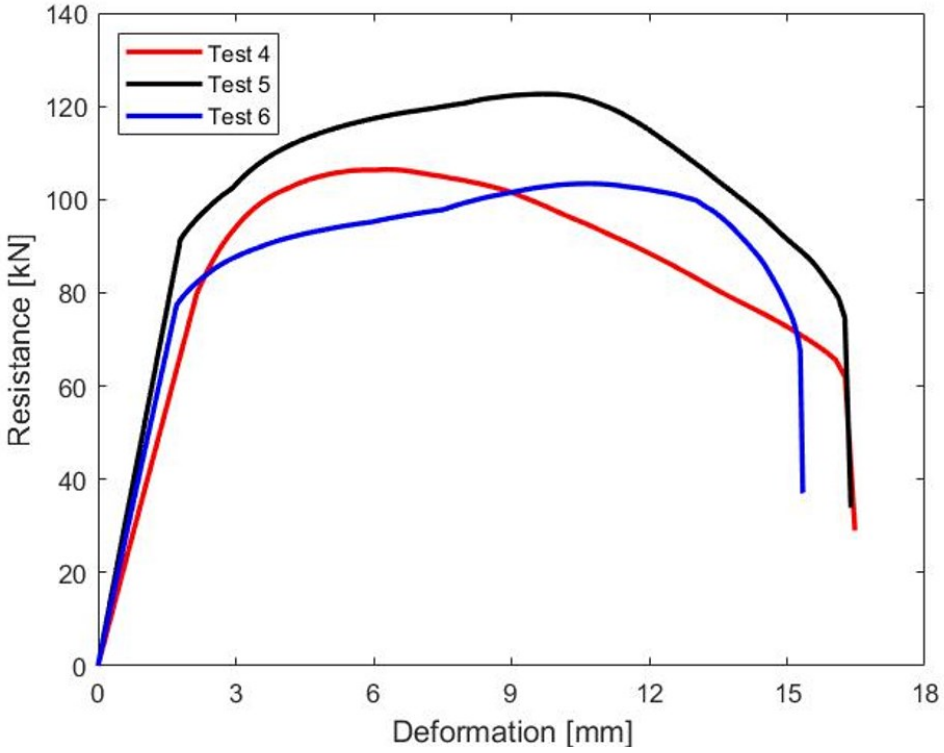

Figure 4.10. Load-deformation curves for test specimens at 400°C

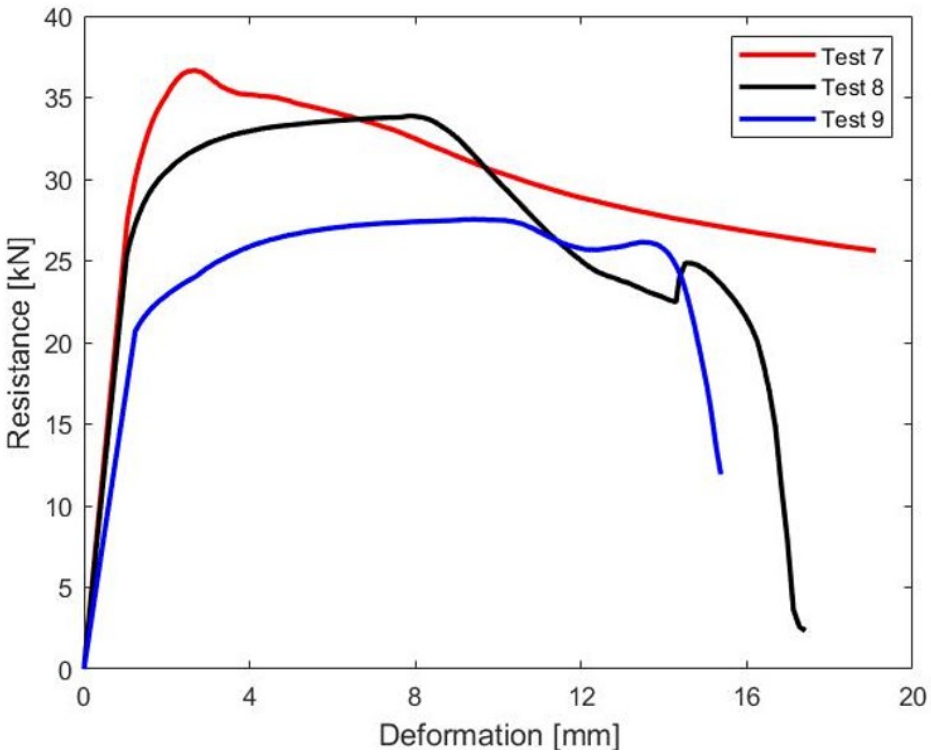

Figure 4.11. Load-deformation curves for test specimens at 600°C

Figure 4.8 and Figure 4.9 depicts the load-deformation curves for test specimens with 4 bolts and 2 bolts at ambient temperature, respectively. It is seen that the test specimens experienced brittle behaviour after bolt fracture at ambient temperature. Figure 4.10 presents the load-deformation behaviour of test specimens at 400°C.

5. Numerical Studies

In this chapter, the solid model for bolted lap joints, the shell model for steel beams, and the CBFEM models for steel joints and members at elevated temperatures are presented. Verification and validation studies are essential to determine the accuracy of the numerical models. The solid model for bolted lap joints is generated to simulate the accurate behavior of bolted lap joints at ambient and elevated temperatures. The author's experimental study and the study [49] are used to validate the solid model. Validation compares the numerical models with the experimental data [104]. Verification studies compare the proposed numerical models with the analytical models or other validated numerical models [104]. The shell model generated in ABAQUS is validated by experimental study in terms of load-deformation curves. Then the validated shell model may be used to verify the CBFEM models for steel members at elevated temperatures. The used material models for steel plates in numerical models are reduced by the Eqs. (32)-(34). The yield strength at temperature θ $(f_{y,\theta})$ is a function of the yield strength (f_y) at 20°C expressed by

$$f_{y,\theta} = k_{y,\theta} f_y \tag{32}$$

The modulus of elasticity for steel plates, bolts and welds is decreased by the reduction factors listed in Table 3.1. In the same way the Young's modulus at temperature θ $\left(E_{a,\theta}\right)$ is a function of the Young's modulus (E_a) at 20°C given by

$$E_{a,\theta} = k_{E,\theta} E_a \tag{33}$$

The proportional limit at elevated temperature is given by:

$$f_{p,\theta} = k_{p,\theta} f_p \tag{34}$$

The reduction factors for yield and ultimate strength of bolts and welds are presented in Table 3.3 and Table 3.4.

5.1. Solid Model for Bolted Lap Joints

prEN-1993-14 [2] defines numerical simulation as an extension of physical experiments to determine the direct resistance of a structure. A finite element solid model has been developed in ABAQUS [11] software to extend the results obtained by experimental studies by authors and Jiang et al. [49] and to verify the numerical design calculation methods. The FE solid model aimed at predicting the resistance and failure modes of bolted lap joints at ambient and elevated temperatures. The solid finite element models were first validated against the test results and subsequently used to verify the shell finite element models. Then, the parametric studies were conducted to generate additional data over a wide range of predicting fire resistance for bolted lap joints. The solid model was validated with different failure modes at different temperature levels. The bearing failure and net section failure at ambient temperature were investigated in the study [74]. The experimental study presented in this study was used to study bolt shear failure at elevated temperatures. The verification of numerical models may be conducted through analytical models or the validated numerical models [104]. In this section, the CBFEM models are verified based on the analytical models presented in Eurocode [7] and the validated numerical simulation.

5.1.1. Material Models

The material properties of tested specimens are listed in Table 5.1. The plates were fabricated from S355 and S700 high-strength steel in experimental studies used for validation of the solid model. The stress–strain characteristics of structural steel at elevated temperatures are well established and presented in the design code []. In this study, the stress–strain characteristics of steel are simulated according to Eurocode as shown in Figure 5.1. The young modulus, proportional limit, and yield

strength of carbon steel at elevated temperatures were reduced by reduction factors proposed by Eurocode. For the sake of simplicity at the design level, the constitutive material model used in numerical simulation does not include linear material softening from 15 to 20% strain which is presented in the Eurocode material model for steel at ambient and elevated temperatures. Figure 5.2 indicates the material models for bolts used in the generated solid model at ambient and elevated temperatures.

Table 5.1. Material properties of tested specimens

Tests	Steel Grade	Bolt Grade	Bolt Diameter	fy [MPa]	fyb [MPa]	fub [MPa]	Elongation [-]
Author test	S355	8.8	M16	355	640	800	0.12
Jiang et al [49]	S700	12.9	M22	700	1080	1200	0.08

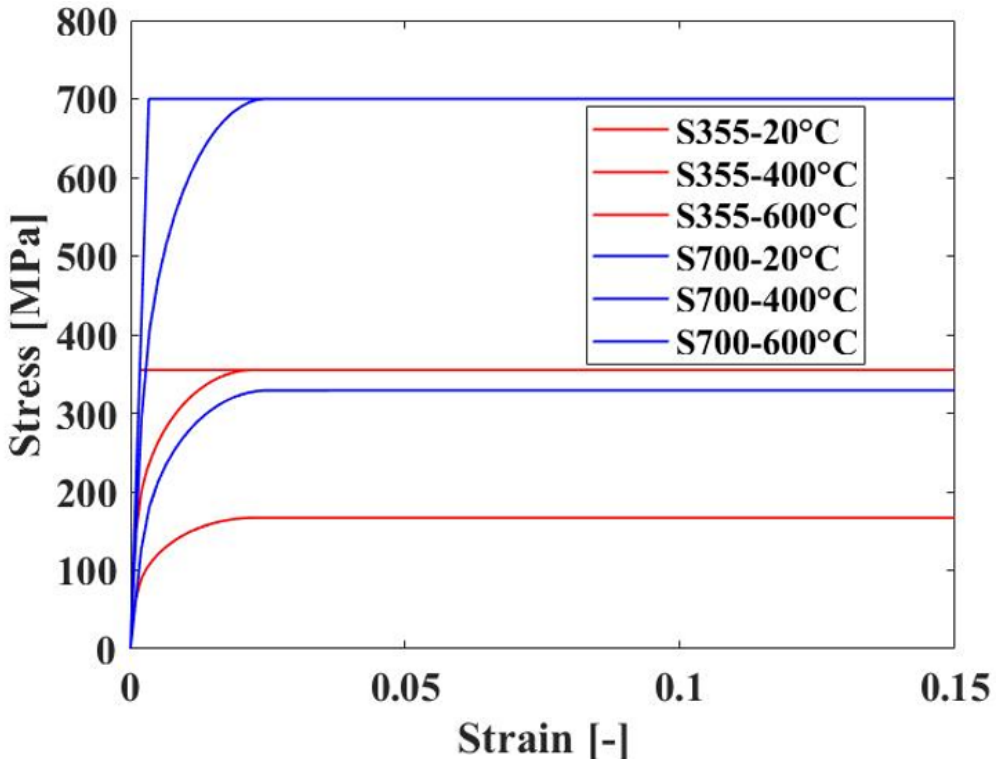

Figure 5.1. Material models for steel plates used in the solid model.

At elevated temperatures, the shape of the stress-strain diagram is modified compared to the shape at room temperature. Instead of a linear-perfectly plastic behaviour as for normal temperature, the model recommended by EN 1993-1-2 at elevated temperature is an elastic-elliptic-perfectly plastic model, followed by a linear descending branch introduced at large strains when the steel is used as material in advanced calculation models to avoid numerical problems.

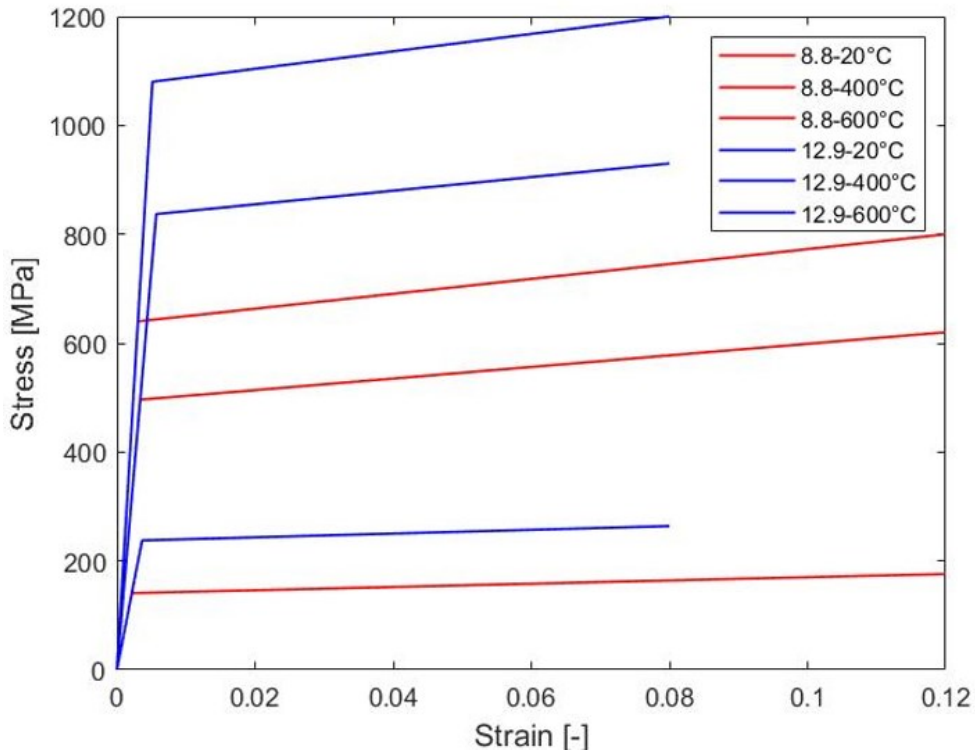

Figure 5.2. Material models for bolts used in the solid model.

For structural bolts, the bilinear material model, shown in Figure 5.2, assumes the onset of yielding at the strain ε_p corresponding to the yield stress and simply uses the value of 25 % of elongation to fracture of a bolt according to EN ISO 898-1 [96] indicated in Table 5.1 as the ultimate strain for the bolt material. The yield strength (σ_y) and ultimate strength (σ_u) for bolt grade 8.8 were taken 640 and 800 MPa, respectively. For both structural steel and bolts, The Young's modulus (E) was taken as 210 GPa, and a value of 0.30 was used for Poisson's ratio (ν). Material nonlinearity analyses were performed based on von Mises yielding criteria. Eurocode reduction factors were used to reduce the stress-strain material properties such as elastic modulus, yield, and ultimate strength at elevated temperatures of the bolts. In order to correctly simulate material behaviour, ABAQUS requires the material properties to be input as functions of true stress and true strain [23]. True stress-strain curves were used since large deformation occurred in the specimens. Since most material data is provided in nominal stresses and nominal strains, a conversion is required using the following relationships provided in Eqs. (35) and (36):

$$\sigma_{true} = \sigma_{nom}(1 + \varepsilon_{nom}) \tag{35}$$

$$\varepsilon_{true} = ln(1 + \varepsilon_{nom}) \tag{36}$$

5.1.2. Element Types

The numerical models of the double lap joints were composed of two plates overlapping the inner plate and connected by bolts. The geometry of the plates and the bolts have been generated by extruding their cross-section. For the sake of simplicity, the hexagonal bolt head and nuts are idealized as circular shapes neglecting the threaded part. Washers are not modelled. Bolt holes are assumed to be equal to the diameter of the bolt shank. Figure 5.3 shows the modelled bolt, inner plate, and splice for the experimental study of the authors.

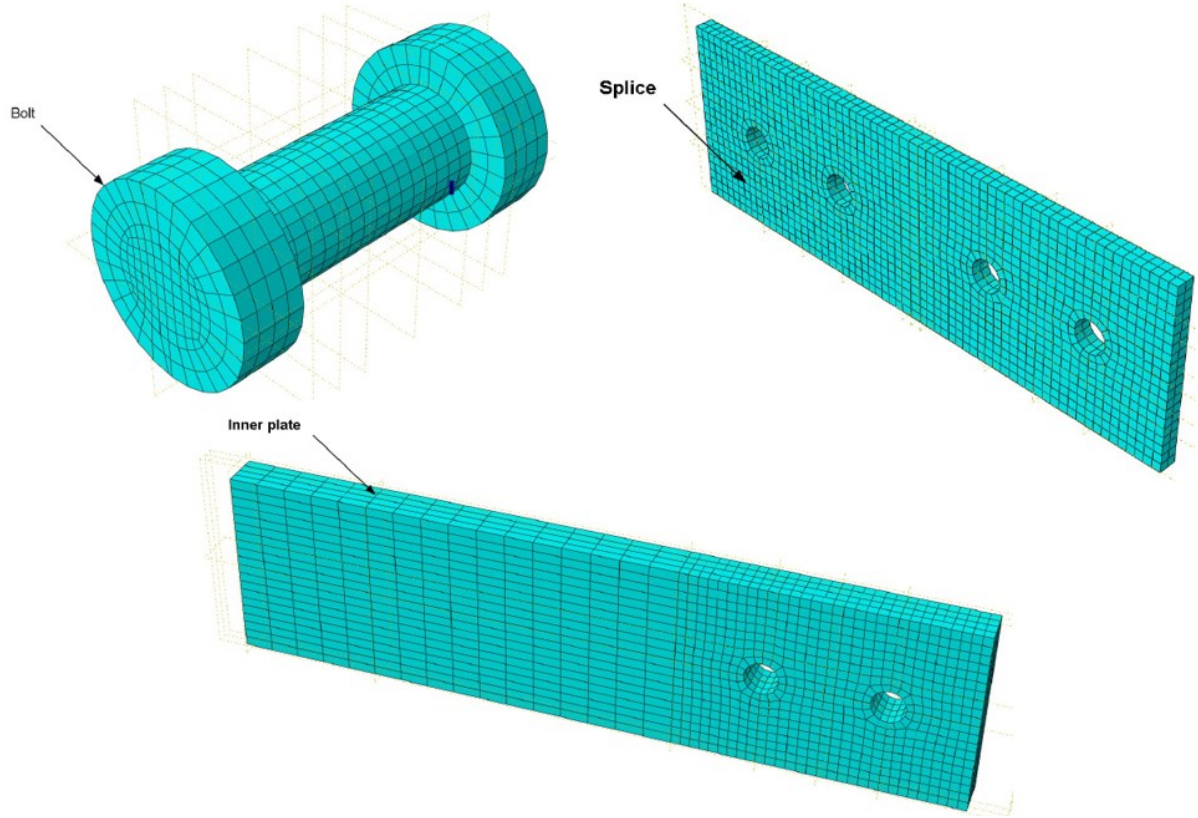

Figure 5.3. Mesh patterns for bolts and plates used in solid model.

All solid models were created using the C3D8R element, which is a three-dimensional continuum (solid) 8-node linear brick element with reduced integration and hourglass control to decrease the computational time [105]. A refined mesh size of 2 mm is used for bolts. Since the bolt is assigned as the master surface, the region around bolt holes has meshed with a 4 mm size. The mesh patterns of the developed FE models are presented in Figure 5.3.

5.1.3. Contact and Solver Types

A general static procedure in ABAQUS standard solver was adopted for numerical simulation. Static analysis utilizes time-independent equilibrium equations to evaluate the displacements, stresses, and strains of the model under the given loading conditions. Geometric nonlinearity was considered in all analyses by a large displacement formulation. ABAQUS adopts a large strain formulation for 3-D solid elements by default. The non-linear geometry parameter (*NLGEOM = ON) was set to deal with local instability and large deformation effects in the ABAQUS step module. No initial imperfection was introduced in the analyses.

Contact between all connected parts was modelled using the surface interaction command in ABAQUS, allowing finite sliding at the interface of the contact surfaces. Friction between the contact surfaces at the connection is modelled using the classical Coulomb model, where the friction coefficient was set at 0.2. The hard-normal contact was used to prevent any penetration of slave nodes into the master surfaces. The bolts were only snug-tightened in the experimental study, therefore the solid model did not consider the bolt preload [106].

5.1.4. Mesh Sensitivity Studies

The mesh sensitivity study is shown in Figure 5.4. This mesh size was decided to be the smallest that can be used to obtain excellent agreement between the simulation results. The non-contact zone in the inner plate was meshed with 4 times the fine mesh size over the contact zone.

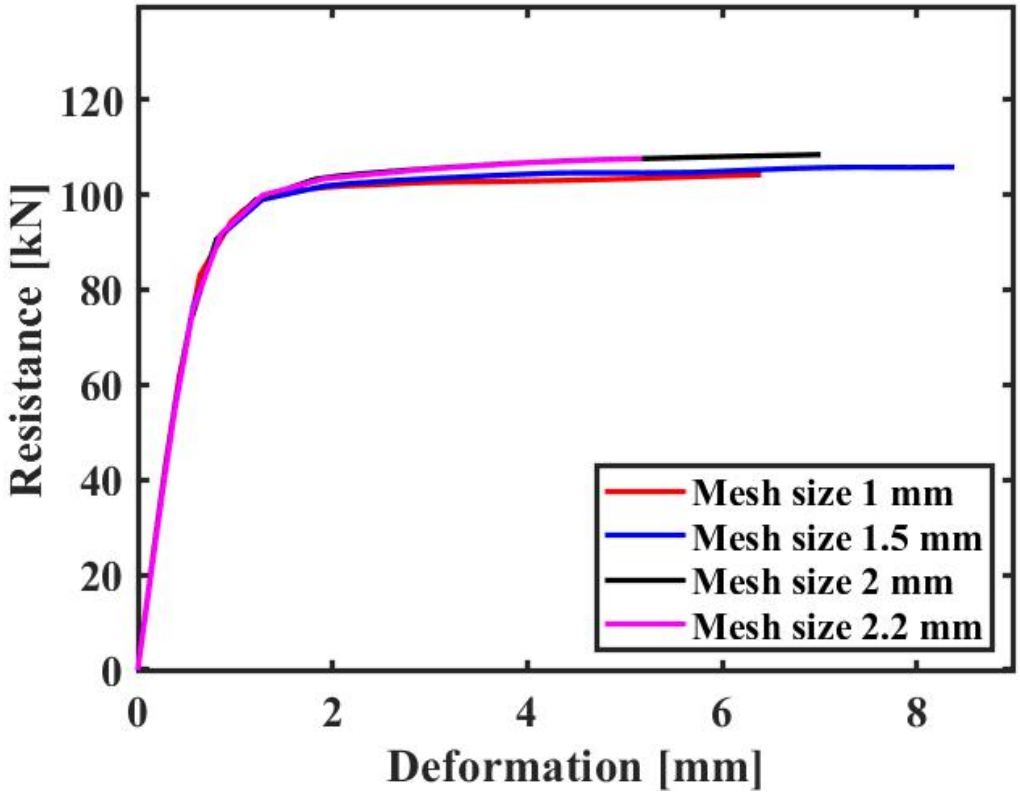

Figure 5.4. Mesh sensitivity study

5.1.5. Validation

Ambient Temperature

The experimental study [49] is utilized to validate the solid model for modelling of bolted lap joints at ambient temperature. The details of the test description are described in Section 3.3.1. The model is fixed in an inner plate and a displacement-controlled loading is applied to the other inner plate until the solid model does not converge. The displacement was obtained from the position where the tensile load applied through the field output in ABAQUS software. Three failure modes were considered in the numerical simulation. In order to investigate different failure modes (net section failure, bolt shear failure, and bearing failure), the following failure criteria were considered comparing the von Mises stress with ultimate stress. The numerical simulation considers the bolt shear failure when the shear plane of bolts reaches the stress value at 25% of the bolt elongation. The accuracy of the numerical simulation was validated against the experimental results on load-deformation relationship, failure mode, and predicting resistance of bolted lap joints at ambient and elevated temperature. The comparisons of the load-deflection graphs obtained from tests and solid models are presented in Figure 5.5-Figure 5.10. It can be seen that the FE models were able to replicate the experimental responses of the bolted lap joints reasonably well. Figure 5.11 indicates the stress distribution that occurred on the steel plates in the solid models. The grey zone on steel plates represents that the stress value reaches the ultimate strength defined in the material model.

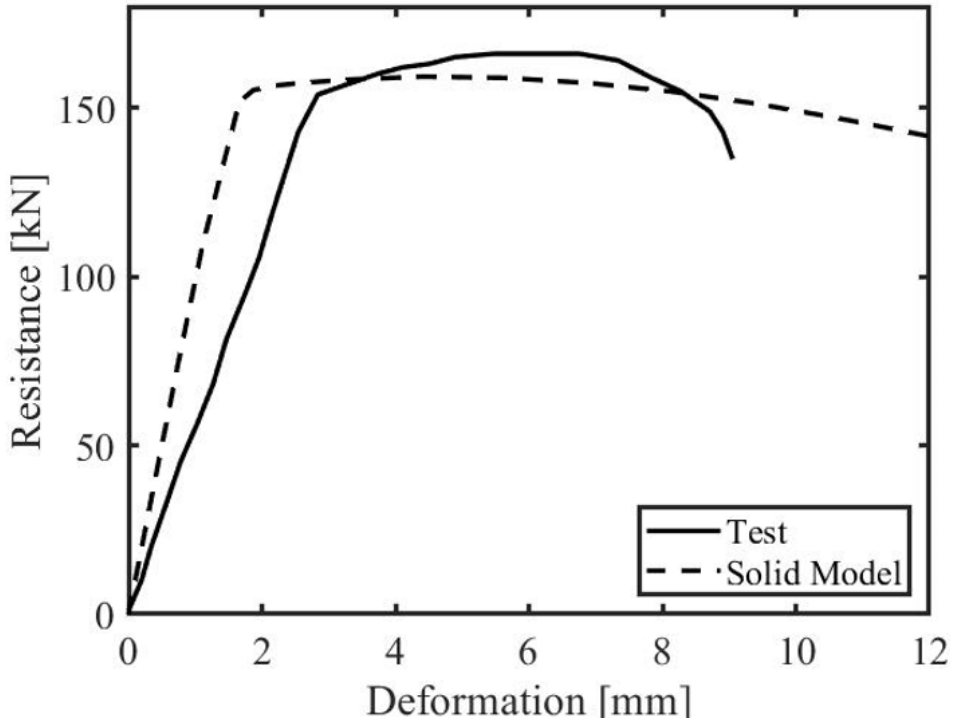

Figure 5.5. Validation of test specimen pa-03

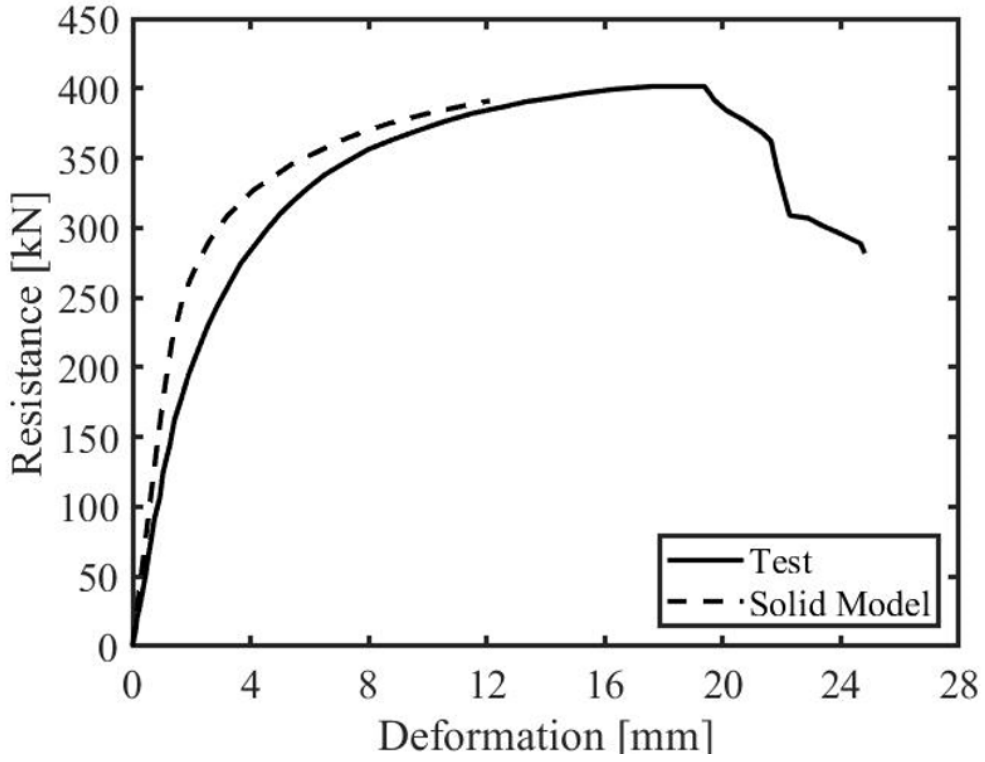

Figure 5.6. Validation of test specimen pa-04

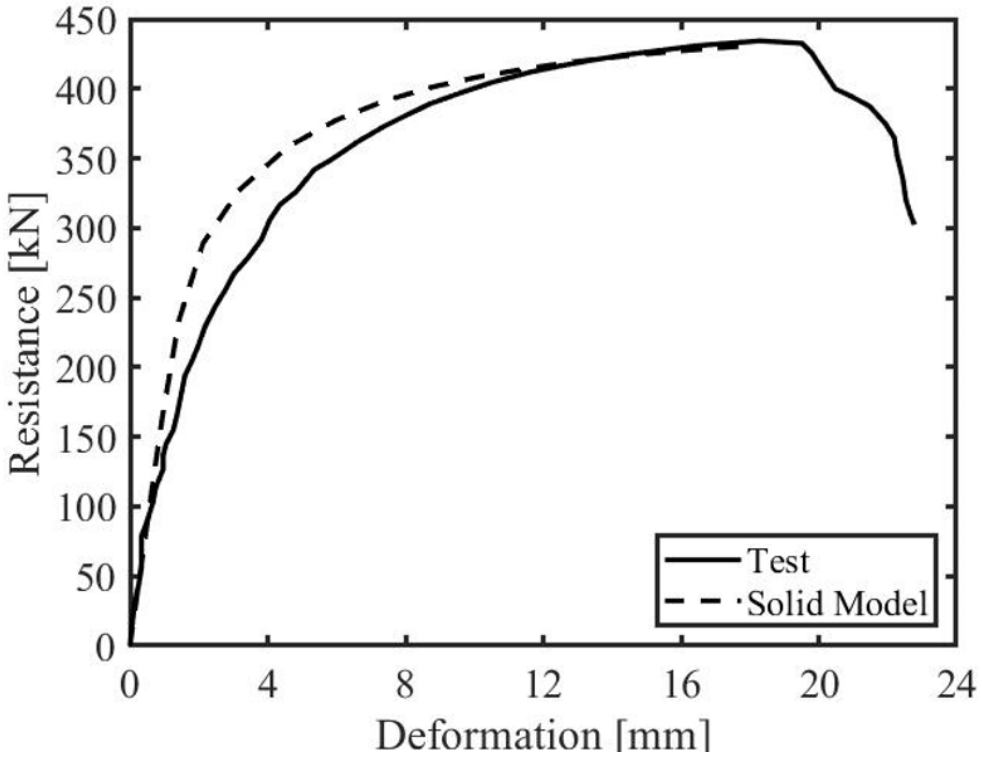

Figure 5.7. Validation of test specimen pa-05

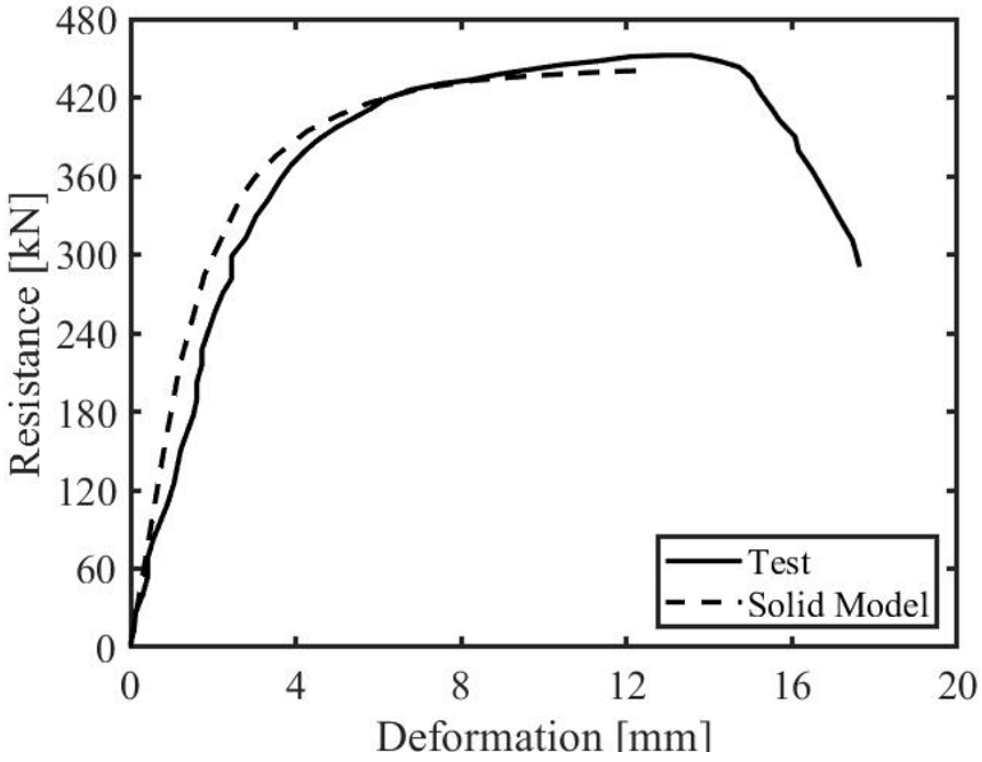

Figure 5.8. Validation of test specimen pa-06

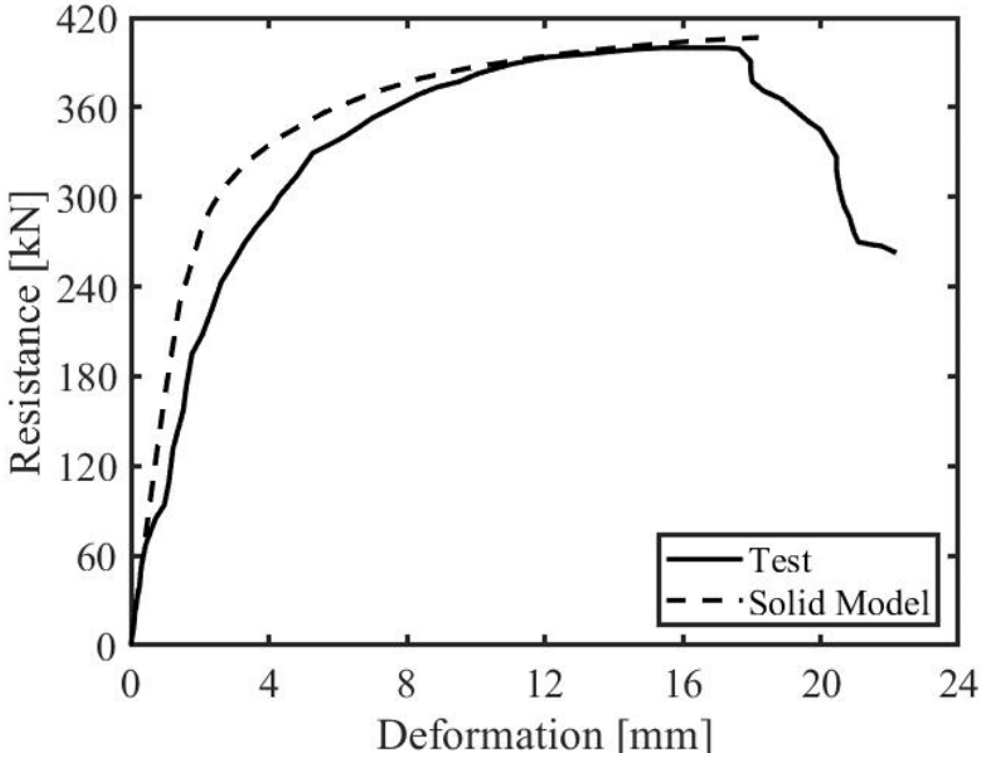

Figure 5.9. Validation of test specimen pa-07

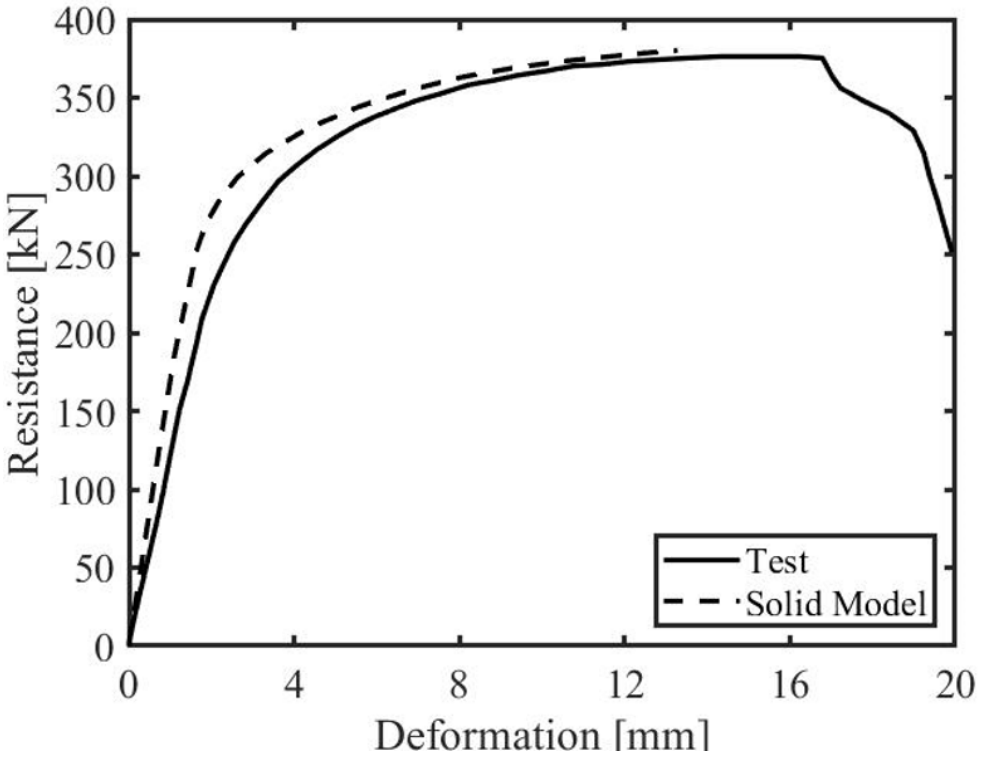

Figure 5.10. Validation of test specimen pa-08

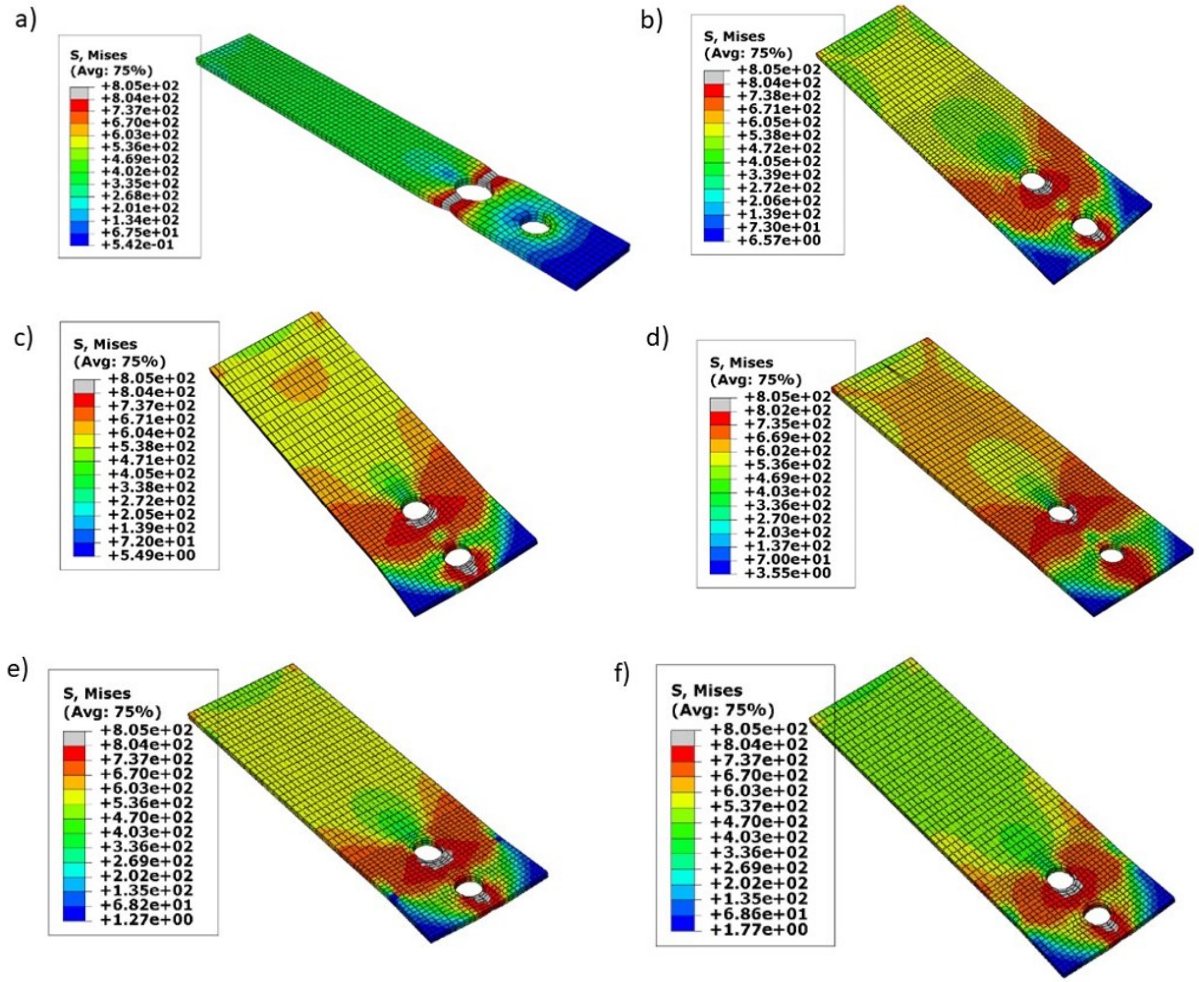

Figure 5.11. Failure Modes for test specimens a-) pa-03, b-) pa-04, c-) pa-05, d-) pa-06, e-) pa-07, f-) pa-08

In general, the load-deformation curve and resistance obtained by the finite element models achieve a good agreement with Jiang's experimental data. Therefore, the finite element models compare well to these experiments and can be used for predicting the resistance of bolted double lap joints. Table 5.2 summarizes the resistance and failure modes of joints from the experimental program and FE analysis. A solid model was established to simulate the mechanical response of bolted lap joints at elevated temperatures. The model was validated against the experimental results obtained from the authors' test and Jiang et al [49]. Due to the high computational time of the solid model and the limitations of the component method, the CBFEM was developed using shell elements and non-linear springs to predict the fire resistance and failure types of bolted lap joints at elevated temperatures. The numerical simulation can predict the mechanical response of bolted lap joint at high temperatures with reasonable accuracy. The solid model also predicts the fire resistance and failure mode of the bolted lap joints. However, high time consumption and costly computational efforts do not make it practical for structural fire design engineers.

Table 5.2. Summary of results from experiments and solid models for lap joint tests

Specimen	Resistance [kN]		Failure Modes		N_{test} / N_{FEM}
	Experiment	Solid Model	Experiment	Solid Model	
pa-03	166.6	159.2	Net section	Net section	0.96
pa-04	402.1	390.3	Bearing	Bearing	0.97
pa-05	433.5	423.6	Bearing	Bearing	0.98
pa-06	450.4	440.7	Bearing	Bearing	0.98
pa-07	400.3	405.4	Bearing	Bearing	1.01
pa-08	376.7	373.5	Bearing	Bearing	0.99

Elevated Temperature

In this section, the experimental study presented in Section 4 was used to validate the solid model in terms of resistance and failure modes of bolted lap joints at elevated temperatures. The observed failure mode was bolt in shear as the analytical model predicted. As seen in Figure 5.12-Figure 5.15, the solid model predicts the mechanical response of bolted lap joints stiffer than experimental curves. However, the results in Table 5.3 confirm that the finite element model was able to accurately predict the failure mode, failure load, and the load–deformation curves of all the tests at elevated temperatures.

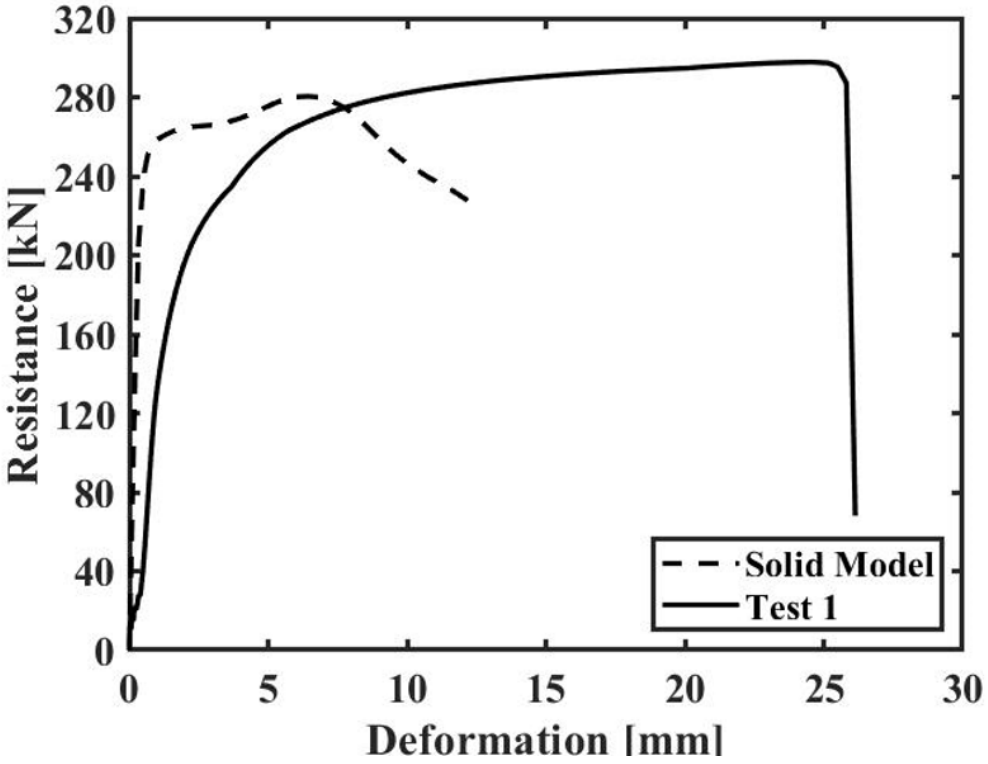

Figure 5.12. Validation of test specimen with 4 bolts at ambient temperature

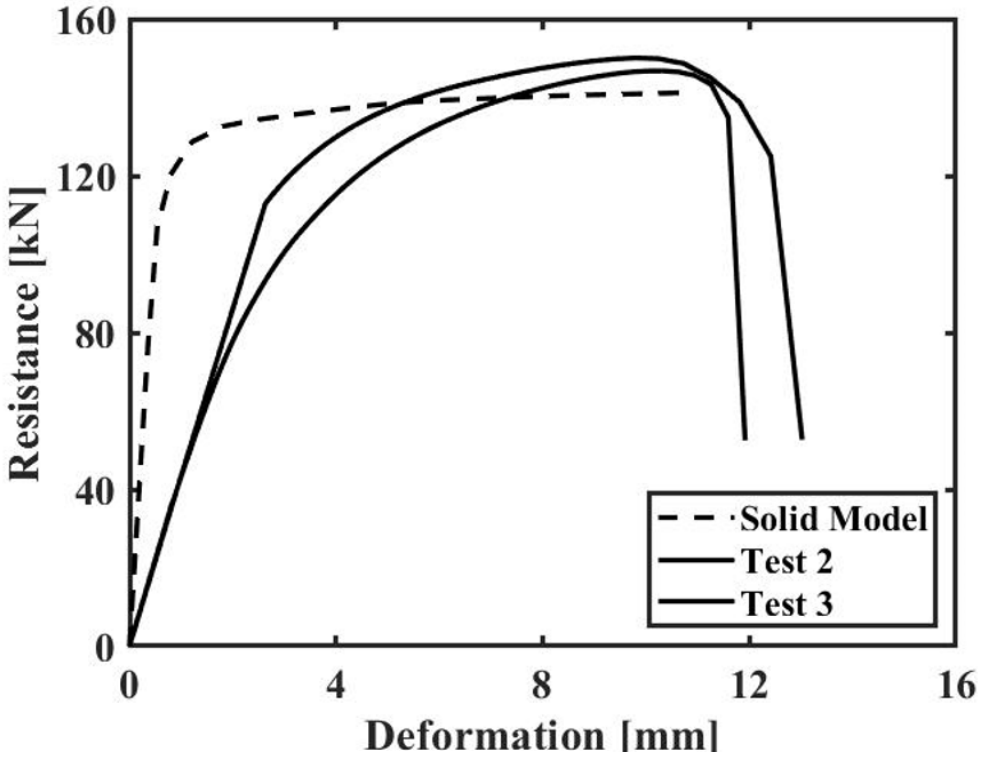

Figure 5.13. Validation of test specimens with 2 bolts at ambient temperature

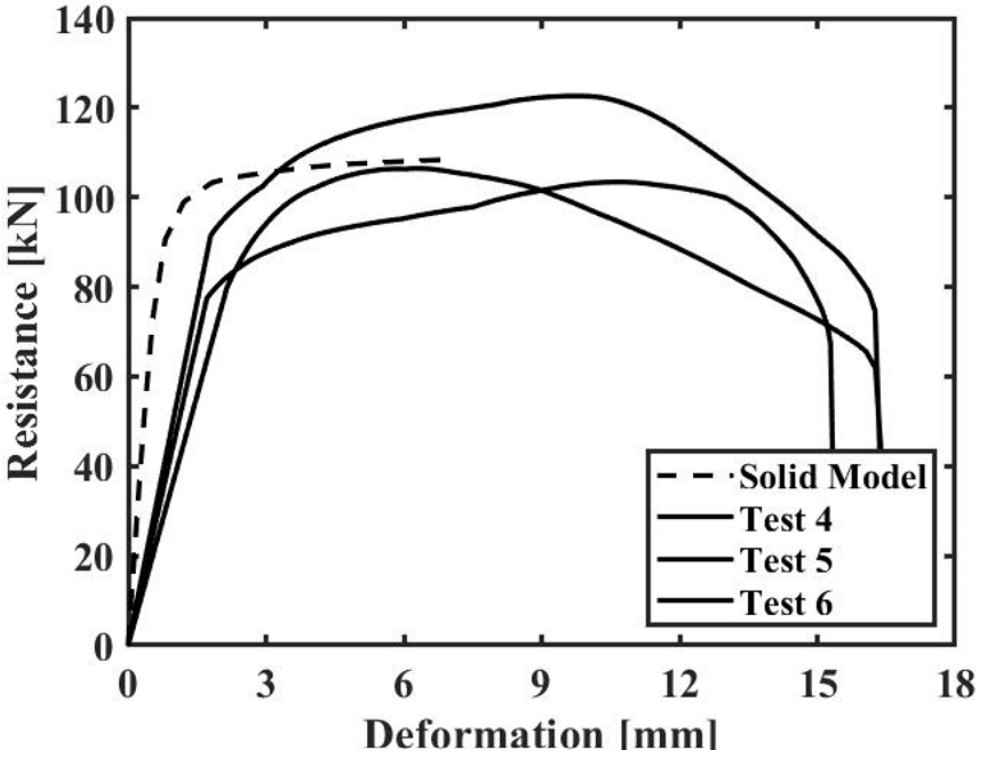

Figure 5.14. Validation of test specimens at 400°C

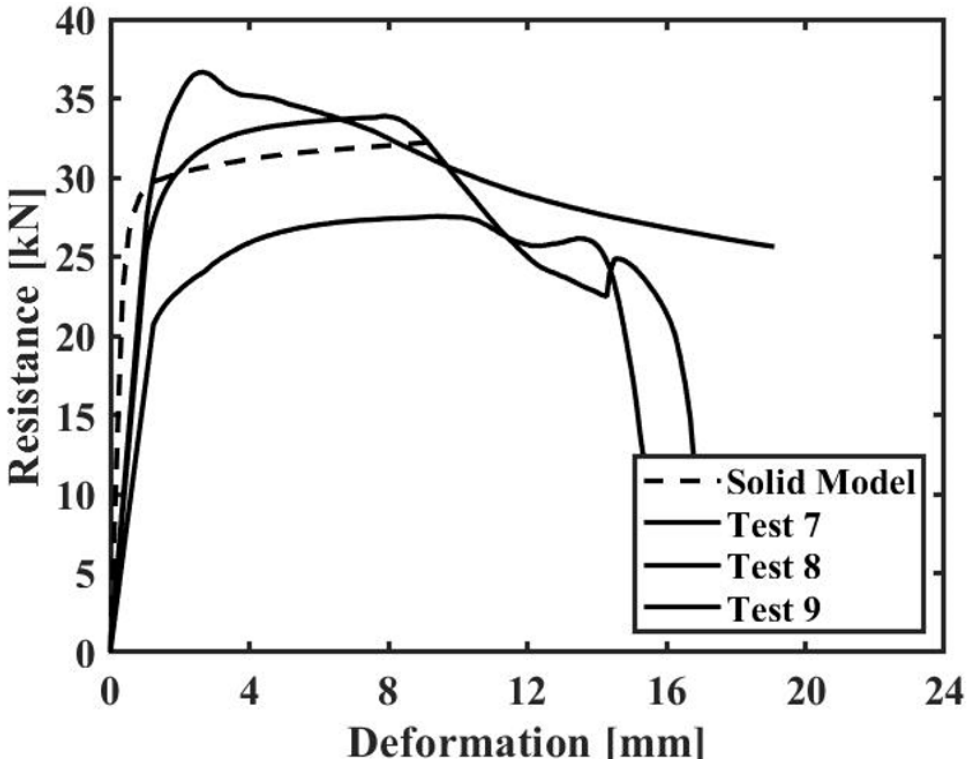

Figure 5.15. Validation of test specimens at 600°C

The comparisons on final deformation states of all bolted lap joints at 20°C, 400°C, and 600°C between numerical simulations and experimental results were indicated in Figure 5.12-Figure 5.15. Furthermore, it is possible to observe a significant difference in terms of stiffness of numerical simulation and experimental results at ambient temperature from the load-displacement curve as indicated in Figure 5.12 and Figure 5.13. It can be seen that good agreements exist on the failure type of bolted lap joints at each temperature level. Although the fracture of the bolts may not be simulated, the grey zone which exceeds the ultimate limit strain at 25% of elongation is able to show the location where the fracture evolves, as exhibited in Figure 5.16. The dominant failure mode of this specimen is clearly bolt shearing as can be seen from the equivalent stress contour plot for the most highly stressed shear planes of the bolt.

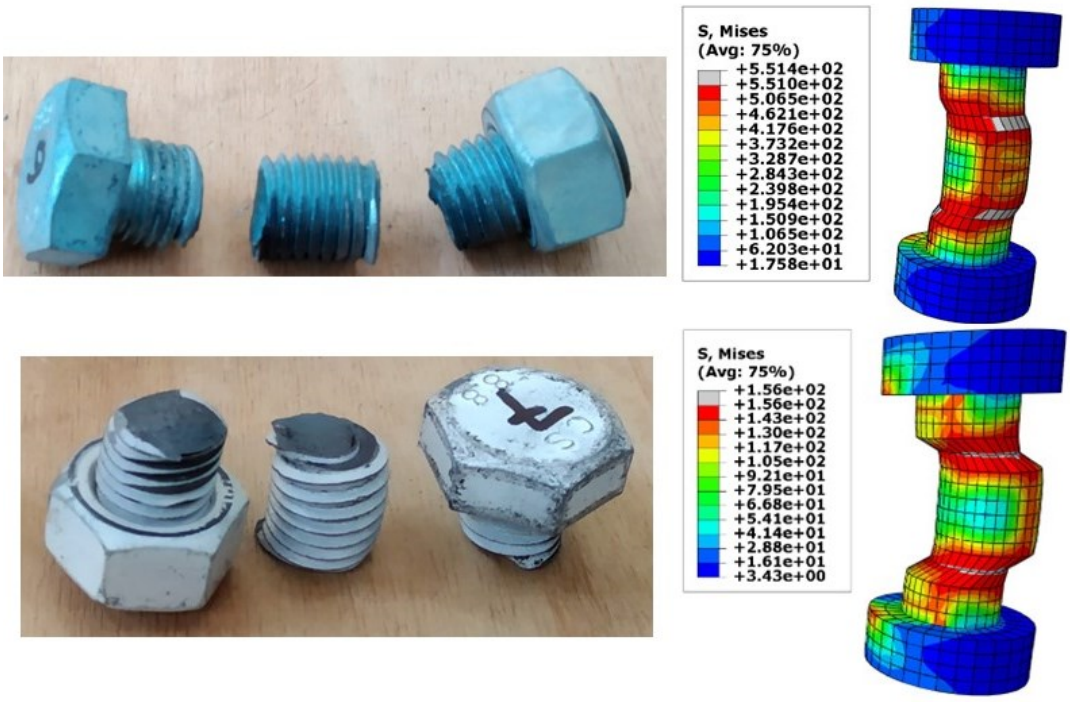

Figure 5.16. Failure modes from test and solid model

Table 5.3 lists the fire resistance derived from experimental results and numerical analysis as well as the failure modes of the specimens. The shear strength of the M16 8.8 bolt at 400°C and 600°C was reduced by 25% and 78% compared with the shear strength of the bolt at ambient temperature. The failure modes for all the specimens were the same as the governing failure modes expected from design calculation as shown in Table 5.3.

Table 5.3. Summary of results from experiments and solid models for lap joint tests

Specimens	Number of bolts	θ (°C)	Test		Solid Model	N_{FEM}/N_{test}	Failure Modes	
			Resistance [kN]	Average [kN]	Resistance [kN]		Test	Solid Model
Test 1	4	20	297.8	297.8	274.25	0.92	Bolts in shear	Bolts in shear
Test 2	2		146.7	148.4	137.84	0.93		
Test 3			150.1					
Test 4	2	400	106.4	110.8	106.49	0.96	Bolts in shear	Bolts in shear
Test 5			122.6					
Test 6			103.4					
Test 7	2	600	36.7	32.7	30.58	0.94	Bolts in shear	Bolts in shear
Test 8			33.9					
Test 9			27.5					

5.1.6. Verification

In order to verify the solid model, the resistance of bolted lap joints at elevated temperatures was evaluated using Eqs (18) and (19). The comparison between the resistances obtained from the solid model and analytical models is presented in Figure 5.17.

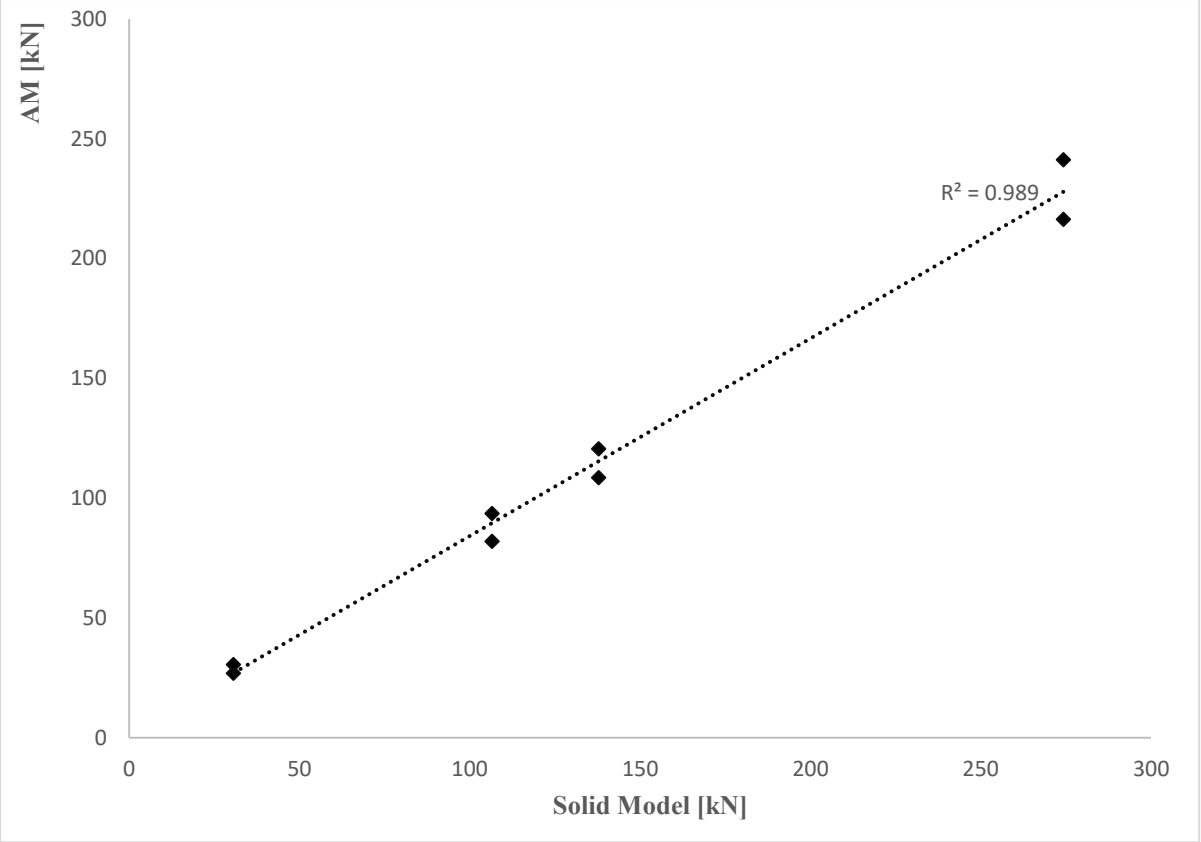

Figure 5.17. Influence of temperature on bolt shear resistance

The effects of temperature on the structural behaviour and failure loads of bolted lap joints are investigated herein. The analytical resistance of bolted lap joints at different temperature levels is plotted against the corresponding resistance obtained from the solid model in Figure 5.17. A very high coefficient of determination R^2 of 0.997 was obtained from a linear regression analysis. It can be concluded that both the numerical simulation and analytical model predict the same failure load. Figure 5.18 depicts the deformed shape of bolted lap joints obtained in the solid model. The bots failed due to shear and the cover plates curled up as observed in Figure 4.7.

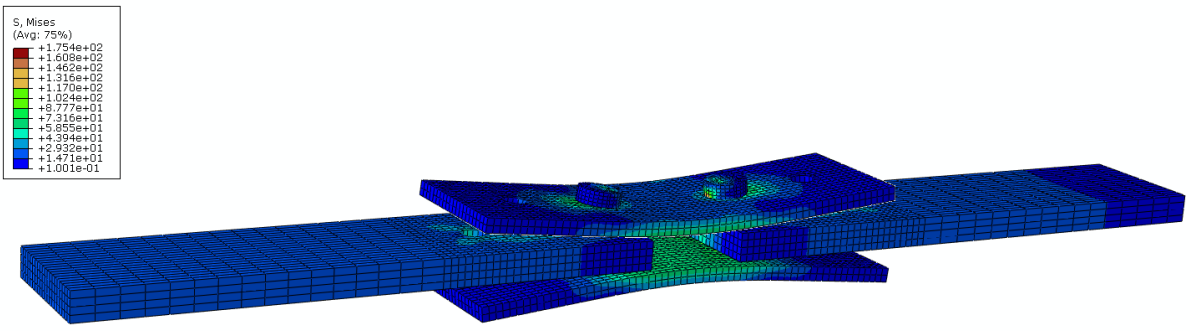

Figure 5.18. Deformed shape of bolted lap joints in the solid model

5.2. Shell Model for Steel Beam

Since the objective of this thesis is to investigate the fire response of steel joints and steel members, the shell model is generated using Abaqus software. Furthermore, the developed model may be used to verify the CBFEM models for steel members at elevated temperatures. However, the verification study requires the validated numerical model. Therefore, the generated model is validated against an experimental study.

5.2.1. Development of finite element model

The finite element models were generated utilizing the finite element analysis software Abaqus [11] in this paper. A four-noded reduced integration shell element (S4R) is used to mesh all the finite element models. S4R may consider transverse shear deformations and membrane stresses. The Simpson integration method was employed with five integration points through the thickness of an element. There are different beam configurations for verification and validation studies. The material model used in the shell model for the steel beam is shown in Figure 5.1. The tested steel beam configuration is presented in Figure 3.11. The details of the experimental study of steel beams are described in Section 3.3.2. The boundary conditions are applied to the bottom flange of a steel beam. The load is applied to the web in the mid-section of the steel beam as a line force. Each portioned part of the steel beam is heated according to Figure 3.12. To define mesh size in the shell model, 20 elements across the web height and 10 elements across the flange width were used.

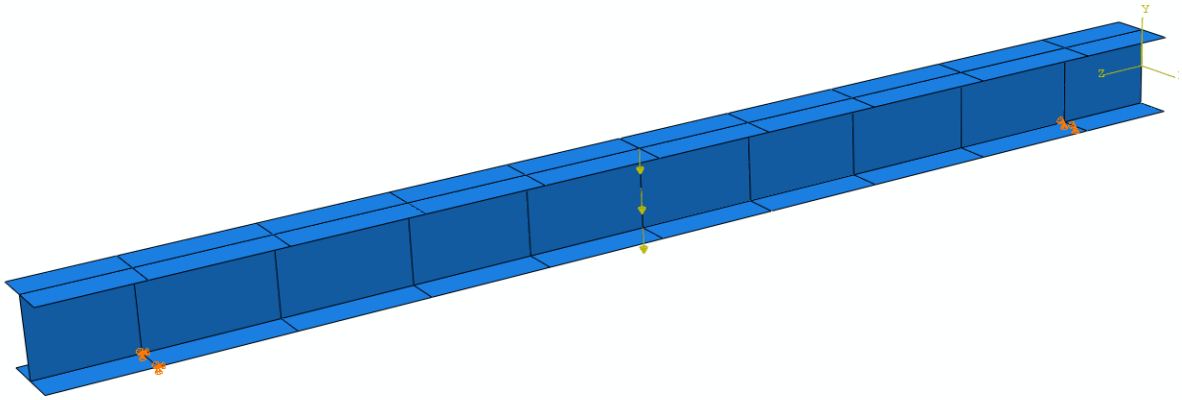

Figure 5.19. Shell model of steel beam for validation

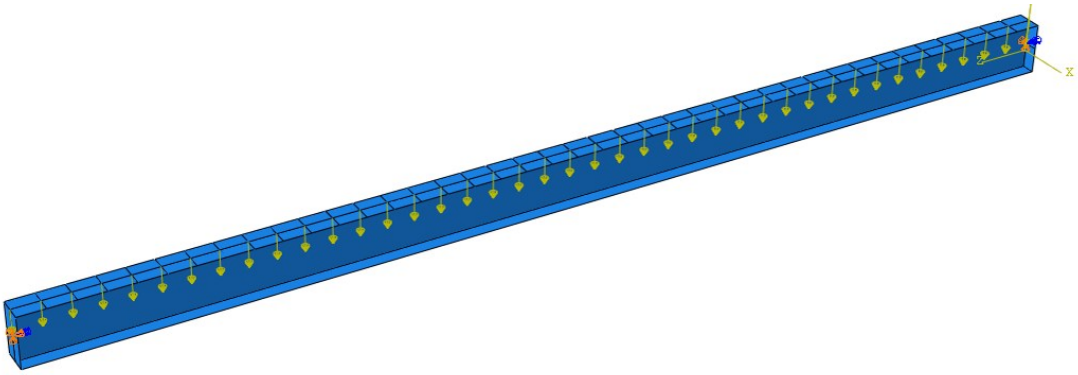

Figure 5.20. Shell Model of steel beam under distributed load for verification study

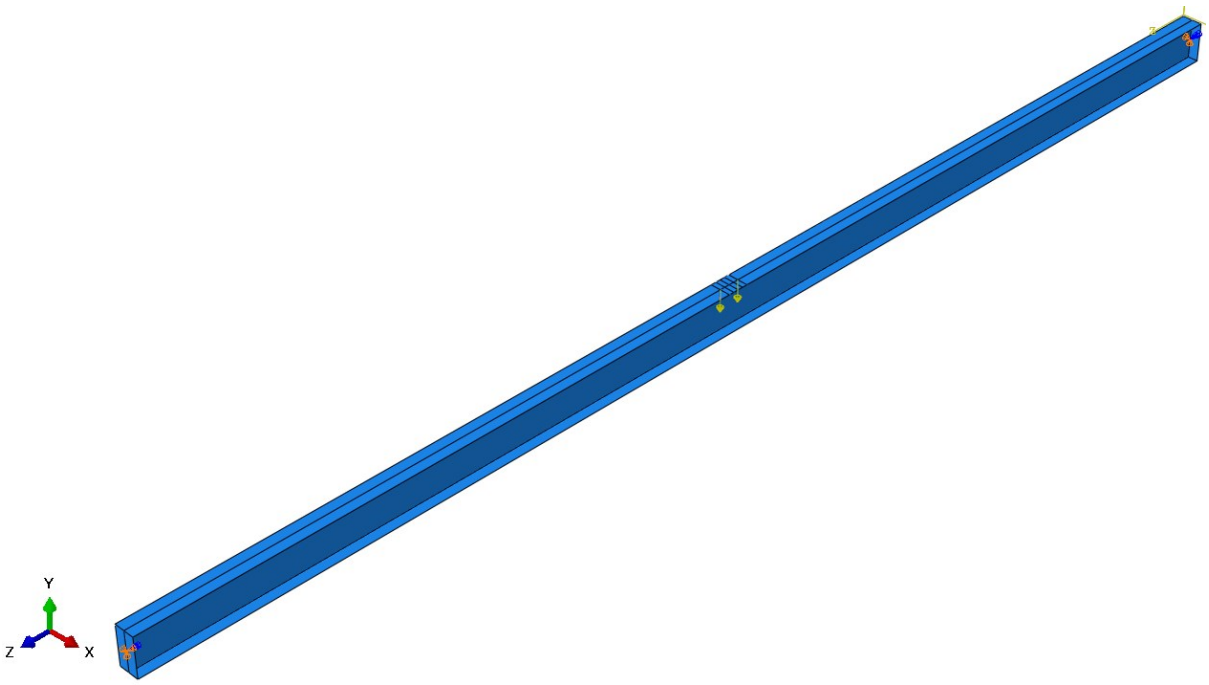

Figure 5.21. Shell Model of steel beam under point load for verification study

Figure 5.20 and Figure 5.21 show the shell model generated for the verification study of steel beams at elevated temperatures. The point at the mass centre of the endplate is coupled to the red line along the width of the endplate using kinematic coupling constraints. On the left side of the model, the movements in all directions and the rotation in the -z direction were constrained, whereas the movement in the -z direction was allowed on the right side of the model to obtain a simply supported beam. The concentrated load was equally applied to five nodes at the top flange with a 25 mm distance to each node. There was no defined constraint in the flanges because it was aimed to provide no warping constraint. Furthermore, the distributed load and fixed-end support were also investigated in this study. The distributed load was applied at the top flange overall span with a 150 mm distance. The total number of nodes used to apply load was 41. To provide fixed-end support conditions, the reference node at the centre of mass was coupled to the beam section including flanges and web. The only degree of freedom that is not constrained is the movement in the z-direction at the right side of the beams. To find the bending resistance of beams, the static general analysis was used without imperfection. Then, a set of simulations was performed with geometric imperfection incorporated from the first mode eigenvalue buckling analysis considering the maximum amplitude of e_0/L (see table 5.1 in EN 1993-1-1[107]). Initial geometric imperfections were applied following the beam's eigenmodes obtained by linear buckling analysis (LBA).

5.2.2. Validation

The validation of the finite element models created in this study against the experiments carried out by Torić et al. [5]. The study involves the numerical result obtained from Vulcan software. The experimental study is explained in Section 3.3.2. The load-deformation curves given from the experimental test, Vulcan software, and the shell model are presented in Figure 5.22 and Figure 5.23. The results show that the shell model is able to fit the test results more accurately than Vulcan software. The discrepancy between the experimental study and the numerical studies, as shown in Figure 5.22, is the additional deformation due to creep strain which is not considered in numerical studies.

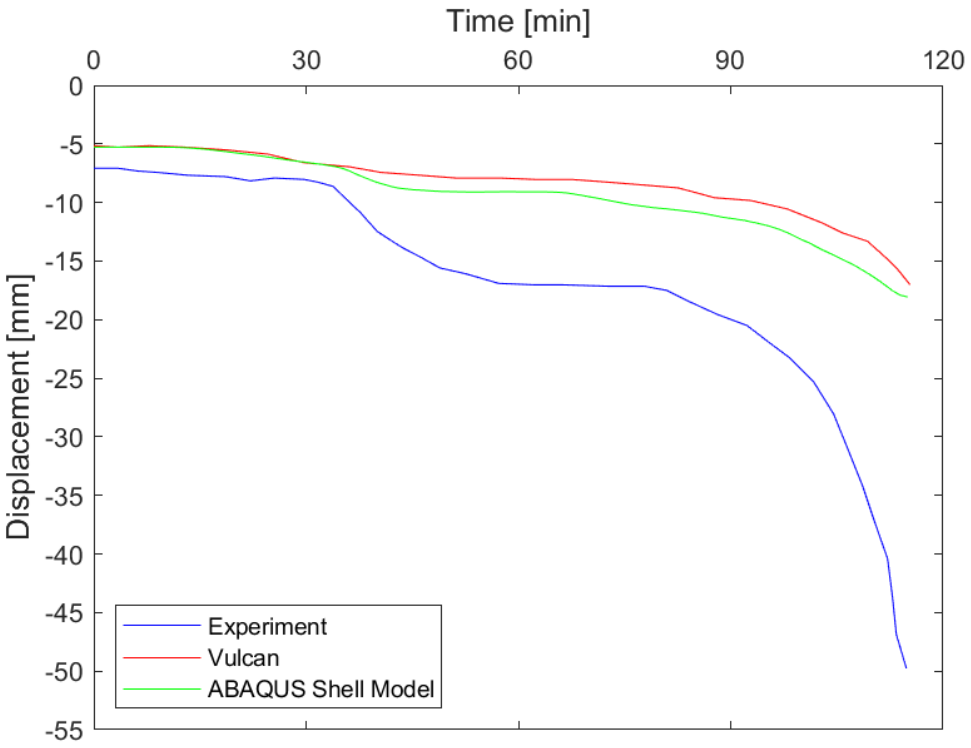

Figure 5.22. Comparison of shell model results with experiment and Vulcan- test 1

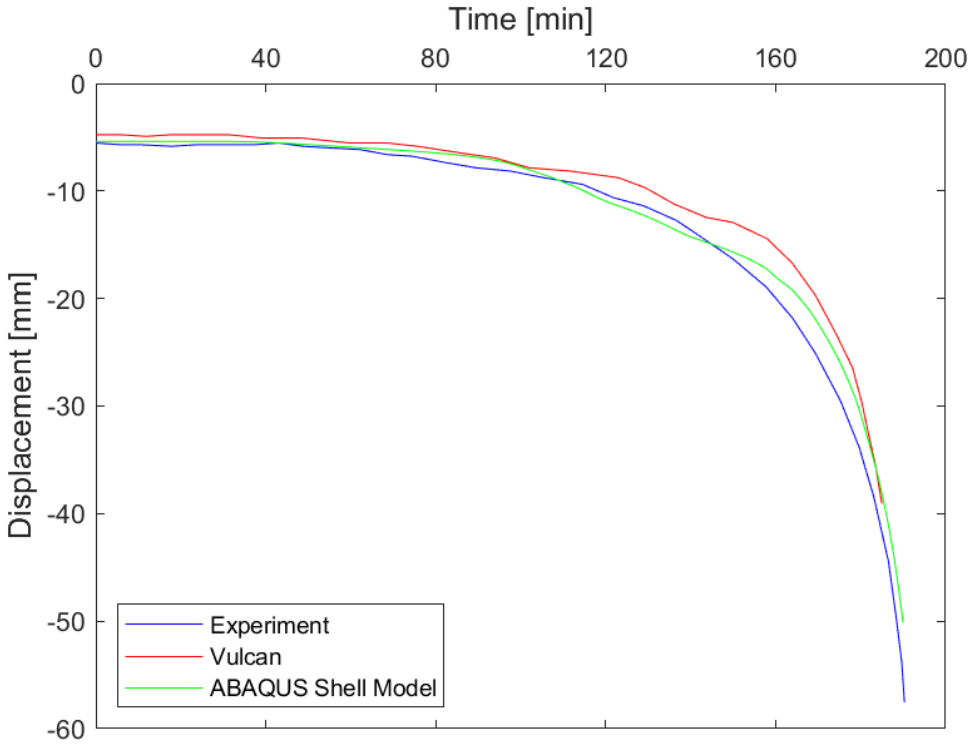

Figure 5.23. Comparison of shell model results with experiment and Vulcan- test 3

5.3. CBFEM Models for Joints

The CBFEM models are generated using the IDEA StatiCa Connection [108] to simulate the behaviour of steel joints at elevated temperatures. IDEA StatiCa Member [109] is used to develop the CBFEM models to investigate the mechanical response of steel members at elevated temperatures.

Design checks are given in Table 3.2 of EN 1993-1-8 for bolts in shear, in tension, and in the interaction of shear and tension. These design checks are modified using the reduction factors in EN 1993-1-2 for the resistance of steel joints at elevated temperatures. EN 1993-1-5 [13] recommends a 5% limit strain for the failure of plates at ambient temperature. One of this thesis's goals is to investigate the use of 5% plastic strain to determine the resistance of steel plates at elevated temperatures. Therefore, the prediction of steel connection and member resistance depends on the recommended plastic strain and design checks for bolts and welds. The CBFEM applies the specific temperature to the components of steel joints. The heat transfer is not included in the CBFEM model.

5.3.1. Bolted Lap Joints

To verify and validate the CBFEM models at elevated temperatures, different types of joints are selected to investigate the components defined in EN 1993-1-8. The selected joints are bolted lap joints, T-stubs, flush endplate joints, and fin plate joints in this thesis. In bolted lap joints, there are four different resistances and deformation modes, that need to be considered: bearing of the plate and/or bolt, shear in the plates, tension in the plates, and shear in the bolt shank, as shown in Figure 5.24. Internal forces (shear, bearing, and tension) may be transferred by bolts and by friction between plates. The main drawback of the component method is the analysis of the stresses and strains of individual components.

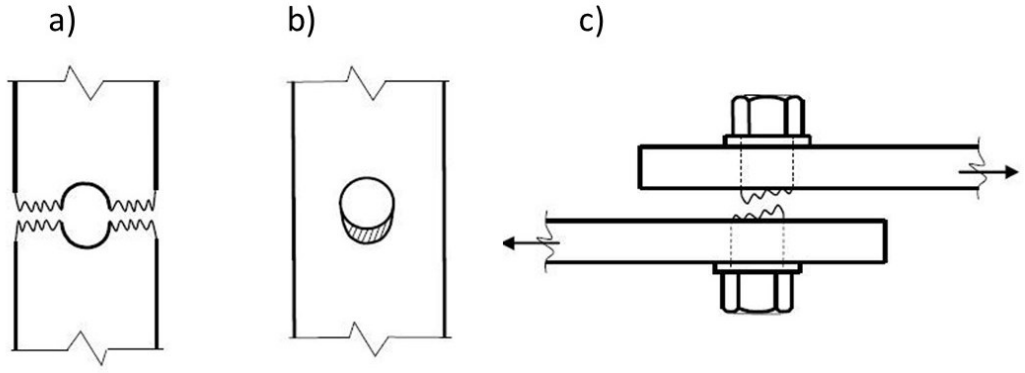

Figure 5.24. Failure modes of bolted lap joints a) net section, b) bearing and c) bolt in shear

The assembly of bolted lap joints is illustrated in Figure 5.25. The inner plate (M1) was fixed, and the member (M2) was chosen as analysed member. Due to the convergence problems, the analysed member was constrained in the rotation when the analysed member was fastened with 1 bolt. The heat transfer in bolted lap joints is not considered. Therefore, the targeted temperature was applied to the components of joints by the author.

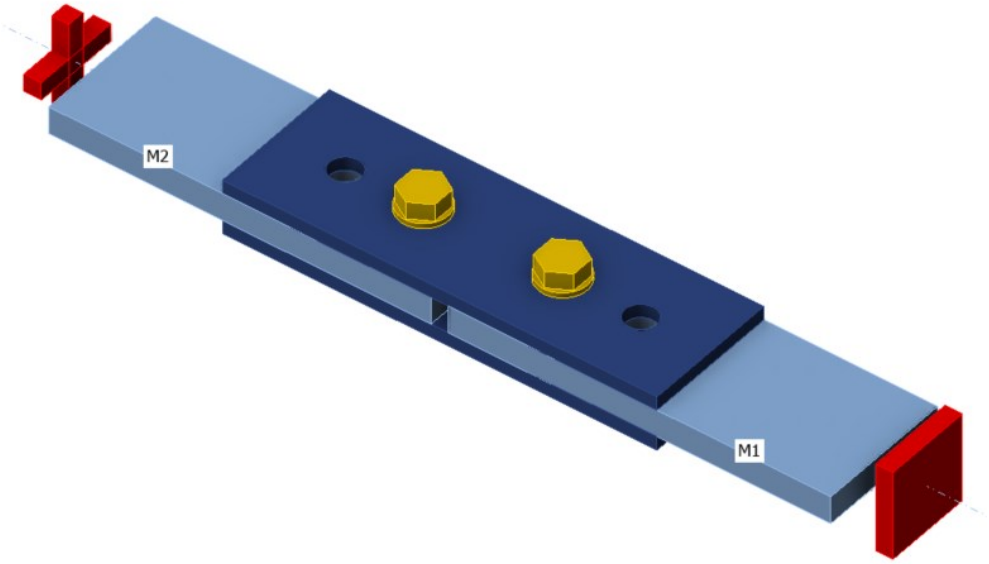

Figure 5.25. Assembly of the studied bolted lap joints

Mesh Sensitivity Study

The resistance of the bolted lap joint for a varying number of elements dividing the plates is shown in Figure 5.26. After using 14 elements on plate meshing, the numerical stability is provided to predict the stable resistances. Therefore, the number of mesh elements used for CBFEM is selected as 16.

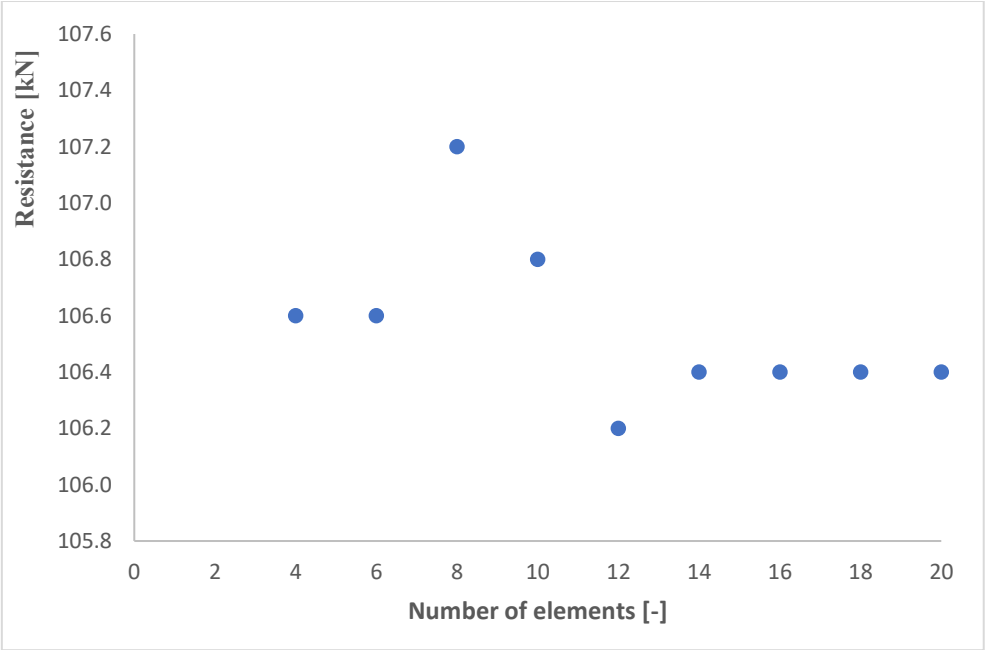

Figure 5.26. Effect of the element number on the resistance at elevated temperature

Verification

The cover and connected plates were fabricated from a single steel plate, grade S355. The specimens were tested at 3 different nominal temperature θ levels, namely, at ambient temperature 20 °C and elevated ones 400 °C and 600 °C. The details of the test specimen and the model are shown in Figure 5.27. The thickness of the inner and cover plates are 8 mm and 16 mm, respectively. More details can be found in the Section 4.

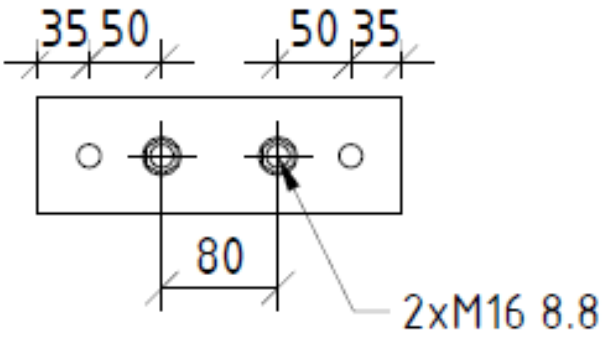

Figure 5.27. Details of the bolted lap joint

A comparison of the bolted lap joint's ultimate resistance for analytical calculation according to EN 1993-1-8 [12] and AISC [110], the solid model, and the CBFEM is shown in Figure 5.28. It can be found that the maximum deviation of ultimate resistances between CBFEM model and analytical solution is 10%, which means good agreement exists. The main difference between Eurocode and CBFEM resistance is the state of tensile force on bolts. The analytical model assumes that the bolt is exposed to pure shear force, however, the CBFEM is able to calculate the tensile force that occurs in the bolt using the advantage of the finite element model. The solid model and analytical model predict the failure mode as a bolt in shear. In CBFEM the model stops due to the interaction of shear and tension.

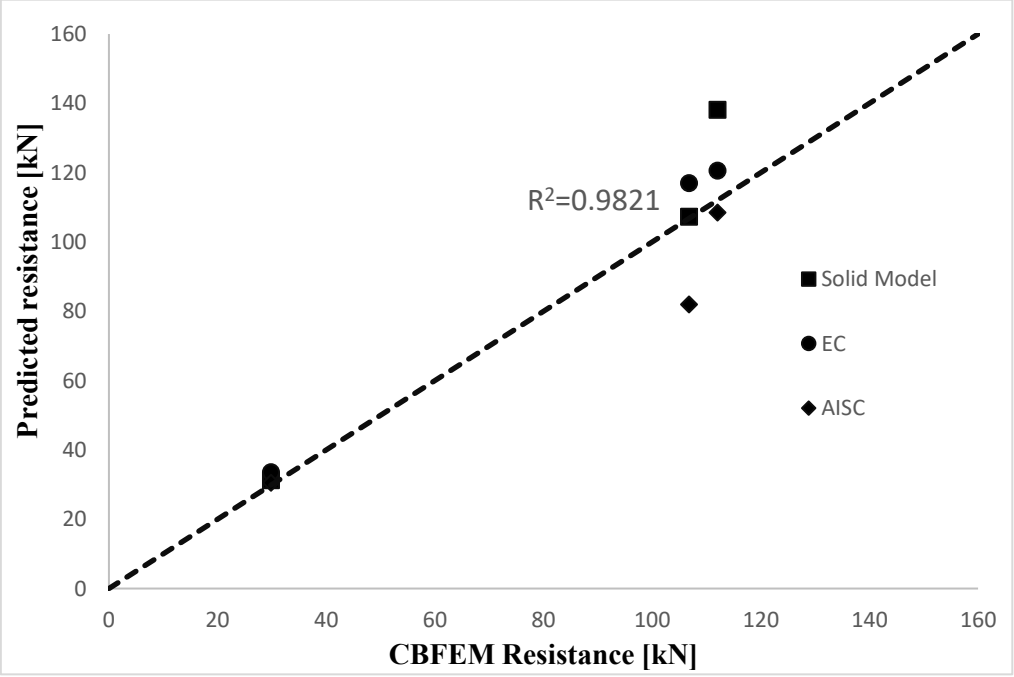

Figure 5.28. Comparison of the resistance between the CBFEM results and the predicted resistance by the solid model and design specifications.

The sensitivity study is carried out by changing several parameters, as listed in Table 5.4, to assess the accuracy of the verification study on the mechanical response of bolted lap joints at elevated temperatures. Design resistances calculated by CBFEM were compared with the results of the analytical model (AM). In order to study the effect of different parameters on the resistance and failure modes of bolted lap joints, sensitivity studies are performed changing several parameters of the tested specimen characteristics. Results are summarized in Table 5.4. Steel grade was in all cases

S355. The parameters are temperature, bolt material, splice thickness, bolt diameter, and bolt distances. The number of bolts is 4 whereas only 2 bolts are used to fasten plates. Figure 5.29-Figure 5.33 graphically presents the comparison of resistance values obtained from analytical and CBFEM models at different temperatures. The results show that the CBFEM predicts the resistance of bolted lap joints less than the analytical model.

Table 5.4. Comparison of resistances from AM and CBFEM

Parameter	Analytical Model (AM)		CBFEM		CBFEM/AM
	Resistance kN	Critical Component	Resistance kN	Critical Component	
Temperature (°C)	Joint description: member plates 80/16 mm, bolts 2xM16 8x8 in distances p=50 mm, e1=35, splices 2x80/8 mm, steel S355				
20	241.2	Bolts in shear	230.2	Bolts in shear	0.95
400	233.6	Bolts in shear	204.2	Tension-shear	0.87
500	165.8	Bolts in shear	140.4	Bolts in shear	0.85
600	66.3	Bolts in shear	55.1	Bolts in shear	0.83
700	30.1	Bolts in shear	24.4	Bolts in shear	0.81
Bolt Material	Joint description (500°C): member plates 80/16 mm, bolts 2xM16 in distances p=50 mm, e1=35, splices 2x80/8 mm, steel S355				
5.8	86.4	Bolts in shear	75.1	Bolts in shear	0.87
6.8	103.6	Bolts in shear	90.1	Tension-shear	0.87
8.8	165.8	Bolts in shear	140.4	Bolts in shear	0.85
10.9	172.7	Bolts in shear	150.2	Tension-shear	0.87
Splice Thickness	Joint description (600°C): member plates 80/16 mm, bolts 2xM16 8x8 in distances p=50 mm, e1=35, splices 2x80/t2 mm, steel S355				
4	22.8	Bearing	22.6	Bearing	0.99
6	34.3	Bearing	34.1	Bearing	1.00
8	45.7	Bearing	45.5	Bearing	1.00
12	57.1	Bolts in shear	56.1	Tension-shear	0.98
Bolt Spacing	Joint description (500°C): member plates 80/16 mm, bolts 2xM16 8x8 in distances, splices 2x80/8 mm, steel S355				
p=40, e1=25 mm	158.4	Bearing	140	Bearing	0.88
p=50, e1=35 mm	165.8	Bolts in shear	140.4	Bolts in shear	0.85
p=55, e1=40 mm	165.8	Bolts in shear	140.5	Bolts in shear	0.85
p=70, e1=55 mm	165.8	Bolts in shear	140.6	Bolts in shear	0.85
Diameter	Joint description (400°C): member plates 80/16 mm, bolts 2x 8x8 in distances p=50 mm, e1=35, splices 2x80 mm, steel S355				
M12	125.0	Bolts in shear	111.8	Tension-shear	0.89
M16	165.8	Bolts in shear	140.4	Bolts in shear	0.85
M20	315.3	Bearing	301.9	Bearing	0.96
M22	311.0	Bearing	296.3	Bearing	0.95

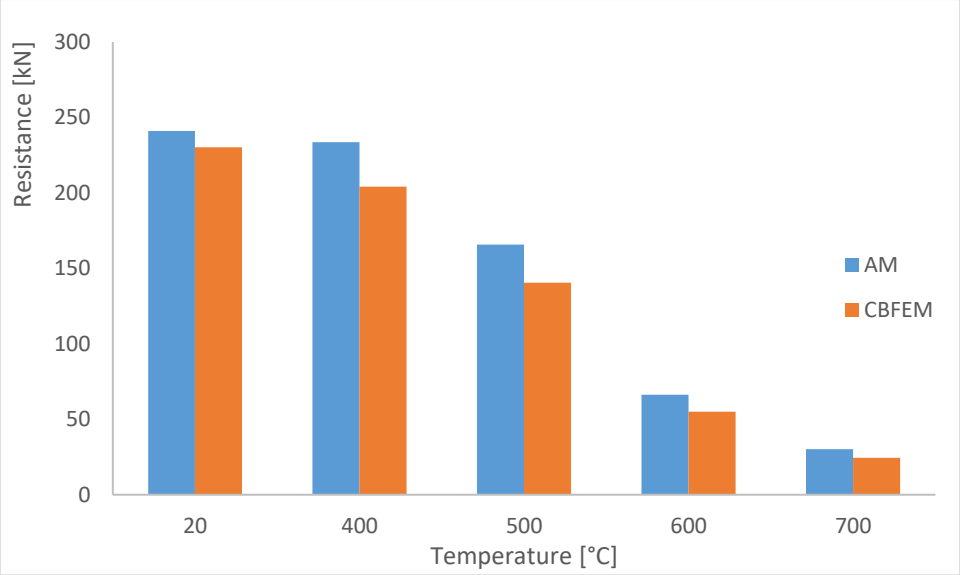

Figure 5.29. Sensitivity study for temperature change

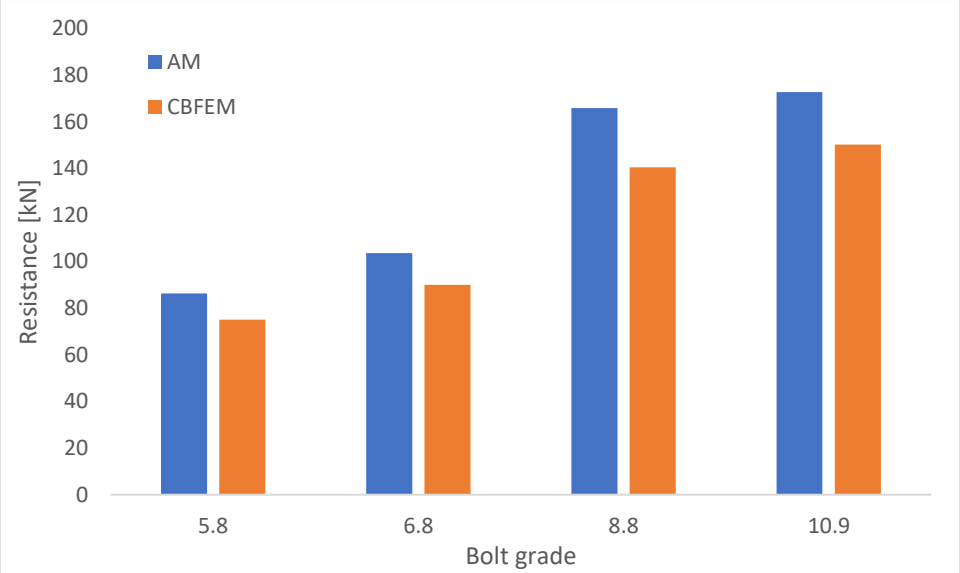

Figure 5.30. Sensitivity study for the bolt grade (500°C)

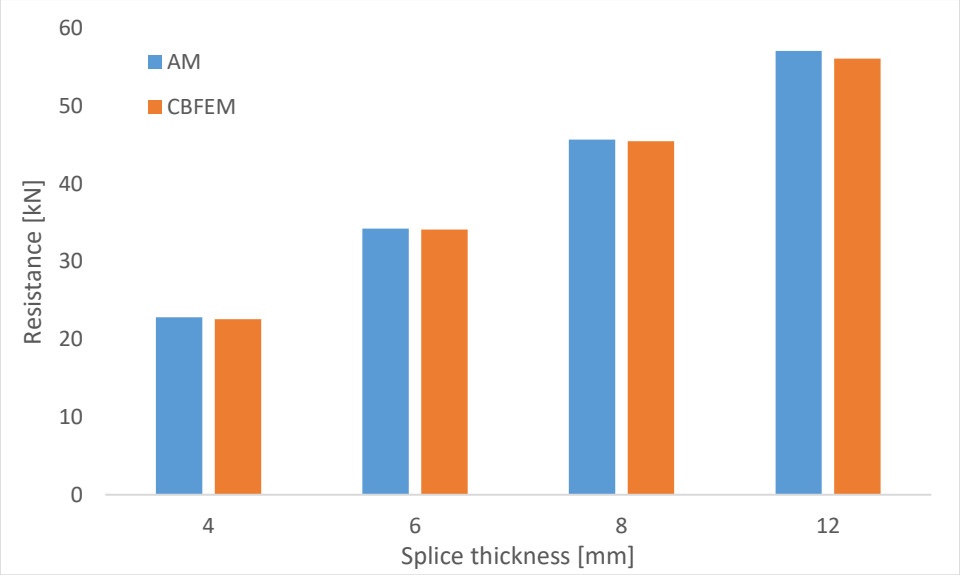

Figure 5.31. Sensitivity study for the splice thickness (600°C)

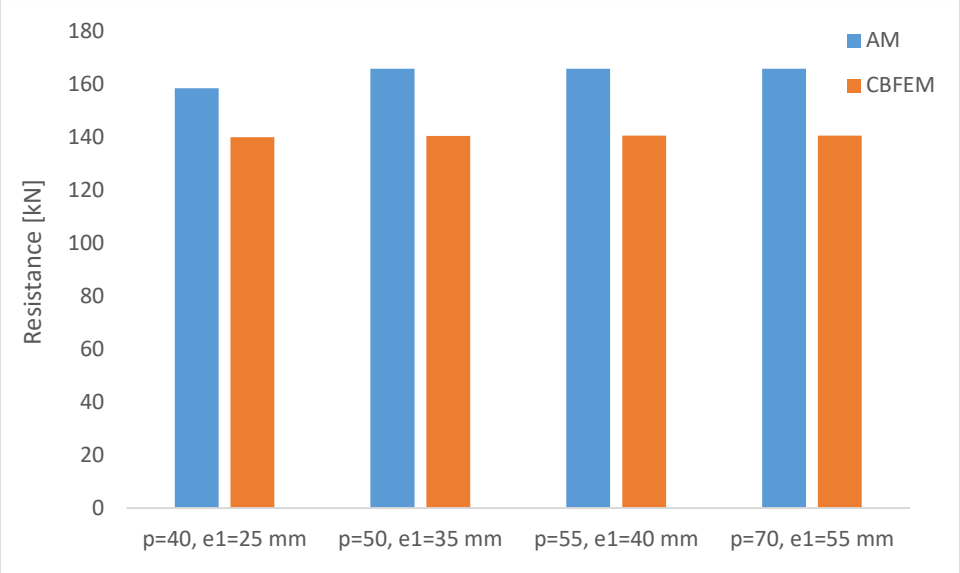

Figure 5.32. Sensitivity study for the bolt spacing (500°C)

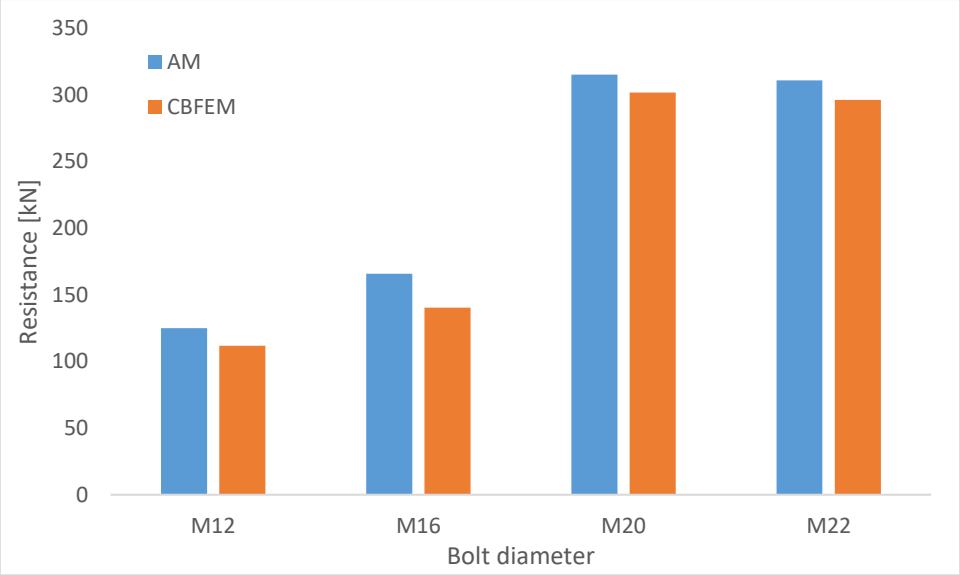

Figure 5.33. Sensitivity study for the bolt size (400°C)

Validation

Validation of the generated CBFEM models was conducted by comparing the experimentally obtained resistances, load– deformation curves, and failure modes against their numerical counterparts. The CBFEM model shows very safe agreement with the test results as displayed in Figure 5.34-Figure 5.37.

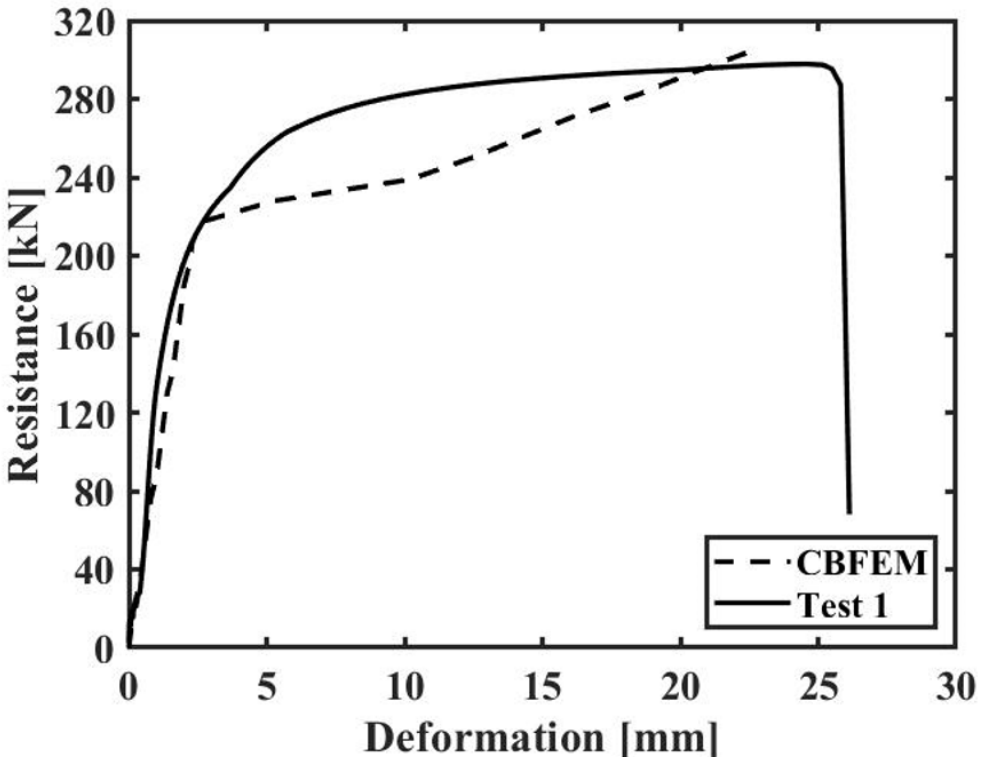

Figure 5.34. Validation of test specimen with 4 bolts at ambient temperature

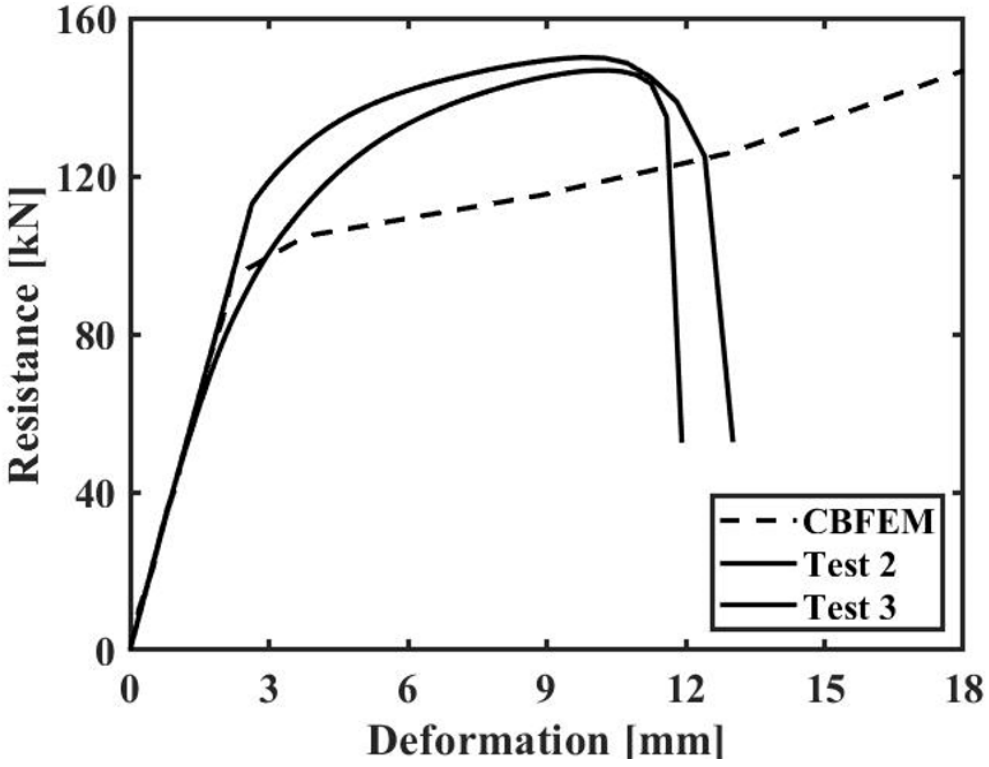

Figure 5.35. Validation of test specimen with 2 bolts at ambient temperature

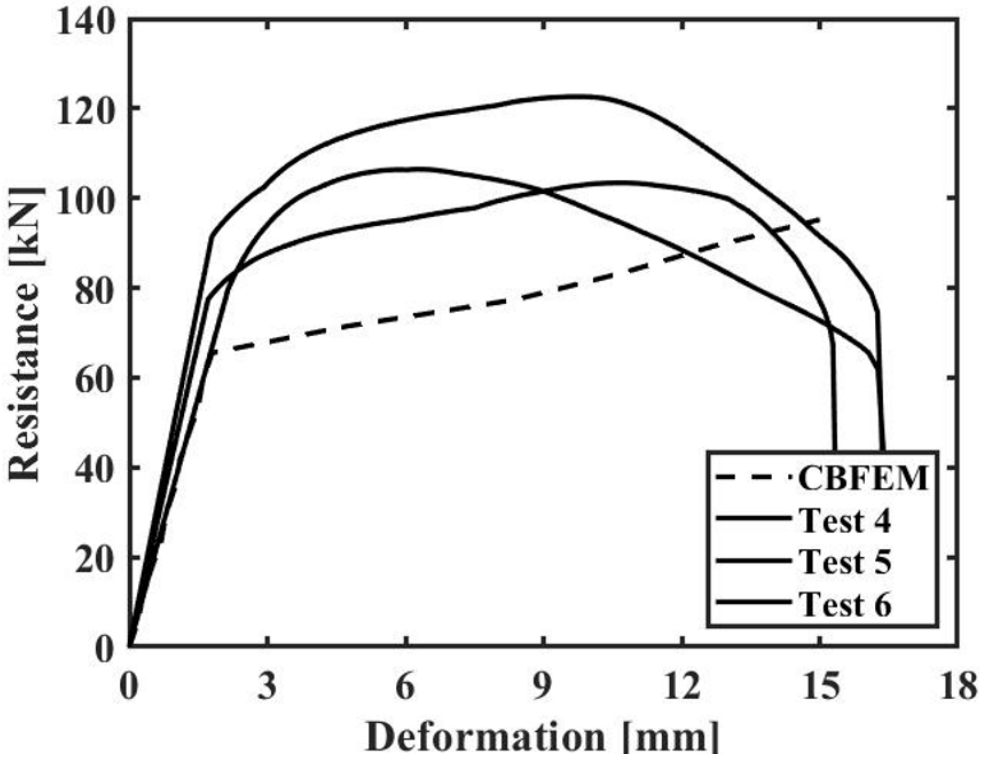

Figure 5.36. Validation of test specimen at 400°C

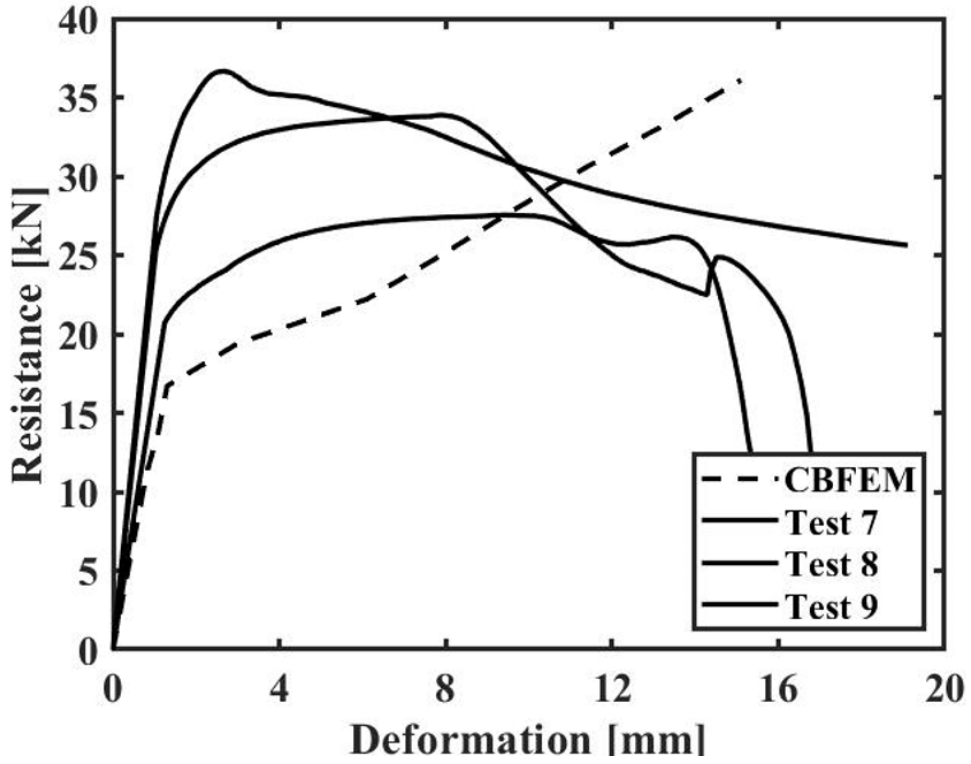

Figure 5.37. Validation of test specimen at 600°C

Table 5.5 reports the ratios of the test resistance to the predicted resistance in CBFEM and the failure mode predictions for the 9 bolted lap joint specimens. The CBFEM provides more conservative resistances at ambient temperature than at elevated temperatures due to the multiplication of the temperature-reduced resistance with the safety factor ($\frac{\gamma_{M2}}{\gamma_{fi}}$) proposed in EN 1993-1-2. As seen in Figure 5.38, the deformation of plates happened in addition to bolt shear failure. This deformation results in the occurrence of tensile force in bolts. The deformed shape of the test specimens obtained from CBFEM is shown in Figure 5.38. It can be seen that the bolts reach the full capacity and the plates curled up. The failure mode of test specimens in CBFEM is the interaction tension and shear.

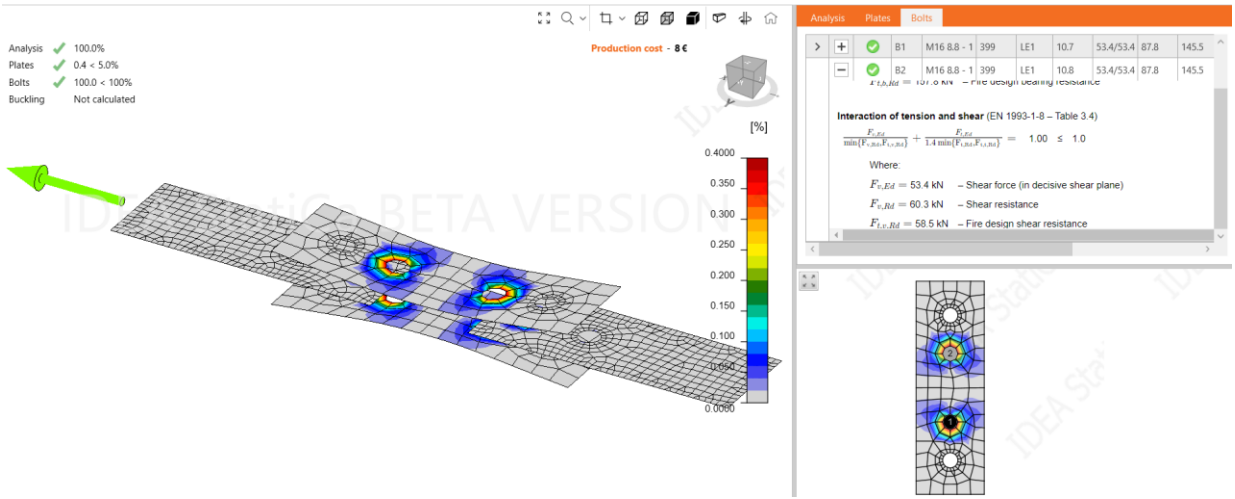

Figure 5.38. Deformed shape of bolted lap joints at 400°C

Table 5.5. Summary of results from experiments and CBFEM for lap joint tests

Specimens	Number of bolts	θ (°C)	Test		CBFEM	N_{CBFEM}/N_{test}	Failure Modes	
			Resistance [kN]	Average [kN]	Resistance [kN]		Test	CBFEM
Test 1	4	20	297.8	297.8	224	0.75	Bolts in shear	Interaction of tension and shear
Test 2	2		146.7	148.4	112	0.75		
Test 3			150.1					
Test 4	2	400	106.4	110.8	106.8	0.96	Bolts in shear	Interaction of tension and shear
Test 5			122.6					
Test 6			103.4					
Test 7	2	600	36.7	32.7	29.8	0.94	Bolts in shear	Interaction of tension and shear
Test 8			33.9					
Test 9			27.5					

Parametric Study

Extensive parametric studies are performed to understand the behaviour of the bolted lap joints and investigate the different failure types at elevated temperatures. The test specimens from Jiang et al [24] and the presented experimental study in Section 4 were used to conduct parametric studies. The tested parameters are temperature, bolt grade and diameter, steel grade, end distance, and plate thickness. Through the validated accurate solid model and CBFEM, the parametric analysis of the mechanical behaviour under fire was carried out to obtain the key influencing factors of the fire resistance and failure modes of bolted double lap joints. Moreover, parametric studies were used to check the accuracy of 5% plastic limit strain in shell elements proposed by EN 199-1-5 at elevated temperatures.

The test specimens pa03 and pa08 from the study [49] were chosen for parametric study since the specimens have two different failure modes: net section and bearing failure. The validated solid model and CBFEM were used to analyse the behaviour of specimens at high temperatures. The effects of temperature on the selected specimens are depicted in Figure 5.39 and Figure 5.40. The targeted temperature values are 400°C, 500°C and 600°C. Figure 5.41 summarizes the comparison of the numerical simulation results and the CBFEM results for test specimens in the study. The coefficient of determination value of the summary equals 0.9918.

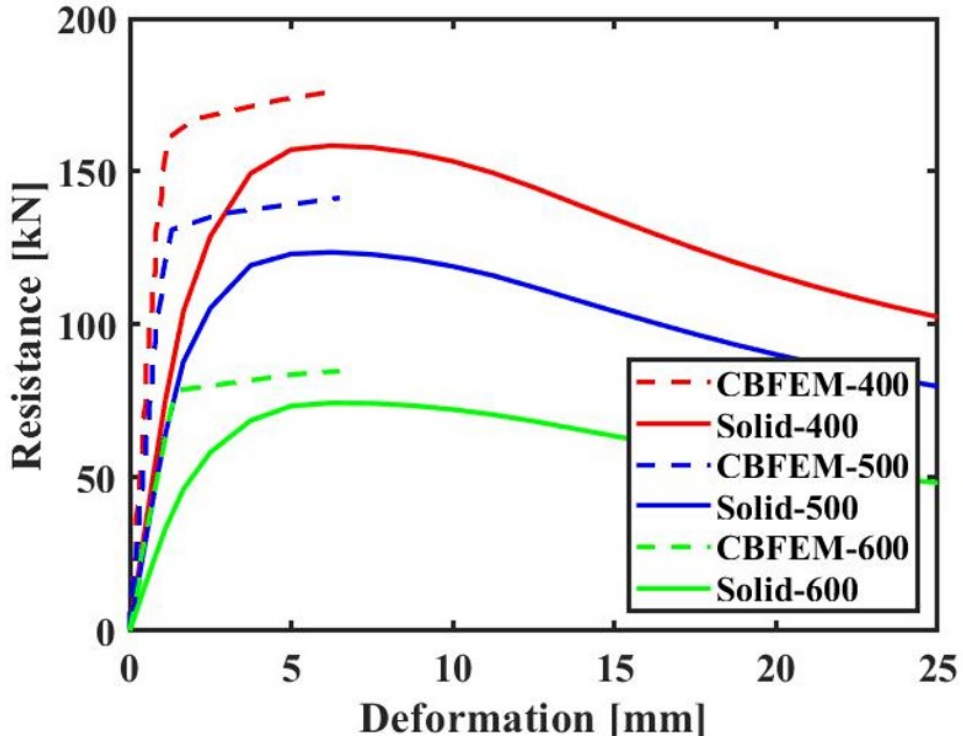

Figure 5.39. Influence of temperature on test specimen pa-03

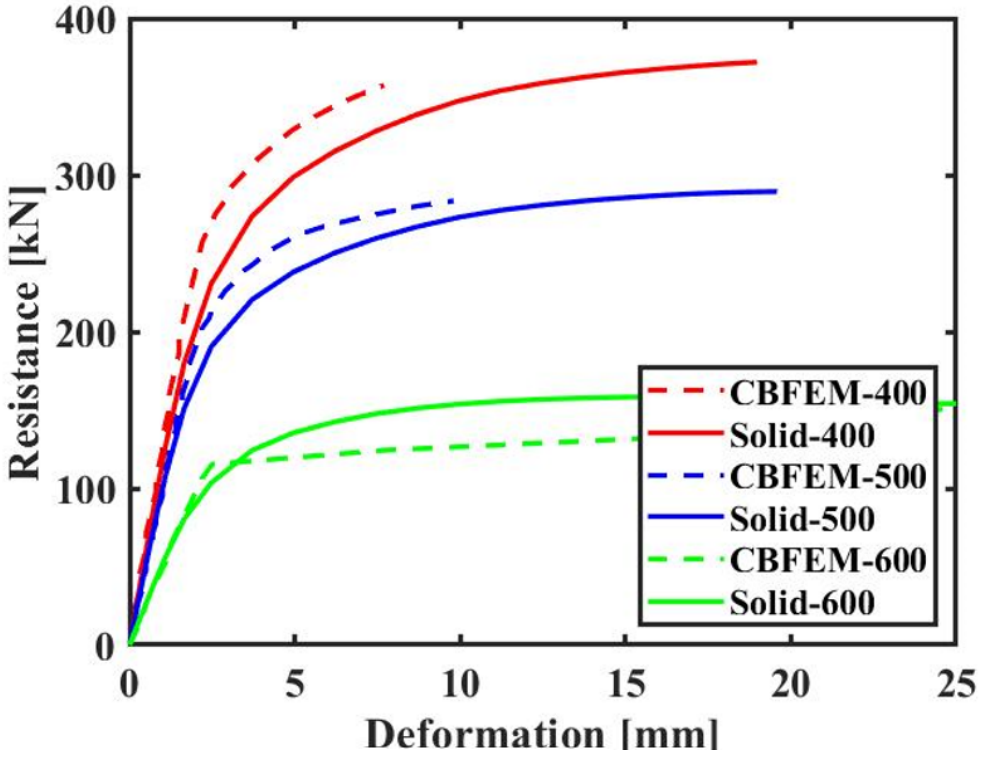

Figure 5.40. Influence of temperature on test specimen pa-08

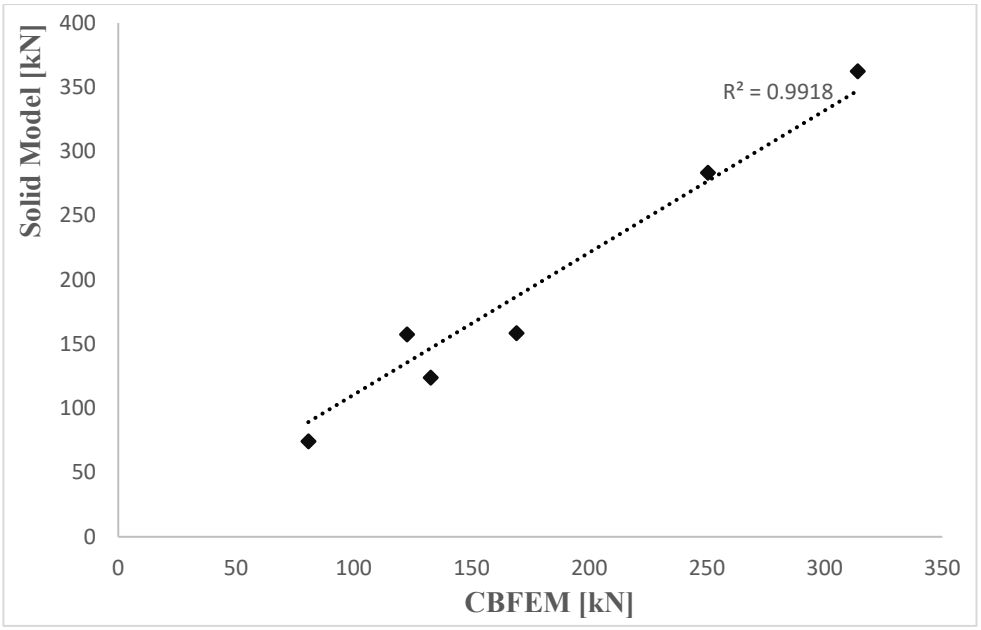

Figure 5.41. Summary of comparison between the solid model and the CBFEM model

The parametric studies were performed using the test specimens from CVUT experiments. The studied factors are bolt grade, steel grade, end distance, and plate thickness. The parametric studies were prepared at different temperature levels to investigate the severity of fire on steel joints. From the previously reported Eqs. (1)-(9), it can be seen that the resistance of bolted lap joints is mainly affected by the geometrical characteristics, bolt, and steel properties. The effect of bolt diameter and grade, steel grade, end distance, and thickness of the inner plate on the bolted lap joint behaviour is studied by comparing CBFEM and the solid finite element models previously validated. Furthermore, many parameters were changed to investigate the net section failure at elevated temperatures for studying the application of 5% limit strain at elevated temperatures.

Load-displacement curves of the joints with the same configuration connected by different bolt types are shown in **Figure 5.42**. In order to observe the effect of bolt diameter on the mechanical response of bolted lap joints at elevated temperatures, the bolt diameter varied from M12 to M24 given in **Figure 5.42**a. Having established in the authors' tests that bolt shear was the predominant failure mode, the effect of bolt grade on the behaviour of bolted lap joints at 500°C was investigated numerically by analysing three models with M16 grade 6.8, 8.8, and 10.9 bolts. Clearly, the bolt diameter and grade also play an important role in the resistance of the analysed joints as seen in **Figure 5.42**. The solid model estimates the resistance higher than the evaluation of the CBFEM model.

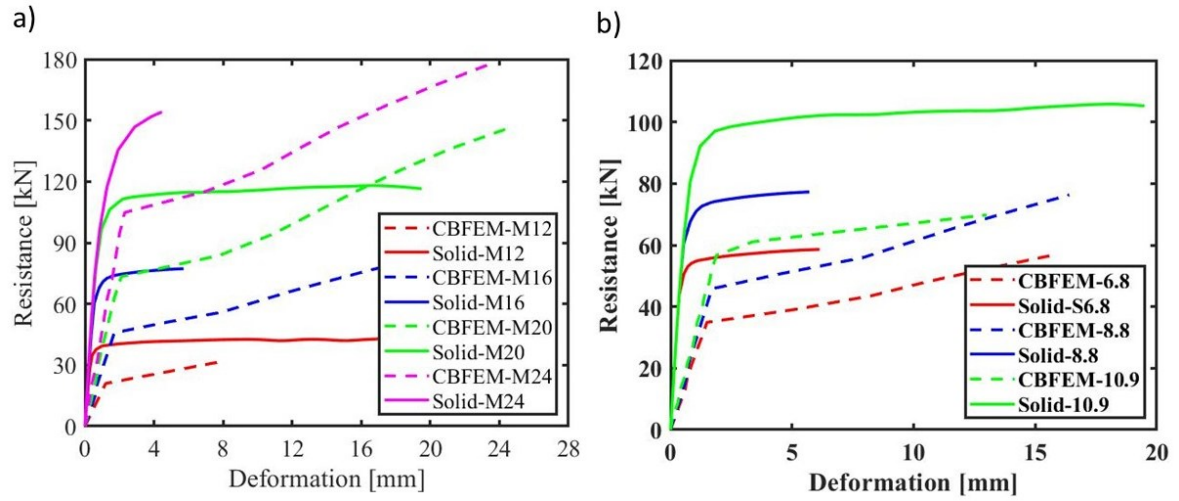

Figure 5.42. The effect of a) bolt diameter and b) grade on the behaviour of bolted lap joints at 500°C

Figure 5.43 illustrates the load-displacement curves showing the influence of steel grade and end distance on the resistance of tested lap joints at 600°C. The effect of steel grade was investigated based on the comparison of the experimental results among three steel grades. The studied steel grades are S235, S275 and S355. The influence of parameter e_1 has been investigated by varying 25 mm, 35 mm, and 45 mm. shows the load-displacement curves of the specimens with varying steel grade end distance e_1. It can be seen that steel grade and end distance do not have a significant influence on bolts in shear resistance at 600°C.

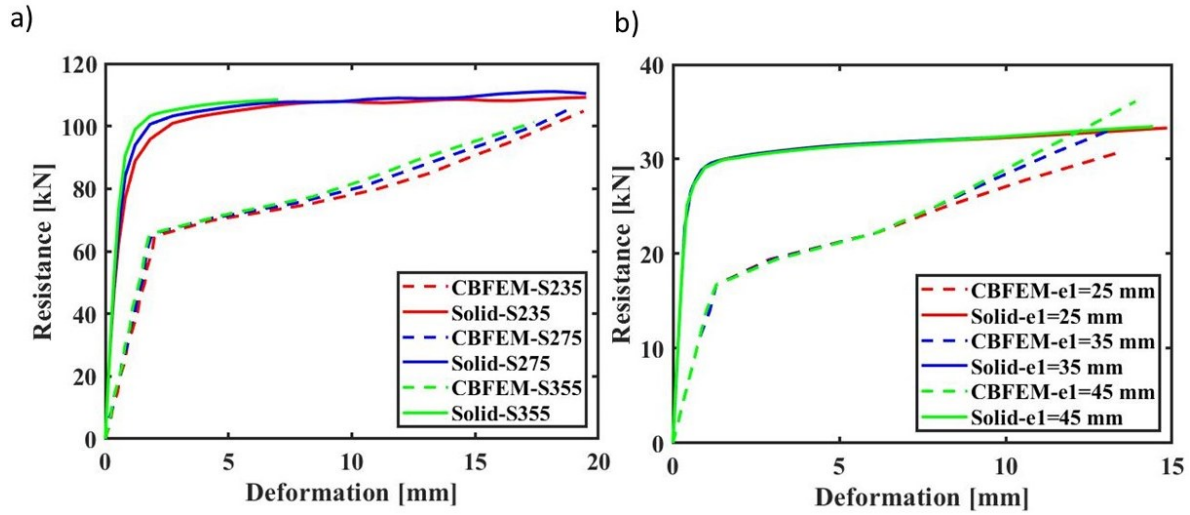

Figure 5.43. The effect of a-) steel grade and b-) end distance on the behaviour of bolted lap joints at 600°C

In Figure 5.44a, the effect of the plate thickness on the mechanical behaviour of bolted lap joints at 600°C. The aim of the parametric study was to determine the degree to which a change in thickness would affect the failure mode at elevated temperatures. In the CBFEM, increasing the thickness of the inner plate has no impact on the trend of the load-deformation curve, however, the solid model keeps the same trend of more than 8 mm. Figure 5.44b illustrates the load-deformation curve for the net section failure at high temperatures obtained from the solid model and CBFEM. To study the applicability of 5% limit strain at elevated temperature on plates, the thickness of the inner plates is taken as 6 mm. The steel grade is S235 whereas M27 bolts are used to fasten the plates. The end distance and the width of the plate are increased to 70 mm and 120 mm to prevent the bearing failure,

respectively. Figure 5.45 indicates the net section failure mode of the bolted lap joint. The CBFEM stops the analyse when the plastic strain of the steel plate is 5% limit strain.

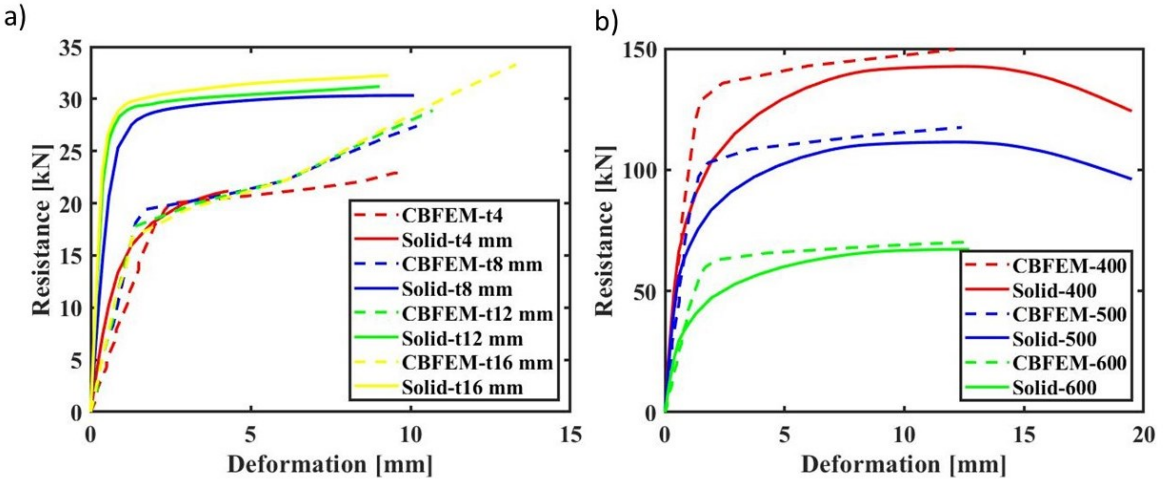

Figure 5.44. The study on a-) the thickness and b-) net section failure

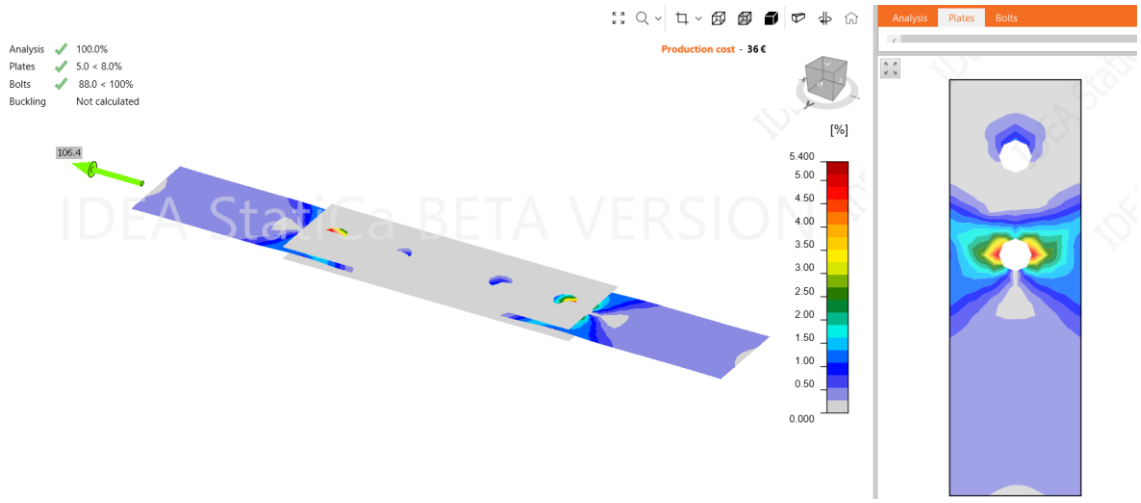

Figure 5.45. Net section failure CBFEM

5.3.2. Welded Lap Joints

The assembly of the model for welded lap joints in the CBFEM is presented in Figure 5.46. For the sake of simplicity, only half of the specimen is developed. The cover plates are cut from the I section member to solve the convergence problems. The cover plates are fixed in all directions. The inner plate which is subjected to the applied load is also restrained for rotations. The failure mode of welds is based on the design check presented in Eq. 26. The stresses in welds are calculated using the advantage of the finite element method. Then, the evaluated stresses are utilized to calculate the resistance of welded lap joints at elevated temperatures. Temperature is applied to each component of welded lap joints. The objective of this section is also to investigate the welds as an important fastener in addition to bolts.

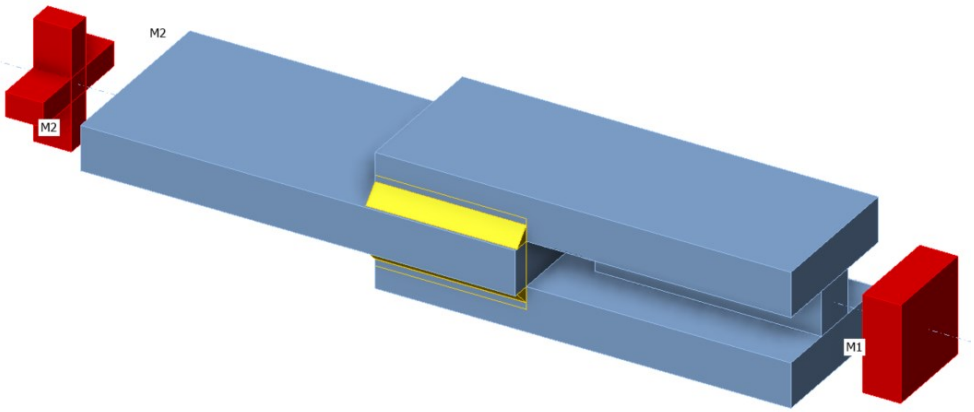

Figure 5.46. Assembly of the studied welded lap joints

The characteristics of test specimens for parallel and longitudinal fillet welds are listed in Table 5.6 and Table 5.7. The verification studies are performed for the test specimens as shown in Figure 5.47 and Figure 5.48.

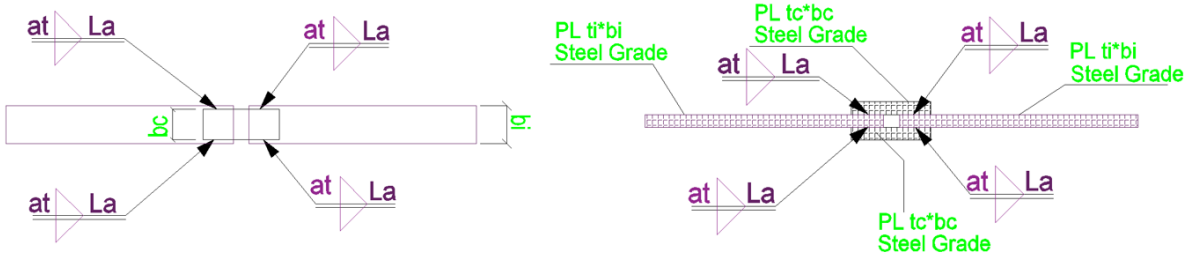

Figure 5.47. The configuration of specimens with parallel fillet weld

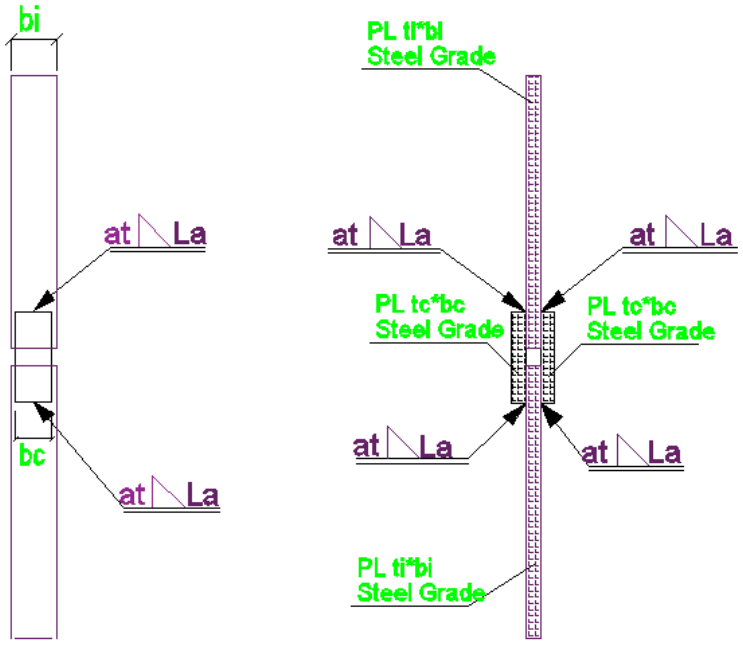

Figure 5.48. The configuration of specimens with longitudinal fillet weld

Verification

The object of this section is the verification of the component-based finite element method (CBFEM) of a fillet weld in a lap joint with the component method (CM). Three plates are connected in two configurations, namely with a parallel weld, with a longitudinal weld. The steel grade, length, and throat thickness of the weld are the changing parameters in the study. The joint is loaded by a normal force.

Table 5.6 presents the results of verification studies for parallel fillet welded lap joints at ambient temperature and elevated temperature. The results highlight that the CBFEM model provides conservative resistances compared to the analytical model at each temperature level. Figure 5.49-Figure 5.51 illustrates the comparison of resistances obtained from the CBFEM model and AM. All studied specimens experienced weld failure. The CBFEM predicts conservative resistances compared to the analytical model. The same failure modes were obtained from the analytical model and the CBFEM. Plates were not exposed to significant plastic strain in the CBFEM.

Table 5.6. Parallel fillet welds

Parameter	Material		Weld			Inner Plate		Cover Plate		AM	CBFEM	CBFEM/AM
θ	Steel	E	at	La	Direction	bi	ti	bc	tc			
[°C]	Grade	[Gpa]	[mm]	[mm]		[mm]	[mm]	[mm]	[mm]	[Kn]	[Kn]	[-]
20	S355	210	3	40	Parallel	50	12	40	12	120.7	118.7	0.98
350	S355	157.5	3	40	Parallel	50	12	40	12	141.5	109	0.77
450	S355	136.5	3	40	Parallel	50	12	40	12	113.4	109	0.96
550	S355	95.55	3	40	Parallel	50	12	40	12	75.8	72.9	0.96
650	S355	46.2	3	40	Parallel	50	12	40	12	38.3	36.8	0.96
Parameter	Material		Weld			Inner Plate		Cover Plate		AM	CBFEM	CBFEM/AM
Steel	θ	E	at	La	Direction	bi	ti	bc	tc			
Grade	[°C]	[Gpa]	[mm]	[mm]		[mm]	[mm]	[mm]	[mm]	[Kn]	[Kn]	[-]
S235	500	126	3	40	Parallel	50	12	40	12	78.2	75.1	0.96
S275	500	126	3	40	Parallel	50	12	40	12	87.9	84.4	0.96
S355	500	126	3	40	Parallel	50	12	40	12	94.6	91	0.96
Parameter	Material		Weld			Inner Plate		Cover Plate		AM	CBFEM	CBFEM/AM
Steel	θ	E	at	La	Direction	bi	ti	bc	tc			
Grade	[°C]	[Gpa]	[mm]	[mm]		[mm]	[mm]	[mm]	[mm]	[Kn]	[Kn]	[-]
S355	600	65.1	3	40	Parallel	100	15	60	15	57.0	54.7	0.96
S355	600	65.1	4	50	Parallel	100	15	60	15	95.1	91.2	0.96
S355	600	65.1	5	60	Parallel	100	15	60	15	142.6	136.9	0.96
S355	600	65.1	7	70	Parallel	100	15	60	15	232.9	222.8	0.96

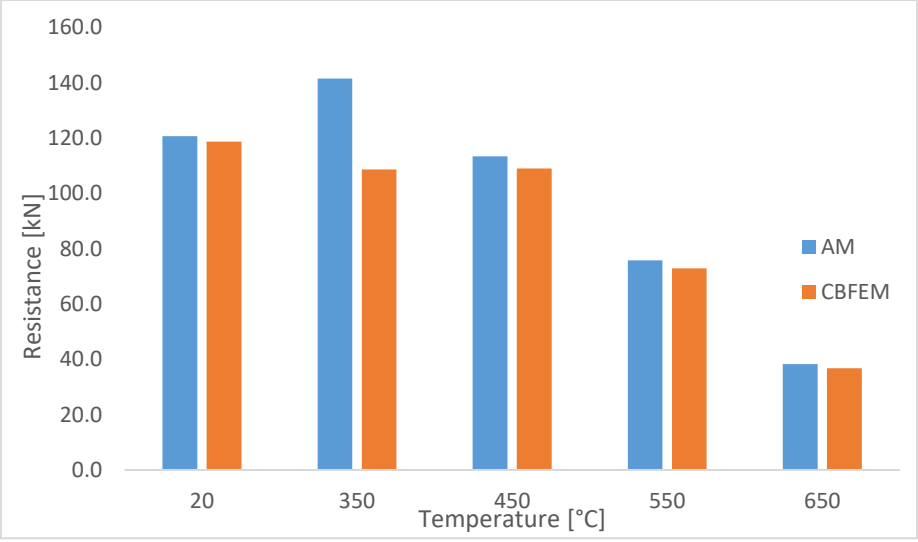

Figure 5.49. Parametric study of temperature for parallel weld

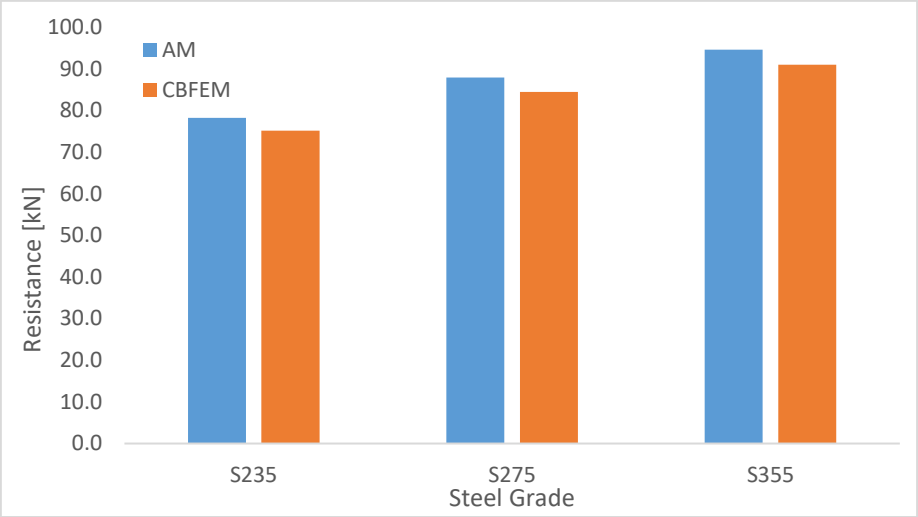

Figure 5.50. Parametric study of steel grade for parallel weld

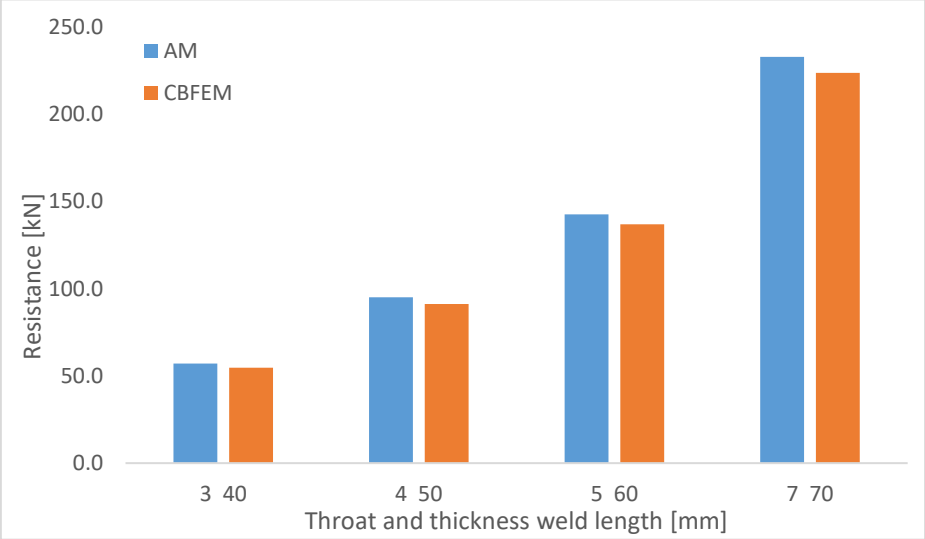

Figure 5.51. Parametric study of weld length throat thickness for parallel weld

Table 5.7 presents the results of verification studies for longitudinal fillet welded lap joints at ambient temperature and elevated temperature. The results highlight that the CBFEM model provides slightly higher than the analytical model at each temperature level. Figure 5.52-Figure 5.54 illustrates the comparison of resistances obtained from the CBFEM model and AM. All studied specimens experienced weld failure. At 350°C, the CBFEM predicts the resistance lower than the analytical model due to the reduced elastic modulus. However, the analytical model does not consider the modulus of elasticity to evaluate the resistance of fillet welds at elevated temperatures.

Table 5.7. Longitudinal fillet welds

Parameter	Material		Weld			Inner Plate		Cover Plate		AM	CBFEM	CBFEM/AM
θ	Steel Grade	E	at	La	Direction	bi	ti	bc	tc			
[°C]		[Gpa]	[mm]	[mm]		[mm]	[mm]	[mm]	[mm]	[Kn]	[Kn]	[-]
20	S355	210	3	40	Longitudinal	50	12	40	12	73.9	77	1.04
350	S355	157.5	3	40	Longitudinal	50	12	40	12	86.7	70.8	0.82
450	S355	136.5	3	40	Longitudinal	50	12	40	12	69.4	71	1.02
550	S355	95.55	3	40	Longitudinal	50	12	40	12	46.4	47.5	1.02
650	S355	46.2	3	40	Longitudinal	50	12	40	12	23.5	24	1.02
Parameter	Material		Weld			Inner Plate		Cover Plate		AM	CBFEM	CBFEM/AM
Steel Grade	θ	E	at	La	Direction	bi	ti	bc	tc			
	[°C]	[Gpa]	[mm]	[mm]		[mm]	[mm]	[mm]	[mm]	[Kn]	[Kn]	[-]
S235	500	126	3	40	Longitudinal	50	12	40	12	47.9	49	1.02
S275	500	126	3	40	Longitudinal	50	12	40	12	53.8	55	1.02
S355	500	126	3	40	Longitudinal	50	12	40	12	57.9	59.2	1.02
Parameter	Material		Weld			Inner Plate		Cover Plate		AM	CBFEM	CBFEM/AM
Steel Grade	θ	E	at	La	Direction	bi	ti	bc	tc			
	[°C]	[Gpa]	[mm]	[mm]		[mm]	[mm]	[mm]	[mm]	[Kn]	[Kn]	[-]
S355	600	65.1	3	40	Longitudinal	100	15	40	15	34.9	36.1	1.03
S355	600	65.1	4	50	Longitudinal	100	15	50	15	58.2	59.9	1.03
S355	600	65.1	5	60	Longitudinal	100	15	60	15	87.3	89.6	1.03
S355	600	65.1	7	70	Longitudinal	100	15	70	15	142.6	145.6	1.02

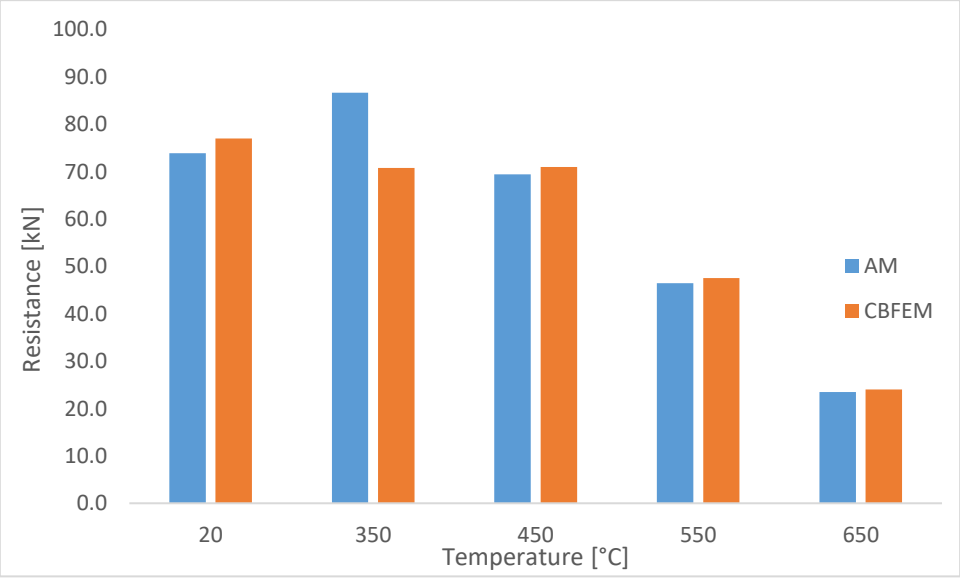

Figure 5.52. Parametric study of temperature for longitudinal weld

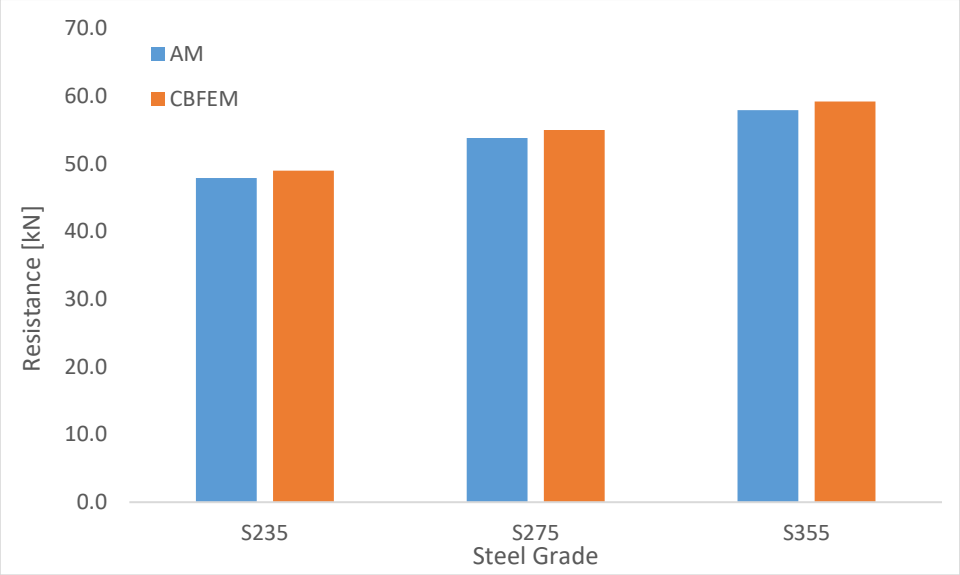

Figure 5.53. Parametric study of steel grade for longitudinal weld

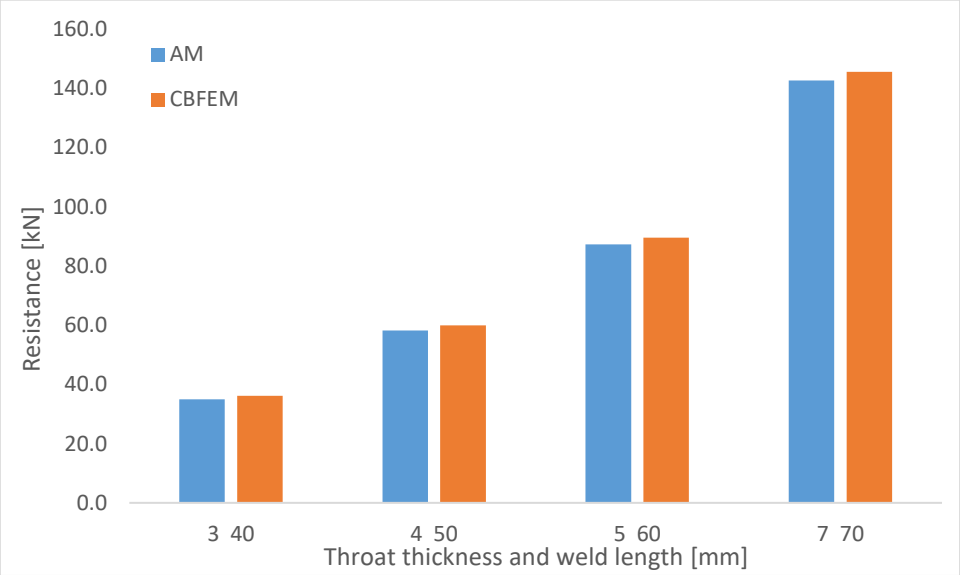

Figure 5.54. Parametric study of weld length throat thickness for longitudinal weld

5.3.3. T-stubs

The assembly of the T-stub model generated in the CBFEM is shown in Figure 5.55. The flange and web of T-stubs consist of steel plates, and these are connected to each other with weld. The member M2 is selected as a bearing member, and it should not be deformed. Therefore, the elastic modulus of the bearing member is magnified by 1000 times than elastic modulus of carbon steel. The CBFEM checks the behaviour of plates, bolts in tension, and welds.

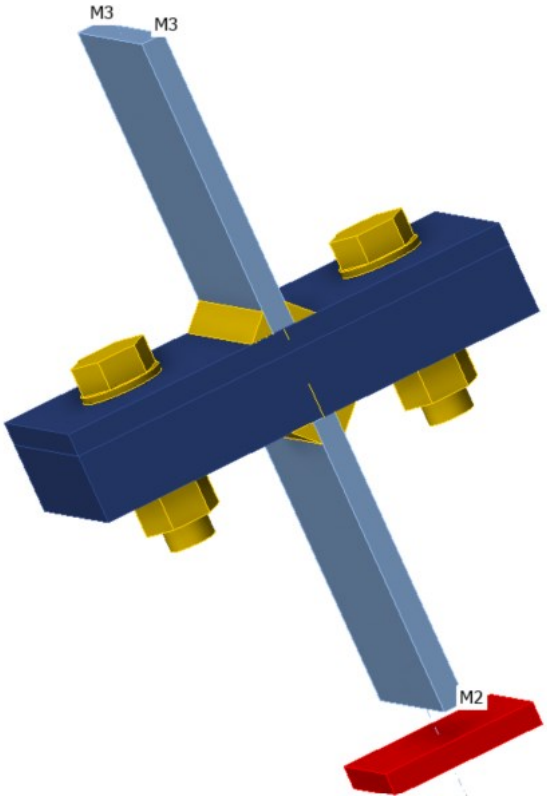

Figure 5.55. Assembly of the studied T-stubs

Mesh Sensitivity Study

A mesh sensitivity study is conducted to optimize the computational cost and to assess the accuracy of the numerical design calculation for predicting the fire resistance of T-stubs. The flange width of the T-stub specimen is subdivided into 8 to 40 elements. The minimum and the maximum element size are set as 1 mm and 5 mm, respectively. The influence of the number of elements on the T-stub resistance at 500°C and 600°C is shown in Figure 5.56. The optimized element number is selected as 16 to divide the plates for T-stubs models in CBFEM.

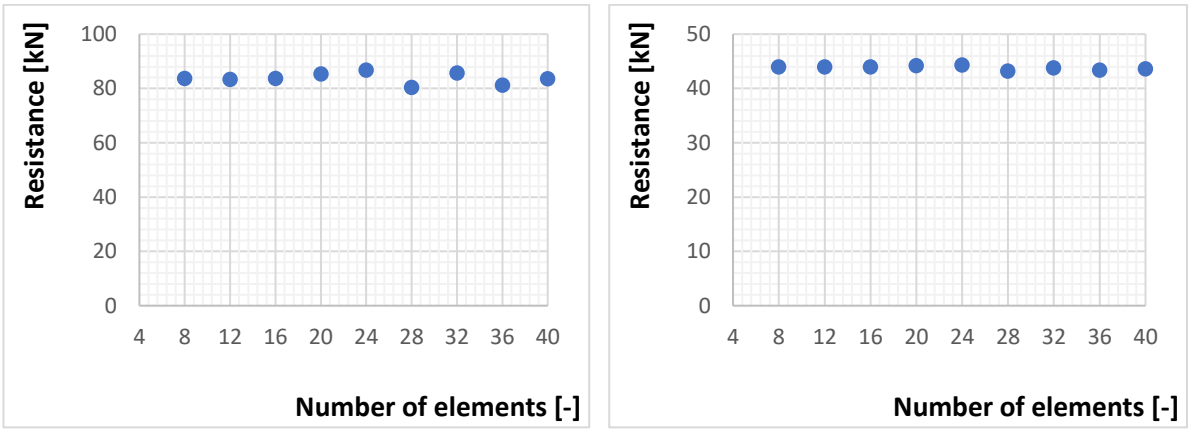

(a) **(b)**

Figure 5.56. Influence of mesh element number on the resistance: (a) at 500°C and (b) at 600°C.

Verification

In this section, the CBFEM models are verified based on the analytical models presented in Eurocode 3. IDEA StatiCa software [108] was used to develop CBFEM models. The test specimens were taken from the study [47] for the comparison of the CBFEM model with the analytical model (AM). The tested T-stubs were analysed in accordance with EN 1993-1-8, considering the reduction factors for carbon steel and bolts at elevated temperatures presented in EN 1993-1-2. The resistance of T-stubs was calculated with nominal dimensions as listed in Table 5.8. The specimens nominated with FL were experimentally studied whereas the specimens nominated with PS were analytically tested in this study in order to increase the accuracy of the CBFEM model. The FL specimens were tested at three different temperature levels: 20°C, 500°C, and 600°C. The resistance of PS specimens was evaluated only at elevated temperatures (500°C, and 600°C). The geometrical characteristics of T-stub specimens are shown in Figure 3.10. The R-squared values are found as 0.993 for both cases in Figure 5.57, the CBFEM can be considered a reliable method instead of analytical models for structural fire designers. Table 5.8 compares the design values obtained from the analytical calculations, in accordance with EN1993-1-8 with the numerical design calculations and indicates that the predicted resistance and failure modes from CBFEM and the analytical resistance and failure modes are consistent. The tested specimens are nominated as the abbreviation of the flange, the thickness of the flange, and the temperature level. In all cases, the AM to CBFEM ratios are ranging from 0.9 to 1.1. The mean value of the ratio between the results from AM and CBFEM is 0.99. In the case of failure Mode 2, sometimes the CBFEM predicts the resistance of T-stubs slightly higher than the analytical resistance.

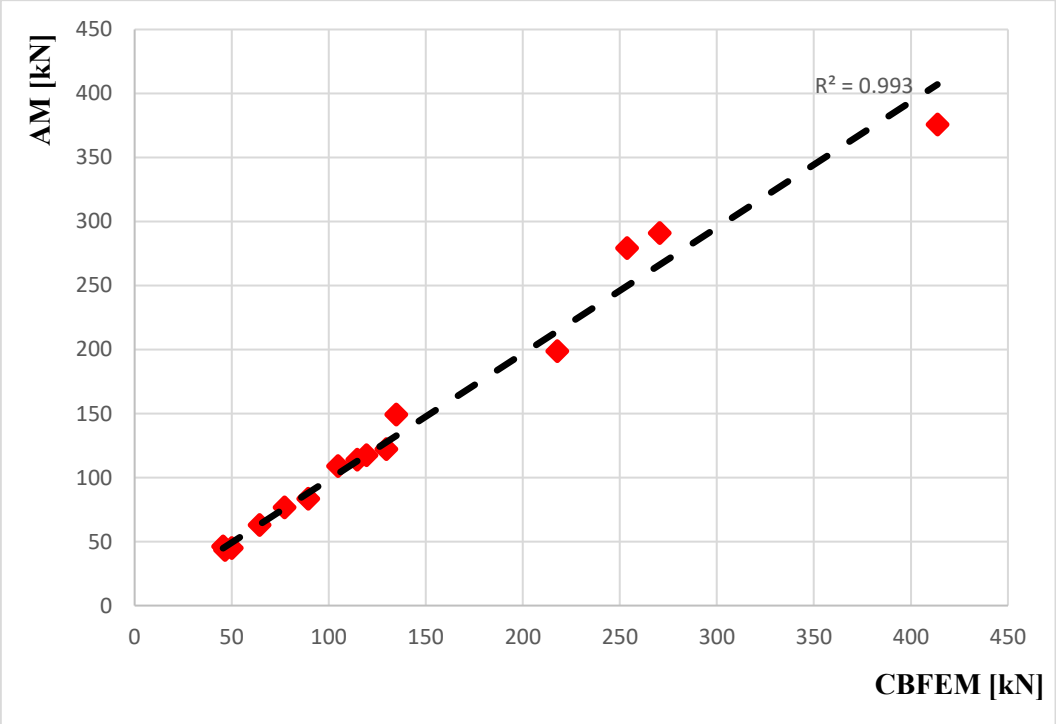

Figure 5.57. This is a figure. Schemes follow the same formatting.

Table 5.8. Resistance values and failure modes: AM vs CBFEM.

Specimen	AM		CBFEM		R_{CBFEM}/R_{AM}
	Resistance [kN]	Failure Mode	Resistance [kN]	Failure Mode	
FL-10-20	114.60	Mode 1	114.22	Mode 1	1.00
FL-10-500	89.39	Mode 1	82.83	Mode 1	0.93
FL-10-600	45.55	Mode 2	46.3	Mode 2	1.02
FL-15-20	217.78	Mode 2	198.87	Mode 1	0.91
FL-15-500	134.81	Mode 2	149.44	Mode 2	1.11
FL-15-600	64.25	Mode 2	62.99	Mode 2	0.98
FL-20-20	413.65	Mode 2	375.98	Mode 1	0.91
FL-20-500	253.63	Mode 2	279.4	Mode 2	1.10
FL-20-600	119.40	Mode 2	117.68	Mode 2	0.99
PS-1-500	104.70	Mode 2	109.15	Mode 2	1.04
PS-1-600	50.00	Mode 3	45	Mode 3	0.90
PS-2-500	270.50	Mode 2	291.25	Mode 2	1.08
PS-2-600	129.56	Mode 2	122.4	Mode 2	0.94
PS-3-500	77.23	Mode 1	76.8	Mode 1	0.99
PS-3-600	46.53	Mode 2	43.68	Mode 2	0.94

The main components in the bolted end-plate connection can be represented using equivalent T-stubs which have been traditionally applied to represent the components in the tension zone. **Figure 5.58** displays the three possible failure modes for T-stubs [72]:

- Complete yielding of the flange;
- Bolt failure with yielding of the flange;
- The T-stub flange remains elastic until fracture of the bolts.

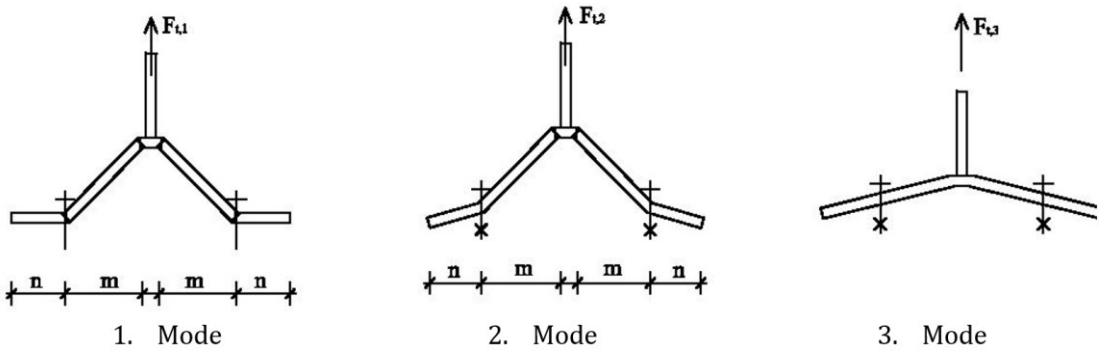

Figure 5.58. Three failure modes of T-stubs [72]

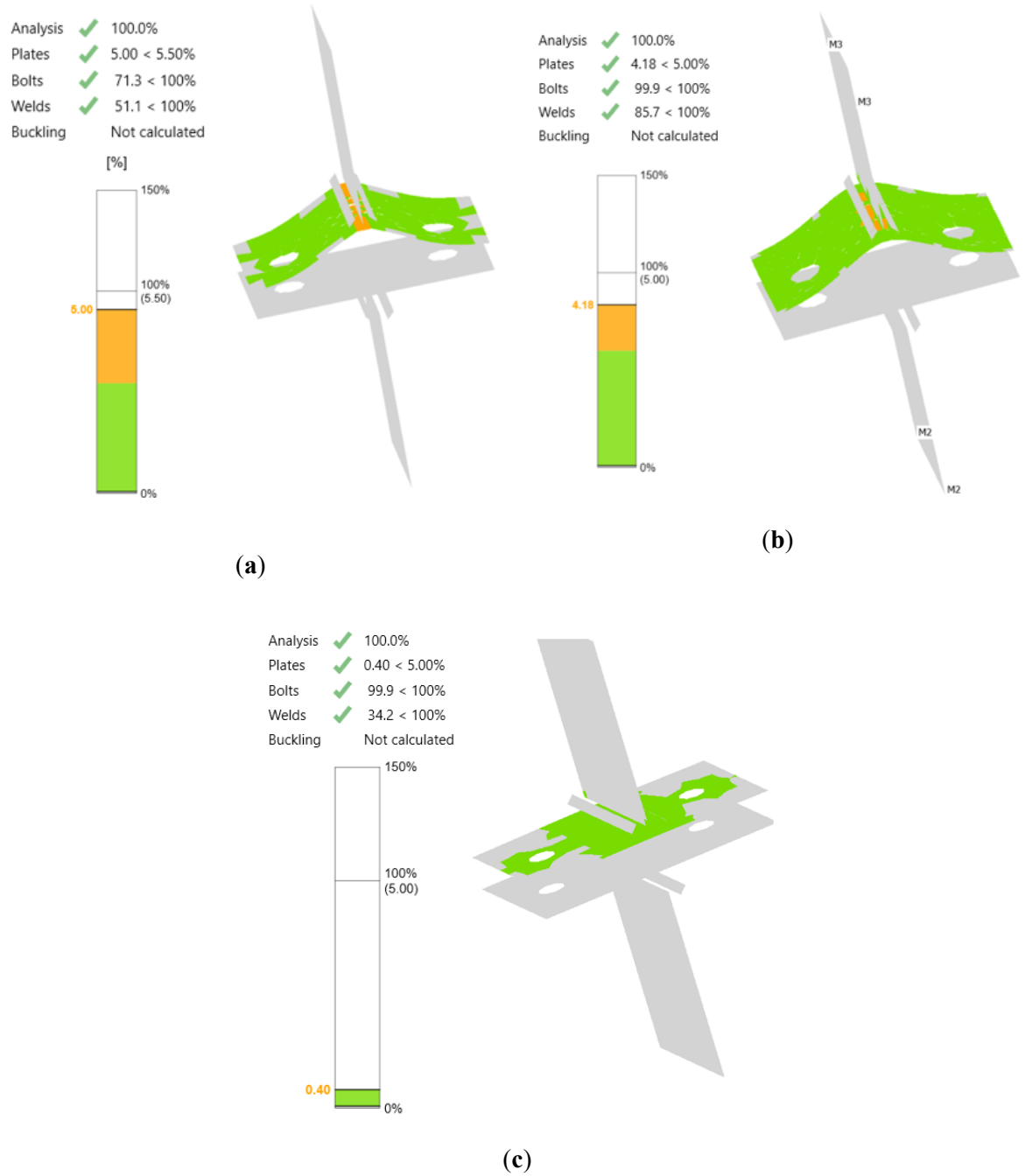

Figure 5.59. Failure modes obtained from the CBFEM: (a) Mode 1; (b) Mode 2; (c) Mode 3.

Figure 5.59 shows the cases of three different failure modes for T-stubs obtained from the CBFEM models. In Mode 1, the flange of T-stubs completely yields and the CBFEM evaluates the plastic strain on the flange as 5%. The EN 1993-1-5 recommends the 5% plastic strain for steel plates to predict the resistance of steel connection components. Therefore, the CBFEM ends the analysis while the steel plate reaches 5% plastic strain before bolts or welds perform their full ultimate capacity. EN 1993-1-8 defines the failure Mode 2 as the yielding of the flange in addition to the bolt failure. As stated in EN 1993-1-2, the bolts use their full ultimate capacity with the occurrence of 4.18% plastic strain in the steel flange. The T-stub flange maintains its elasticity until the bolts fracture in Mode 3. As seen in Figure 5.59c, the steel flange has only 0.4% plastic strain before the bolts reach full capacity. Table 3 presents the comparison of the resistance and failure modes obtained from the AM

and the CBFEM. Generally, the same failure modes were obtained in the CBFEM models as the AM predicts. There are only two test specimens experienced with different failure modes. For the specimen FL-15-20, the AM evaluates the resistances of Mode 1 and Mode 2 as 276 kN and 218 kN, respectively. The difference between the resistances of the two modes is 21%. Table 5.9 indicates the plastic strain of the steel flange and the bolt capacity ratio of the tested specimens measured in the CBFEM models. The plastic limit strain is obtained on the steel flange of the specimen FL-15-20 whereas the bolt capacity reaches 91.7% which is highly close to the full capacity. A similar situation happened for the test specimen with 20 mm flange thickness at ambient temperature. The bolt capacity of specimen FL-20-20 is slightly higher than that of specimen FL-15-20.

Validation

This section presents the validation of the CBFEM model using experimental results on T-stub specimens [47]. The CBFEM model is validated in terms of the load-deformation curves, resistance, and failure modes. The experimental study involves nine test specimens with three different thicknesses of flange (t_f is 10mm, 15mm, and 20mm), two different bolts (M20, grade 8.8 and M24, grade 10.9) and three temperature levels (20°C, 500°C and 600°C). Figure 5.60 demonstrates the load-deformation curves from the experimental study (solid lines) and the CBFEM (dashed lines) for the test specimens with three different thickness values. It can be seen that the CBFEM models can safely predict the global behaviour of the T-stub component at ambient temperature and 500°C up to the failure defined for steel connection components in Eurocode 3. At 600°C, the prediction of the T-stub response is accurately consistent with the recorded graphs. The numerical curve only exceeds the experimental graph at 600°C after the failure deformation of the tested specimen FL-15.

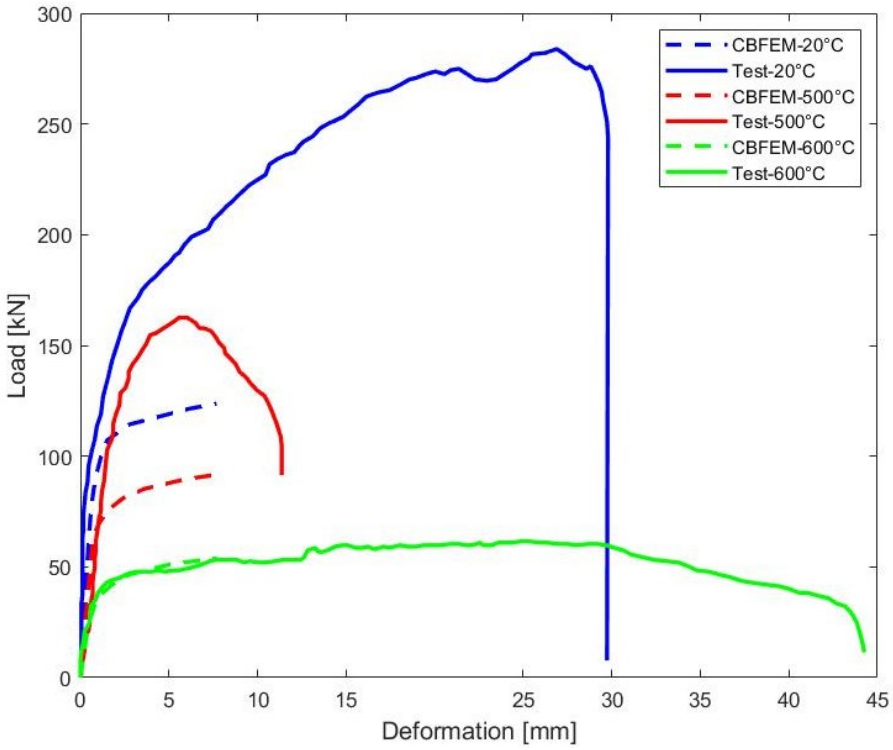

(a)

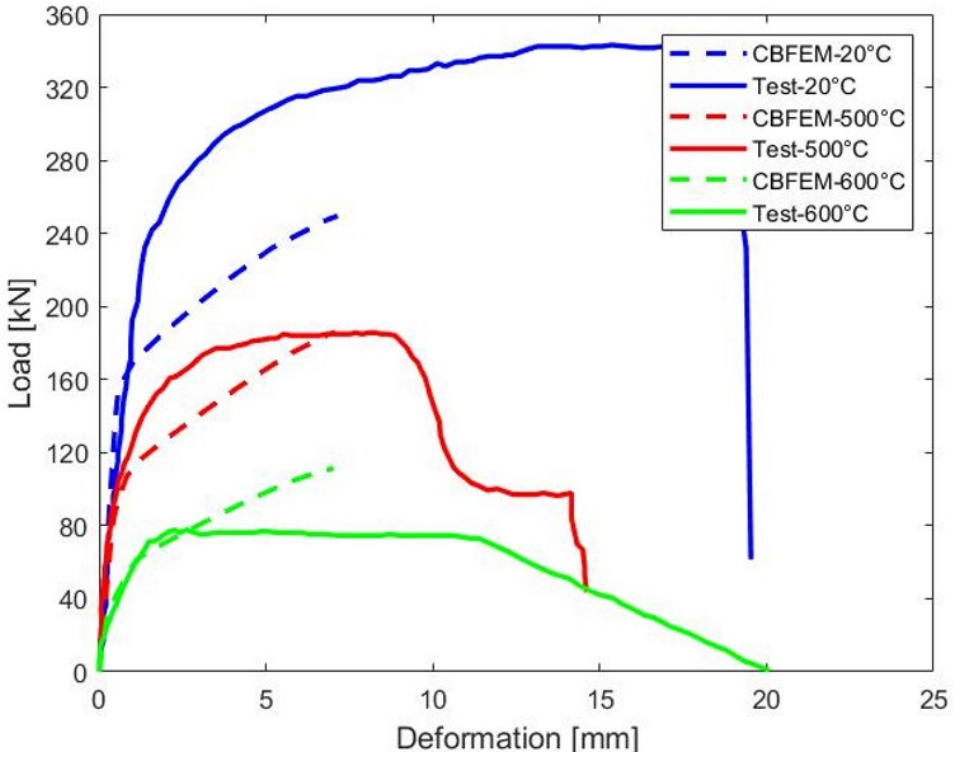

(**b**)

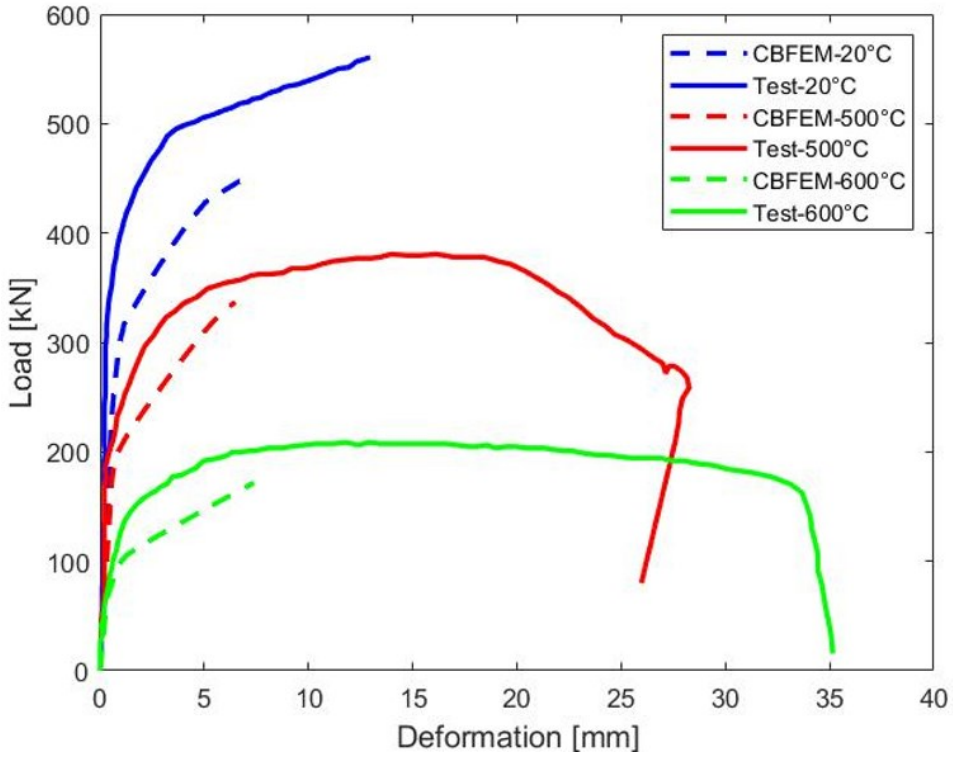

(**c**)

Figure 5.60. Comparison of test results with the CBFEM results: (a) Thickness of the flange is 10 mm; (b) Thickness of the flange is 15 mm; (c) Thickness of the flange is 20 mm.

Table 5.9 lists the comparison of resistance values and failure modes between test results and the CBFEM models. PS refers to the plastic strain on steel flange and BC means the bolt capacity. During

the experimental study, the authors observed the following failures: (a) weld fracture, (b) bolt fracture, (c) the flange crack near the weld toe, and (d) the yielding of the flange. Since there was no information on the material properties of welding metal, the fillet welds in the CBFEM were designed so that no failure could be observed. As can be seen in Table 5.9, the CBFEM provides conservative resistance values compared to the test results. The measured resistance is only 5% higher than the calculated resistance for the specimen T10-600. The logic behind this difference can be the modelling of the fillet welds because the weld failure was observed during the test, but the weld cannot fail in the developed model due to the lack of material properties. Numerical design calculation models failed due to the plastic limit strain or the use of bolt full capacity.

Table 5.9. Resistance values and failure modes: Experiment vs CBFEM.

Specimen	Experiment		CBFEM		R_{CBFEM}/R_{EXP}
	Resistance [kN]	Failure Mode	Resistance [kN]	Failure Mode	
T10-20	170.45	b, d	114.22	PS=5%, BC=71.3%	0.67
T10-500	137	a, c	83.7	PS=5%, BC=77.3%	0.61
T10-600	43.9	a, c	46.3	PS=4.18%, BC=100%	1.05
T15-20	295.9	b, d	198.87	PS=5%, BC=91.7%	0.67
T15-500	177	a, c, d	149.44	PS=3.69%, BC=100%	0.84
T15-600	77.8	b	62.99	PS=0.77%, BC=100%	0.81
T20-20	494.15	a	375.98	PS=5%, BC=93.4%	0.76
T20-500	335	b, d	279.4	PS=3.96%, BC=100%	0.83
T20-600	187	a, c, d	117.68	PS=0.82%, BC=100%	0.63

Barata et al. [47] stated that the specimen with 15 mm of flange thickness failed due to the bolt fracture at 600°C. The CBFEM check also ended due to the bolt fracture when the plastic limit strain reaches only 0.7 % as shown in Figure 5.61. The 10 mm thickness of specimens at 500°C and 600°C, the development of the plastic hinges was first observed during the tests. As indicated in Figure 5.62, the flange reached to 5% plastic limit strain while the bolts still had 20% more capacity to resist the load. Furthermore, similar failure modes were observed for the specimens with 20 mm thickness and CBFEM captured the failure modes correctly.

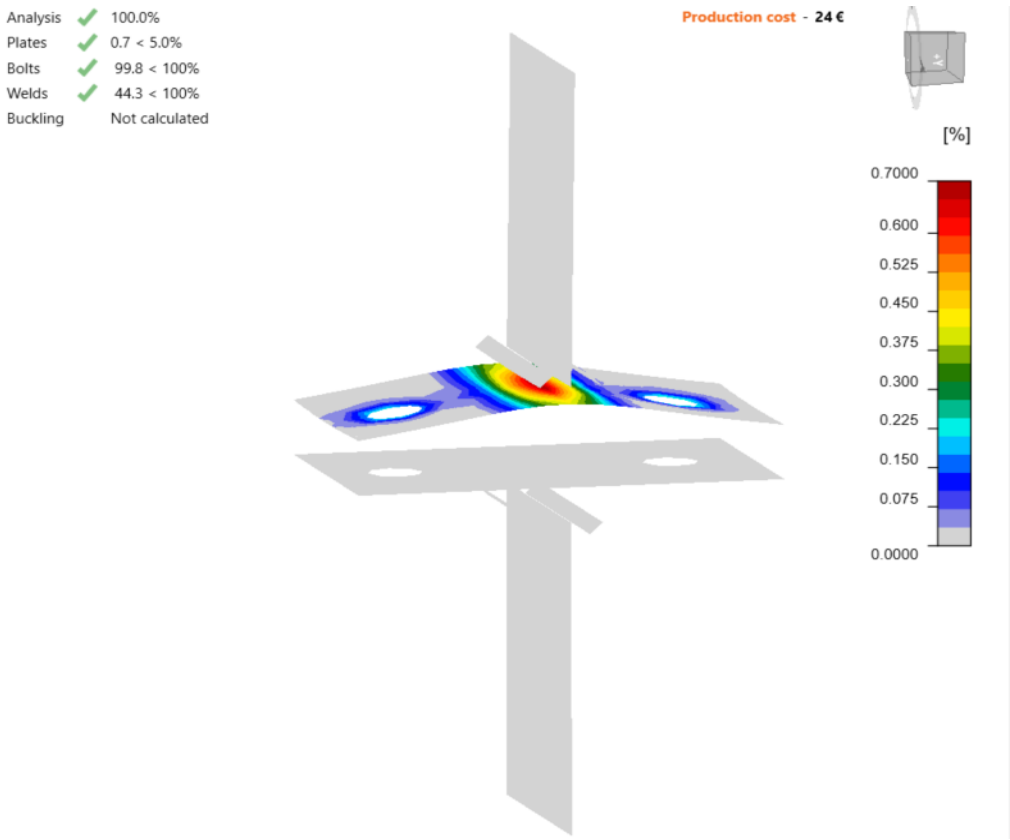

Figure 5.61. The plastic strain in T-stub (15 mm) at 600°C before the bolt failure by CBFEM model

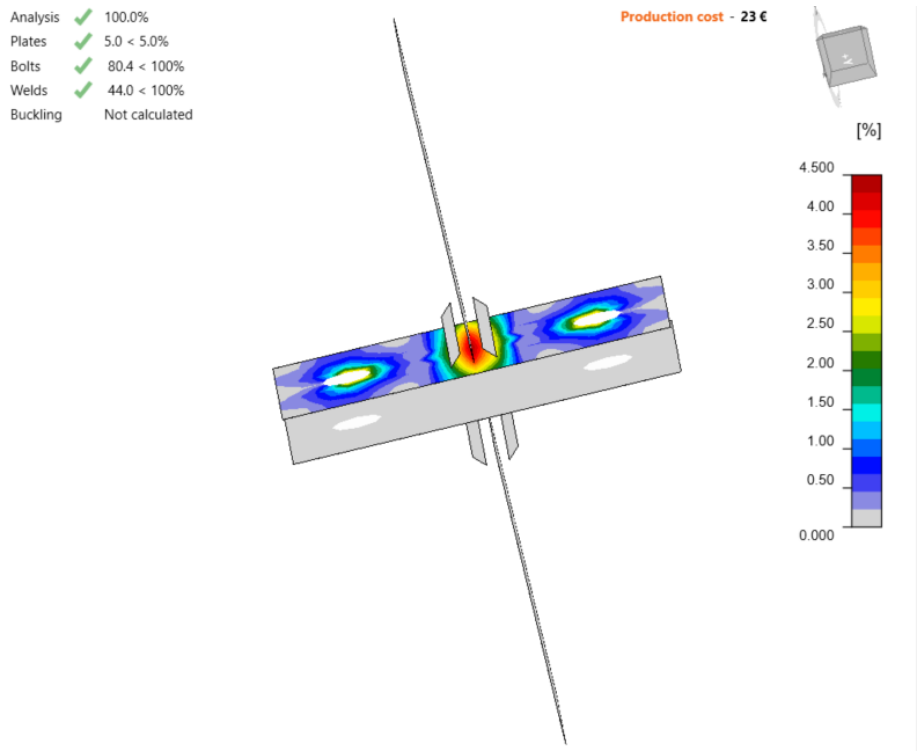

Figure 5.62. The limiting plastic strain in T-stub (10 mm) at 500°C by CBFEM model

Parametric studies were performed to understand the effect of temperature better on the response of T-stub specimens for each flange thickness. 400°C and 700°C were added to the studied temperature

levels. Figure 5.63 demonstrates the load-deformation curves predicted from the numerical design calculations for the extended temperature level. The initial stiffness and resistance decline with the increase in temperature for the examined T-stubs.

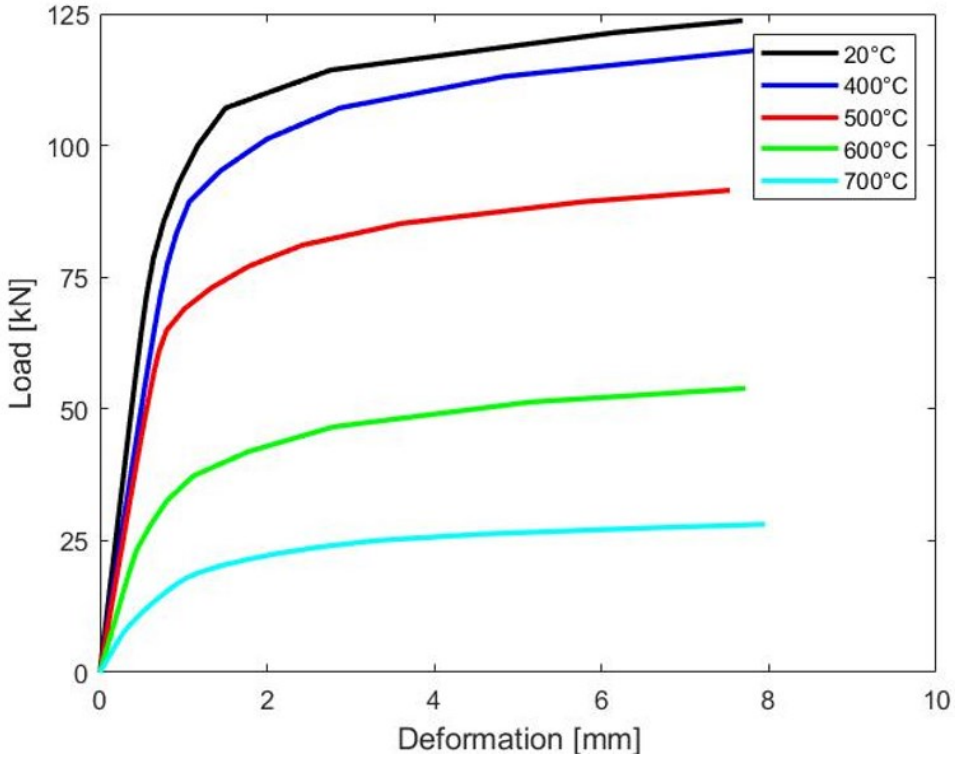

(a)

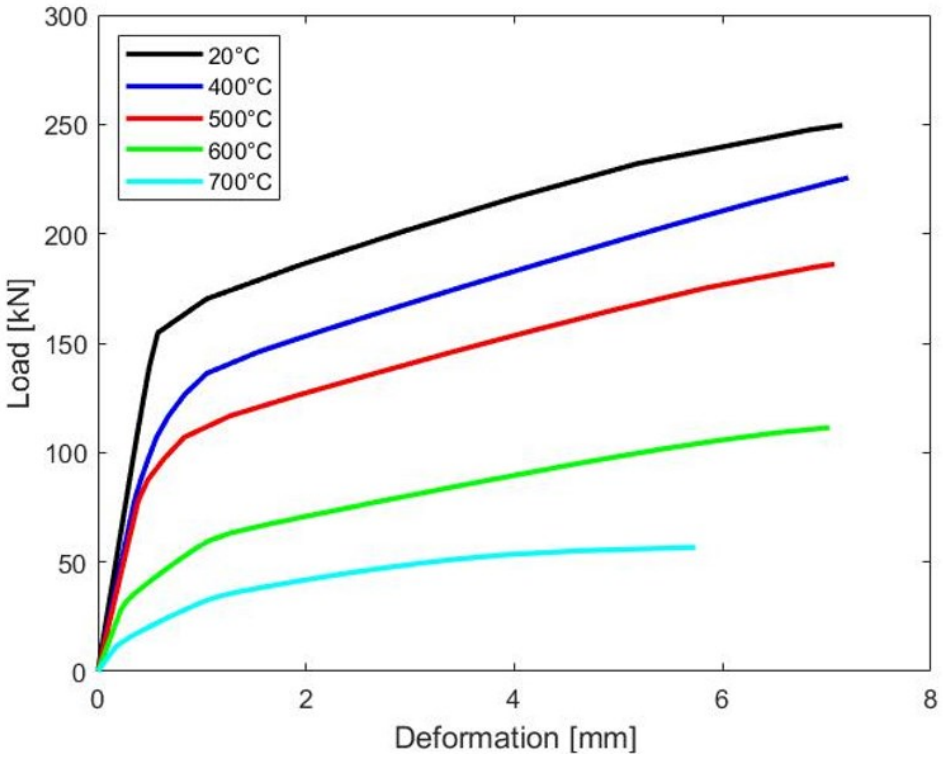

(b)

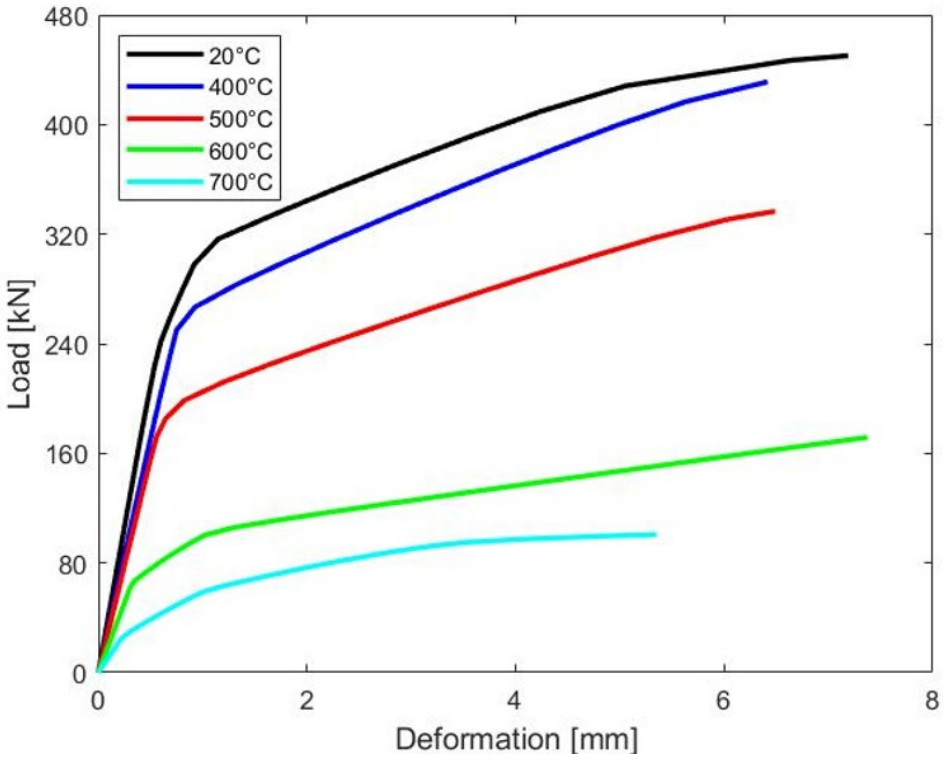

(c)

Figure 5.63. The effect of temperature on the response of tested T-stub specimens (a) Thickness of the flange is 10 mm; (b) Thickness of the flange is 15 mm; (c) Thickness of the flange is 20 mm.

Figure 5.64 depicts the evolution of the plastic strain in the flange and the tension bolt force according to temperature ranging from 400°C to 700°C. The T-stub specimen with 10 mm thickness is selected for conducting the parametric study. The plastic strain distribution in the specimen FL-10 at ambient temperature is shown in **Figure 5.64**a. The selected specimen is designed to fail in Mode 1. However, the failure mode of the specimen is changed from 1 to 2 at 600°C and 700°C. It proves that the temperature has a significant effect on the failure mode of the T-stub components.

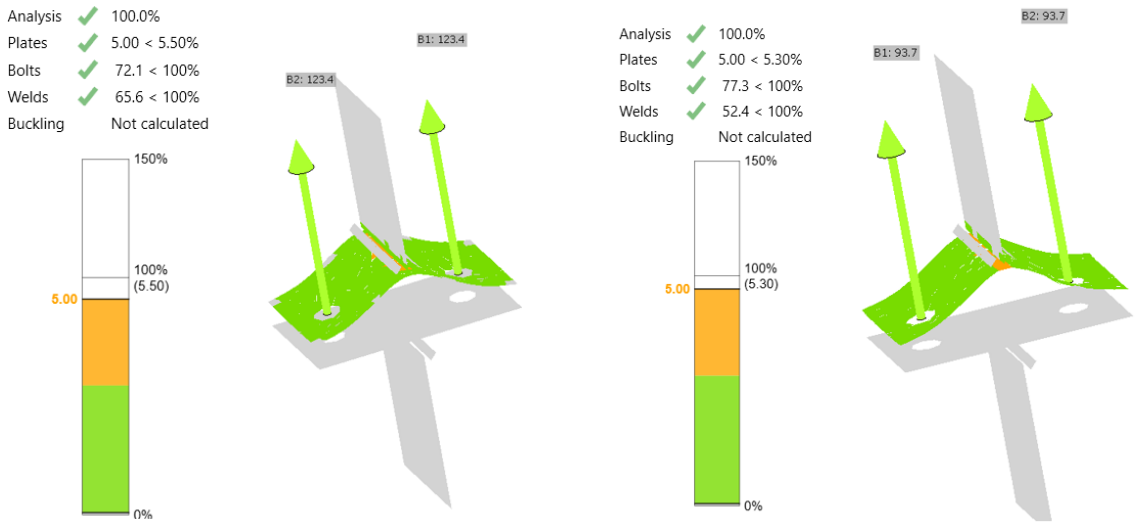

(a)

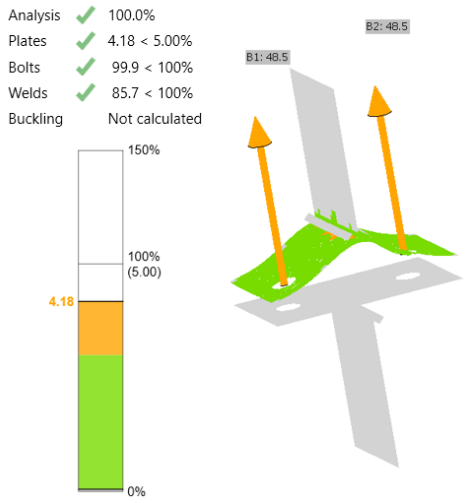

(b)

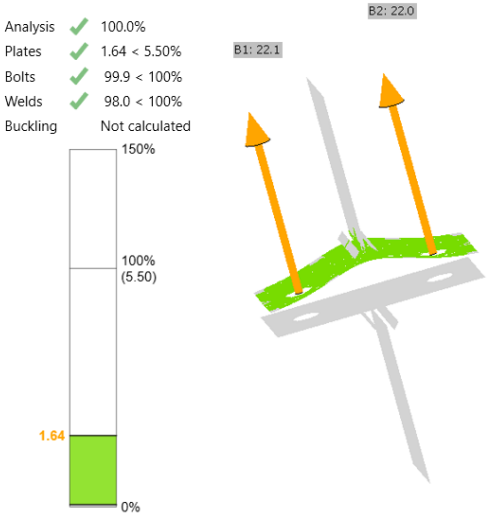

(c)

(d)

Figure 5.64. The influence of the elevated temperatures on the plastic strain and the bolt force at: (a) 400°C; (b) 500°C; (c) 600°C; (d) 700°C.

Fire design of endplate joints is crucial for structural fire engineering because the parametric study highlighted that the temperature has a remarkable effect on the load-deformation curves and the failure modes of T-stubs which are defined as the main component of the endplate joints in EN 1993-1-2. Therefore, this section presented a CBFEM model to investigate the behaviour of T-stubs at elevated temperatures. The equivalent T-stub method proposed in EN 1993-1-8 was used to verify the CBFEM model in terms of resistance and failure modes. The CBFEM model was validated based on test results evaluating the load-deformation curves, fire resistances, and failure modes. To predict the resistance of the T-stubs at ambient and elevated temperatures, the 5% plastic limit strain recommended in EN 1993-1-5 for steel plate elements and the analytical model for the bolts in tension proposed in EN 1993-1-8 were used in the CBFEM model. The influence of temperature on the resistance is considered using the reduction factors for carbon steel and bolts presented in EN 1993-1-2. The parametric study was carried out to investigate the influence of different temperature temperature levels (ranging from 20°C to 700°C) on the load-deformation curves and the failure modes of T-stub specimens.

5.3.4. Fin Plate Joints

Fin plate joints are one of the most common shear connection types in construction due to their ease of assembly. The fin plate is a joint made with a vertical plate usually welded to the column and bolted to the beam. The fin plate may be considered as a pinned joint with possible small bending moments. The main components of fin plate joints are bolts in shear, plate bearing, and weld failure according to EN 1993-1-8. Sarraj [111] reported the following six potential failure modes for this type of connection based on the previous studies: yielding of the gross area of the plate, bearing failure of bolt holes, fracture of net section of plate, fracture of edge distance of plate, bolt fracture and welds fracture. Therefore, based on these failure mechanisms, the potential active components for fin plate joints are bolts in shear, beam web in bearing, plate in bearing, welds in shear/tension, and column web in compression, as shown in Figure 5.65. The assembly of the beam-to-column fin plate joint is

shown in Figure 5.66. The load is applied to the beam using an inclined rod with a specific angle, but the loads are applied to the tested specimen in the CBFEM as normal, and shear forces.

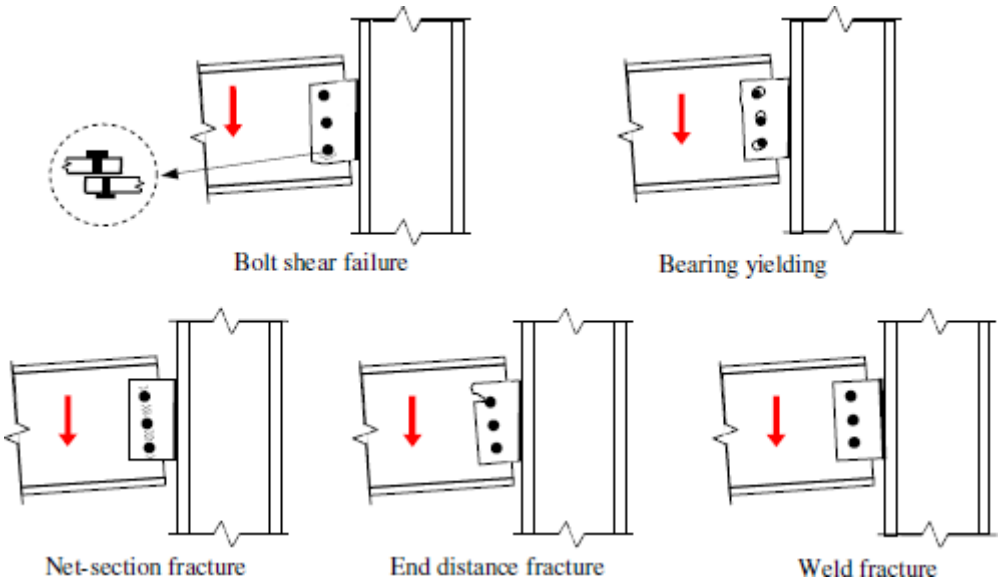

Figure 5.65. Failure modes for fin plate connections [111]

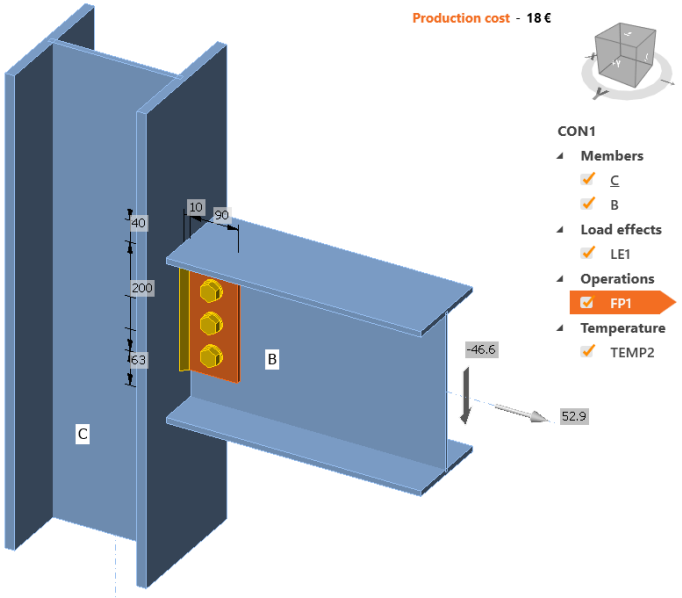

Figure 5.66. Assembly of the studied fin plate connection

Verification

According to the study [10], verification is a process where the computational solution is compared with a highly accurate analytical or numerical benchmark solution. In this paper, CBFEM models are compared with the component analytical models presented in EN 1993-1-2. The most critical components in the experimental study were bolts in shear and bearing. Since the beam web is 2 mm thinner than the fin plate, the bearing may be calculated in the web of the beam. EN 1993-1-8 Table 3.4 predicts the shear resistance of one bolt and bolt bearing resistance in the beam web. Table 5.10 presents the bolt resistances calculated from Eurocode and CBFEM. Eurocode predicts the bearing failure for each specimen. CBFEM calculated the applied loads to bolts using the advantage of the finite element model when the fin plate joints were subjected to the maximum force. Therefore, the bolts were not exposed to pure shear load as assumed in connection resistance. Bending moments also

caused extra shear and bearing loads affecting bolts. The CBFEM models predicted the failure modes as bearing and utilization of shear capacity in loads as Eurocode design specification determined.

Table 5.10. The bolt forces from Eurocode and CBFEM

Specimen	CBFEM		Eurocode – Failure Loads		Specimen	CBFEM		Eurocode – Failure Loads	
	Applied Load [kN]	Load on bolt [kN]	Shear [kN]	Bearing [kN]		Applied Load [kN]	Load on bolt [kN]	Shear [kN]	Bearing [kN]
20-35	36.65	69.6	86.4	69.6	550-55	14.6	33.5	41.6	33.5
450-35	31.09	57.6	71.5	57.6	650-55	5.76	13.9	17.3	13.9
550-35	18.99	33.5	41.6	33.5	10.9-20	41.75	69.6	98	69.6
650-35	8.15	13.9	17.3	13.9	10.9-550	25.46	33.5	47.2	33.5
20-55	38.38	69.6	86.4	69.6	M24-20	30.06	51.1	124.5	51.1
450-55	25.37	57.6	71.5	57.6	M24-550	15.54	24.6	59.9	24.6

Validation

EN 1993-1-8 underestimates the resistance of fin plate joints, hence the CBFEM also gives conservative results. The difference between resistances obtained from tests and the CBFEM at ambient temperature is higher than at elevated temperatures. Since the Eurocode reduces the bearing resistance with the reduction factor for structural steel, the amount of difference between resistances decreases as seen in Figure 5.67-Figure 5.69.

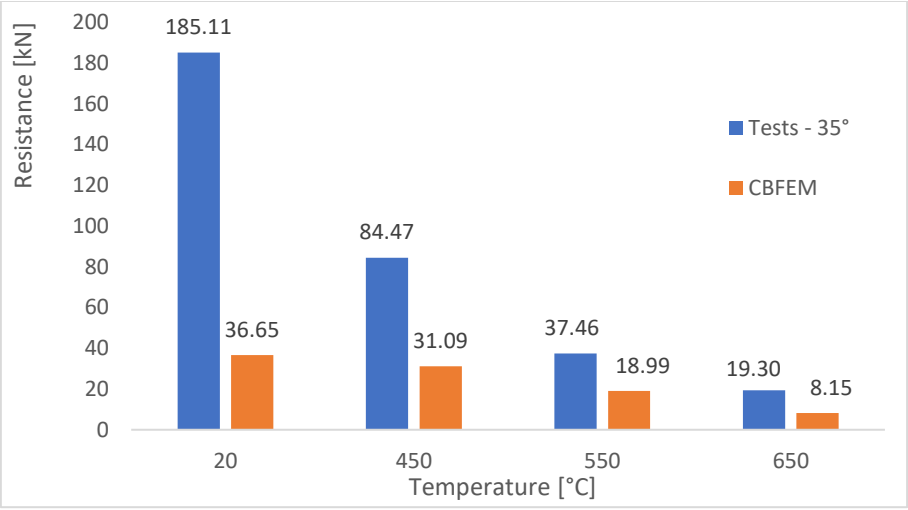

Figure 5.67. Comparison of test results (35°C) with CBFEM

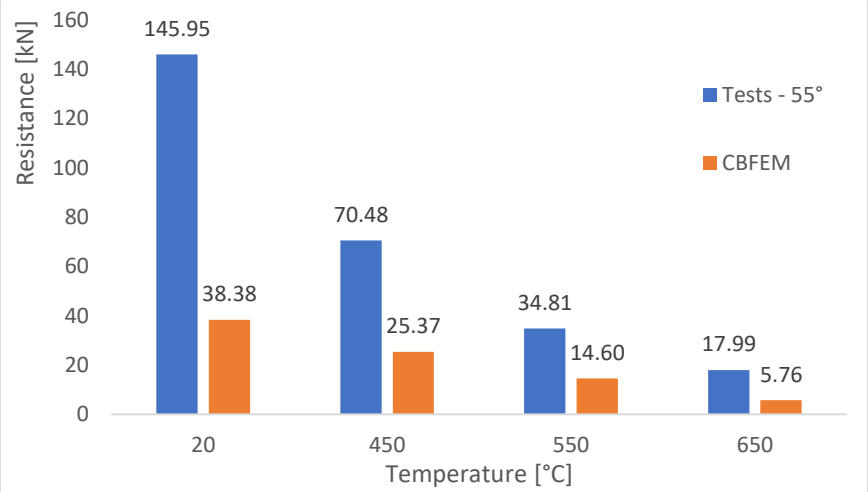

Figure 5.68. Comparison of test results (55°C) with CBFEM

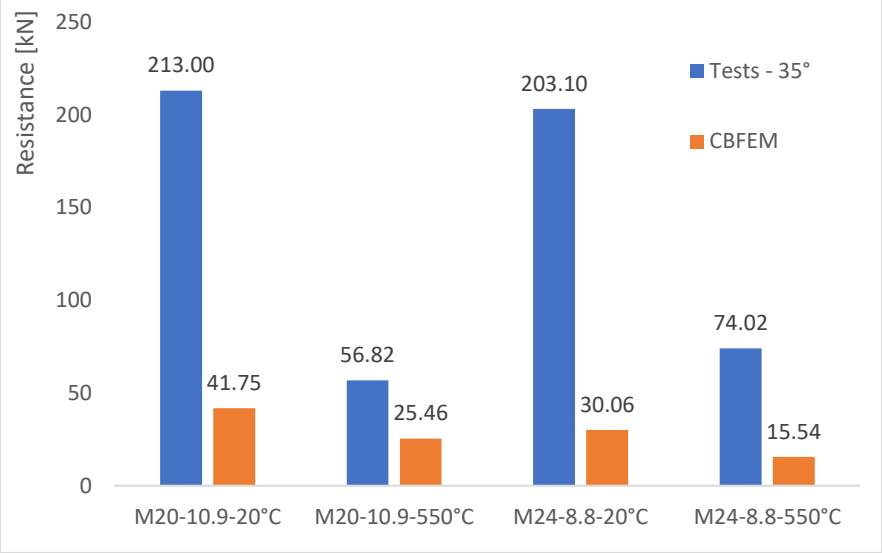

Figure 5.69. Comparison of test results (35°C) with CBFEM – bolt grade and diameter

The most critical components in the experimental study were bolts in shear and bearing. Since the beam web is 2 mm thinner than the fin plate, the bearing may be calculated in the web of the beam. Figure 5.70 indicates the failure mode of the test specimen with bolt grade 10.9 at 550°C and the strain distribution on the fin plate in CBFEM. The failure mode is observed as bolts in shear during experimental studies, whereas the CBFEM predicts the bearing failure. It is reported in a study [11] that the top bolt failed earlier than the other 2 bolts failed. In the CBFEM the plastic strain occurs around the top bolt hole with the bolt failure. Figure 5.71 provides the stress distribution on the fin plate joints at 650°C. The higher stress values concentrated around the top bolt hole as the same as in other specimens.

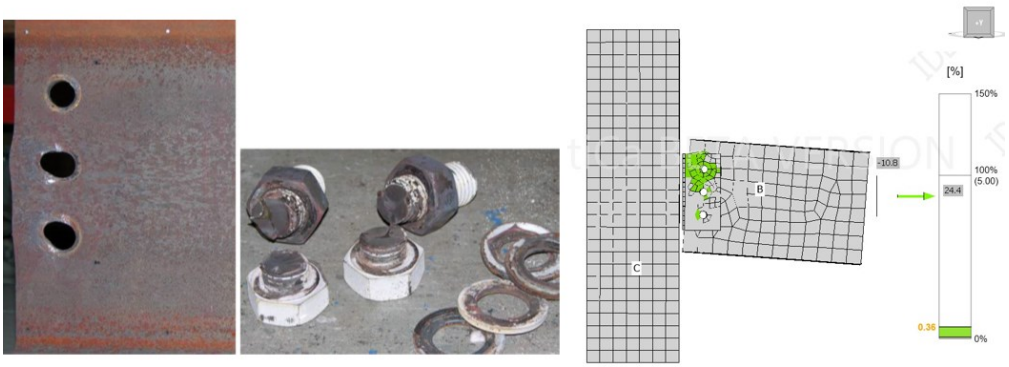

Figure 5.70. Strain check for test specimen with bolt grade 10.9 at elevated temperatures

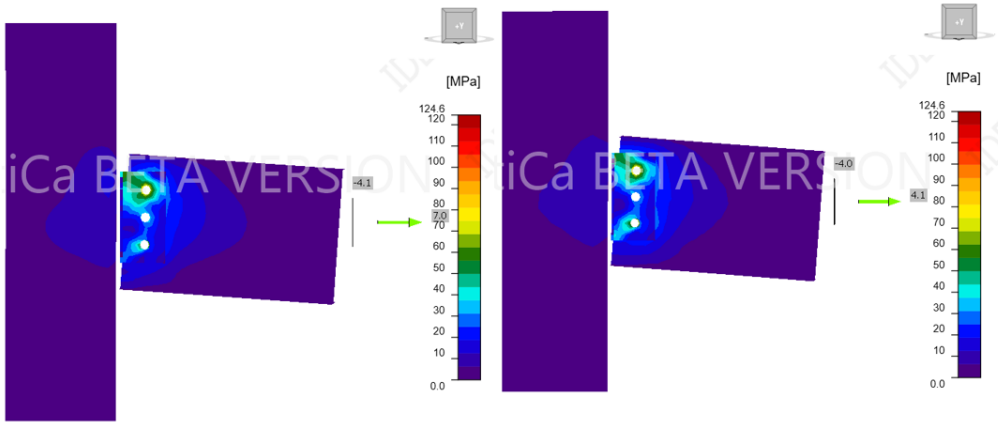

Figure 5.71. Stress distribution of fin plate joints with 35° (left) and 55° (right) at 650°C

5.3.5. Flush Endplate Joints

The assembly of the flush endplate joint is depicted in Figure 5.72. The column is restrained on both ends. The beam is subjected to normal and shear force to simulate the inclined forces in tests. All components of the modelled joints are exposed to the targeted temperature. The beam is modelled without any constraints in order to obtain the load-rotation graphs.

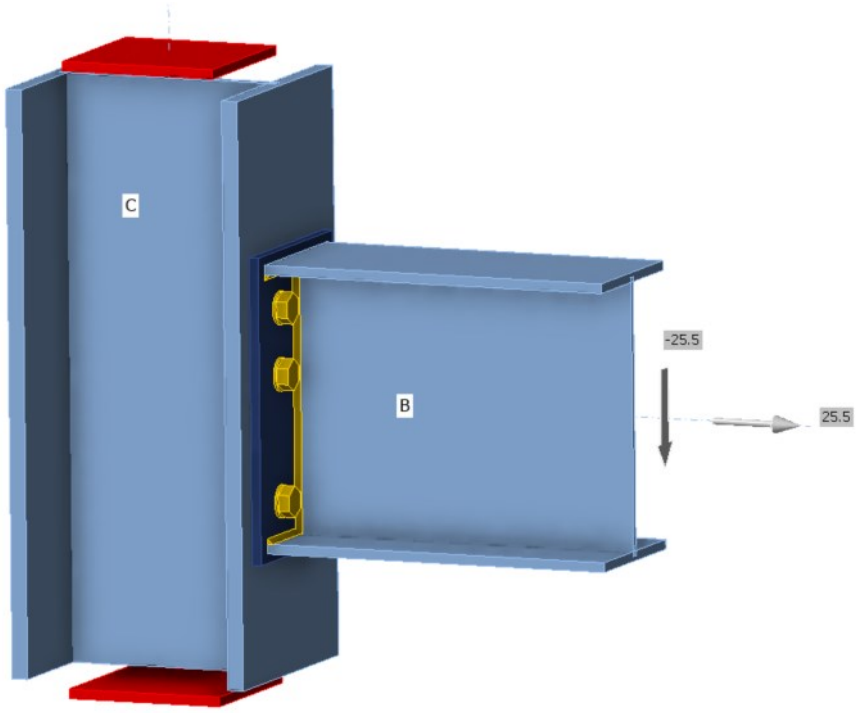

Figure 5.72. Assembly of the studied flush endplate connection

Mesh Sensitivity Study

A mesh sensitivity study is a critical issue for finite element modelling. To assess the accuracy of the numerical design calculations and optimize the computational cost, a mesh sensitivity study is performed for flush endplate joints. The study shows that the coarse mesh predicts higher resistance than the fine mesh. Figure 5.73 shows the influence of the number of elements on the connection resistance. However, increasing the number of mesh elements leads to higher computational costs. Therefore, the optimized element number is selected as 30 to divide the plates in the CBFEM.

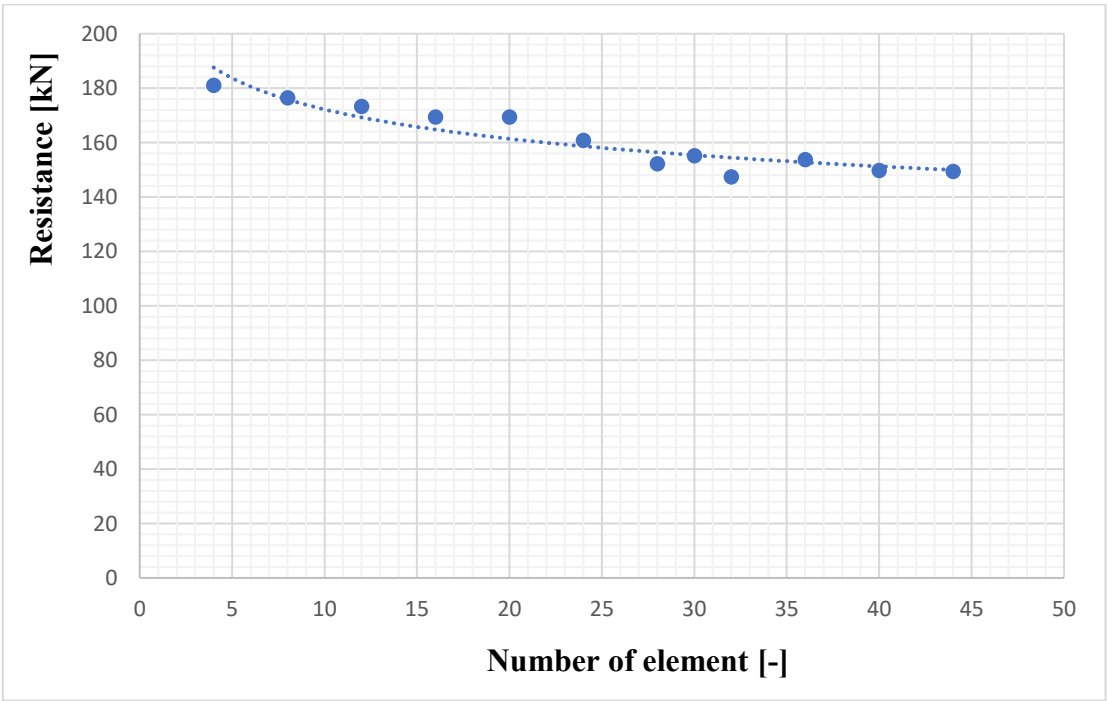

Figure 5.73. Mesh sensitivity study for flush endplate joints

Validation

In order to understand the mechanical response of flush endplate joints at high temperatures, the study of Yu et al. [37] on bolted beam-to-column joints was selected since several failure modes were observed. This chapter presents the validation of the CBFEM model using experimental results. The CBFEM model is validated in terms of the load-deformation curves and failure modes.

In the numerical model, the applied load is divided into its components using trigonometric equations as normal and shear force. In this section, Figure 5.74-Figure 5.77 shows the comparison between the load-rotation curves obtained from the experimental study (solid lines) and the CBFEM (dashed lines). In Figure 5.74, the results from the test and the CBFEM for the 35° loading angle are presented. At 35°, the load capacity of the flush endplate joints is underestimated by the CBFEM.

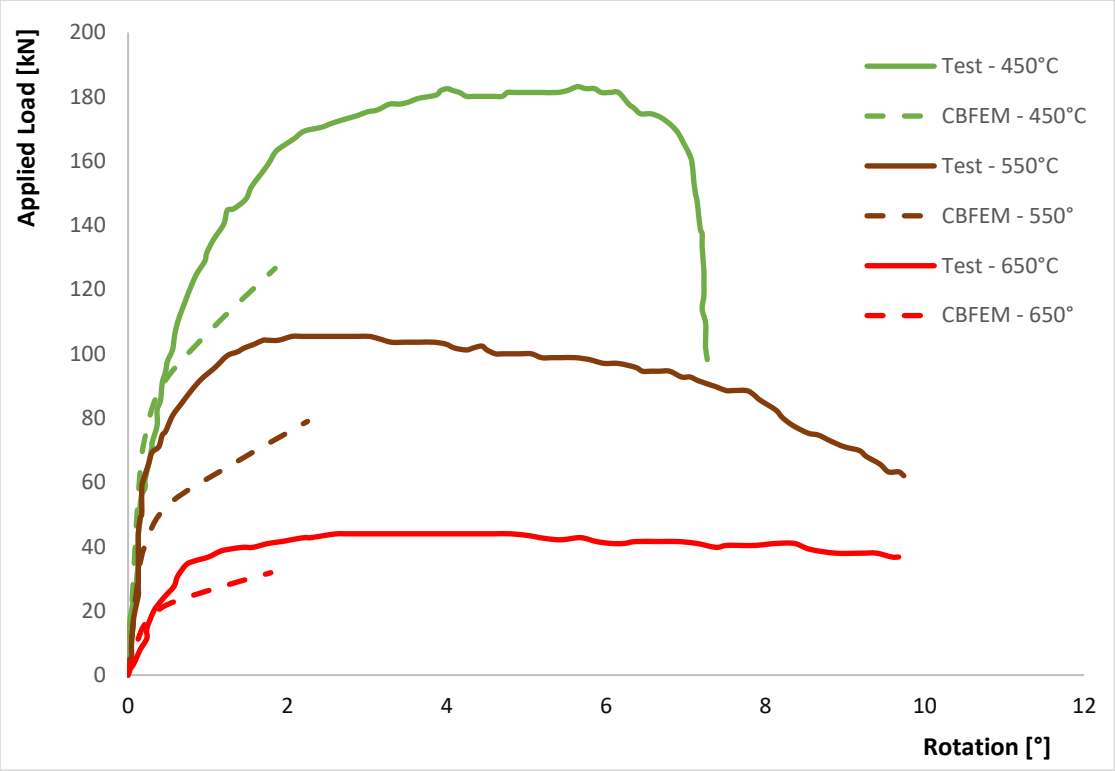

Figure 5.74. The load-rotation graph - 35°

A comparison of the load–rotation response of the joint loaded with 45° is shown in Figure 5.74. It can be seen that the load–rotation response curves of the joint agree well with tests and the CBFEM model. Furthermore, there exists a strong correlation between the initial stiffness derived from the CBFEM analysis and the results obtained through tests.

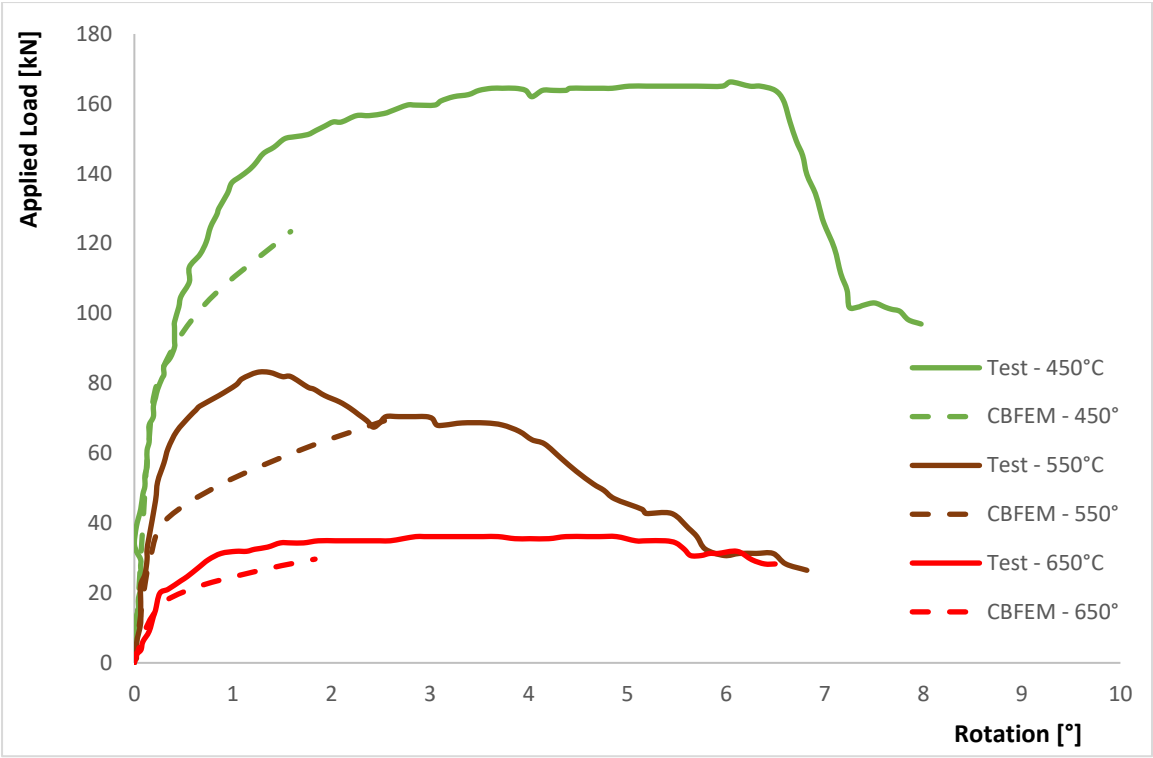

Figure 5.75. The load-rotation graph - 45°

The load-rotation behaviour of the tested connection, calculated by the CBFEM, is shown in Figure 5.76 for ambient and elevated temperatures. It can be seen that there is a good correlation for rotations up to 2° between test results and calculated load-rotation behaviour. The influence of endplate thickness on the behaviours of the connection at 550°C is depicted in Figure 5.77. Increasing the thickness of endplates enhances the resistance of flush endplate joints, however, the ductility of the joints is decreasing.

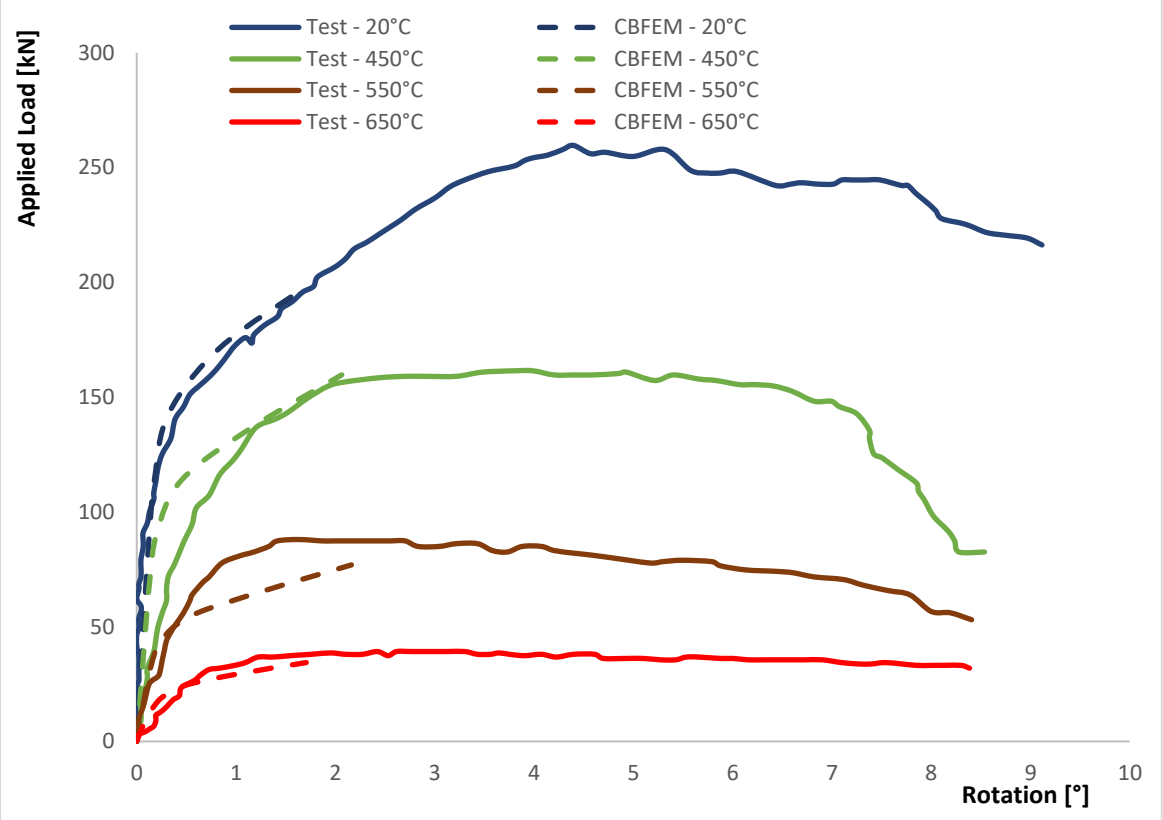

Figure 5.76. The load-rotation graph - 55°

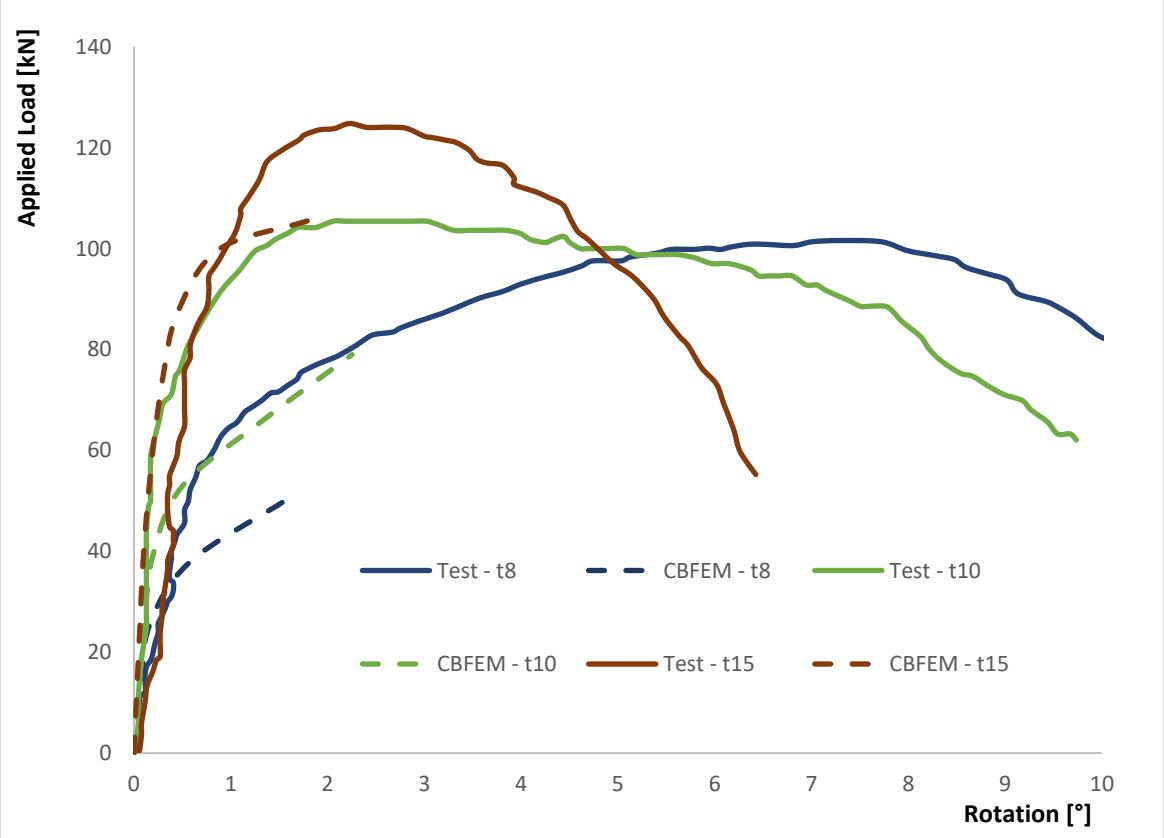

Figure 5.77. The load-rotation graphs of different thickness plates at 550°C

Authors from the experimental study reported that the test specimens with 10 mm plate thickness failed due to two failure modes [38]. Fracture of the endplate governs the failure mode of testes specimens at ambient and 450°C. However, the bolts in the top row also have significant deformation, but no fracture is observed at 450°C, as seen in Figure 5.78. It can be seen that a small crack is developed during tests and the plastic strain on the beam web near the weld equals the limit strain.

a)

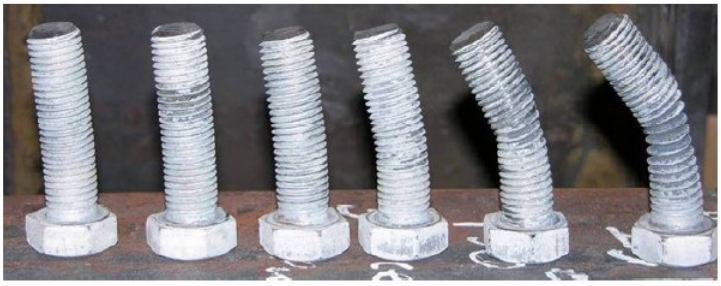

b)

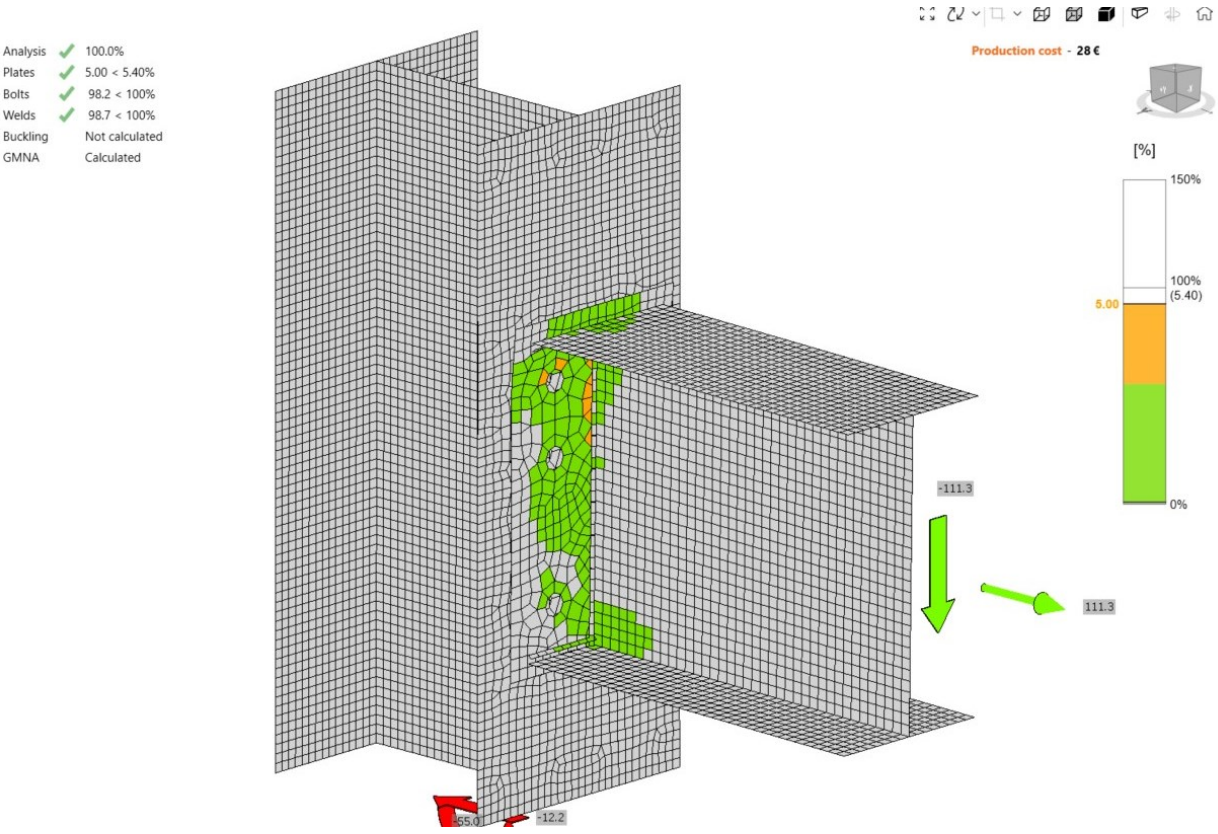

Figure 5.78. Deformed shape of the connection at 450°C, a-) test, b-) CBFEM

At 550°C and 650°C, the top two bolts were completely fractured with high ductile behaviour and a moderate bending deformation occurred in the endplate. Figure 5.79 indicates the endplate and bolts at 650°C after failure and plastic strain distribution on the test specimen obtained from the CBFEM. As observed in the test, the CBFEM measures only 0.3% plastic strain while the bolts in the top row reach their ultimate capacity.

a)

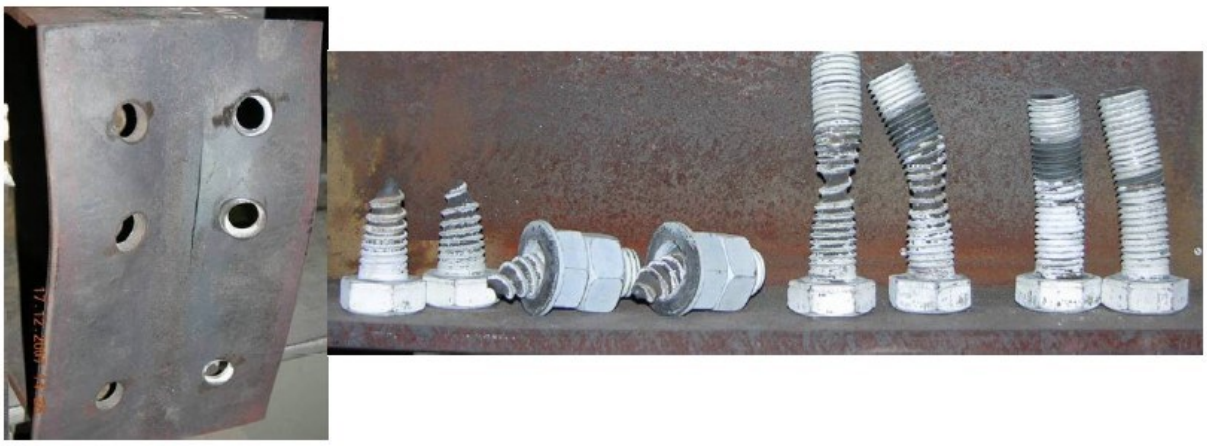

b)

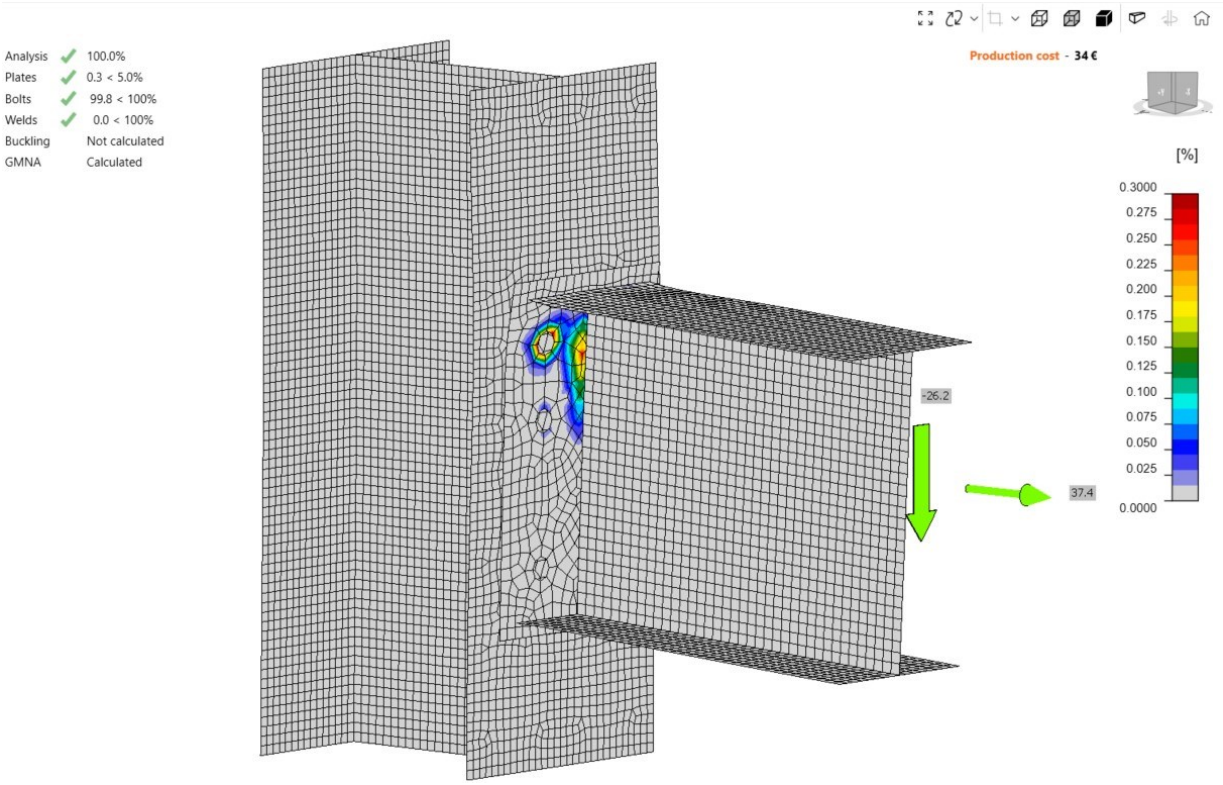

Figure 5.79. Deformed shape of the connection at 650°C a-) test, b-) CBFEM

The flush endplate joints using the endplate thickness of 8 mm are tested at ambient temperature and 550°C. At room temperature, the endplate deformation leads to the failure of the test specimen. The bolts don't have significant deformation. Figure 5.80 shows that the observed deformations of the connection components were followed by the CBFEM model at 550°C. It can be observed that the failure is controlled by the bolt fracture. In CBFEM, the bolts at the top row reach 99.9% capacity. Severe bending occurred in the endplate and the plastic strain of the endplate equals to 4.34% which is close to the limit strain.

a)

b)

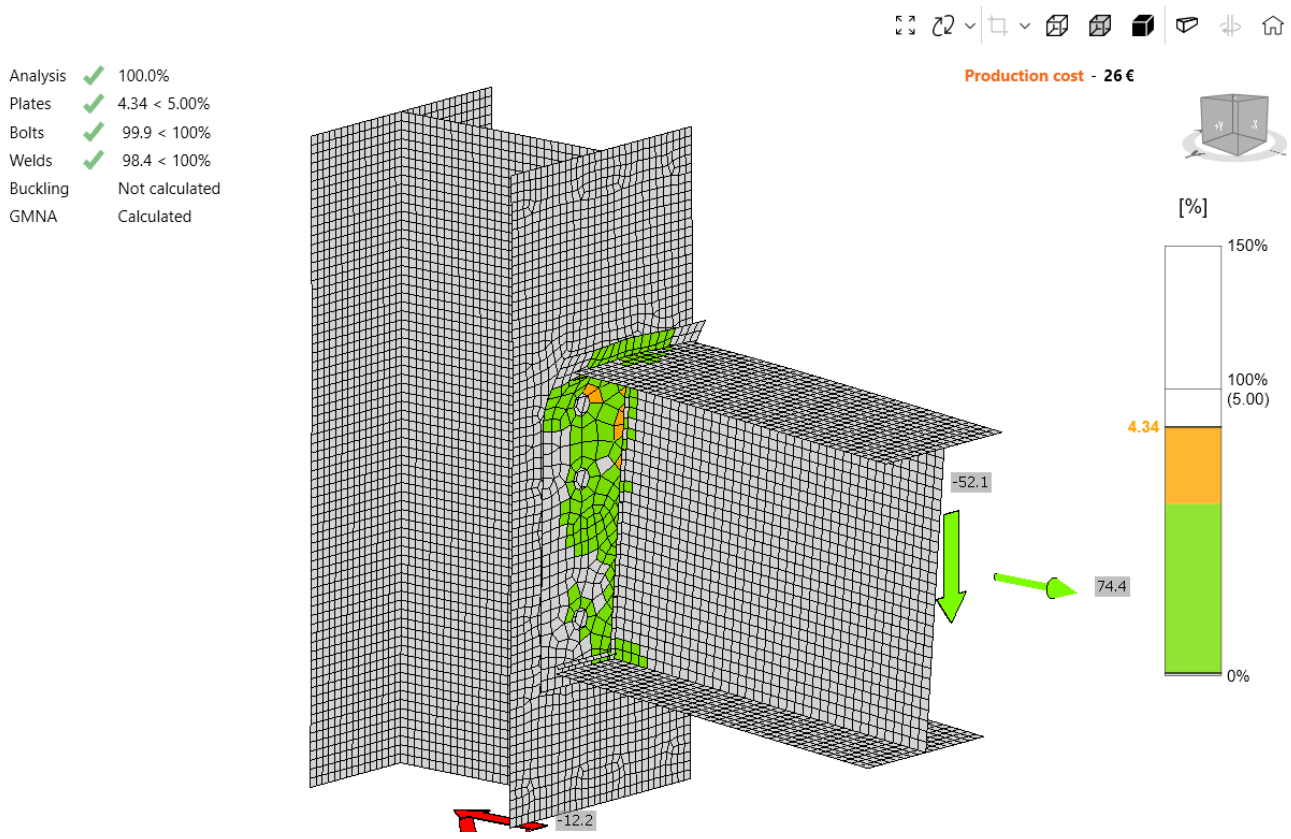

Figure 5.80. Deformed shape of the connection with 8 mm endplate at 550°C a-) test, b-) CBFEM

Table 5.11 lists the comparison of the failure modes from test results and the CBFEM models. In the CBFEM, the 5% plastic strain on the endplate means that the failure happens in the endplate. Meanwhile, if the bolt capacity reaches 100% capacity before steel plates have 5% plastic strain, the connection fails due to the bolt failure. The capacity of bolts is calculated using the equations for bolts in tension, shear, and bearing according to Eurocode. As can be seen in Table 5.11, the CBFEM

models predicted the same failure modes for all test specimens as observed during the experimental study. Although the load-deformation curves indicated that the resistance is changing according to the loading angle, there is no influence on the failure modes of flush endplate joints.

Table 5.11. Comparison of failure modes from test and the CBFEM model

Test Number	Test Description		CBFEM	Test	Test Number	Test Description		CBFEM	Test
	Angle [°]	T [°C]	Failure Mode			Angle [°]	T [°C]	Failure Mode	
2	35	450	5% plastic strain on endplate	Plate fracture	9	55	20	5% plastic strain on endplate	Plate fracture
3		550	100% bolt capacity	Bolt fracture	10		450	100% bolt capacity	Plate fracture
4		650	100% bolt capacity	Bolt fracture	11		550	100% bolt capacity	Bolt fracture
6		450	5% plastic strain on endplate	Plate fracture	12		650	100% bolt capacity	Bolt fracture
7	45	550	100% bolt capacity	Bolt fracture	13	35	20	5% plastic strain on endplate	Plate fracture
8		650	100% bolt capacity	Bolt fracture	14		550	100% bolt capacity	Bolt fracture
					15		550	100% bolt capacity	Bolt fracture

Parametric studies for finite element models are performed to investigate the sensitivity of the model and its responses to variations in key parameters. The investigated parameters are plastic limit strain, bolt elongation, and bolt diameter. The specimens from Test 6 and Test 8 are selected for parametric studies since two different failures were observed. To investigate the influence of the plastic limit strain which is recommended in EN 1993-1-5 [13] on the load-rotation curves of flush endplate joints at 450°C and 650°C, the plastic limit strain varies from 5% to 15%. Increasing the plastic limit strain of steel plates does not change the trend of the load-rotation curve; however, the rotation capacity is increased from 2.26° to 3.7° at 450°C. Figure 5.81 and Figure 5.82 present the influence of the plastic limit strain at 450°C and 650°C, respectively.

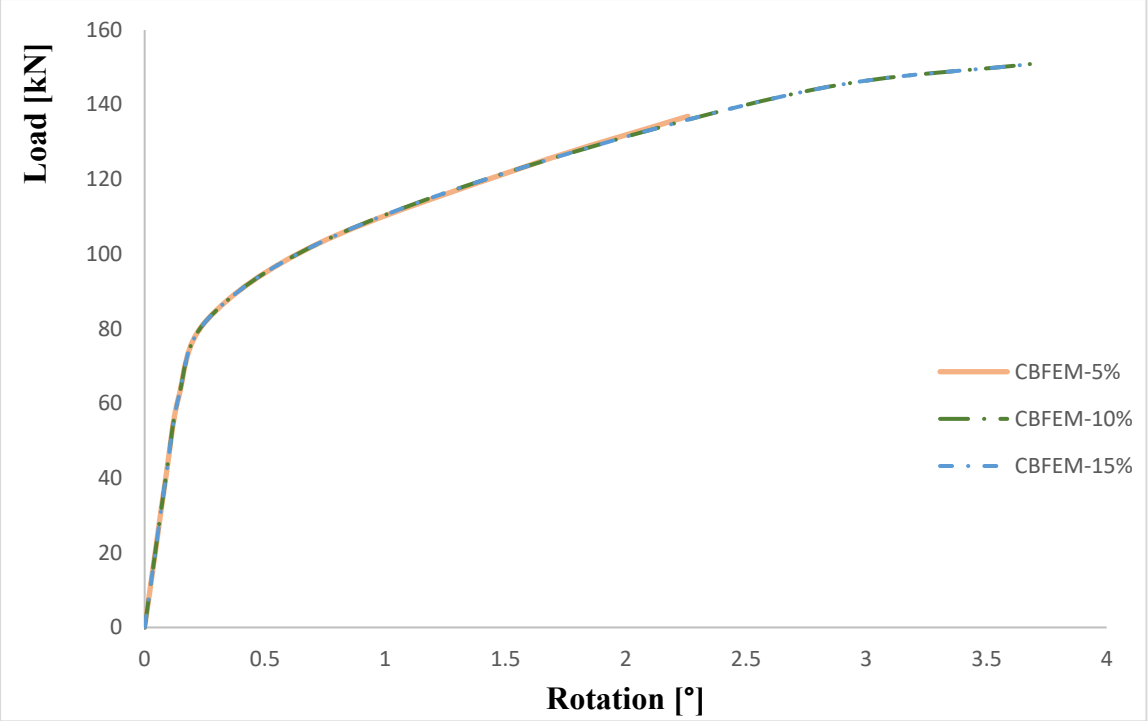

Figure 5.81. The influence of the plastic limit strain at 450°C

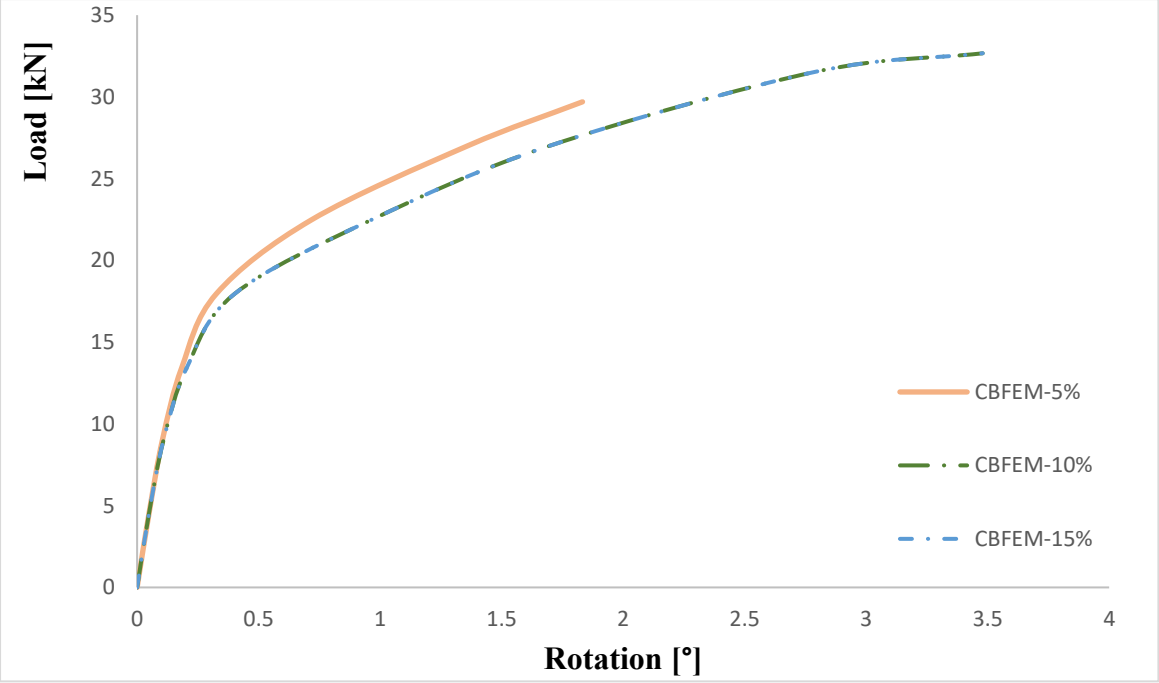

Figure 5.82. The influence of the plastic limit strain at 650°C

ISO 898 [96] proposes the values of bolt elongation for different bolt types at ambient temperature. The CBFEM uses these values to prepare the load-deformation model for bolts to model the bolted connection. Furthermore, the test results showed that the bolt behaviour is highly ductile at elevated temperatures. Therefore, the influence of bolt elongation on the mechanical response of the tested joints is analysed by varying the bolt elongation from 12% to 20%. The results of the CBFEM in terms of load-rotation curves for each value of the bolt elongation are depicted in Figure 5.83 and Figure 5.84. Figure 5.83 shows that bolt elongation does not have a significant effect on the joint behaviour if the joints fail due to the plate fracture. While the bolt elongation is increased, the

resistance of the joint is decreased with higher rotation capacity. As the bolt elongation increases, the joint's resistance is reduced, accompanied by an enhanced rotation capacity, as depicted in Figure 5.84.

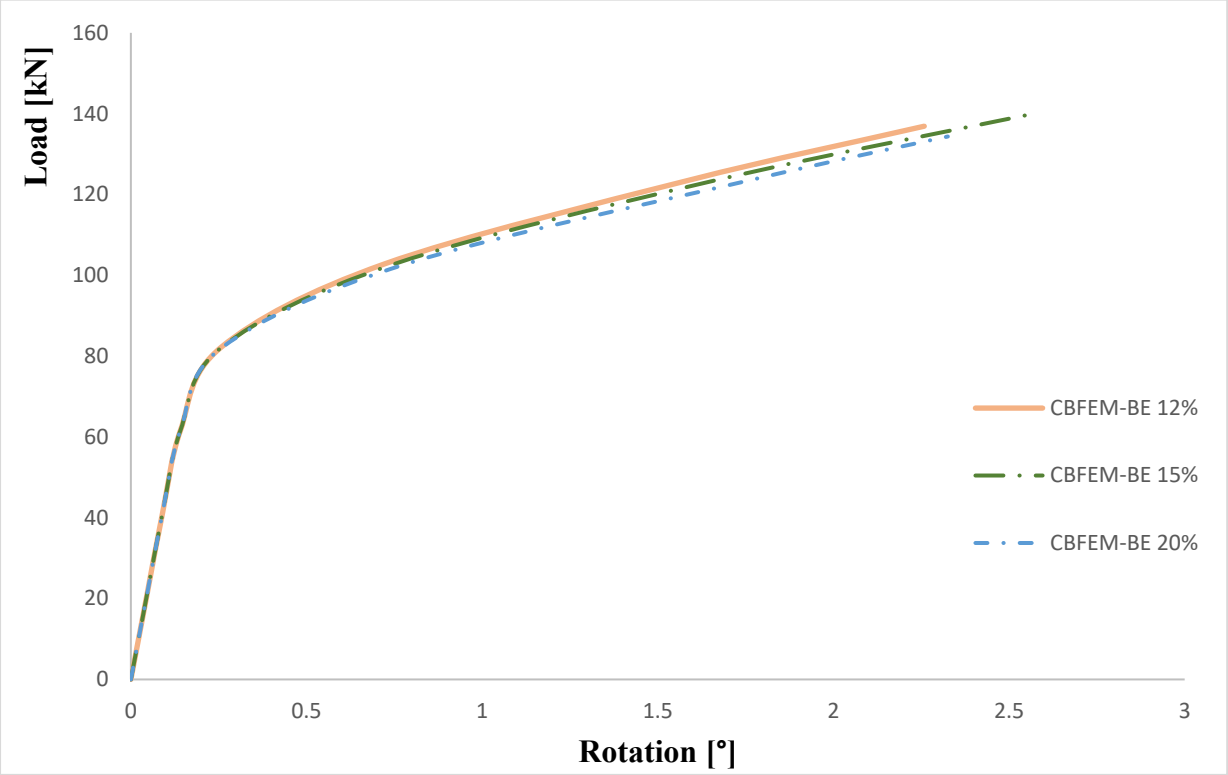

Figure 5.83. The influence of the bolt elongation at 450°C

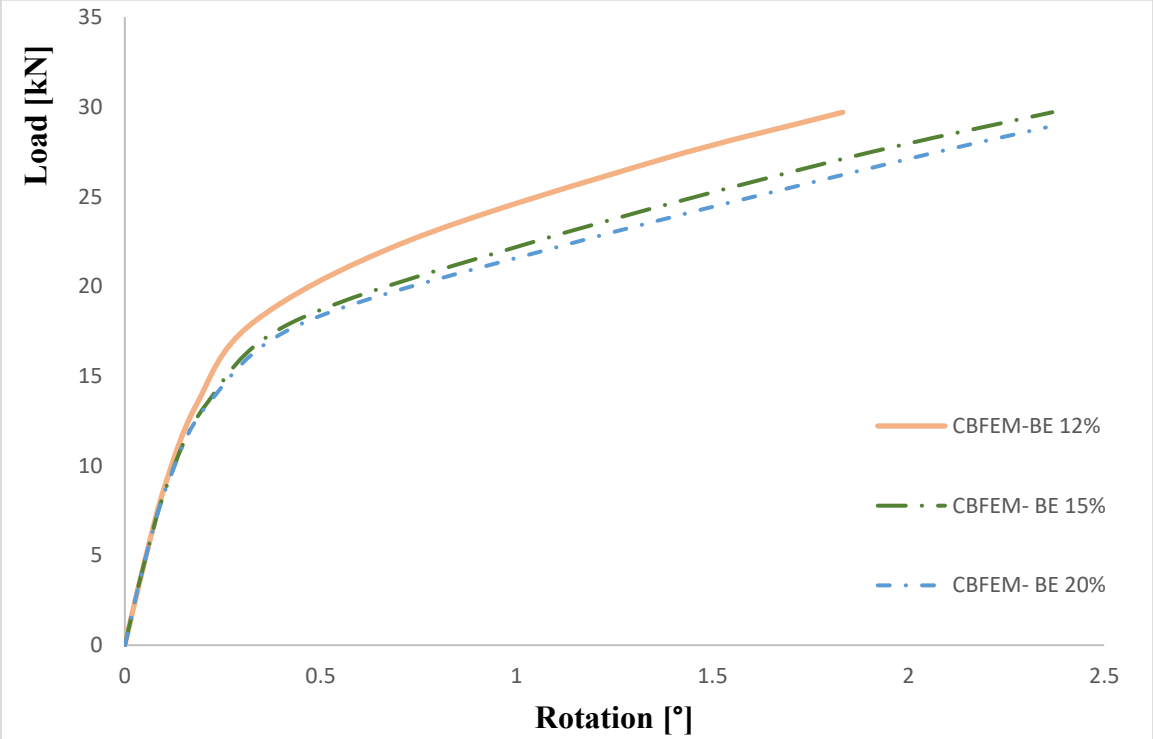

Figure 5.84. The influence of the bolt elongation at 650°C

The bolt diameter also plays an important role in the behaviour of the analysed joints at elevated temperatures. In fact, the increase in the bolt diameter results in a progressive increase in the joint resistance. Conversely, the decrease in the bolt diameter leads to an increase of the joint rotation capacity at 450°C and 650°C, as shown in **Figure 5.85** and **Figure 5.86**.

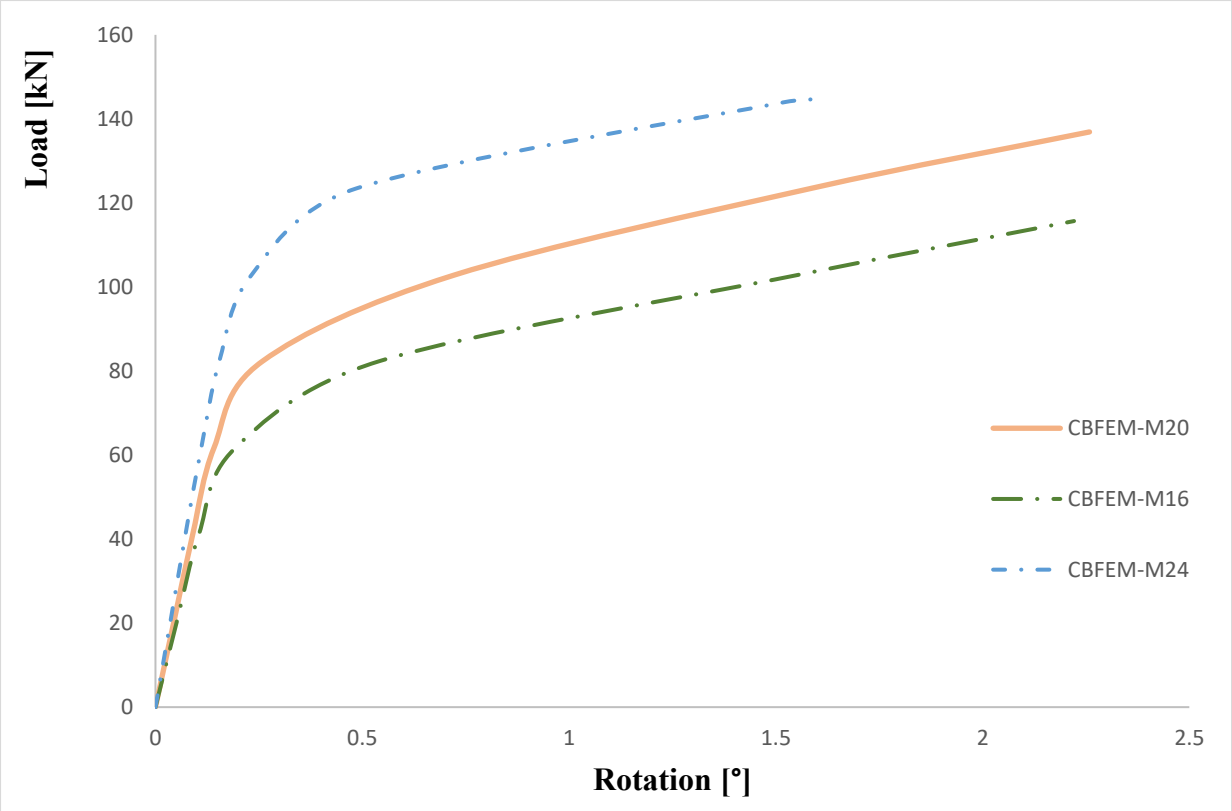

Figure 5.85. The influence of the bolt diameter at 450°C

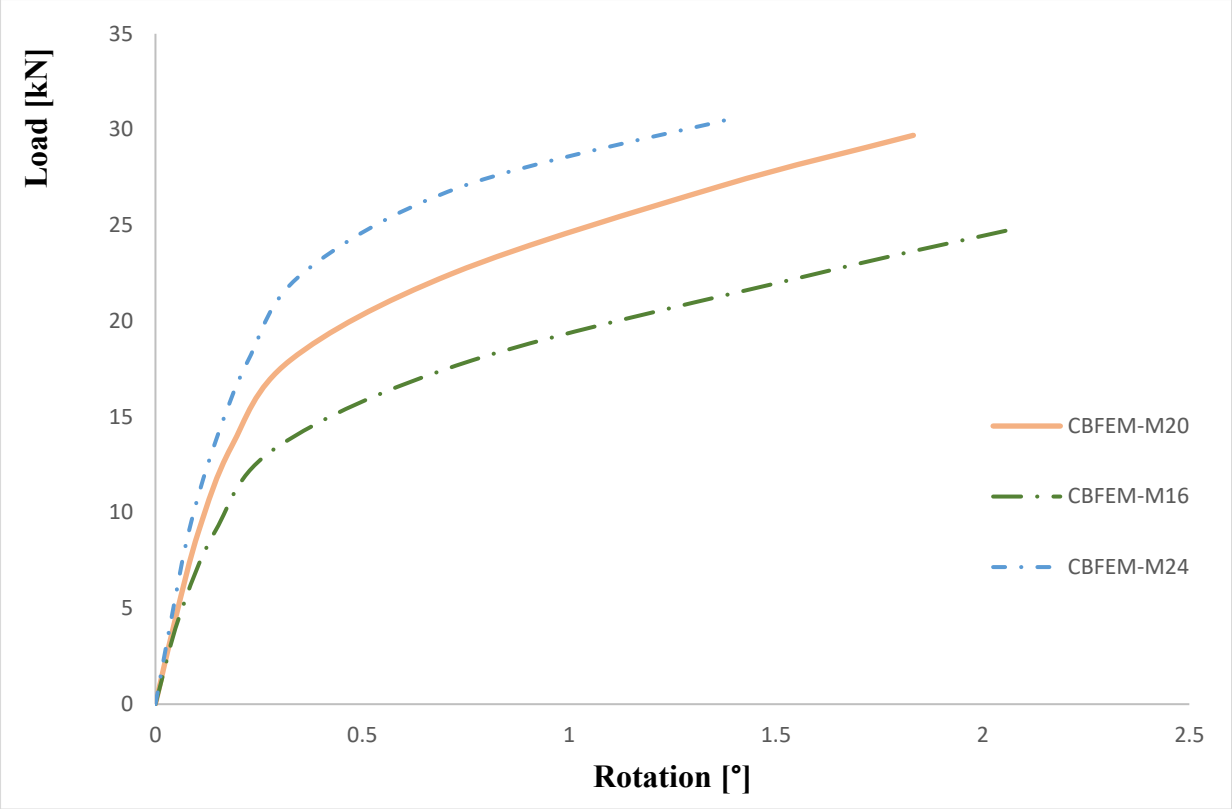

Figure 5.86. The influence of the bolt diameter at 650°C

The CBFEM model was generated to develop a numerical design calculation for flush endplate joints at elevated temperatures. The CBFEM model is validated based on test results from the literature and is verified against Eurocode design specifications. Then, parametric studies were employed to assess the influence of key parameters on the behaviour of flush endplate joints at elevated temperatures.

The experimental and numerical plots demonstrated that the NDC models may predict the bolted connection behaviour at both ambient and elevated temperatures. It was also observed that the connections, both in the CBFEM models and the experiments, failed by the same failure modes. The characteristics of load-rotation curves, developed by the CBFEM, are in good agreement with measured test data. The CBFEM model was verified by comparing the resistance of the T-stub specimens calculated from Eurocode equations. The coefficient of determination was evaluated as 0.95. It can be concluded that the CBFEM is a reliable method to design bolted connections compared to the analytical model, The parametric study investigated the effect of three parameters on the load-deformation curves. The results stated that the most effective parameter on the behaviour of flush endplate joints at elevated temperatures was the bolt diameter.

5.4. CBFEM Models for Steel Members

4-node quadrangle shell elements with nodes at their corners are used to simulate plates. The material behaviour is based on the Von Mises yield criterion. It is assumed to be elastic before reaching the yield strength f_y. The value of a 5% plastic limit strain is recommended for predicting the resistance. The uniform temperature distribution is applied to each member of the study. The numerical model is able to predict the resistance at the target temperature by user-defined. EN 1993-1-2 [10] proposes design methods to evaluate the fire resistance of steel members as follows:

- Simplified calculation models

- Advanced calculation models
- Testing

Simple calculation models are used to simply design individual members considering conservative assumptions. In this thesis, a benchmark study for steel beams and steel columns exposed to fire is prepared using simple models to provide safe design values for designers. To use these simplified rules the cross-sections may be classified as normal temperature design with a reduced value, $\varepsilon = 0.85$. As recommended in Eurocode 3, the steel member can be tested from global analyses at ambient temperatures. Then, a cross-section check may be done reducing the material properties of steel members.

5.4.1. Steel Beams

The mechanical response of the steel beam was studied using the CBFEM model. In order to apply boundary conditions, the columns were used to constrain the movement of a steel beam. The beam and columns were connected by the endplates to allow the beam ends to rotate, as shown in Figure 5.87. The columns and endplates were not subjected to high temperature. Therefore, material degradation happens only in steel beams due to the elevated temperature.

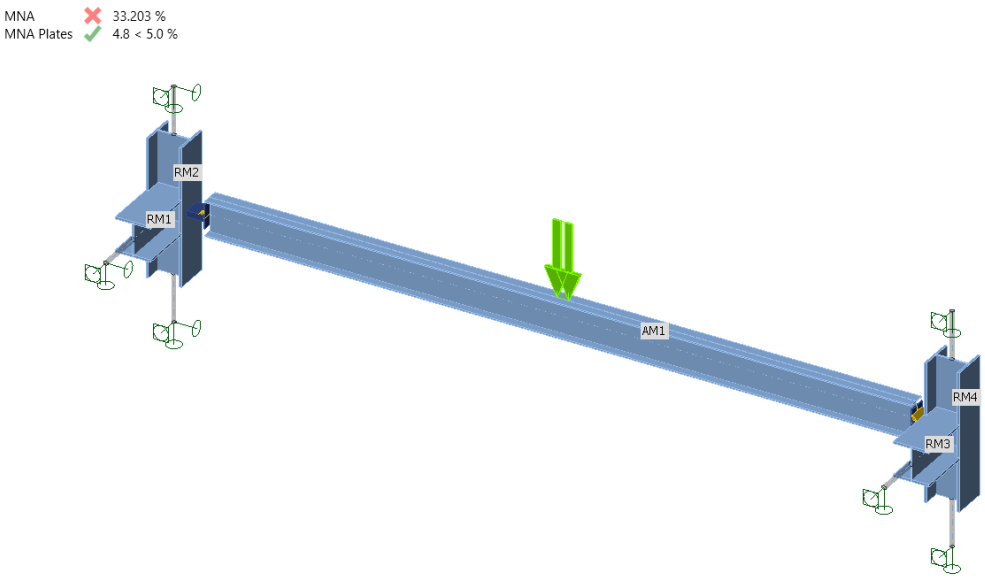

Figure 5.87. Assembly of steel beam in the CBFEM

Mesh Sensitivity Study

A mesh sensitivity study of a steel beam under distributed load at elevated temperature is presented. The geometry of the steel beam is shown in Figure 5.88. The web and flange of the steel beam are subdivided into 8 to 40 elements, and the minimal element size is set to 1 mm. The influence of the number of elements on the bending resistance is shown in Figure 5.89 and Figure 5.90. The dashed lines represent the 5 %, 10 %, and 15 % differences. It is recommended to use 16 elements on the web and the flange width of steel beams in the fire.

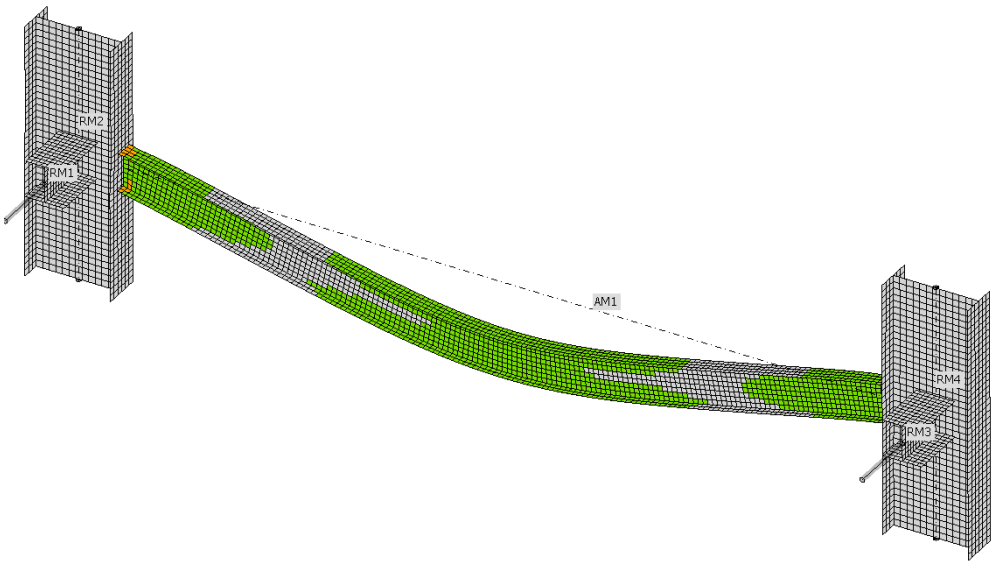

Figure 5.88. Mesh distribution over the web and flange of steel beam

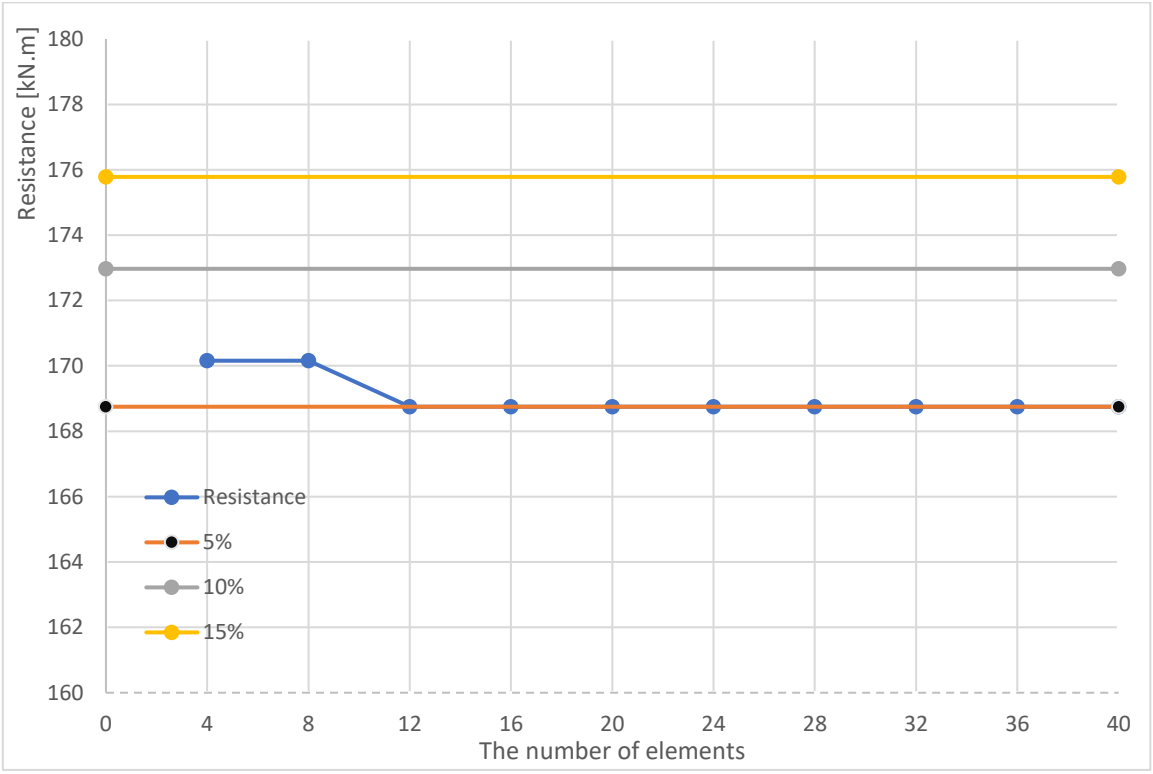

Figure 5.89. Influence of number of elements on the steel beam (IPE 300 - simply support) bending resistance at 500°C.

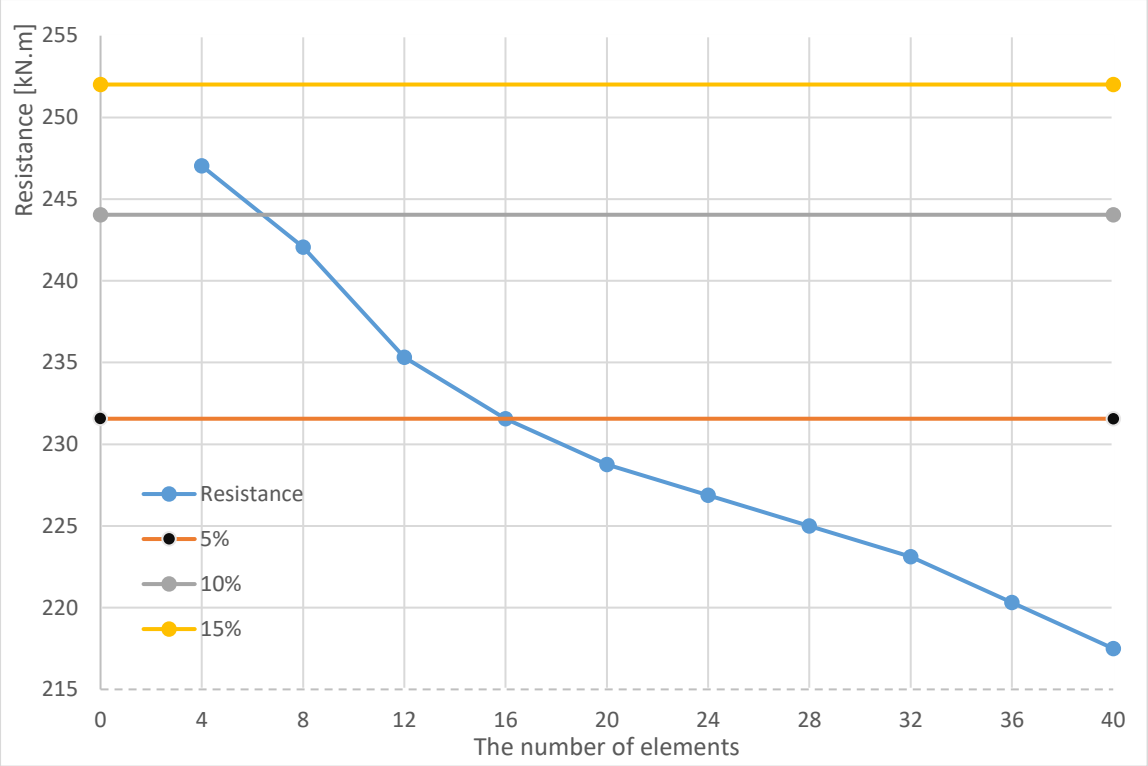

Figure 5.90. Influence of number of elements on the steel beam (IPE 300 – fixed end) bending resistance at 450°C.

Verification

The study includes a beam from the IPE300 section with a span of L = 6 m, which is loaded by concentrated force at the midspan at the top flange. The beam is assumed to have a uniform temperature along the cross-section and length of the beam. Elastic modulus and yield strength of steel beam at room temperature are taken as 210000 N/mm^2 and 355 N/mm^2, respectively. In all cases, Poisson's ratio is 0.3 and non-temperature dependent. Then, the three different moment resistance values, (bending, critical elastic, and lateral-torsional buckling) are calculated through the equations proposed in EN 1993-1-2 [10] to verify results from the proposed shell model. Finally, parametric studies are prepared changing the different parameters such as cross-section, length of the span, loading, and boundary conditions. The objective of this study is to provide numerical and analytical results using the shell model generated in FEA software [11] and EN 1993-1-2 equations to show the applicability of the simple shell model in structural fire engineering.

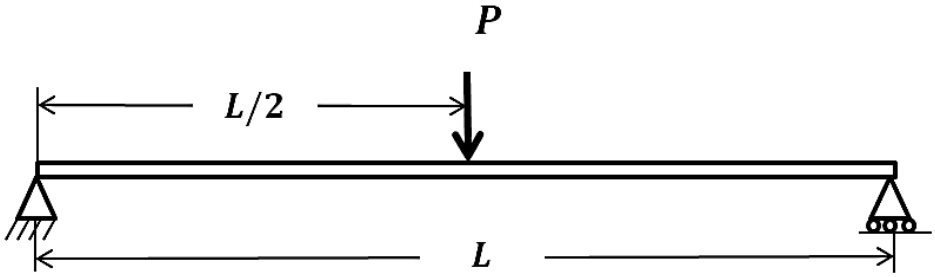

Figure 5.91. Model description

The moment resistance of the steel beams at elevated temperatures is calculated according to clause 4.2.3.3 in EN 1993-1-2 [10]. The design moment resistance $M_{fi,\theta,Rd}$ of a Class 1, Class 2 or Class 3 cross-section with a uniform temperature θ_a should be determined from:

$$M_{fi,\theta,Rd} = k_{y,\theta}[\gamma_{M0}/\gamma_{Mfi}]M_{Rd} \tag{36}$$

where $k_{y,\theta}$ is the reduction factor for the yield strength of steel at a uniform temperature θ_a, reached at time t, γ_{M0} is a partial safety factor for the resistance of cross-sections, γ_{Mfi} is a partial safety factor for the relevant material property, for the fire situation, M_{Rd} is the design resistance for bending about one principal axis of a cross-section for normal temperature design. Clause 6.2.5 in EN 1993-1-1 [107] gives the following expressions to calculate the design bending resistance of sections class 1 and 2 at ambient temperature:

$$M_{Rd} = M_{pl,Rd} = \frac{W_{pl}f_y}{\gamma_{M0}} \tag{37}$$

There is no formulation or guidance for the calculation of the elastic critical moment (M_{cr}) in Clause 6.3.2.2(2) of EN 1993-1-1. A general expression proposed by NCCI SN003 [112] is used to calculate the elastic critical moment for lateral-torsional buckling considering the shape of the bending moment diagram, different end restraint conditions, warping restraints, in-plane curvature before buckling, and the level at which the load is applied.

$$M_{cr} = C_1 \frac{\pi^2 EI_z}{(kL)^2}\left(\sqrt{\left(\frac{k}{k_w}\right)^2 \frac{I_w}{I_z} + \frac{(kL)^2 GI_t}{\pi^2 EI_z} + \left(C_2 z_g\right)^2} - C_2 z_g\right) \tag{38}$$

in which I_t is the torsion constant, I_w is the warping constant, E is the modulus of elasticity, G is the shear modulus, I_z is the second moment of area about the minor axis, L is the length of the beam between points of lateral restraint, z_g is the distance between the level of application of the loading and the shear centre (and is positive for destabilising loads applied above the shear centre when the load is acting downwards), C_1 and C_2 are parameters, which can be taken from Table 5.12, k_w is a warping restraint parameter. Where warping restraint is not provided, and as a conservative assumption when the degree of warping restraint is not certain, k_w should be taken equal to unity [107]. According to clause 4.2.3.3 in EN 1993-1-2, the design lateral-torsional buckling resistance moment $M_{b,fi,t,Rd}$ at time t of a laterally unrestrained member with a Class 1 or Class 2 cross-section should be determined from:

$$M_{b,fi,t,Rd} = \chi_{LT,fi} W_{pl,y} \frac{k_{y,\theta,com} f_y}{\gamma_{M1}} \tag{39}$$

where $W_{pl,y}$ is the plastic section modulus of cross-section, $k_{y,\theta,com}$ is the reduction factor for the yield strength of steel considering the maximum temperature in the compression flange θ_{com} reached at time t, and $\chi_{LT,fi}$ is the reduction factor for lateral-torsional buckling in the fire design situation, which is calculated using the following equation:

$$\chi_{LT,fi} = \frac{1}{\phi_{LT,\theta,com} + \sqrt{[\phi_{LT,\theta,com}]^2 - [\lambda_{LT,\theta,com}]^2}} \tag{40}$$

with

$$\phi_{LT,\theta,com} = \frac{1}{2}[1 + \alpha\bar{\lambda}_{LT,\theta,com} + \left(\bar{\lambda}_{LT,\theta com}\right)^2] \tag{41}$$

and the imperfection factor, α, which was proposed by Vila Real et al. [113] , is given by

$$\alpha = 0.65\sqrt{\frac{235}{f_y}} \tag{42}$$

and, for Class 1, 2 and 3 the non-dimensional elevated temperature LTB slenderness of a steel beam $\bar{\lambda}_{LT,\theta,com}$ is determined through the following expression:

$$\bar{\lambda}_{LT,\theta,com} = \bar{\lambda}_{LT}\sqrt{k_{y,\theta,com}/k_{E,\theta,com}} \tag{43}$$

in which $k_{E,\theta,com}$ is the modulus of elasticity reduction factor at the maximum steel temperature in the compression flange,

$$\bar{\lambda}_{LT} = \sqrt{\frac{W_y f_y}{M_{cr}}} \tag{44}$$

Table 5.12, C_1 and C_2 values for transverse loading [112]

Loading and support conditions	Bending moment diagram	C_1	C_2
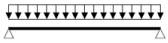		1.127	0.454
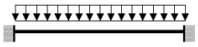		2.578	1.554
		1.348	0.63
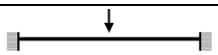		1.683	1.645

The results were presented here in terms of bending resistance, critical elastic moment, and lateral-torsional buckling resistance. Even though the presence of endplates in the shell model creates some amount of the warping restraint, it is assumed that k_w equals unity due to the uncertainty of warping restraint degree in the analytical model. This assumption may result in a difference between numerical and analytical results in the evaluation of critical elastic moment and lateral-torsional buckling resistance. The bending resistance of steel beams at high temperatures according to Eq. 37 is dependent on the steel grade and the cross-section type. In this study, only the cross-section type was changed in the shell model and the results are presented in Table 5.13.

Table 5.13. Bending resistance (kN.m)

T (°C)	IPE 200			IPE 300			IPE 400		
	Eurocode	Shell	CBFEM	Eurocode	Shell	IDEA	Eurocode	Shell	IDEA
20	78.31	77.40	78.95	223.08	222.32	226.87	463.99	456.64	467.59
100	78.31	77.40	78.95	223.08	222.32	226.87	463.99	456.64	467.59
200	78.31	76.79	77.34	223.08	218.09	222.19	463.99	444.53	457.76
300	78.31	76.65	77.02	223.08	216.92	222.19	463.99	440.51	455.30
400	78.31	76.56	77.02	223.08	215.48	221.26	463.99	436.69	455.30
500	61.08	59.77	59.94	174.00	168.44	172.51	361.91	341.70	354.38
600	36.81	35.98	36.09	104.85	100.67	104.06	218.07	204.57	214.07
700	18.01	17.60	17.72	51.31	49.03	50.62	106.72	98.69	103.38
800	8.61	8.43	8.38	24.54	23.74	24.38	51.04	48.06	49.20

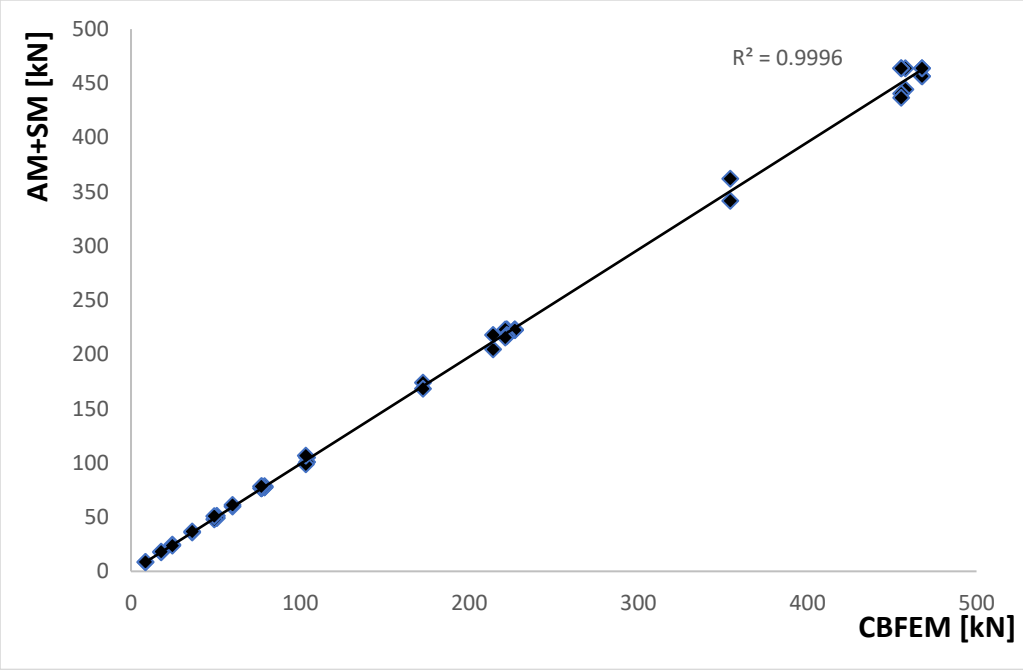

Figure 5.92. Summary of bending resistance comparison

The goal of this section is the verification of the linear buckling analysis (LBA) module of the IDEA Member application. The influence of different loading conditions, boundary conditions, and the beam span are investigated. The resulting elastic critical moments from IDEA Member are compared to the elastic critical moments based on analytical and numerical models. The LBA provides the buckling shapes of steel beams in order to consider the imperfection effect on steel beams. In Table 5.14, the results are shown to investigate the influence of the cross-section type on the elastic critical

moment resistance of steel beams at elevated temperatures. The tested beam is 6 m in length and is exposed to concentrated load in the mid-section of the beam. Table 5.15 indicates the elastic critical moment resistance of steel beams under different boundary and loading conditions. Furthermore, the beam span length was changed from 5 m to 7 m and the results can be seen in Table 5.16.

Table 5.14. Critical Elastic Moment (kN.m) – cross section

T (°C)	IPE 200 - 6 m				IPE 300 - 6 m				IPE 400 - 6 m			
	Analytical	Shell	LTBeam	CBFEM	Analytical	Shell	LTBeam	CBFEM	Analytical	Shell	LTBeam	CBFEM
20	24.37	22.35	25.07	24.89	85.54	82.60	88.65	86.18	207.18	195.37	215.71	202.73
100	24.37	22.35	25.07	24.89	85.54	82.60	88.65	86.18	207.18	195.37	215.71	202.73
200	21.93	20.11	22.56	22.57	76.98	74.34	79.79	77.95	186.46	175.83	194.14	183.08
300	19.49	17.88	20.06	20.25	68.43	66.08	70.92	69.70	165.74	156.30	172.57	163.36
400	17.06	15.64	17.55	17.90	59.87	57.82	62.06	61.42	145.03	136.76	151.00	143.64
500	14.62	13.41	15.04	15.53	51.32	49.56	53.19	53.16	124.31	117.22	129.43	123.86
600	7.55	6.93	7.77	8.51	26.52	25.61	27.48	28.75	64.23	60.56	66.87	66.15
700	3.17	2.91	3.26	3.88	11.12	10.74	11.52	13.34	26.93	25.40	28.04	29.80
800	2.19	2.01	2.26	2.77	7.70	7.43	7.98	9.77	18.65	17.58	19.41	21.55

Table 5.15. The elastic critical moment – boundary and loading conditions (kN.m)

T (°C)	Simply supported - point load				Fix supported - point load				Simply supported - distributed load			
	Analytical	Shell	LTBeam	CBFEM	Analytical	Shell	LTBeam	CBFEM	Analytical	Shell	LTBeam	CBFEM
20	85.54	82.60	88.65	86.18	138.68	124.37	134.71	124.39	78.78	75.11	78.36	76.72
100	85.54	82.60	88.65	86.18	138.68	124.37	134.71	124.39	78.78	75.11	78.36	76.72
200	76.98	74.34	79.79	77.95	124.81	111.93	121.24	112.13	70.9	67.6	70.52	69.41
300	68.43	66.08	70.92	69.70	110.95	99.50	107.77	99.83	63.02	60.09	62.69	62.14
400	59.87	57.82	62.06	61.42	97.08	87.06	94.30	87.49	55.14	52.58	54.85	54.83
500	51.32	49.56	53.19	53.16	83.21	74.62	80.83	75.11	47.27	45.07	47.02	47.52
600	26.52	25.61	27.48	28.75	42.99	38.55	41.76	39.00	24.42	23.29	24.29	25.85
700	11.12	10.74	11.52	13.34	18.03	16.17	17.51	16.39	10.24	9.76	10.19	12.17
800	7.70	7.43	7.98	9.77	12.48	11.19	12.12	11.36	7.09	6.76	7.05	9.00

Table 5.16. The elastic critical moment – span length (kN.m)

T (°C)	IPE 300 - 5 m				IPE 300 - 6 m				IPE 300 - 7 m			
	Analytical	Shell	LTBeam	CBFEM	Analytical	Shell	LTBeam	CBFEM	Analytical	Shell	LTBeam	CBFEM
20	104.88	103.16	109.33	107.6	85.54	82.60	88.65	86.18	72.81	69.19	75.08	62.17
100	104.88	103.16	109.33	107.6	85.54	82.60	88.65	86.18	72.81	69.19	75.08	62.17
200	94.39	92.84	98.4	97.3	76.98	74.34	79.79	77.95	65.53	62.27	67.57	56.23
300	83.9	82.53	87.46	86.95	68.43	66.08	70.92	69.70	58.25	55.35	60.07	50.27
400	73.42	72.21	76.53	76.6	59.87	57.82	62.06	61.42	50.97	48.43	52.56	44.28
500	62.93	61.9	65.6	66.3	51.32	49.56	53.19	53.16	43.69	41.51	45.05	38.34
600	32.51	31.98	33.89	35.75	26.52	25.61	27.48	28.75	22.57	21.45	23.28	20.70
700	13.63	13.41	14.21	17.3	11.12	10.74	11.52	13.34	9.47	8.99	9.76	9.56
800	9.44	9.28	9.84	12.15	7.70	7.43	7.98	9.77	6.55	6.23	6.76	6.98

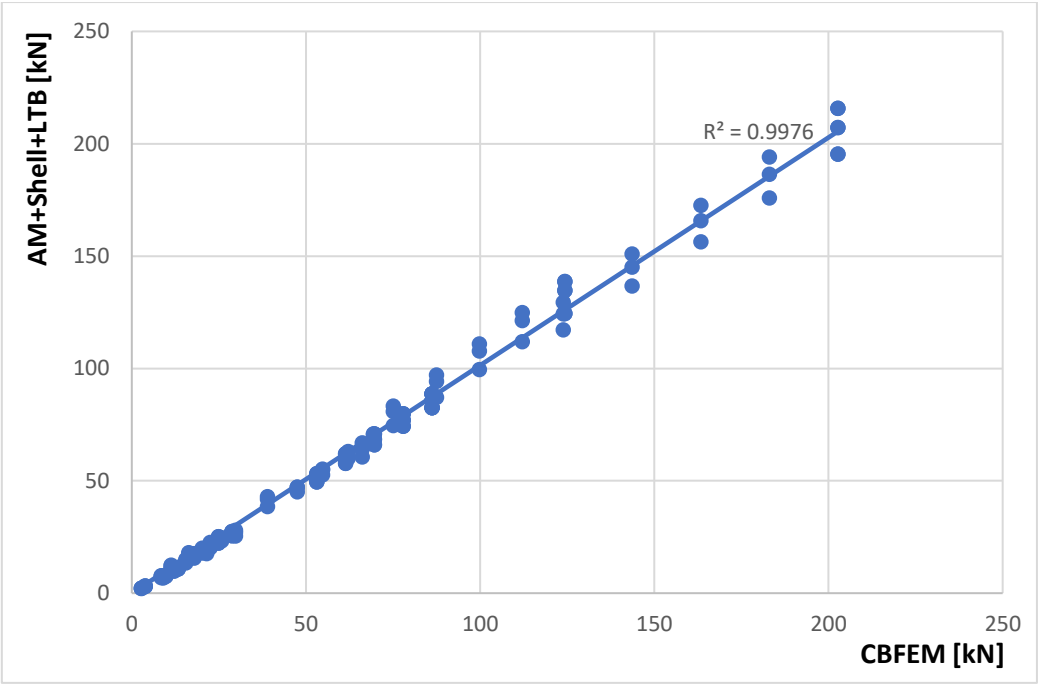

Figure 5.93. Summary of the elastic critical moment comparison

The GMNIA (geometrically and materially nonlinear analysis with imperfections) module of the IDEA Member provides the lateral torsional buckling moment resistance. Initial geometric imperfections were applied following the beam's eigenmodes obtained by linear buckling analysis (LBA).

Table 5.17. The lateral torsional buckling – cross-section (kN.m)

T (°C)	IPE 200 - 6 m			IPE 300 - 6 m			IPE 400 - 6 m		
	Analytical	Shell	CBFEM	Analytical	Shell	CBFEM	Analytical	Shell	CBFEM
20	21.32	19.73	20.95	72.28	64.54	66.55	157.67	135.78	140.30
100	21.32	19.73	20.95	72.28	64.54	66.55	157.67	135.78	140.30
200	16.21	17.44	18.69	54.55	56.65	59.06	127.51	118.86	123.04
300	14.71	15.08	16.43	49.70	48.47	52.51	116.55	101.51	108.30
400	13.16	12.48	14.18	44.60	40.10	45.00	104.93	83.79	93.49
500	11.11	10.60	11.92	37.56	33.18	37.51	88.18	70.81	78.75
600	5.88	5.50	6.12	19.96	17.34	20.62	47.02	37.10	41.83
700	2.52	2.33	2.58	8.58	7.40	9.38	20.28	15.90	19.72
800	1.65	1.45	1.61	5.57	4.95	5.62	13.04	10.29	12.29

Table 5.17 indicates the lateral torsional buckling moment results from the CBFEM using different types of the cross-section. In Table 5.18, the lateral torsional buckling resistance of steel beam under different boundary and loading conditions. The lateral torsional buckling moment resistance of steel beams with different lengths is shown in Table 5.19.

Table 5.18. The lateral torsional buckling – boundary and loading conditions (kN.m)

T (°C)	Simply supported - point load			Fix supported - point load			Simply supported - distributed load		
	Analytical	Shell Model	CBFEM	Analytical	Shell Model	CBFEM	Analytical	Shell Model	CBFEM
20	72.28	64.54	66.55	83.27	81.70	82.05	55.54	52.02	61.88
100	72.28	64.54	66.55	83.27	81.70	82.05	55.54	52.02	61.88
200	54.55	56.65	59.06	77.67	71.89	73.24	51.12	45.73	54.83
300	49.70	48.47	52.51	71.61	62.51	64.46	46.51	39.22	47.81
400	44.60	40.10	45.00	65.04	52.98	55.65	41.67	32.4	40.79
500	37.56	33.18	37.51	54.32	43.54	46.88	35.13	27.57	32.33
600	19.96	17.34	20.62	29.25	23.16	24.90	18.64	14.29	18.29
700	8.58	7.40	9.38	12.72	10.24	10.24	8	6.06	8.42
800	5.57	4.95	5.62	8.00	6.25	6.39	5.21	3.85	5.62

Table 5.19. The lateral torsional buckling – span length (kN.m)

T (°C)	IPE300 - 5 m			IPE 300 - 6 m			IPE300 - 7 m		
	Analytical	Shell Model	CBFEM	Analytical	Shell Model	CBFEM	Analytical	Shell Model	CBFEM
20	68.80	74.73	70.3	72.28	64.54	66.55	52.21	57.45	50.11
100	68.80	74.73	70.3	72.28	64.54	66.55	52.21	57.45	50.11
200	63.71	65.53	68.35	54.55	56.65	59.06	48.00	50.42	44.82
300	58.30	56.04	60.55	49.70	48.47	52.51	43.60	43.21	38.68
400	52.56	46.23	50.8	44.60	40.10	45.00	39.01	35.89	34.27
500	44.13	39.15	42.95	37.56	33.18	37.51	32.93	30.41	28.13
600	23.56	20.44	23.45	19.96	17.34	20.62	17.44	15.86	15.82
700	10.17	8.73	11.7	8.58	7.40	9.38	7.48	6.76	7.04
800	6.52	5.69	5.85	5.57	4.95	5.62	4.89	4.43	4.51

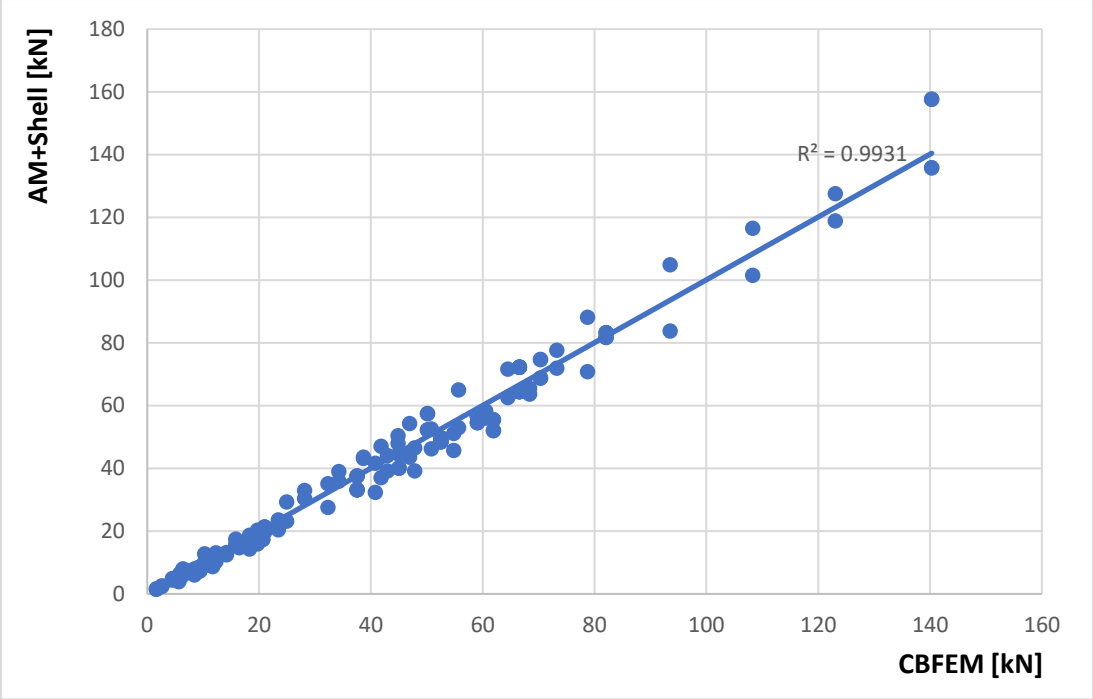

Figure 5.94. Summary of LTB resistance comparison

The section proposed a CBFEM model to calculate the fire resistance of steel beams in terms of different moment values. The CBFEM model was verified by the shell model and analytical models. The main drawbacks of the shell model can be defined as the uncertainty in the degree of warping constraint and the differences between real section dimensions and the geometry used in the shell model leading to different torsion and warping constants. The lateral-torsional buckling resistance from the analytical model becomes higher than that from the shell model because the analytical model includes bending resistance depending on the reduction factor in the yield strength of steel. According to Eurocode, the yield strength of steel does not have a reduction until 400°C. However, the results from the shell model were consistent with analytical results and they showed that using a simple shell model is possible to predict the moment resistance of the beam at elevated temperature.

5.4.2. Steel Columns

The steel column is modelled using IDEA StatiCa Member, as seen in Figure 5.95. The ends of steel columns are simulated using rigid end plates differently from steel beam models. The boundary conditions are applied to the midpoint in the end plates. The targeted temperature is applied to the column by the author.

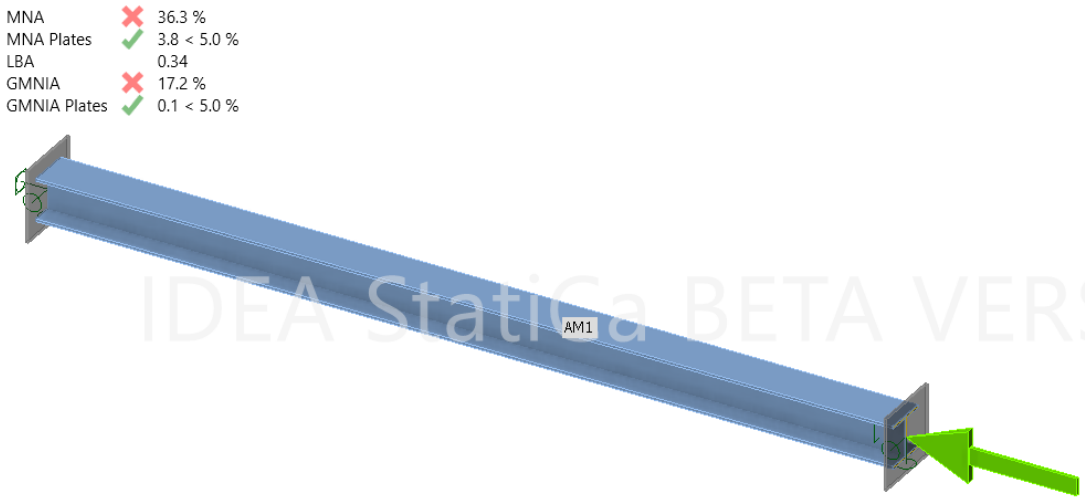

Figure 5.95. The configuration of the studied steel column

Verification

The study includes a column from the HEB300 section with a span of L = 6 m, which is loaded by concentrated force at the end of the column. The column is assumed to have a uniform temperature along the cross-section. Elastic modulus and yield strength of the steel beam at room temperature are taken as 210000 N/mm^2 and 355 N/mm^2, respectively. In contrast to steel beam model, the joint is modelled using the rigid plates welded to the ends of steel columns. The warping is not allowed due to the weld between flanges and rigid plates. The design buckling resistance $N_{b,fi,t,Rd}$ at time t of a compression member with Class 1, Class 2, or Class 3 cross-section and uniform temperature θ_a can be determined from clause 6.3.1 of EN 1993-1-1:

$$N_{b,fi,t,Rd} = \chi_{fi} A k_{y,\theta} f_y / \gamma_{M,fi} \tag{45}$$

where χ_{fi} is the reduction factor for flexural buckling in the fire design situation; $k_{y,\theta}$ is the reduction factor for yield strength of steel at temperature θ_a. The minimum value of $\chi_{y,fi}$ and $\chi_{z,fi}$ can be taken as the value of χ_{fi}.

$$\chi_{\text{fi}} = \frac{1}{\Phi + \sqrt{\Phi^2 - \bar{\bar{\lambda}}^2}} \text{ but } \chi \leq 1.0 \tag{46}$$

with

$$\Phi = 0.5\left[1 + \alpha\bar{\bar{\lambda}}_\theta + \bar{\lambda}_\theta^2\right] \tag{47}$$

and for all steel grades $\alpha = 0.65\sqrt{235/f_y}$, where f_y is the yield strength of steel at ambient temperature. The relative slenderness $\bar{\bar{\lambda}}_\theta$ at temperature θ_a is calculated by

$$\bar{\bar{\lambda}}_\theta = \bar{\lambda}\sqrt{k_{y,\theta}/k_{E,\theta}} \tag{48}$$

in which $k_{E,\theta}$ is the reduction factor for modulus of elasticity of steel at temperature θ_a and $\bar{\lambda}$ is the non-dimensional slenderness at room temperature given by the following equations using the buckling length in fire situation l_{fi}. The non-dimensional slenderness at room temperature ($\bar{\lambda}$) is given by Eq. 49

$$\bar{\lambda} = \sqrt{\frac{Af_y}{N_{cr}}} \; for\ Class\ 1, 2\ and\ 3\ cross\ sections \tag{49}$$

where N_{cr} is the elastic critical force for flexural buckling based on the gross cross-sectional properties and in the buckling length in fire situation l_{fi}.

$$N_{cr} = \frac{\pi^2 EI}{l_{fi}^2} \tag{50}$$

where E is the Young's modulus at room temperature, I is the second moment of area about y-y or x-x axis based on the gross cross-sectional properties and l_{fi} is the buckling length in fire situation.

Table 5.20. The critical loads for buckling

T (°C)	HEB 300 -PP - 6 m		HEB 300 -FP - 6 m		HEB 300 -FF - 6 m	
	AM [Kn]	CBFEM [Kn]	AM [Kn]	CBFEM [Kn]	AM [Kn]	CBFEM [Kn]
20	4930	4896	10061	9936	19720	18768
500	4930	4896	10061	9936	19720	18768

In Table 5.20, it can be seen that the results from CBFEM are not changed according to the temperature of the steel member as defined in analytical model and the CBFEM provides conservative results compared to the analytical result. The results of LBA are slightly conservative (< 5 %) for columns with fixed-end supports. For simply supported columns, the critical loads are very close to the expected analytical value. Figure 5.96. shows the buckling load values at different temperatures for the benchmark study of the column. In Table 5.21, the resistance values for buckling loads from parametric studies are presented. The boundary conditions and length of the column are changed at 500°C and 600°C, respectively.

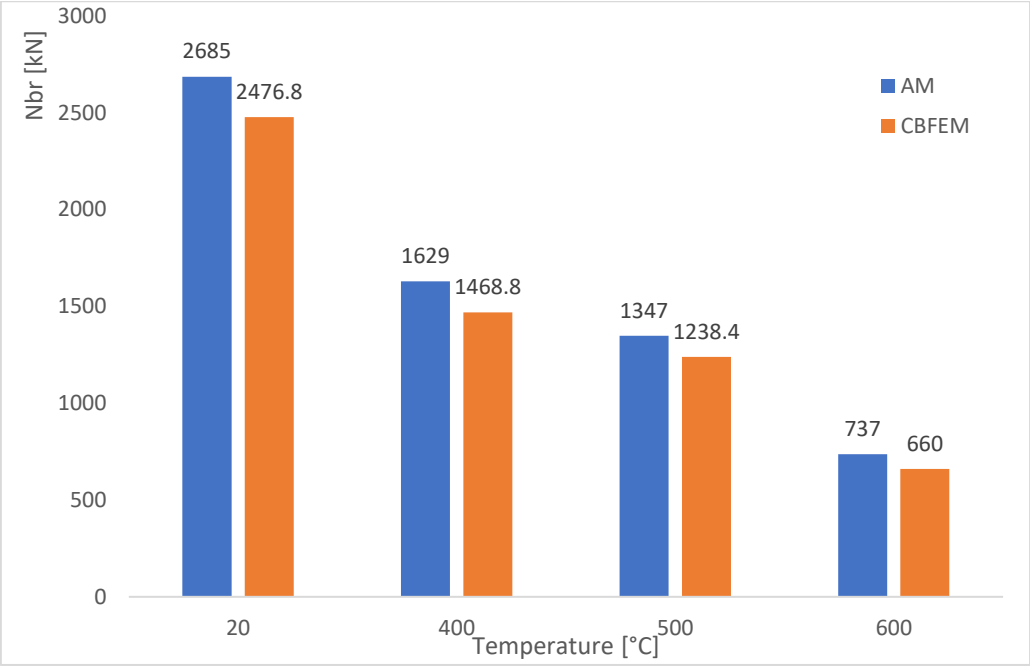

Figure 5.96. The buckling loads for the benchmark study

Table 5.21. The buckling loads changing supports and length of column

L (m)	HEB 300 -PP - 600°C		BC	HEB 300 -6m - 500°C	
	AM	CBFEM		AM	CBFEM
4	1129	1020	PP	1347	1238.4
6	737	660	FP	1915	1742.4
7	596	550	FF	2334	2226.4

6. Conclusion

6.1. Research summary

This thesis may be divided into six main chapters. The third chapter explains the effect of high temperatures on the response of steel structures. The material properties of components for steel joints and members at elevated temperatures are described in terms of thermal and mechanical properties. Then, the experimental studies on the behaviour of steel joints and members at elevated temperatures are listed. Finally, the different modelling types for steel joint design are presented in order to indicate the literature review on steel connections in the fire. The CBFEM model explains how to model steel joints at elevated temperatures. The chapter describes the material model for plate and bolts in shear and tension at elevated temperatures and the element type used for plate modelling.

In the fourth chapter, the experimental study is described. The details of test procedures and test results are given. Test results include the load-deformation curves, ultimate resistances, and failure modes at ambient temperature, 400°C and 600°C.

The fifth chapter presents the numerical studies performed by the author to model steel joints and members at elevated temperatures. To investigate the fire behaviour of steel joints and members, the solid model for bolted lap joints, the shell model for steel beams, and the CBFEM models for several joints and members are prepared. The verification and validation process of numerical models is an integral part of the procedure to check the accuracy of the numerical models [104]. The verification and validation studies on the CBFEM models for different joints and member types are performed. The failure modes for each component are explained to define the resistance of steel joints at high temperatures.

The sixth chapter finalises this study presenting the findings from the thesis and possible future research topics.

6.2. Findings

This thesis introduced the component-based finite element method (CBFEM) which is a numerical design calculation model to analyse and design steel connections and steel members at elevated temperatures. The connection and members in the CBFEM model were analysed by finite element models. The correct response of components is simulated by introducing its behaviour in terms of initial stiffness, ultimate strength, and deformation capacity of bolts and welds at elevated temperatures. The studied connection types were bolted and welded lap joints, flush endplate, and fin plate joints, and T-stubs to investigate the main components such as bolts in tension and shear, welds in shear, plate bearing, and plate fractures at elevated temperatures. In this study, the CBFEM was employed to analyse steel beams and steel columns at elevated temperatures, as well. The primary conclusions from this research are:

- The verification studies highlighted that the CBFEM is a reliable model to design bolted and welded connections and steel members at elevated temperatures. The numerical design calculation models may replace the curve fitting and component methods for designing steel connections and steel members at elevated temperatures.
- The developed CBFEM model is able to evaluate the mechanical response of different bolted connections subjected to different loading conditions at elevated temperatures. Since the CBFEM provided smaller resistance values than test results and predicted the same failure mode as observed in tests, it may be utilized as a design tool for structural fire engineers.
- The results showed that the recommended plastic limit strain may be used to calculate the resistance and failure modes of steel connections and members at elevated temperatures. The recommended 5% plastic limit strain for steel plates can be also used for the fire design of steel connections.

6.3. Future research

Due to the lack of time and the difficulties in the development of IDEA StatiCa Fire Module, there are some uncompleted studies for future research.

Experimental studies were preformed to study the behaviour of welded lap joints at ambient temperatures, 450°C and 650°C at the laboratory of Czech Technical University in Prague. Since the IDEA StatiCa current version is not running when the elastic modulus of welds is decreased based on Eurocode reduction factors at elevated temperatures, the validation study could not be performed for modelling welded lap joints at elevated temperatures. The test results will be used to validate the CBFEM model for fillet welds at elevated temperatures.

Mostly, the verification studies were done using the analytical models according to Eurocode. The CBFEM models will be compared with other finite element models as studied in bolted lap joints.

The CBFEM models for steel members at elevated temperatures were only verified compared to analytical results. In the future the CBFEM model will be validated using experimental results from literature in terms of isolated beams, columns, and steel frames published in FISHWALL project.

List of figures

List of tables

References

[1] A. H. Buchanan and A. K. Abu, “Front Matter,” in *Structural Design for Fire Safety*, Wiley, 2016. doi: 10.1002/9781118700402.fmatter.

[2] “CEN/TC 250 Eurocode 3: Design of steel structures-Part 1-14: Design assisted by finite element analysis,” 2021.

[3] B. Der, F. Wald, M. Vild, and C. Batuhan Der, “Modelling of bolted joints in fire using the component-based finite element method Proceedings in civil engineering,” 2023, doi: 10.1002/cepa.

[4] B. Der, F. Wald, M. Vild, and J. Kabeláč, “Bolted joints in fire by the component-based finite element method,” *Proceedings of the International Conference - Celebrating 60 Years of IBST*, pp. 71–76, Nov. 2023, doi: 10.59382/pro.intl.con-ibst.2023.ses1-4.

[5] B. Der, F. Wald, M. Vild, and C. Batuhan Der, “Modelling of bolted joints in fire using the component-based finite element method Proceedings in civil engineering,” 2023, doi: 10.1002/cepa.

[6] Lubomír Šabatka, František Wald, Jaromír Kabeláč, Drahoslav Kolaja, and Martin Pospíšil, “Structural Analysis and Design of Steel Connections Using Component-Based Finite Element Model,” *Journal of Civil Engineering and Architecture*, vol. 9, no. 8, Aug. 2015, doi: 10.17265/1934-7359/2015.08.002.

[7] F. Wald *et al.*, “Component based finite element design of steel joints,” *Civil Engineering Design*, vol. 2, no. 3, pp. 78–89, Jul. 2020, doi: 10.1002/cend.202000015.

[8] G. M. Newman, J. T. Robinson, and C. G. Bailey, “Fire Safe Design: A New Approach to Multi-Storey Steel-Framed Buildings,” p. 116, 2006.

[9] C. M. Gutierrez and P. D. Gallagher, “NIST NCSTAR 1A Federal Building and Fire Safety Investigation of the World Trade Center Disaster Final Report on the Collapse of World Trade Center Building 7,” 2008.

[10] “EN 1993-1-2: Eurocode 3: Design of steel structures - Part 1-2: General rules - Structural fire design,” 2005.

[11] “Abaqus theory manual,” *Abaqus 6.13 documentation*, no. Dassault Systemes Simulia Corp., Providence, RI, USA., 2014.

[12] CEN, “EN 1993-1-8: Eurocode 3: Design of steel structures - Part 1-8: Design of joints,” 2005.

[13] EN 1993-1-5: Eurocode 3: Design of steel structures - Part 1-5: Plated structural elements,” 2006.

[14] B. Der *et al.*, “Emissivity of hot-dip galvanized surfaces in future development of EN 1993-1-2,” *Journal of Structural Fire Engineering*, 2022, doi: 10.1108/JSFE-11-2021-0070.

[15] Sakumoto, Y., Keira, K., Furumura, F., & Ave, T. (1993). Tests of fire-resistant bolts and joints. Journal of Structural Engineering, 119(11), 3131-3150

[16] B. R. Kirby, “The behaviour of high-strength grade 8.8 bolts in fire,” *J Constr Steel Res*, vol. 33, no. 1–2, pp. 3–38, 1995, doi: 10.1016/0143-974X(94)00013-8.

[17] G.-Q. Li, Y.-Z. Yin, and M.-F. Li, “Experimental studies on the material properties of high-strength bolt connection at elevated temperatures,” *Steel and Composite Structures*, vol. 2, no. 4, pp. 247–258, Aug. 2002, doi: 10.12989/scs.2002.2.4.247.

[18] L. Yu, “Behavior of bolted connections during and after a fire,” vol. PhD Disser, p. 196, 2006, [Online]. Available: http://search.ebscohost.com/login.aspx?direct=true&db=edsndl&AN=edsndl.oai.union.ndltd.org.UTEXAS.oai.repositories.lib.utexas.edu.2152.2959&site=eds-live

[19] Y. Hu, J. B. , Davison, I. W. Burgess, and R. J. Plank, “Comparative study of the behaviour of BS 4190 and BS EN ISO 4014 bolts in fire,” in *The 3rd International Conference on Steel and Composite Structures* , Manchester: Francis, 2007, pp. 587–592.

[20] V. Kodur, S. Kand, and W. Khaliq, “Effect of Temperature on Thermal and Mechanical Properties of Steel Bolts,” *Journal of Materials in Civil Engineering*, vol. 24, no. 6, pp. 765–774, 2012, doi: 10.1061/(ASCE)MT.1943-5533.0000445.

[21] R. M. Peixoto, M. S. Seif, and L. C. M. Vieira, “Double-shear tests of high-strength structural bolts at elevated temperatures,” *Fire Saf J*, vol. 94, pp. 8–21, Dec. 2017, doi: 10.1016/j.firesaf.2017.09.003.

[22] X. P. Pang *et al.*, “Physical properties of high-strength bolt materials at elevated temperatures,” *Results Phys*, vol. 13, Jun. 2019, doi: 10.1016/j.rinp.2019.102156.

[23] A. Rezaeian, M. Shafiei, and M. Eskandari, “Effect of Temperature on Mechanical Properties of Steel Bolts,” *Journal of Materials in Civil Engineering*, vol. 32, no. 9, Sep. 2020, doi: 10.1061/(asce)mt.1943-5533.0003314.

[24] H. Ban, Q. Yang, Y. Shi, and Z. Luo, “Constitutive model of high-performance bolts at elevated temperatures,” *Eng Struct*, vol. 233, Apr. 2021, doi: 10.1016/j.engstruct.2021.111889.

[25] H. Yu, “Experimental investigation of structural steel welds at high temperature,” in *Advanced Materials Research*, 2011, pp. 3350–3354. doi: 10.4028/www.scientific.net/AMR.250-253.3350.

[26] A. Rezaeian, M. Keshavarz, and E. Hajjari, “Mechanical properties of steel welds at elevated temperatures,” *J Constr Steel Res*, vol. 167, Apr. 2020, doi: 10.1016/j.jcsr.2019.105853.

[27] Da Silva, L. Simoes, and AM Girão Coelho. "An analytical evaluation of the response of steel joints under bending and axial force." Computers & Structures 79.8 (2001): 873-881.

[28] Wald, F., Silva, L. S., Moore, D., & Santiago, A. (2004). Experimental behaviour of steel joints under natural fire. ECCS – AISC Workshop June 3-4, 2004

[29] Lawson, R. (1990). Behaviour of steel beam-to-column connections in fire. The Structural Engineer, 68, 263-271.

[30] L. C. Leston-Jones, “THE INFLUENCE OF SEMI-RIGID CONNECTIONS ON THE PERFORMANCE OF STEEL FRAMED STRUCTURES IN FIRE,” 1997.

[31] Al-Jabri, K. S. (1999). *The behaviour of steel and composite beam-to-column connections in fire.* Department of Civil and Structural Engineering. Sheffield, UK: University of Sheffield.

[32] J. Kruppa, “Resistance en feu des assemblages par boulons haute resistance,” *Centre Technique Industriel de la Construction Metallique.*, 1976.

[33] British, S. (1982). The performance of beam/column/beam connections in the BS476: art 8 fire test. Reports T/RS/1380/33/82D and T/RS/1380/34/82D: British Steel.

[34] L. C. Leston-Jones, “The influence of semi-rigid connections on the performance of steel framed structures in fire.,” no. July 1997, 1997, [Online]. Available: http://etheses.whiterose.ac.uk/3047/

[35] H. Yu, I. W. Burgess, J. B. Davison, and R. J. Plank, “Tying capacity of web cleat connections in fire, Part 1: Test and finite element simulation,” *Eng Struct*, vol. 31, no. 3, pp. 651–663, Mar. 2009, doi: 10.1016/j.engstruct.2008.11.005.

[36] Hu, Ying, et al. "Experimental study on flexible end plate connections in fire." Proceedings of 5th European conference on steel structures, Graz, Austria. 2008.

[37] Yu, Hongxia, et al. "Experimental investigation of the behaviour of flush endplate connections in fire." Proceedings of 5th international conference Structures in Fire, Singapore. 2008.

[38] Yu, Hongxia, et al. "Experimental and numerical investigations of the behavior of flush end plate connections at elevated temperatures." Journal of structural engineering 137.1 (2011): 80-87.

[39] H. Yu, I. W. Burgess, J. B. Davison, and R. J. Plank, “Experimental investigation of the behaviour of fin plate connections in fire,” *J Constr Steel Res*, vol. 65, no. 3, pp. 723–736, Mar. 2009, doi: 10.1016/j.jcsr.2008.02.015.

[40] Yu, Hongxia, et al. "Experimental investigation of the robustness of fin plate connections in fire." Proceedings of 5th ICASS (Advances in Steel Structures) (2007).

[41] “SCI P358. (2014). Joints in steel construction: Simple joints to Eurocode 3.

[42] Liu, T. C. H., M. K. Fahad, and J. M. Davies. "Experimental investigation of behaviour of axially restrained steel beams in fire." Journal of Constructional Steel Research 58.9 (2002): 1211-1230.

[43] Z. H. Qian, K. H. Tan, and I. W. Burgess, “Behavior of steel beam-to-column joints at elevated temperature: Experimental investigation,” *Journal of Structural Engineering*, vol. 134, no. 5, pp. 713–726, 2008, doi: 10.1061/(ASCE)0733-9445(2008)134:5(713).

[44] A. Santiago, L. S. Da Silva, G. Vaz, P. V. Real, and A. G. Lopes, “Experimental investigation of the behaviour of a steel sub-frame under a natural fire,” in *Steel and Composite Structures*, Techno Press, 2008, pp. 243–264. doi: 10.12989/scs.2008.8.3.243.

[45] Y. C. Wang, X. H. Dai, and C. G. Bailey, “An experimental study of relative structural fire behaviour and robustness of different types of steel joint in restrained steel frames,” *J Constr Steel Res*, vol. 67, no. 7, pp. 1149–1163, Jul. 2011, doi: 10.1016/j.jcsr.2011.02.008.

[46] S. V. Khonsari, S. Nejati, M. Rahdan, and M. Ahmadi, “Behaviour of thin flush end-plate connections in a 3D bare steel frame under fire loading: experimental study,” *Journal of Structural Fire Engineering*, vol. 14, no. 1, pp. 15–33, Feb. 2023, doi: 10.1108/JSFE-08-2021-0050.

[47] Barata, Pedro, Aldina Santiago, and João P. Rodrigues. "Experimental behaviour of T-stub joint component at elevated temperatures." 2º CILASCI–Congresso Ibero-Latino-Americano sobre Segurança Contra Incêndios. 2013.

[48] Y. You, M. Liu, Y. Liu, P. Wang, S. Zhou, and J. Chen, “Experimental studies on thread-fixed one-side bolted T-stubs in tension at elevated temperatures,” *J Constr Steel Res*, vol. 171, Aug. 2020, doi: 10.1016/j.jcsr.2020.106139.

[49] K. Jiang, O. Zhao, and K. H. Tan, “Experimental and numerical study of S700 high strength steel double shear bolted connections in tension,” *Eng Struct*, vol. 225, Dec. 2020, doi: 10.1016/j.engstruct.2020.111175.

[50] Y. Dong and X. Li, “The behaviors of h-section steel beam in fire,” in *Fire Safety Science*, International Association for Fire Safety Science, 2005, pp. 201–209. doi: 10.3801/IAFSS.FSS.8-201.

[51] R. B. Dharma and K. H. Tan, “Rotational capacity of steel I-beams under fire conditions Part I: Experimental study,” *Eng Struct*, vol. 29, no. 9, pp. 2391–2402, Sep. 2007, doi: 10.1016/j.engstruct.2006.11.031.

[52] S. Ramesh, L. Choe, and C. Zhang, “Experimental investigation of structural steel beams subjected to localized fire,” *Eng Struct*, vol. 218, Sep. 2020, doi: 10.1016/j.engstruct.2020.110844.

[53] P. Woźniczka, “Experimental study of lateral-torsional buckling of class 4 beams at elevated temperature,” *Materials*, vol. 14, no. 17, Sep. 2021, doi: 10.3390/ma14174825.

[54] F. Wald and European Cooperation in the Field of Scientific and Technical Research (organizace), *Benchmark studies : experimental validation of numerical models in fire engineering*. CTU Publishing House, Czech Technical University, 2014.

[55] N. Torić, A. Harapin, and I. Boko, “Experimental verification of a newly developed implicit creep model for steel structures exposed to fire,” *Eng Struct*, vol. 57, pp. 116–124, Dec. 2013, doi: 10.1016/j.engstruct.2013.09.024.

[56] Choe, Lisa, Amit H. Varma, and Andrea Surovek. "Behavior of steel columns under fire loading." Structures Congress 2011. 2011.

[57] K. C. Yang and R. Hsu, “Structural behavior of centrally loaded steel columns at elevated temperature,” *J Constr Steel Res*, vol. 65, no. 10–11, pp. 2062–2068, Oct. 2009, doi: 10.1016/j.jcsr.2009.06.007.

[58] J. ; Pauli, D. ; Somaini, M. ; Knobloch, and M. Fontana, “Experiments on steel columns under fire conditions”, doi: 10.3929/ethz-a-007600651.

[59] W. Wang, L. Zhang, Y. Ge, and L. Xu, “Behaviour of restrained high strength steel columns at elevated temperature,” *J Constr Steel Res*, vol. 148, pp. 251–264, Sep. 2018, doi: 10.1016/j.jcsr.2018.05.022.

[60] W. Wang, H. Zhou, and L. Xu, “Creep buckling of high strength Q460 steel columns at elevated temperatures,” *J Constr Steel Res*, vol. 157, pp. 414–425, Jun. 2019, doi: 10.1016/j.jcsr.2019.03.003.

[61] Steel Construction Institute., *Structural fire engineering : investigation of Broadgate Phase 8 fire.* Steel Construction Institute, 1991.

[62] Wang, Yong C., ed. Steel and composite structures: behaviour and design for fire safety. CRC Press, 2002.

[63] C. G. Bailey, “Fire engineering design of steel structures,” *Advances in Structural Engineering*, vol. 8, no. 3, pp. 185–202, 2005, doi: 10.1260/1369433054349141.

[64] C. G. Bailey, T. Lennon, and D. B. Moore, “The behaviour of full-scale steel-framed buildings subjected to compartment fires,” *Structural Engineer*, vol. 77, no. 8, pp. 15–21, 1999.

[65] A. S. Usmani, Y. C. Chung, and J. L. Torero, “How did the WTC towers collapse: A new theory,” *Fire Saf J*, vol. 38, no. 6, pp. 501–533, 2003, doi: 10.1016/S0379-7112(03)00069-9.

[66] M. A. Orabi, L. Jiang, A. Usmani, and J. Torero, “The Collapse of World Trade Center 7: Revisited,” *Fire Technol*, 2022, doi: 10.1007/s10694-022-01225-2.

[67] F. Wald *et al.*, “Experimental behaviour of a steel structure under natural fire,” *Fire Saf J*, vol. 41, no. 7, pp. 509–522, Oct. 2006, doi: 10.1016/j.firesaf.2006.05.006.

[68] Wang, Y. C. "An analysis of the global structural behaviour of the Cardington steel-framed building during the two BRE fire tests." Engineering Structures 22.5 (2000): 401-412.

[69] W. Y. Wang, G. Q. Li, and Y. L. Dong, “Experimental study and spring-component modelling of extended end-plate joints in fire,” *J Constr Steel Res*, vol. 63, no. 8, pp. 1127–1137, Aug. 2007, doi: 10.1016/j.jcsr.2006.10.006.

[70] J. P. Jaspart, “General report: Session on connections,” *J Constr Steel Res*, vol. 55, no. 1–3, pp. 69–89, 2000, doi: 10.1016/S0143-974X(99)00078-4.

[71] Da Silva, L. Simoes, Aldina Santiago, and Paulo Vila Real. "A component model for the behaviour of steel joints at elevated temperatures." Journal of Constructional Steel Research 57.11 (2001): 1169-1195.

[72] S. Spyrou, “Development of a Component-Based Model of Steel Beam-To-Column Joints At Elevated Temperatures,” no. January, 2002.

[73] F. M. Block, I. W. Burgess, J. B. Davison, and R. J. Plank, “The development of a component-based connection element for endplate connections in fire,” *Fire Saf J*, vol. 42, no. 6–7, pp. 498–506, Sep. 2007, doi: 10.1016/j.firesaf.2007.01.008.

[74] M. Sarraj, I. W. Burgess, J. B. Davison, and R. J. Plank, “Finite element modelling of steel fin plate connections in fire,” *Fire Saf J*, vol. 42, no. 6–7, pp. 408–415, 2007, doi: 10.1016/j.firesaf.2007.01.007.

[75] W. Y. Wang, G. Q. Li, and Y. L. Dong, “Experimental study and spring-component modelling of extended end-plate joints in fire,” *J Constr Steel Res*, vol. 63, no. 8, pp. 1127–1137, 2007, doi: 10.1016/j.jcsr.2006.10.006.

[76] Santiago, Aldina Maria da Cruz. Behaviour of beam-to-column steel joints under natural fire. Diss. 2008.

[77] Taib, M. (2012). The performance of steel framed structures with fin-plate connections in fire (Doctoral dissertation, University of Sheffield).

[78] G. Quan, S. S. Huang, and I. Burgess, “Component-based model of buckling panels of steel beams at elevated temperatures,” *J Constr Steel Res*, vol. 118, pp. 91–104, Mar. 2016, doi: 10.1016/j.jcsr.2015.10.024.

[79] K. S. Al Jabri, “Modelling of the behaviour of beam-to-column connections at elevated temperature,” *High Performance Structures and Materials*, vol. 7, pp. 319–328, 2004.

[80] K. S. Al-Jabri, A. Seibi, and A. Karrech, “Modelling of unstiffened flush end-plate bolted connections in fire,” *J Constr Steel Res*, vol. 62, no. 1–2, pp. 151–159, 2006, doi: 10.1016/j.jcsr.2005.04.016.

[81] S. Selamet and M. E. Garlock, “Fire resistance of steel shear connections,” *Fire Saf J*, vol. 68, pp. 52–60, 2014, doi: 10.1016/j.firesaf.2014.05.016.

[82] T. Gernay and J. M. Franssen, “The introduction and the influence of semi-rigid connections in framed structures subjected to fire,” *Fire Saf J*, vol. 114, Jun. 2020, doi: 10.1016/j.firesaf.2020.103007.

[83] Bursi, Oreste S., and Jean-Pierre Jaspart. "Benchmarks for finite element modelling of bolted steel connections." Journal of Constructional Steel Research 43.1-3 (1997): 17-42.

[84] J. Kim, J. C. Yoon, and B. S. Kang, “Finite element analysis and modeling of structure with bolted joints,” *Appl Math Model*, vol. 31, no. 5, pp. 895–911, 2007, doi: 10.1016/j.apm.2006.03.020.

[85] Rutman, Alexander, et al. "Fastener modeling for joining parts modeled by shell and solid elements." Americas Virtual Product Development Conference. 2007.

[86] Gödrich, Lukáš, František Wald, and Zdeněk Sokol. "To advanced modelling of end plate joints." Journal of Civil Engineering, Environment and Architecture 30.60 (2013): 2.

[87] Z. Wu, S. Zhang, and S. F. Jiang, “Simulation of tensile bolts in finite element modeling of semi-rigid beam-to-column connections,” *International Journal of Steel Structures*, vol. 12, no. 3, pp. 339–350, 2012, doi: 10.1007/s13296-012-3004-8.

[88] Aygül, Mustafa. Fatigue analysis of welded structures using the finite element method. Chalmers Tekniska Hogskola (Sweden), 2012.

[89] Niemi, Erkki, ed. Stress determination for fatigue analysis of welded components. Woodhead Publishing, 1995.

[90] Fayard, J-L., Andre Bignonnet, and K. Dang Van. "Fatigue design criterion for welded structures." Fatigue & Fracture of Engineering Materials & Structures 19.6 (1996): 723-729.

[91] Eriksson, Å., Lignell, A. M., Olsson, C., & Spennare, H. (2003). Weld evaluation using FEM: a guide to fatigue-loaded structures. Industrilitteratur.

[92] “https://www.ideastatica.com/support-center/material-model.”

[93] “https://www.ideastatica.com/support-center/cbfem-how-it-works-code-compliance-validation-and-verification.”

[94] “VEREIN DEUTSCHER INGENIEURE Systematische Berechnung hochbeanspruchter Schraubenverbindungen Zylindrische Einschraubenverbindungen Systematic calculation of high duty bolted joints Joints with one cylindrical bolt VDI-Gesellschaft Entwicklung Konstruktion Vertrieb VDI-Handbuch Konstruktion,” 2003.

[95] H. Agerskov, “High-Strength Bolted Connections Subject to Prying,” *Journal of the Structural Division*, vol. 102, no. 1, pp. 161–175, Jan. 1976, doi: 10.1061/JSDEAG.0004253.

[96] ISO 898-1. "Mechanical properties of fasteners made of carbon steel and alloy steel." Bolts, screws and stud (2009).

[97] “https://www.ideastatica.com/support-center/welds.”

[98] K.-H. Tan and Z.-F. Huang, “Structural Responses of Axially Restrained Steel Beams with Semirigid Moment Connection in Fire,” *Journal of Structural Engineering*, vol. 131, no. 4, pp. 541–551, Apr. 2005, doi: 10.1061/(asce)0733-9445(2005)131:4(541).

[99] Y. Z. Yin and Y. C. Wang, “A numerical study of large deflection behaviour of restrained steel beams at elevated temperatures,” *J Constr Steel Res*, vol. 60, no. 7, pp. 1029–1047, Jul. 2004, doi: 10.1016/j.jcsr.2003.09.005.

[100] A. Heidarpour and M. A. Bradford, “Generic nonlinear modelling of restrained steel beams at elevated temperatures,” *Eng Struct*, vol. 31, no. 11, pp. 2787–2796, Nov. 2009, doi: 10.1016/j.engstruct.2009.07.006.

[101] M. Kucukler, “Lateral instability of steel beams in fire: Behaviour, numerical modelling and design,” *J Constr Steel Res*, vol. 170, Jul. 2020, doi: 10.1016/j.jcsr.2020.106095.

[102] H. Fang and T. M. Chan, “Axial compressive strength of welded S460 steel columns at elevated temperatures,” *Thin-Walled Structures*, vol. 129, pp. 213–224, Aug. 2018, doi: 10.1016/j.tws.2018.04.006.

[103] H. Murtaza and M. Kucukler, “Fire design of steel columns through second-order inelastic analysis with strain limits,” *Thin-Walled Structures*, vol. 184, Mar. 2023, doi: 10.1016/j.tws.2022.110458.

[104] Wald, František, et al. "Validation and verification procedures for connection design in steel structures." 12th International Conference on Steel, Space and Composite Structures. 2014.

[105] Selamet, Serdar, and Maria Garlock. "Guidelines for modeling three dimensional structural connection models using finite element methods." International symposium: steel structures: culture & sustainability. 2010.

[106] H. Wen and H. Mahmoud, “Simulation of block shear fracture in bolted connections,” *J Constr Steel Res*, vol. 134, pp. 1–16, Jul. 2017, doi: 10.1016/j.jcsr.2017.03.006.

[107] “EN 1993-1-1: Eurocode 3: Design of steel structures - Part 1-1: General rules and rules for buildings.”

[108] “IDEA StatiCa Connection 23.1.” 2023, Product documentation. Retrieved from www.idea-rs.com.

[109] “IDEA StatiCa Member 23.1.” 2023, Product documentation. Retrieved from www.idea-rs.com.

[110] AISC (American Institute of Steel Construction), “Specification for Structural Steel Buildings, ANSI / AISC 360-16,” *American Institute of Steel Construction*, p. 676, 2016.

[111] M. Sarraj, “The behaviour of steel fin plate connections in fire,” *The University of Sheffield Department of Civil and Structural Engineering*, no. July, 2007, doi: 10.1016/j.ijppaw.2013.04.002.

[112] Bureau, Alain. "NCCI: Elastic critical moment for lateral torsional buckling." SN003a-EN-EU, Access Steel< project. access-steel. com/Content/Content. htm>[26.11. 06] (2006).

[113] Real, PMM Vila, P. A. G. Piloto, and J-M. Franssen. "A new proposal of a simple model for the lateral-torsional buckling of unrestrained steel I-beams in case of fire: experimental and numerical validation." Journal of Constructional Steel Research 59.2 (2003): 179-199.

Authors Publications

Peer Reviewed Journals:

- DER, B., et al. Emissivity of hot-dip galvanized surfaces in future development of EN 1993-1-2. Journal of Structural Fire Engineering. 2022, 13(4), 535-557. ISSN 2040-2317. DOI 10.1108/JSFE-11-2021-0070
- Der, B., Wald, F., Vild, M. Numerical Design Calculation of Fin Plate Connections in Fire, 2024, Proceedings of the 7th International Conference on Geotechnics, Civil Engineering and Structures; CIGOS 2024; 04-05 April, Ho Chi Minh City, Vietnam, A Springer book series Lecture Notes in Civil Engineering [ACCEPTED]
- Der, B., Wald, F., Vild, M. Numerical Design Calculation of Flush Endplate Connections at Elevated Temperatures, 2024, Fire and Materials, Under Review
- Der, B., Wald, F. Numerical Design Calculation of Bolted Lap Joints at Elevated Temperatures, 2024, Fire Safety Journal, Under Review
- Der, B., Wald, F., Vild, M. Numerical Design Calculation of T-stubs at Elevated Temperatures, 2024, Fire Technology, Under Editorial Review

International Conference Proceedings:

- DER, B., F. WALD, and M. VILD. BENCHMARK STUDY FOR FIRE DESIGN OF STEEL BEAM. In: PEČENKO, R.P., et al., eds. Proceedings of the International Conference In Ljubljana, 10-11 June 2021. Applications of Structural Fire Engineering 2021, Ljubljana, 2021-06-10/2021-06-11. Lublaň: University of Ljubljana, Faculty of Civil and Geod, 2021. p. 394-399. 1. vydání. ISSN 2570-8074. ISBN 978-961-6884-71-6. Available from: https://www.asfe21conference.com/static/Proceeding_asfe_2021.pdf
- DER, B. and F. WALD. Experimental and Numerical Studies of Bolted Lap Joints at Elevated Temperature. In: VILA REAL, P. and N. LOPES, eds. The International Colloquium on Stability and Ductility of Steel Structures (SDSS 2022). The International Colloquium on Stability and Ductility of Steel Structures, Aveiro, 2022-09- 14/2022-09-16. Berlin: Ernst & Sohn, 2022. p. 204-209. 4. vol. 5. ISSN 2509-7075. DOI 10.1002/cepa.1746
- DER, B. NUMERICAL DESIGN CALCULATION OF STEEL MEMBERS AND JOINTS IN FIRE. In: Young Engineers Colloquium Dresden 2023. Dresden, 2023-05-30/2023-05-31. Berlin: IABSE Colloqium, 2023. p. 10-11. ISBN 978-3-85748-193-2.
- DER, B., F. WALD, and M. VILD. Modelling of bolted joints in fire using the component-based finite element method. In: EUROSTEEL Amsterdam 2023. Amsterdam, 2023-09-12/2023-09-14. Berlin: Ernst & Sohn, 2023. p. 2103-2107. 3-4. vol. 6. ISSN 2509-7075. DOI 10.1002/cepa.2485
- DER, B., F. WALD, and M. VILD. NUMERICAL CALCULATION OF JOINTS IN FIRE. In: Zborník prednášok zo 46.aktívu pracovníkov odboru oceľových konštrukcií. 46. aktívu pracovníkov odboru oceľových konštrukcií, Oščadnica, 2023-05-25/2023-05-26. Žilina: Žilinská universita, Strojnícka fakulta, 2023. p. 30-39. ISBN 978-80-554-1967-1.
- DER, B., et al. Bolted joints in fire by the component-based finite element method. In: PROCEEDINGS OF THE INTERNATIONAL CONFERENCE CONSTRUCTION SCIENCE AND TECHNOLOGY TOWARD SUSTAINABLE DEVELOPMENT. Hanoi, 2023-11-10. Hanoi: Construction Publishing House, 2023. p. 71-76. ISBN 978-604-82-7527-3. DOI 10.59382/pro.intl.con-ibst.2023.ses1-4
- WALD, F., et al. Component Based Finite Element Method for Steel Joints at Ambient and Elevated Temperatures. In: PROCEEDINGS OF THE INTERNATIONAL CONFERENCE CONSTRUCTION SCIENCE AND TECHNOLOGY TOWARD SUSTAINABLE

DEVELOPMENT. Hanoi, 2023-11-10. Hanoi: Construction Publishing House, 2023. p. 14-23. ISBN 978-604-82-2586-5. DOI 10.59382/pro.intl.con-ibst.2023.keynotes-2

- DER, B., F. WALD, and M. VILD, FIRE DESIGN OF STEEL MEMBER BY COMPONENT-BASED FINITE ELEMENT METHOD, XIV Conference on Steel and Composite Construction, Coimbra, Portugal, 23-24/11/2023, Wiley c/e papers, Berlin: Ernst & Sohn, DOI:10.1002/cepa.3020.
- DER, B., F. WALD, and M. VILD, Component-Based Finite Element Method for Flush Endplate Connections in Fire, 15th Nordic Steel Construction Conference in Luleå, 26-28 June, Wiley c/e papers, Berlin: Ernst & Sohn [UNDER REVIEW]

National Conference Proceedings:

- DER, B., et al. NÁVRH STYČNÍKŮ OCELOVÝCH KONSTRUKCÍ NA ÚČINKY POŽÁRU. In: Sborník přednášek KONSTRUKCE 2022. 12. odborná konference České asociace ocelových konstrukcí 2022, Špindlerův Mlýn, 2022-11-03/2022-11-04. Ostrava: Česká asociace ocelových konstrukcí (ČAOK), 2022. p. 28-33. ISSN 1803-8433.
- WALD, F., B. DER, and K. CÁBOVÁ. CHEMICKÉ SLOŽENÍ OCELÍ A ZVÝŠENÍ POŽÁRNÍ ODOLNOSTI ŽÁROVÝM ZINKOVÁNÍM V prEN1993-1-2:2022. In: Sborník přednášek KONSTRUKCE 2022. 12. odborná conference České asociace ocelových konstrukcí 2022, Špindlerův Mlýn, 2022-11-03/2022-11-04. Ostrava: Česká asociace ocelových konstrukcí (ČAOK), 2022. p. 17-23. ISSN 1803-8433.
- DER, B., F. WALD, and M. VILD. NUMERICKÁ PODPORA NÁVRHU PRVKŮ ZA ZVÝŠENÉ TEPLOTY PŘI POŽÁRU. In: SBORNÍK PŘEDNÁŠEK KONSTRUKCE 2023. 13. odbornou konferenci KONSTRUKCE 2023, Olomouc, 2023- 11-02. Ostrava: Česká asociace ocelových konstrukcí (ČAOK), 2023. p. 19-26

Others:

- DER, B. EXPERIMENTAL STUDIES OF BOLTED LAP JOINT AT ELEVATED TEMPERATURE. In: STUDNIČKA, J. and J. MAREŠ, eds. Sborník semináře doktorandů katedry ocelových a dřevěných konstrukcí 2021. Seminář doktorandů katedry ocelových a dřevěných konstrukcí 2021, Praha, 2021-02-02/2021-09-14. Praha: Czech Technical University in Prague, 2021. p. 20-23. ISBN 978-80-01-06856-4.